Swansea University
Prifysgol Abertawe

The role of STEAP2 in aggressive prostate cancer traits and androgen responses

Leia Ashleigh Jones

Submitted to Swansea University in fulfilment of the requirements for the Degree of

Doctor of Philosophy

Swansea University

July 2021

Summary

The prognosis of localised prostate cancer is generally promising, as many tumours remain dormant and therefore do not require immediate intervention. In contrast, once metastasised, the prognosis for aggressive prostate cancer is often poor, highlighting the need for novel, effective treatment approaches. The expression of the six transmembrane epithelial antigen of the prostate2 (STEAP2) cell surface protein is increased in aggressive prostate cancer compared to normal prostate tissue. *In vitro* studies have shown STEAP2 to aid in prostate cancer progression, and as such this molecule shows promise as a potential novel therapeutic target in the treatment of advanced disease. The aim of this thesis was to develop a comprehensive understanding of the mechanistic role of STEAP2 in promoting aggressive prostate cancer traits and evaluate if its knock-out has the capacity to reduce the invasive potential of prostate cancer cells *in vitro*. As prostate cancer is a largely androgen dependent disease, this thesis also aimed to evaluate the effects of STEAP2 inhibition on the expression of the androgen receptor and androgen-regulated genes.

This study developed and optimised a protocol for generating a set of 3D prostate cancer spheroids to provide more representative models of the *in vivo* prostate cancer environment. In this thesis, one commercial anti-STEAP2 polyclonal antibody and a panel of anti-STEAP2 monoclonal antibodies were selected for proof-of-concept studies where their effects on reducing prostate cancer cell viability were assessed. Receptor internalisation of STEAP2 was evaluated upon anti-STEAP2 monoclonal antibody binding to determine its suitability for use with antibody-drug conjugate technology. STEAP2 expression was knocked out using CRISPR/Cas9 genome engineering technology in two prostate cancer cell lines to evaluate its impact on cell proliferation, migration and invasion. Furthermore, gene expression profiling was conducted to explore interactions between *STEAP2,* the androgen receptor and a panel of androgen-regulated genes (*PSA, FKBP5, GPRC6A* and *TMPRSS2)* following: 1) anti-STEAP2 antibody treatment, 2) STEAP2-knockout and 3) the growth of prostate cancer cells in androgen-depleted conditions.

The data presented in this thesis demonstrate that inhibition of STEAP2 by both the polyclonal anti-STEAP2 antibody and lead anti-STEAP2 monoclonal antibody significantly reduced prostate cancer cell viability. STEAP2 receptor internalisation was triggered following treatment of prostate cancer cells with the anti-STEAP2 monoclonal antibody, demonstrating its potential utility with antibody-drug conjugate technology in the future. STEAP2 knockout prostate cancer cells exhibited decreased cell proliferation, migration and invasion in comparison to wild-type cells. These promising findings highlight the therapeutic value of STEAP2-knockout in inhibiting invasive tumour cell traits. Gene expression data from both STEAP2-knockout cells and androgen-depleted cells suggest that STEAP2 may be involved in crosstalk between the androgen receptor and androgen-regulated genes. STEAP2 could therefore provide a novel target in conjunction with current conventional androgen deprivation therapy. In conclusion, the *in vitro* findings presented herein suggest STEAP2 as a viable target for the development of more tailored and personalised therapeutic agents to improve the clinical management of men with aggressive prostate cancer.

Declaration

This work has not previously been accepted in substance for any degree and is not being concurrently submitted in candidature for any degree.

Signed  (candidate)

Date: 21.07.2021

STATEMENT 1

This thesis is the result of my own investigations, except where otherwise stated. Where correction services have been used, the extent and nature of the correction is clearly marked in a footnote(s).

Other sources are acknowledged by footnotes giving explicit references. A bibliography is appended.

Signed  (candidate)

Date: 21.07.2021

STATEMENT 2

I hereby give consent for my thesis, if accepted, to be available for photocopying and for inter-library loan, and for the title and summary to be made available to outside organisations.

Signed  (candidate)

Date: 21.07.2021

Table of Contents

Chapter 2

“Materials and methods”

Chapter 3

"Development and characterisation of 3D *in vitro* prostate cancer-stromal cell co-culture models"

“Appendices”

Acknowledgements

Firstly, I would like to extend my sincere thanks and gratitude to my supervisor Professor Shareen Doak for her endless support and guidance from both sides of the Atlantic. I would also like to thank my secondary supervisor Professor Gareth Jenkins for his support throughout my research. Thank you to my supervisory team and colleagues at Houston Methodist Research Institute, Texas, for your expertise during my year in Houston.

I would also like to thank my colleagues on the 4th floor of ILS1 at Swansea University, especially Sally James for her technical expertise. I would like to thank Demi, Harriet, Linda, and Sarah for keeping me on track and sane through what was a very challenging period.

Completing this research whilst also relocating to and from America, followed by the impact of the COVID-19 pandemic, and finally starting full time employment was challenging to say the least. All of this would not have been possible without the constant support of my friends Alice, Becca, Jess, Katie, and Mel – thank you for always being there to cheer me on either in person or virtually.

Last but certainly not least I would like to thank my Dad, Phil, to whom I dedicate this thesis, for teaching me to never give up and without whom I wouldn't have had the motivation to undertake this research. Thank you to you and Gill for always being there when completing this seemed impossible, despite the time differences and many miles between us. I'd also like to thank my Nan for her constant support and encouragement.

As always, this work was undertaken in memory of my Mum, Christine, who has been my inspiration every step of the way.

List of Figures

List of Tables

List of Abbreviations

aa	Amino acids
AAV	Adeno-associated viruses
ACRATA	Apoptosis, cancer and redox associated transmembrane domain
ADC	Antibody-drug conjugate
ADCC	Antibody-dependent cellular cytotoxicity
ADCP	Antibody-dependent cell phagocytosis
ADT	Androgen deprivation therapy
AKR1C3	Aldo-keto reductase family-1 member-
Akt	Protein kinase B
AP-1	Activating protein 1
APS	Ammonium persulphate
AR	Androgen receptor
ARBS	Androgen receptor binding site
ARE	Androgen response elements
ARv7	Androgen receptor splice variant 7
ATCC	American type culture collection
ATP	Adenosine triphosphate
Bcl-2	B-cell lymphoma 2
BMP	Bone morphogenetic protein
BPH	Benign prostate hyperplasia
C4-2B	LNCaP-derived prostate cancer cells
CAF	Cancer-associated fibroblast
Cas9	CRISPR-associated protein 9
CBP	cAMP response element-binding protein
CDC	Complement-dependent cytotoxicity
CDKI	Cyclin-dependent kinase inhibitor
CH	Constant heavy chain
CL	Constant light chain
CREB5	Cyclin AMP-responsive element-binding protein 5
CRISPR	Clustered regularly interspaced short palindromic repeat
CRPC	Castrate resistant prostate cancer
crRNA	CRISPR RNA
CRUK	Cancer Research UK
CSS	Charcoal stripped serum
CTL	Cytotoxic t-lymphocyte
CTLA	Cytotoxic T-lymphocyte associated
CYP17A1	Cytochrome P450 17A1
DAPI	4’,6-diamidino-2-phenylindole
DBD	DNA binding domain
DHT	Dihydrotestosterone

DISC	Death inducing signal complex
DMEM	Dulbecco's Modified Eagle Medium
DMSO	Dimethyl sulfoxide
DNA	Deoxyribose nucleic acid
DRE	Digital rectal examination
DSB	Double strand break
DU145	Prostate cancer cells metastatic to the brain
EBRT	External beam radiotherapy
ECL	Extracellular loop
ECM	Extracellular matrix
EGF	Epidermal growth factor
EGFR	Epidermal growth factor receptor
EMT	Epithelial mesenchymal transition
eNAMPT	Extracellular nicotinamide phosphoribosyltransferase
ERG	ETS-related gene
ERK	Extracellular signal regulated kinase
ETS	Erythroblast transformation-specific
ETV	ETS translocation variant
EV	Extracellular vesicle
EZH2	Enhancer of zeste homolog 2
FAK	Focal adhesion kinase
FBS	Foetal bovine serum
FGF	Fibroblast growth factor
FKBP5	FK506 binding protein 5
FNO	$F_{420}H_2$:$NADP^+$ oxidoreductase
GFP	Green fluorescent protein
GLUT1	Glucose transporter 1
GM-CSF	Granulocyte-macrophage colony-stimulating factor
GOF	Gain of function
GPRC6A	G-protein coupled receptor family C group 6 member A
gRNA	Guide RNA
HDR	Homology-directed repair
HIF	Hypoxia inducible factor
HS5	Bone stromal cells
HSD3β1	Hydroxy-delta-5-steroid dehydrogenase beta-1
HSP	Heat shock protein
Ig	Immunoglobulin
IGF	Insulin-like growth factor
IL-6	Interleukin-6
ISUP	International Society of Urological Pathology
IVT	*In vitro* transcribed
kDa	Kilodaltons
KLK	Kallikrein

KO	Knockout
LBD	Ligand binding domain
LHRH	Luteinising hormone releasing hormone
LNCaP	Prostate cancer cells metastatic to lymph nodes
LOF	Loss of function
lrECM	Laminin-rich extracellular matrix
LTGF-β	Latent TGF-β
LUTS	Lower urinary tract symptoms
mAb	Monoclonal antibody
MHC	Major histocompatibility complex
MMAE	Monomethyl auristatin E
MMAF	Monomethyl auristatin F
MMP	Matrix metalloproteinase
mRNA	Messenger RNA
MSC	Mesenchymal stem cell
MTT	3-(4,5-Dimethyl-2thiazoyl)-2,5-diphenyl-2H-tetrazolium bromide
MVA	Modified vaccinia virus Ankara
NADPH	Nicotinamide adenine di-nucleotide phosphate
NCCN	National Comprehensive Cancer Network
NCoA2	Nuclear receptor coactivator 2
NEP	Neutral endopeptidase 24.11
NFκB	Nuclear factor kappaB
NHEJ	Non-homologous end joining
NICE	National Institute for Health and Care Excellence
Nox	NADPH oxidase
nsSNP	Non-synonymous single nucleotide polymorphism
NTD	N-terminal domain
P/S	Penicillin/streptomycin
p53	Tumour suppressor 53
pAb	Polyclonal antibody
PAM	Proto-spacer adjacent motif
PBMC	Peripheral blood mononuclear cells
PBS	Phosphate buffered saline
PC3	Prostate cancer cells metastatic to the bone
PCa	Prostate cancer
PDX	Patient derived xenograft
PFA	paraformaldehyde
PI	Propidium iodide
PI3K	Phosphoinositide 3-kinase
PIN	Prostate intraepithelial neoplasia
PNT2	Normal prostate epithelial cells
PolII	RNA polymerase II

PPARα	Peroxisome proliferator-activated receptor alpha
PRF	Phenol red free
PRK1	Protein-kinase-C-related kinase
PSA	Prostate specific antigen
PSMA	Prostate specific membrane antigen
PTEN	Phosphatase and tensin homolog
PTH	Parathyroid hormone
PTHrP	Parathyroid hormone related protein
qRT-PCR	Quantitative reverse transcriptase polymerase chain reaction
RANK	Receptor activator of nuclear factor kappa- β
RANKL	Receptor activator of nuclear factor kappa- β ligand
RIPA	Radioimmunoprecipitation assay
RNA	Ribonucleic acid
RNAi	RNA interference
ROS	Reactive oxygen species
RPMI	Roswell Memorial Park Medium
scFvs	Single chain variable fragments
SDS	Sodium-dodecyl sulphate
SFM	Serum free medium
sgRNA	Single guide RNA
Shh	Sonic hedgehog
siRNA	Small interfering RNA
Src	Steroid receptor coactivator
ssODN	Single stranded DNA oligonucleotides
STAMP	Six transmembrane protein of prostate
STAT	Signal transducer and activator of transcription
STEAP	Six transmembrane epithelial antigen of the prostate
STRO-1	Stromal specific antibody 1
T	Testosterone
TEMED	N, N, N', N' Tetramethylenethylenediamine
TfR	Transferrin receptor
TGF	Transforming growth factor
TIARP	TNF-a-induced adipose-related protein
TIL	Tumour infiltrating lymphocyte
TKI	Tyrosine kinase inhibitor
TKR	Tyrosine kinase receptor
TMPRSS2	Transmembrane protease serine 2
TNF-α	Tumour necrosis factor alpha
TNFR	Tumour necrosis factor alpha receptor
TNM	Tumour, Node, Metastasis
tracrRNA	Trans-activating crRNA
TRAIL	Tumour necrosis factor–related apoptosis-inducing ligand
TRIS	Tris(hydroxymethyl)aminomethane

TRUS	Transrectal ultrasound
TSAP6	Tumour-suppressor activated pathway-6
VEGF	Vascular endothelial growth factor
VH	Variable heavy chain
VISTA	V-domain Ig suppressor of T-cell activation
VL	Variable light chain
WHO	World Health Organisation
WT	Wild-type
α	Alpha
β	Beta
cm	Centimetre
et al.	*Et al., ii*
e.g.	*exempli gratia*
g	Grams
Gy	Gray
i.e.	*id est*
h	Hour(s)
κ	Kappa
μg	Microgram
μl	Microlitre
μm	Micrometre
μM	Micromolar
mg	Milligram
ml	Millilitre
mm	Millimetre
mM	Millimolar
min	Minute(s)
nm	Nanometre
nmol	Nanomole
s	Second(s)
V	Volts
W	Watts
=	Equal
<	Less than
>	More than
≤	Less than or equal to
≥	More than or equal to
%	Percent

Chapter 1

General introduction

1.1 The biology of cancer

Cancer is the general term given to the abnormal growth of cells, which typically occur in epithelial tissues, which are sheets of cells that line the walls of cavities and channels or cover the outside of the body as layers of cells forming skin. The epithelia play an important role in oncogenesis – the onset of cancerous tumours – as they give rise to the most common of human cancers: carcinomas. Carcinomas arise from cells originating in the endodermal (inner) or ectodermal (outer) germ layer which form during embryogenesis and cause 80% of cancer related deaths in the Western World (Weinberg, 2014). The World Health Organisation (WHO) deems cancer as the leading cause of mortality globally (Stewart & Wild, 2014). Figures suggest that over 1,000 people are diagnosed with cancer each day in the UK, with statistics showing 1 in 2 people will be diagnosed with cancer at some point throughout their lifetime (Cancer Research UK (CRUK), 2019).

1.1.2 The Hallmarks of Cancer

Hanahan and Weinberg first suggested six hallmarks of cancer, which are acquired properties of almost all cancer cells that influence the onset and progression of the disease (Hanahan & Weinberg, 2000). These include excessive proliferation, the ability of cancer cells to evade growth suppressors, immortality, invasion and metastasis, angiogenesis and the prevention of apoptosis (Hanahan & Weinberg).

1.1.2.1 Uncontrolled proliferation

The ability of cancer cells to sustain chronic proliferation and grow uncontrollably is fundamental to disease progression (Hanahan & Weinberg, 2011). Normal cell growth is carefully maintained by multiple growth factors that control cell cycle progression (Hanahan & Weinberg, 2011). Cancer cells utilise a variety of mechanisms to overcome these inhibitory signals, and as such are able to grow in an uncontrolled and abnormal manner (Hanahan &

Weinberg, 2011). Many cancer types upregulate the expression of growth factor receptors, and as such are able to overcome the rate limiting step posed by the rapid depletion of growth factors produced by neighbouring cells (Witsch *et al*., 2010). This ability leads to independent cell growth and increased proliferative capacity of cancer cells (Witsch *et al*., 2010). Another mechanism by which cancer cells overcome the rate limiting step is by triggering neighbouring cells to overproduce growth factors (Witsch *et al*., 2010). In many cancers, excessive proliferation can be the result of activation of downstream pathways such as phosphoinositide 3-kinase (PI3K), which induces mutations allowing for the proliferation of cells (Jiang & Liu, 2009). These various mechanisms by which cancer cells are able to rapidly proliferate in an uncontrolled manner result in an increase in cell numbers and subsequent tumour formation.

1.1.2.2 Evading growth suppressors

To overcome negative regulators of cell proliferation, cancer cells largely depend on the actions of tumour suppressor genes (Hanahan & Weinberg, 2011). Tumour suppressor genes act as either control points to regulate cell proliferation, or activate cell senescence and apoptotic mechanisms (Hanahan & Weinberg, 2011). The most widely studied of these is tumour suppressor 53 (p53), a 53-kDa tumour suppressor protein located on chromosome 17 and is the most frequently mutated gene in cancers (Yue *et al*., 2017). p53 acts mainly as a transcriptional regulator and can activate genes involved in apoptosis, cellular senescence, repair of deoxyribose nucleic acid (DNA) and cell cycle arrest (Yue *et al*., 2017).

1.1.2.3 Activating invasion and metastasis

When confined to the primary site, tumours are deemed localised, yet still have the potential to mobilise and spread to other parts of the body. Metastasis is the term given to this migration of cancerous cells from their original primary tumours. Metastasis can give rise to new colonies known as metastases, which are usually traceable back to the site of the primary tumour (Fares *et al*., 2020; Lambert *et al*., 2017). The most common sites for metastases to

occur are the liver, lungs, brain and bones (Fares *et al*., 2020; Lambert *et al*., 2017). Cancer cells leaving primary tumours are carried by blood and lymphatic vessels until they relocate and form new colonies. The occurrence of metastases is the principal cause of death in patients with cancer (Fares *et al*., 2020; Lambert *et al*., 2017; Weinberg, 2014).

The invasion-metastasis cascade is the term given to the events cancer cells undergo in order to achieve metastasis (Hanahan & Weinberg, 2011; Welch & Hurst, 2019). Once a tumour has become established at a primary site, the cells begin to invade the local tissues, leading to locally advanced disease (Hanahan & Weinberg, 2011; Welch & Hurst, 2019). A series of molecular events within the invasion-metastasis cascade trigger distinct cellular changes that allow cancer cells to become mobile and enter the blood stream, enabling them to spread to distant sites via the circulatory system (Hanahan & Weinberg, 2011; Lambert *et al*., 2017; Welch & Hurst, 2019). A process known as epithelial to mesenchymal transition (EMT) is required for cells to gain mobility and relies upon a switch in cadherin (Lamouille *et al*., 2014; Pal *et al*., 2018). E-cadherin, expressed in epithelial cells, interacts with β-catenin to anchor cells in place, yet when cells undergo EMT, E-cadherin is switched for N-cadherin, expressed in mesenchymal cells (Lamouille *et al*., 2014; Pal *et al*., 2018). In order to become mobile, cancer cells must also be able to degrade the extracellular membrane (ECM), consisting of the basement membrane and connective tissue (Hanahan & Weinberg, 2011). Mobilised cancer cells often aggregate with platelets in order to survive in circulation before attaching to secondary tissues to form micro-metastases, which subsequently proliferate and expand to form metastatic tumours (McGowan *et al*., 2009; Yan & Jurasz, 2016). The “seed and soil” idea first hypothesised in 1989 states that cancer cells use molecular signalling to seek out distant organs with similar characteristics to their primary sites in order to survive (Paget, 1989; Welch & Hurst, 2019). Activation of the invasion-metastasis cascade triggers a multi-step process which allows cancer cells to migrate from their primary sites and form metastases (**Figure 1.1**).

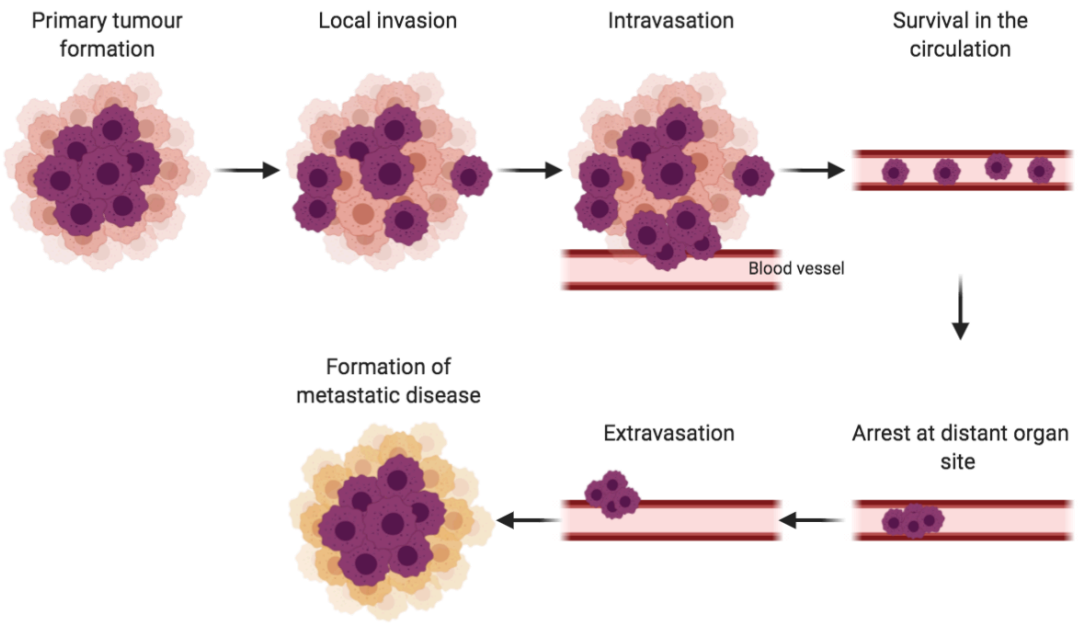

Figure 1.1. The invasion-metastasis cascade. Following the initiation of a tumour at a primary site, cancer cells exit their primary sites (local invasion, intravasation). Cancer cells are then able to enter circulation and translocate systemically (extravasation). If the cells are able to survive the circulation, they arrest at distant sites and adapt to survive in secondary tissue (micro-metastasis formation, metastatic colonisation). Cells then continue to divide and become clinically detectable metastatic disease. Adapted from (Valastyan & Weinberg, 2011). Created using BioRender.

1.1.2.4 Inducing angiogenesis

Angiogenesis is the process of forming new blood vessels from existing vasculature, which in cancers generates tumour-associated neovasculature and is required for cancer cells to obtain the required volumes of nutrients to allow for exponential growth (Hanahan & Weinberg, 2011). This tumour-associated neovasculature often contains an unstable mix of pro-angiogenic signals which lead to disproportionate vessel branching, abnormal blood flow, micro-haemorrhaging and abnormal levels of endothelial cell proliferation and apoptosis (Ebrahem *et al*., 2010; Nagy *et al*., 2012). One of the main pro-angiogenic growth factors is the vascular endothelial growth factor (VEGF), which acts upon tyrosine kinase receptors (TKRs) (Aslam *et al*., 2013; Wu *et al*., 2018). Interactions between VEGF and TKRs trigger increased vascular permeability and endothelial sprouting, subsequently allowing new vessels to form and aid in tumour growth and progression (Aslam *et al*., 2013; Hanahan & Weinberg, 2011; Wu *et al*., 2018).

1.1.2.5 Enabling replicative immortality

The ability of cancer cells to divide and replicate indefinitely plays a key role in the development of macroscopic tumours (Hanahan & Weinberg, 2011). Under normal conditions, once a cell has reached its replicative capacity it enters an exit phase known as senescence, during which cells are no longer proliferative but remain viable (Hanahan & Weinberg, 2011). The length of a cell's life is dependent on multiple factors, with the presence of telomeres being the most important (Lulkiewicz *et al*., 2020). Telomeres protect cells from DNA damage and gradually shorten with age as a section of the telomere is lost during each cell replication cycle, resulting in a definite life span for cells (Artandi & DePinho, 2010; Lulkiewicz *et al*., 2020). In cancer cells the expression of telomerase, an enzyme able to synthesis telomeric DNA sequences, is often upregulated and provides cancer cells with replicative immortality (Artandi & DePinho, 2010; Lulkiewicz *et al*., 2020).

1.1.2.6 Evading cell death

Programmed cell death, known as apoptosis, acts as a natural defence mechanism to cancer development (D'Arcy, 2019; Hanahan & Weinberg, 2011). The ability to evade this signalling pathway is key to tumourigenesis (D'Arcy, 2019; Hanahan & Weinberg, 2011). Apoptosis is activated either by an extrinsic or intrinsic pathway, both of which result in caspase activation and cell degradation (D'Arcy, 2019). Regulation of apoptosis is essential for maintaining cellular homeostasis and is mediated by a variety of pro- and anti-apoptotic mechanisms (D'Arcy, 2019). Pro-apoptotic factors including Bak and Bax become activated by cell stress and trigger cytochrome c production in the mitochondria (Singh *et al*., 2019). An apoptosome is then generated which results in the downstream activation of caspases and eventual cell death by degradation (D'Arcy, 2019; Dorstyn *et al*., 2018; Singh *et al*., 2019). A mechanism used by cancer cells to overcome cell death by apoptosis is through increased expression of the B-cell lymphoma 2 (Bcl-2) anti-apoptotic pathway (Singh *et al*., 2019). Bcl-2 prevents Bak and Bax activation and subsequent cytochrome c release, suggesting a mechanism for cancer cells

to evade cell death signals and continue to grow uncontrollably (Singh *et al*., 2019).

Another mechanism by which cancer cells evade death is through autophagy. The main purpose of autophagy is to recycle cellular components in response to nutrient starvation, allowing for cells to survive for extended periods of time (Glick *et al*., 2010). With regards to cancer progression, autophagy plays a dual role as it can act either as a quality control mechanism or in promoting tumour survival under harsh growth conditions (Yun & Lee, 2018). In terms of the hallmarks of cancer, autophagy influences mechanisms involved in resisting cell death and activation of invasion and metastasis (Hanahan & Weinberg, 2011). This dual-role theory also involves p53 which modulates autophagy both positively and negatively (Ryan, 2011; Wawrzynow *et al*., 2018). Despite the dual role autophagy plays in cancer, it has been suggested that this role is not equally divided, yet favours tumour cell survival by increasing stress tolerance levels (Degenhardt *et al*., 2006; Wawrzynow *et al*., 2018; Yun & Lee, 2018). Tumour cell survival is notably promoted by autophagy-proficient cells when used to combat high cytotoxic and metabolic stresses, such as hypoxia, nutrient deprivation, and an increase in proliferation (Towers *et al*., 2020; Yun & Lee, 2018). Due to increased cellular proliferation, tumour cells have increased metabolic needs to maintain the survival of the tumour cells. To do so, autophagy becomes activated to stimulate the recycling of adenosine triphosphate (ATP), which if maintained can lead to continuous growth and proliferation (Towers *et al*., 2020; Yun & Lee, 2018).

1.1.2.7 Emerging Hallmark: Evading immune destruction

Emerging hallmarks have also since been identified as the ability of cancer cells to evade the immune system, and alterations to energy metabolism (Hanahan & Weinberg, 2011). Cancer cells are able to avoid immune surveillance, the process by which the immune system monitors, recognizes and eliminates the vast majority of foreign cells and tissues (Hanahan & Weinberg, 2011). In immunocompromised patients, the absence of a fully functioning immune system does promote an increase in the onset of some

cancers, which has also been noted in patients following organ transplantation who later develop donor-derived cancers (Vajdic & van Leeuwen, 2009). However, as the majority of cancers arise in immune-competent patients, the mechanism by which cancer cells evade the immune system remains unclear. The “elimination, equilibrium, escape” theory has been suggested as a mechanism of immune system avoidance (Mittal *et al*., 2014). In the first phase, elimination, cells are detected and destroyed by the immune system, however, sporadic tumour cells enter an equilibrium phase where editing and mutations occur (Mittal *et al*., 2014). Finally, during the escape phase, immunologically sculpted tumour cells are able to grow exponentially, and establish an immunosuppressive tumour microenvironment (Mittal *et al*., 2014).

1.1.2.8 Emerging Hallmark: Reprogramming energy metabolism

Alterations to energy metabolism are required to fuel cell growth and division, and ultimately enable the uncontrolled proliferation of cancer cells (Hanahan & Weinberg, 2011; Pavlova & Thompson; 2016). Cancer cells undergo a metabolic switch, enabling them to reprogram their glucose metabolism and energy production to a state known as aerobic glycolysis (Hanahan & Weinberg, 2011; Pavlova & Thompson; 2016). Glucose transporters, predominantly glucose transporter 1 (GLUT1), are upregulated by cancer cells to substantially increase the import of glucose into the cytoplasm (de Castro, 2019; Pavlova & Thompson; 2016). This increase in glycolysis has been reported to correlate with alterations in oncogene and tumour suppressor expression, which drive other hallmarks of cancer including cell proliferation and avoidance of apoptosis (de Castro, 2019; Hanahan & Weinberg, 2011; Pavlova & Thompson; 2016).

1.1.3 Enabling Characteristics

Since the first proposal of the original six hallmarks of cancer and addition of the two new emerging hallmarks, two enabling characteristics were added: inflammation and genomic instability (Hanahan & Weinberg, 2011). These characteristics are known to influence the occurrence of the known hallmarks of cancer and lead to disease progression (Hanahan & Weinberg, 2011).

1.1.3.1 Tumour-promoting inflammation

The recruitment of inflammatory cells to the site of tumours was initially thought of as a process by which to destroy tumour cells, yet has since been suggested to benefit tumour survival and neoplastic formation (deNardo *et al*., 2010; Hanahan & Weinberg, 2011). Tumour growth and survival may benefit from inflammatory cell recruitment due to an increased supply of growth factors, pro-angiogenic factors and signalling to facilitate invasion and metastasis (deNardo *et al*., 2010; Grivennikov *et al*., 2010). A more aggressive phenotype may also be generated as a result of inflammatory cells producing and releasing reactive oxygen species (ROS) into the tumour microenvironment (Grivennikov *et al*., 2010).

1.1.3.2 Genome instability and mutation

Alterations in the genomes of cancer cells allows them to acquire the properties identified as the hallmarks of cancer to aid in disease progression (Fares *et al*., 2020; Hanahan & Weinberg, 2011; Macheret *et al*., 2015; Negrini *et al*., 2010). Mutant genotypes confer advantageous characteristics to enable cell growth, proliferation and metastasis (Hanahan & Weinberg, 2011; Macheret *et al*., 2015). Some of these mutations may be the result of epigenetic changes such as DNA methylation and histone modifications, or heritable phenotypes including inactivation of tumour suppressor genes (Flavahan *et al*., 2017; Negrini *et al*., 2010). Mutations in genes involved in DNA damage repair mechanisms result in a loss of function and subsequent increase in cancer development and progression (Negrini *et al*., 2010; Turgeon *et al*., 2018).

1.2 The prostate

The prostate is an accessory gland around the size of a walnut found only in the reproductive system of males (**Figure 1.2**; Flint *et al*., 2015). The prostate is located in the pelvis and sits behind the urinary bladder, with the urethra running through it (**Figure 1.2**; Fine *et al*., 2012; Flint *et al*., 2015). The part of the urethra passing through the prostate is known as the prostatic urethra, which joins the two ejaculatory ducts (**Figure 1.3**; Fine *et al*., 2012; Flint *et al*., 2015). The prostate is surrounded by a fibromuscular capsule known as the prostatic capsule and contains both glandular and connective tissues (**Figure 1.3**; Fine *et al*., 2012). The primary function of the prostate is related to reproduction, as the gland secretes substances including prostatic fluid, which is required to nourish sperm, which subsequently alters the viscosity of semen (Flint *et al*., 2015).

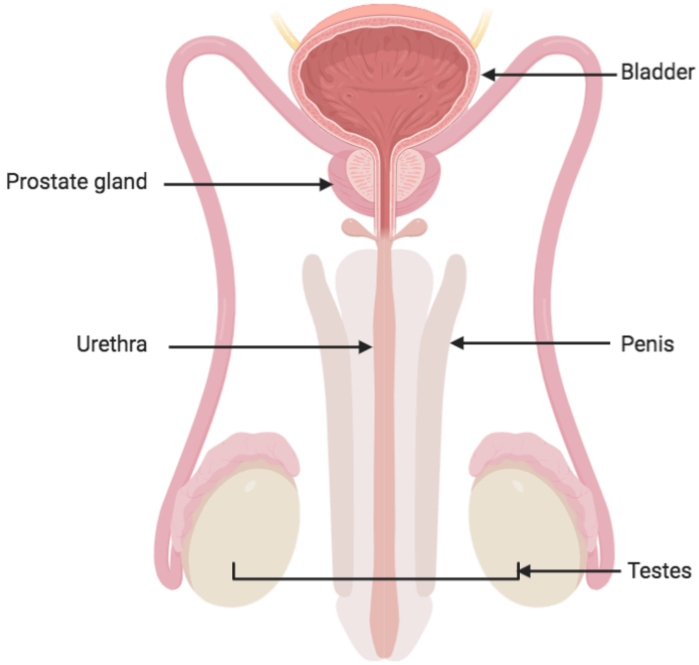

Figure 1.2. Diagram of the human male reproductive system showing the location of the prostate. The prostate is found only in the reproductive system of males and sits below the bladder. The main organs of the male reproductive system are the testes, penis, urethra and prostate gland. Adapted from (CRUK, 2019). Created using BioRender.

The internal structure of the prostate is described in gross anatomy as consisting of four lobes: lateral, anterior, median and posterior (Packer & Maitland, 2010). In microanatomy the prostate is divided into three zones known as the transitional, central and peripheral zones (**Figure 1.3**; Fine *et al*., 2012; Packer & Maitland, 2010). The peripheral zone lies beneath the capsule and is found at the posterior of the gland, making up 70% of the prostate and surrounding the distal urethra (Fine *et al*., 2012; Packer & Maitland, 2010). The ejaculatory ducts are surrounded by the central zone which contains the ductal tube from the seminal vesicle to the descending urethra and makes up 20% of the prostate and also has a separate embryological origin (Fine *et al*., 2012; Packer & Maitland, 2010). The transitional zone is found directly below the bladder and surrounds the transitional urethra and makes up 5% of the prostate (Fine *et al*., 2012; Packer & Maitland, 2010). Finally, the anterior fibromuscular stroma is usually absent of glandular components and, as the name suggests, is composed only of muscle and fibrous tissue (Fine *et al*., 2012; Packer & Maitland, 2010).

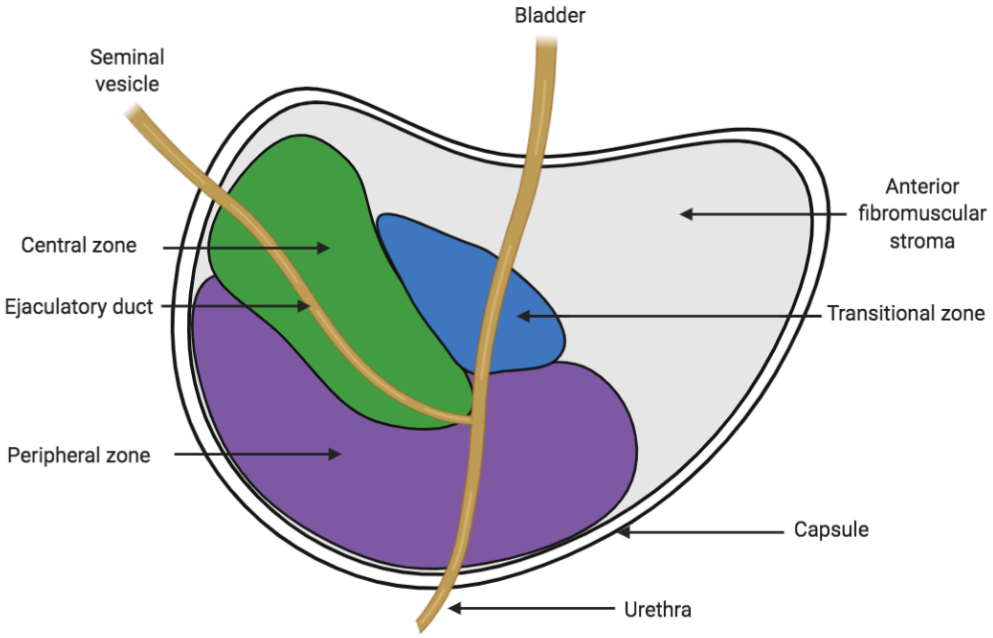

Figure 1.3. Diagram showing the anatomy of the human prostate. The prostate is located beneath the bladder and is composed of 3 distinct zones: the central zone (green), the peripheral zone (purple), and the transitional zone (blue). The urethra runs through the prostate to the bladder and seminal vesicles. Adapted from (Packer & Maitland, 2010). Created using BioRender.

1.3 Prostate cancer

1.3.1 Epidemiology

Prostate cancer is the most common non-cutaneous cancers in men, accounting for 15% of all male cancer diagnoses globally (Ferlay *et al*., 2015). In the UK, 130 new cases of prostate cancer are diagnosed each day, totalling 47,700 per year, leading to 11,300 deaths annually (CRUK, 2019). The lifetime risk of a man being diagnosed with prostate cancer is 1 in 8, with statistics showing that one man in the UK dies from prostate cancer every 45 minutes (Nelson & Shah, 2019; Prostate Cancer UK, 2020). Prostate cancer is largely a disease of the elderly, with over half (54%) of new cases being diagnosed in those aged over 70 and is rarely detected in men under the age of 40 (Center *et al*., 2012; CRUK, 2019). As such, given the ageing population, prostate cancer incidence has increased over recent years (Center *et al*., 2012).

Ethnicity can largely affect the incidence of prostate cancer, which varies widely between countries leading to a difference of up to 90-fold between populations (Odedina *et al.,* 2009). The risk of a black man being diagnosed with prostate cancer is much higher than that of a white man (1 in 4 compared to 1 in 8 respectively), yet the reason behind this is unclear (Prostate Cancer UK, 2020). A difference in genetics, particularly the androgen receptor (*AR*) gene, is thought to play a role in this increase in incidence amongst black men (Platz, 2000; Spratt *et al*., 2018). Incidence of prostate cancer is lowest in Asian countries, notably China (1.9 per 100,000 per year), and highest in North America, with African American men more commonly diagnosed (137 per 100,000 per year) (Kitagawa *et al*., 2013; Odedina *et al*., 2009; Pernar *et al*., 2018). Studies exploring international variation in prostate cancer aggressiveness found that more men of African descent were diagnosed with higher grade disease than those from the Caribbean or UK, which also correlated with higher Gleason scores upon diagnosis (Rebbeck *et al*., 2013).

1.3.2 Risk factors

Whilst defined risk factors are yet to be established, other than age, a man's risk of developing prostate cancer may be increased by lifestyle factors including smoking, poor diet and obesity, however these risk factors apply to cancer development in general and have not been specifically linked to prostate cancer (CRUK, 2019). To date, prostate cancer is not thought to be clearly linked to any specific preventable risk factors (CRUK, 2019).

Excluding age and race, the only determined risk factor for prostate cancer is a family history of the disease (Leitzmann & Rohrmann, 2012; Kicinski *et al*., 2011). Compared to men in the general population, the risk for first-degree relatives of men with the disease is initially doubled and increases to up to four times higher when the first-degree relative is diagnosed at younger than 60 years of age (Johns & Houlston, 2003; Pernar *et al.,* 2018). When more than two-first degree relatives are affected, this risk increases four- to five-fold (Kicinski *et al*., 2011). In terms of first-degree relatives, men who have a brother diagnosed with prostate cancer are more likely to develop the disease themselves compared to those with their father diagnosed, indicating that prostate cancer may be recessive or linked to the X-chromosome (Barber *et al.,* 2018; Johns & Houlston, 2003; Monroe *et al*., 1995). Overall, 10-15% of men diagnosed with prostate cancer have at least one relative who has also been diagnosed with the disease (Barber *et al*., 2018; Schaid, 2004). Another factor that may influence the risk of prostate cancer is a family history of other cancers such as breast, ovarian, bladder and kidney (Barber *et al*., 2018; Negri *et al*., 2005). This is thought to be the result of germline mutations in BRCA1 and BRCA2 genes, which can increase the risk of prostate cancer three-fold compared to the general population (Negri *et al*., 2005).

Hormonal factors have also been linked to the onset of prostate cancer, with the peak age of prostate cancer development coinciding with the age at which serum testosterone levels decline, whilst serum oestrogen levels remain constant (Leitzmann & Rohrmann, 2012). A change in the serum testosterone to oestrogen ratio has been found to be a determinant of prostate cancer risk,

which also correlates with the risks exposed by ethnicity (Leitzmann & Rohrmann, 2012; Nelson *et al*., 2014). In men of Afro-Caribbean origin, serum oestrogen levels are highest when compared to Caucasian and Asian men, resulting in a more profound difference in the testosterone to oestrogen ratio (Leitzmann & Rohrmann, 2012; Nelson *et al*., 2014).

1.3.3 Disorders of the prostate

As men age, the prostate becomes increasingly susceptible to undergo changes, such as the onset of benign prostatic hyperplasia (BPH), which occurs primarily in the transitional zone, and prostate intraepithelial neoplasia (PIN), which often develops in the peripheral zone (see **Section 1.2**; Packer & Maitland, 2010). BPH is the most common non-malignant condition of the prostate and can be categorized as either microscopic or macroscopic, with a vast majority of men developing microscopic BPH as they age (Roehrborn *et al*., 2002). PIN is also another common disorder of the prostate and is found during approximately 5% of initial prostate biopsies (Pullar & Shah, 2016). PIN displays similar morphological changes to prostate cancer yet does not correlate with an increase in prostate specific antigen (PSA), and in men with high-grade PIN additional biopsies are often required as subsequent development of prostate cancer occurs in approximately 40% of cases (Pullar & Shah, 2016). PIN is categorised as low- or high-grade depending on the prominence of nucleoli, with high-grade PIN progressing to cross the epithelial basement membrane and becoming invasive adenocarcinoma (Pullar & Shah, 2016).

Adenocarcinomas account for the vast majority of prostate cancers (>95%), which develop from glandular structures in epithelial tissues (Goldstein *et al*., 2010). During cancer development, the basal cell layer is lost, and malignant cells enter the basement membrane, leading to local invasion (Goldstein *et al*., 2010). The remaining minority of prostate cancers include transitional cell carcinoma, intra-ductal carcinomas which arise from prostatic ducts, sarcomas, small cell carcinomas and metastases forming in the prostate from other sites, all of which are very rare and often aggressive forms of the disease which have a poor prognosis for the patient (Pullar & Shah, 2016).

With regards to **Figure 1.3**, the prostate is often referred to according to its distinct anatomical zones, known as McNeil's zones (Packer & Maitland, 2016). The majority (70-80%) of prostate cancers develop in the peripheral zone, and 10-20% manifest in the transitional zone (Packer & Maitland, 2010). The transitional zone is usually anterior in the gland and is difficult to target using traditional transrectal ultrasound (TRUS) biopsy techniques (Pullar & Shah, 2016). The central zone gives rise to approximately 2.5% of prostate cancers, which tend to be more aggressive and are more likely to invade the seminal vesicles (Cohen *et al*., 2008; Packer & Maitland, 2010; Pullar & Shah, 2016).

When confined to the gland, prostate cancer is not usually life threatening, as localised tumours often remain dormant and can be removed surgically through radical prostatectomies, or effectively managed through routine observations (Moschini *et al*., 2017; Wilt *et al*., 2012). The two main systems used to determine the progression of prostate cancer are the tumour, node, metastasis (TNM) staging system which is applied to all cancers, and the Gleason scoring system which is reserved specifically for prostate cancer staging (CRUK, 2019; Chen & Zhou, 2016). The TNM staging system is widely used in cancer research, and, in terms of prostate cancer, Stage 3 refers to a tumour that has broken through the prostate capsule, whereas Stage 4 indicates metastases to lymph nodes or other organs (**Figure 1.3**; CRUK, 2019). Once prostate cancer has metastasised, the prognosis for the patient decreases significantly, with only 30% of men with Stage 4 disease surviving for more than 5 years, compared to up to 95% of men with Stage 3 disease (**Figure 1.4;** CRUK, 2019; National Comprehensive Cancer Network (NCCN), 2018).

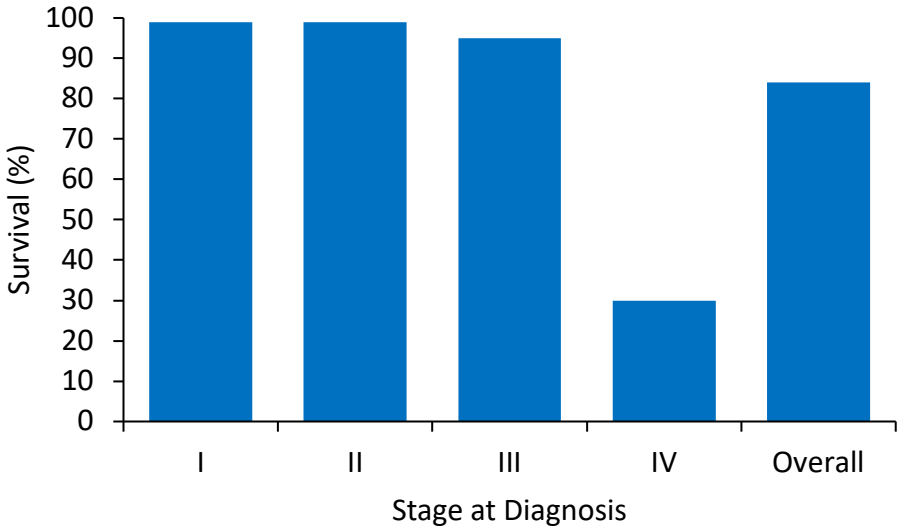

Figure 1.4. Five-year survival of men with prostate cancer based on stage at diagnosis. Graph showing the percentage of men aged 15-99 diagnosed with prostate cancer surviving 5-years after diagnosis dependent on stage at diagnosis and net overall survival. Adapted from (CRUK, 2019; NCCN, 2018).

1.3.4 Prostate cancer diagnosis

A combination of tools are employed to confirm a diagnosis of prostate cancer. To date, the current gold standards are a blood test to detect circulating PSA levels, the digital rectal examination (DRE), and TRUS-guided biopsies (Nelson & Shah, 2019). Over the last 30 years, the incidence of prostate cancer in the UK has increased dramatically by almost 150%, partly due to increased detection from PSA testing, or incidental detection from resected tissue following lower urinary tract symptoms (LUTS)-related surgery (Nelson & Shah, 2019). Once a suspicion of prostate cancer is apparent, the patient is referred to a urologist to repeat the prostate examination and check for a family history of the disease (Moschini *et al*., 2017). Symptoms of advanced disease which would prompt an urgent referral include, but are not limited to, back pain, leg swelling, or peripheral neurological symptoms (Pullar & Shah, 2016). Once a diagnosis is confirmed, the disease requires grading by TNM staging, Gleason score, and more recently the International Society of Urological Pathology (ISUP) scoring system (National Institute for Health and Care Excellence (NICE), 2019; Nelson & Shah, 2019).

Screening is currently not universally available in the UK and is only recommended as an opportunistic screening approach in the form of PSA blood testing in men over the age of 55 presenting with prostate cancer symptoms (Basch *et al*., 2012; Lee *et al*., 2017; Nelson & Shah, 2019). However, there is controversy over the age at which to begin screening by PSA blood tests, with the European Association of Urology recommending a baseline PSA test at 40-45 years, yet the American Urological Association suggests reserving this to over 55 years (Cabarkapa *et al*., 2016; Carter *et al*., 2013). Randomised trials of PSA screening have proven inconclusive, with one reporting that no improvement in prostate cancer mortality was observed following the screening of 420,000 men (Martin *et al*., 2018). As such, a PSA screening programme is not currently recommended by NICE or supported by the WHO (Nelson & Shah, 2019).

1.3.4.1 Prostate specific antigen test

To date, the most widely used diagnostic tool in prostate cancer is the detection of PSA (Crawford *et al*., 2013; Schröder *et al*., 2009). PSA is a glycoprotein serine protease enzyme, part of the kallikrein (KLK) family (Pullar & Shah, 2016). PSA is made solely by the epithelial cells of the prostate gland, hence its use as a biomarker for prostate cancer in the diagnosis, monitoring and risk prediction of the disease (Pullar & Shah, 2016). Circulating PSA levels can be indicative of prostate health, as when leaked into the blood stream and causing an increase in PSA levels detected by a blood test, an enlarged prostate is often present (Nelson & Shah, 2019). Thus, increases in PSA levels are often deemed prostate specific yet not prostate cancer specific, warranting the need for more specific biomarkers of prostate cancer detection and progression (Pullar & Shah, 2016). As shown in **Table 1.1**, PSA levels also increase naturally with age, yet there is no determined PSA level at which prostate cancer can be completely excluded. PSA also provides a useful tool in the active surveillance of men with prostate cancer following radical treatment, as biochemical recurrence may indicate a need for further treatment (Nelson & Shah, 2019). PSA detection comes with a risk of over-diagnosis,

which has been linked with up to 50% of diagnoses (Crawford *et al*., 2013; Schröder *et al*., 2009).

Table 1.1. Normal physiological PSA values dependent on age. Adapted from (Nelson & Shah, 2019).

Age (years)	PSA value (ng/ml)
All ages	<4.0
40-49	<2.5
50-59	<3.5
60-69	<4.5
>70	<6.5

1.3.4.2 Digital rectal examination

DREs are often performed to confirm a diagnosis following an elevated PSA result, as PSA can also increase as a result of BPH, but not PIN (Packer & Maitland, 2010). A DRE may also be beneficial, particularly in more elderly patients, as they avoid the risks associated with TRUS biopsies (Nelson & Shah, 2019). During the DRE, the size and softness of the prostate is evaluated by the physician assessing the gland by placing their fingers into the rectum of the patient (Kim *et al*., 2014). The DRE often follows the detection of elevated PSA levels and may be of particular use in patients presenting with urinary problems which could influence the results of the PSA test (Cornford *et al*., 2020). Abnormalities found in a DRE alongside elevated PSA levels warrant further investigations in the form of biopsies of prostate tissue being collected, as DRE alone has a sensitivity and specificity below 60%, and therefore cannot be used to either diagnose or exclude the presence of prostate cancer (Naji *et al*., 2018; Nelson & Shah, 2019).

1.3.4.3 Biopsies

TRUS-guided biopsies are traditionally used in the diagnosis of prostate cancer, during which 12 cores are taken from the prostate via the rectum using an ultrasound-guided probe (Nelson & Shah, 2019). Ultrasound waves are used to visualise the prostate and the seminal vesicles, with a low echo of the ultrasound indicative of prostate cancer, whereas strong echoes usually

signify the bone (Lam *et al*., 2019). TRUS biopsies have the advantage of simultaneously imaging and taking biopsies at desired locations of the prostate (Nelson & Shah, 2019). TRUS biopsies come with a number of risks, both short-term for the patient in the form of pain or infection, and clinically as a negative biopsy does not necessarily rule out prostate cancer as approximately 30% give false-negative results (Lam *et al*., 2019; Nelson & Shah, 2019; Pullar & Shah, 2016). When a TRUS biopsy returns a negative result yet a suspicion of prostate cancer remains, further investigations are considered such as MRI scanning or repeated biopsies (Nelson & Shah, 2019). Biopsied tissue is assessed microscopically by a pathologist and determined as either positive, where cancer is present, or negative when a cancer diagnosis can be excluded (Lam *et al*., 2019). Positive biopsies are then categorised according to various scoring systems to aid in giving a prognosis for the patient (Lam *et al*., 2019).

1.3.4.4 Gleason Grading System

Since its development in the 1960s by Dr Donald F Gleason, prostate cancers have been graded according to the Gleason grading system, which gives the disease a grade between one and five dependent on the degree of gland differentiation and glandular architecture, as evaluated under microscopy (Chen & Zhou, 2016). A higher grade correlates with a more aggressive cancer, with two grades given to represent the two most dominant patterns observed, or, if only one pattern is found, the single grade is doubled, giving an overall score between 2 and 10 (Humphrey, 2004). For instance, if by prostate biopsy or radical prostatectomy a specimen is found to have a Gleason 4 as its most dominant pattern, yet some Gleason 3 characteristics are present, the patient will be reported as having a Gleason 7 (4 + 3). When a man is first diagnosed with prostate cancer, the Gleason score is vital when determining the patient's clinical management and is the most important prognostic indicator (Pullar & Shah, 2016). However, not all Gleason 7 scores are classified as the same phenotype, as there is a clear distinction between a Gleason 7 (3 + 4) and a Gleason 7 (4 + 3) when considering the prognosis for the patient (Nelson & Shah, 2019). Prostate cancers with a Gleason 7 score

are the most difficult category to manage clinically as a Gleason 6 prostate cancer is usually indolent, whereas a Gleason 8 – 10 represents aggressive tumours (Nelson & Shah, 2019). Gleason 7 therefore sits in between these stages of disease and are much more difficult to predict in terms of prognosis for the patient (Nelson & Shah, 2019). In clinical practice, Gleason scores of 1 and 2 are no longer regarded as cancerous, and as such the lowest possible Gleason score indicative of prostate cancer is Gleason 6 (3+3), and the highest is Gleason 10 (5+5) (Nelson & Shah, 2019).

With the purpose of simplifying the Gleason scoring system for patients, a new 5-point grading system was developed in 2016 by ISUP (**Table 1.2**; Nelson & Shah, 2019). The aim of this system was to overcome any confusion regarding the Gleason 7 score, and to give patients a more easily recognisable 1 to 5 score, with 1 being the least aggressive, compared to 6 in the Gleason grading system (**Table 1.2;** Nelson & Shah, 2019; Pullar & Shar, 2016).

Table 1.2. ISUP Grading system for prostate cancer for risk stratification. The Gleason sum scores translate to ISUP grades. Adapted from (Nelson & Shah, 2019).

ISUP Grade	Gleason Score	Gleason Score breakdown
1	6	3 + 3
2	7	3 + 4
3	7	4 + 3
4	8	4 + 4 / 5 + 3 or 3 + 5
5	9 / 10	4 + 5 or 5 + 4 / 5 + 5

1.3.4.4 Tumour Node Metastasis staging

Following a confirmed diagnosis of prostate cancer, staging the disease must be carefully considered as this is the most important process during diagnosis as it aids in the choice of treatment, and is often determined following a CT or MRI scan, or biopsy to assess whether the lesion is confined to the prostate or has metastasised (Pullar & Shah, 2016). Each individual case will then be discussed by a multidisciplinary team involving urologists, oncologists,

radiologists and pathologists, to review the patient's imaging and histology results in order to produce a treatment plan. A universally used TNM staging system is commonly used to classify prostate cancer cases (Sobin *et al*., 2009). This system is used in conjunction with the Stage I – Stage IV system, which indicates the degree of metastasis present, with Stage I indicating a locally contained tumour and Stage IV indicating metastasis involving the lymph nodes (CRUK, 2019). 10-year prostate cancer mortality is significantly higher in patients diagnosed with metastatic (M1) disease when compared to metastatic Stage IV prostate cancer (Shukla *et al*., 2015). It has also been found that the majority of men who die of prostate cancer were diagnosed with node-positive (N+), or metastatic (M1) disease, and often had detectable distant metastases at diagnosis (Helgstrand *et al*., 2017; Patrikidou *et al*., 2014). Prostate cancers are categorised into three broad categories: localised disease (T1/2, N-, M-), locally advanced (T1/2, N+, M- or T3/4, N-/+, M-) and metastatic (Any T/N, M+) (Nelson & Shah, 2019). When a high-risk or advanced disease is diagnosed, often a bone scan will be requested to exclude the possibility of bone metastatic disease, as 80% of prostate cancer metastases develop in the bone (CRUK, 2019; Pullar & Shah, 2016).

A newly diagnosed patient must also be categorised into either low-, intermediate- or high-risk for risk stratification. A system developed by D'Amico, aids in this process and also assists clinicians in determining the most appropriate treatment for the patient and determines whether any further diagnostic tests are required (**Table 1.3**; D'Amico *et al*., 1998).

Table 1.3. D'Amico risk categories for prostate cancer. Adapted from (D'Amico *et al*., 1998; Nelson & Shah, 2019).

Risk	**PSA (ng/ml)**	**Gleason score**	**Clinical Stage (DRE)**
Low	<10	≤ 6	Tumour confined to prostate (T1-T2a)
Intermediate	10-20	7	Tumour involves more than one half of one lobe – both lobes (T2b)
High	>20	8-10	Tumour extends through prostate capsule and may have spread to distant organs (≥ T2c)

Upon diagnosis, 39-56% of patients in the main age demographic (60-80+ years) present with Stage III or Stage IV metastatic prostate cancer due to the lack of specific symptoms in the earlier stages of the disease (CRUK, 2019). At the later stages of disease, these patients present a clinical problem as due to the patient's age and progress of disease, little chemotherapeutic intervention is available, resulting in a poor prognosis for these patients as the risk of disease recurrence also increases with stage upon diagnosis (CRUK, 2019).

1.3.5 Prostate cancer metastasis

When metastasis occurs, locally advanced prostate cancer often invades surrounding structures such as the penis, seminal vesicles, bladder and distal ureter, or, more rarely, the rectum (Pullar & Shah, 2016). Metastasis to the regional nodes most commonly affects the obturator and iliac nodes, located in the pelvis and detected by lymph node dissection when performed alongside radical prostatectomy (Heidenreich *et al*., 2002). Less frequent sites of metastases are the liver, lung and brain (Pullar & Shah, 2016).

The most common site for metastases to manifest is the bones, termed osteotropism, which occurs in up to 80% of metastatic cases, with the axial skeleton, especially the spine, most frequently effected (Bubendorf *et al*., 2000; Shiozawa *et al*, 2011). Contrary to other cancers which also metastasise to the bone and form osteolytic lesions, the bone metastases of prostate cancer lead to dysregulation of bone formation and are characterised by an osteoblastic appearance (Hensel *et al*., 2016; Ibrahim, 2010; Wang *et al*., 2005). Additional cytogenetic abnormalities and an increased metastatic potential of prostate cancer cells has been observed following interaction with bone stromal cells (Chung, 2003; Hensel *et al*., 2016). These alterations in tumour microenvironment have been suggested to be controlled by matrix metalloproteinases (MMPs) which can degrade various cell adhesion molecules and alter cell-cell and cell-ECM interactions (Gialeli *et al*., 2011). MMPs can either promote cancer metastasis through the release of interleukins and growth factors when released by fibroblasts, or inhibit disease progression (Gialeli *et al*., 2011). Cells involved in bone function include osteoprogenitor cells, osteoblasts, osteoclasts and osteocytes (Vela *et al*., 2007). The formation and degradation of bone is controlled by two specialized cell types; osteoblasts, which produce bone matrix and assist in its mineralisation, and osteoclasts, which dissolve bone mineral (Karsenty *et al*., 2009).

In order for bone metastases to successfully develop, the bone microenvironment must be suitable and sustainable, which is contributed to through the regulation of both osteoblastic and osteoclastic activities (Ibrahim *et al*., 2010). Metastases of the bone are characterized as osteolytic (bone destructive), or osteoblastic (bone forming), yet a combination of the two is often displayed (Ibrahim *et al*., 2010). Osteoblastic behaviour is a more common occurrence in prostate cancer metastases and develops as a result of growth factors produced by tumours, such as bone morphogenetic protein (BMP), tumour growth factor β (TGF-β), insulin-like growth factor (IGF), and Wnt (Logothetis & Lin, 2005). Parathyroid hormone (PTH) related protein (PTHrP) is highly expressed by osteoblastic prostate cancer, and although this

is normally characteristic of osteolytic behaviour, it induces osteoblastic metastatic lesions (Liao *et al*., 2008).

One of the most common nutrients associated with bone formation and metabolism is calcium (Ca^{2+}), which is taken up by osteoblasts from the blood in order to produce bone (Xing & Boyce, 2005). When metastasis of prostate cancer to the bone occurs, so does disruption of the natural equilibrium of bone homeostasis and calcium levels (Farhat *et al*., 2017). One of the main reasons for this is the production of large amounts of Wnt by prostate cancer cells, in comparison with usual levels of Wnt in the body (Dai *et al*., 2008). Wnt proteins are mainly used for developmental control of body axis symmetry *in utero*, however in mature tissues, Wnt are involved in the self-renewal of stem cells and upkeep of normal tissues, whilst sometimes contributing to oncogenesis (Dai *et al*., 2008; Hall *et al*., 2006). Levels of osteoblasts and their precursors increase as a result of Wnt overexpression, which leads to rapid bone formation whilst simultaneously triggering the production of osteoclasts, initiating rapid bone resorption (Xing & Boyce, 2005; Dai *et al*., 2008). The resulting large bone turnover subsequently releases latent TGF-β (LTGF-β), which when activated, assists in the proliferation of late-stage disease (Dallas *et al*., 2002). Wnt concentration is then increased, which in turn creates a two-way crosstalk during which the growing tumour sustains its additional growth through bone remodelling, known as the “vicious cycle” of prostate cancer metastasis (Cook *et al*., 2014).

1.3.6 Clinical management of prostate cancer

Prostate cancer treatment is broadly divided into the management of localised, locally advance and metastatic disease, with high-risk localised disease and locally advanced disease often considered in the same category (Nelson & Shah, 2019). Given that prostate cancer is predominantly a disease which effects older men, radical treatment is often reserved for patients with a life expectancy of more than 10 years post-treatment (Bill-Axelson *et al*., 2014).

1.3.6.1 Active surveillance

Active surveillance, sometimes known as the “watch and wait” strategy, is reserved for men with localised disease, as treatment is avoided until necessary for symptom relief (Nelson & Shah, 2019). Watch and wait is also employed for elderly men or those with co-morbidities, for whom radical treatment is deemed inappropriate (Graham *et al*., 2014; Nelson & Shah 2019). In these patients, PSA progression is carefully monitored along with any symptomatic developments, and as such this approach is palliative as opposed to curative (Graham *et al*., 2014). In younger men, or those with an increased life expectancy due to age at diagnosis, active surveillance is used to defer radical treatment until it is absolutely necessary, as a way of avoiding surgery for low-risk tumours that may not progress or cause harm to the patient if left *in situ* (Graham *et al*., 2014). A number of factors are considered to switch from active surveillance to radical treatment, including patient choice, PSA progression, or disease progression determined by repeat biopsies or imaging (Nelson & Shah, 2019). One of the main risks posed by active surveillance is that once there is evidence of disease progression to warrant radical treatment, the disease may no longer be curable, however 10-year survival rates following active surveillance remain extremely promising (Bill-Axelson *et al*., 2014; Hamdy *et al*., 2016).

1.3.6.2 Surgical treatment

A radical prostatectomy involves the surgical removal of the entire prostate and seminal vesicles, requiring the urethra to be reconnected to the neck of the bladder (NICE, 2019). This treatment approach is often utilised in men with localised disease, where the entire cancer is contained within the prostate capsule (NICE, 2019). The most common side effects of radical prostatectomies are urinary incontinence and erectile dysfunction, both of which can be managed clinically through further surgery and hormone therapy respectively (Haglind *et al*., 2015). Over recent years, the development and implementation of robot-assisted radical prostatectomy has become increasingly popular and has the added benefits of reducing intraoperative blood loss, along with increased continence and erectile function post-surgery

(Ficarra *et al*., 2012; Haglind *et al*., 2015; Huynh *et al*., 2018). Following surgery, PSA levels are expected to fall to an undetectable level and are monitored for 5-years to detect any biochemical recurrence, which may indicate a need for further treatment (Nelson & Shah, 2019).

1.3.6.3 Radiotherapy

Radical radiotherapy is used to treat men with localised or locally advanced disease (Cornford *et al*., 2020). Radiation is delivered either internally (brachytherapy) or by external beam radiotherapy (EBRT) (Bolla *et al*., 2019; Nelson & Shah, 2019; Potters *et al*., 2004). Traditional radiotherapy is generated by a linear accelerator which delivers x-rays containing high-energy proton beams directly to the prostate, initiating DNA damage, double-strand breaks and ultimately cell death (Bolla *et al*., 2019; Mavragani *et al*., 2019; Reuvers *et al*., 2020). A daily dose of 2 Gy per treatment is given 5 days a week for a period of 7-8 weeks, with a minimum total dose of 78 Gy delivered over the treatment period (Dearnaley *et al*., 2014; Kuban *et al*., 2008; Pollack *et al*., 2002). Technological developments in the delivery of radiotherapy have allowed for more precision, therefore limiting toxicity to neighbouring organs such as the rectum (Bolla *et al*., 2019; Soni *et al*., 2017).

Brachytherapy uses radioactive seeds containing low doses of radioactive iodine (^{125}Iodine) or palladium (^{103}Palladium), which are implanted directly into the prostate under the guidance of ultrasound (Peschel *et al*., 2004; Stish *et al*., 2017). The most commonly used, ^{125}Iodine, has a half-life of 60 days and delivers a dose of 145 Gy (Nelson & Shah, 2019). This treatment method is best suited to patients with low-risk localised disease, however, can be used alongside external beam radiotherapy to treat higher-risk patients (Stish *et al*., 2017). Side effects of both external radiotherapy and brachytherapy are similar and include worsening LUTS, erectile dysfunction, seed migration (brachytherapy) and radiation cystitis (external radiotherapy) (Nelson & Shah, 2019; Onishi *et al*., 2019).

1.3.6.4 Hormone therapy

Androgen deprivation therapy (ADT) is commonly used to treat advanced and metastatic prostate cancer, or relapsed disease following radical treatment (Nelson & Shah, 2019). Prostate cancer cells are reliant on circulating levels of testosterone, and therefore the aim of ADT is to reduce these levels (Massard & Fizazi, 2011). ADT is delivered in a number of different formats, including luteinising hormone releasing hormone (LHRH) agonists (e.g., Goserelin), LHRH antagonists (e.g., Degarelix), anti-androgens (e.g., Bicalutamide) and surgical castration (Cornford *et al*., 2020; Nelson & Shah, 2019). LHRH agonist have become the gold standard form of ADT, replacing surgical castration as they offer reversibility whilst avoiding the physical and psychological discomfort of surgery (Cornford *et al*., 2020). Surgical castration, or bilateral subcapsular orchiectomy, involves the removal of both androgen-producing testicles, and is considered successful when the patients' serum testosterone falls below 20 – 50 ng/ml, with these levels carefully monitored post-surgery to determine response (Nelson & Shah, 2019). ADT drugs work by interfering with the hypothalamus-pituitary-gonadal axis and the LHRH receptor, and therefore LHRH agonists downregulate the production of androgens through a negative feedback mechanism (Tolkach *et al*., 2013). One of the side effects of ADT is osteoporosis, and as such patients with bone metastases must be carefully considered and require a bone density scan before commencing treatment (NICE, 2019).

1.3.6.5 Chemotherapy

Docetaxel, a taxane chemotherapeutic, is the standard first-line treatment for men with metastatic, late-stage disease (Tannock *et al*., 2004; Quinn *et al*., 2017). Cell death is achieved through the inhibitory effects of docetaxel on microtubule dynamics, triggering mitotic arrest (Herbst *et al*., 2003). However, some metastatic prostate cancers develop resistance to docetaxel, and as such a second-generation taxane, cabazitaxel was approved for the treatment of patients who had previously received docetaxel-based regimens (D'Amico, 2014; de Bono *et al*., 2010). Chemotherapeutic drugs are delivered systemically through intravenous drips in cycles and are often accompanied

with severe side effects such as nausea, hair loss and extreme fatigue (CRUK, 2019; Tannock *et al*., 2004). A recent study – the STAMPEDE trial – found that docetaxel has potential to be used in combination with hormone therapy to illicit a significant clinical response when compared to hormone therapy alone (James *et al*., 2016). In this study, median survival was increased by 10 months and this treatment regimen is now considered the standard of care for newly diagnosed locally advanced or metastatic prostate cancer (James *et al*., 2016; Sathianathen *et al*., 2018). Docetaxel has also been used in combination with radiotherapy, which achieved a biochemical recurrence-free survival of 94% after two years (Chen *et al*., 2012). Whilst chemotherapy is non-selective, it may provide potential to sensitise cells to radiation and therefore increase the efficacy of radiotherapies.

1.3.6.6 Immunotherapy

Recent advances in immunotherapy have allowed for developments in the treatment of many types of cancer to be made, including prostate cancer. In the treatment of prostate cancer, the potential of vaccines, checkpoint inhibitors and immune cytokines are being explored (Gao *et al*., 2017; Redman *et al*., 2017). The regulation of immune homeostasis relies upon immune checkpoint receptors and co-inhibitory molecules, which mediate the functions of effector and regulatory cells by altering their expressions on T-cells (Marshall & Djamgoz, 2018). V-domain Ig suppressor of T-cell activation (VISTA) negatively regulates T-cell responses and is overexpressed on tumour infiltrating myeloid and regulatory cells (Lines *et al*., 2014). In prostate cancers, VISTA expression has been identified as a compensatory inhibitory pathway as cytotoxic T-lymphocyte-associated (CTLA) protein 4 (CTLA-4) blockade triggered an increase in VISTA expression in response to ipilimumab, a CTLA-4 inhibitor (Alaia *et al*., 2018; Gao *et al*., 2017). A Phase III clinical trial of ipilimumab triggered a promising PSA response rate compared to a placebo group, and increased progression-free survival (Beer *et al*., 2017). Ipilimumab has also shown promise in reducing PSA levels when delivered in combination with ADT or radiotherapy (Hossain *et al*., 2018).

However, ipilimumab treatment was accompanied with adverse effects in 10% of patients, including a rash, nausea, vomiting and fatigue (Beer *et al*., 2017).

A dendritic cell vaccine, Sipuleucel-T, was approved for the treatment of metastatic prostate cancer in 2010 (Anassi & Ndefo, 2011; Kantoff *et al*., 2017; Patel *et al*., 2008; Redman *et al*., 2017). Sipuleucel-T uses active cellular products harvested from a patient's own peripheral blood (Anassi & Ndefo, 2011; Redman *et al*., 2017). The vaccine consists of autologous peripheral blood mononuclear cells (PBMC), including antigen-presenting cells, which have been activated *ex vivo* with a recombinant fusion protein (PA2024) (Anassi & Ndefo, 2011; Redman *et al*., 2017). PA2024 consists of prostatic acid phosphatase, an antigen highly expressed in the majority of prostate cancers, fused to granulocyte-macrophage colony-stimulating factor (GM-CSF), an important activator of immune response (Anassi & Ndefo, 2011; Kantoff *et al*., 2017; Redman *et al*., 2017).

1.3.7 Castrate resistant prostate cancer

Castrate resistant prostate cancer (CRPC) develops in 10-20% of men following ADT treatment due to loss of normal AR activity and is a much more aggressive form of the disease (Scher *et al*., 2004; Kirby *et al*., 2011). The prognosis for men diagnosed with CRPC is generally poor, with a median survival of 18 months (Scher *et al*., 2004). CRPC is defined as castrate serum testosterone <50 ng/dL or 1.7 nmol/L plus either biochemical resurgence of PSA, or radiological progression detected by the appearance of new lesions despite castrate levels of serum testosterone (Scher *et al*., 2004; Cornford *et al*., 2020). In men who have yet to receive chemotherapy, docetaxel is offered as the first-line treatment for CRPC, yet for those who have already received docetaxel or have developed resistance, anti-androgens abiraterone and enzalutamide are given which can improve median survival by up to 3 months (Arsov *et al*., 2012; Cornford *et al*., 2020; Nelson & Shah, 2019; Tannock *et al*., 2004). Abiraterone functions by inhibiting the androgen producing enzyme in the adrenal gland, whilst enzalutamide blocks AR from entering the cell nucleus to trigger DNA activation (Arsov *et al*., 2012). The STAMPEDE trial also found that abiraterone improves overall survival in non-CRPC compared

to standard ADT alone (James *et al*., 2016). Serum testosterone levels have proven a useful biomarker in the selection of treatment methods for CRPC, with patients presenting with very low levels having a better outcome when treated with abiraterone compared to enzalutamide (Hashimoto *et al*., 2019). Recent studies have also shown that dual targeting a co-activator of AR-mediated gene expression, enhancer of zeste homolog 2 (EZH2), alongside enzalutamide treatment results in a synergistic anti-tumour effect (Shankar *et al*., 2020).

1.4 Current challenges

One of the main challenges in the treatment of all cancers is the resistance to established therapeutic approaches (Zugazagoitia *et al*., 2016). Through recent advances in the modelling of the human genome, a more targeted and personalised approach has become available (Nevedomskaya *et al*., 2018). Through this research, the development of more viably therapeutic antibodies has been made possible, the clinical application of which has increased rapidly. Another challenge in the treatment of cancers, particularly with regards to prostate cancer, is the toxic side-effects associated with current treatment regimes, which can have a significant negative impact upon a patient's quality of life (Herbst *et al*., 2003; Onishi *et al*., 2019). To overcome this, ongoing research into the potential of immunotherapies, such as ipilimumab and Sipuleucel-T, have allowed for more patient-specific treatments (Gao *et al*., 2017). However, given the relatively new field of immune-oncology, more efficient drugs are still needed for the treatment of advanced or metastatic prostate cancer, whilst limiting any side effects for patients. The onset of CRPC also presents clinical challenges, with many cases developing resistance to first-line docetaxel treatment (Arsov *et al*., 2012). The identification of novel drug targets for clinical application is therefore still needed to improve the management of prostate cancer patients.

1.5 The STEAP family

Through the identification of novel biomarkers for cancer progression, a further insight into the mechanisms behind metastasis can be developed, which may subsequently aid in the management of the disease (see **Section 1.1.2.3**). Of particular interest is the six transmembrane epithelial antigen of the prostate (STEAP) family, which warrants further evaluation into its role in prostate cancer progression (Grunewald *et al*., 2012; Sikkeland *et al*., 2016; Whiteland *et al*., 2014). The STEAP family has four members, STEAP1 – 4, all of which comprise of six transmembrane helices (Porkka *et al*., 2002; Grunewald *et al*., 2012; Sikkeland *et al*., 2016).

All four members of the STEAP family have a COOH-terminal domain, which shares significant homology with the yeast FRE family of b-type cytochrome metalloreductases (Gomes *et al*., 2012). They also all have an N-terminal with homology to the archaeal and bacterial $F_{420}H_2$:$NADP^+$ oxidoreductase (FNO)-binding proteins (Ohgami *et al*., 2006). Two conserved histidine residues are present which allow for the uptake of iron and copper by STEAP proteins by binding to an intramembranous heme group (Ohgami *et al*., 2005). STEAP proteins contain a heme-binding domain known as the apoptosis, cancer and redox associated transmembrane domain (ACRATA) (Sanchez-Polido *et al*., 2004). This ACRATA domain is also present in a structurally related family which includes STEAP family members, the bacterial NADPH oxidase (Nox) family, and the oxidoreductase family YedZ (Ohgami *et al*., 2005 & 2006; Sanchez-Polido *et al*., 2004). Electron transfer may be supported through this heme-binding function, which has been found to affect cell growth and metabolism in Nox proteins, and electron transport across membranes in both Nox and STEAP proteins (Oosterheert *et al*., 2020; Yamada *et al*., 2004).

Another shared property of the STEAP family members is the Rossman fold (GXGXXG/A motif), which is a common feature of proteins with oxidoreductase and dehydrogenase functions (Ohgami *et al*., 2005). The first identified role of the STEAP family of proteins, with the exception of STEAP1 due to the absence of the FNO-like domain in the Rossman fold, was their

function in metal homeostasis and metabolism through reducing iron and copper, allowing for their uptake (Gomes *et al*., 2012; Ohgami *et al*., 2006).

1.5.1 STEAP1

The first member of the STEAP family to be identified was STEAP1 (Hubert *et al*., 1999). STEAP1 is located on chromosome 7q21.13 and comprises of 5 exons and 4 introns (Gomes *et al*., 2012). When transcribed, the *STEAP1* gene gives rise to two different messenger ribonucleic acid (mRNA) transcripts of 1.4 kb and 4.0 kb, yet only the 1.4 kb transcript is processed into the mature protein, consisting of 339 amino acids (aa) with an estimated molecular weight of 36 kilodaltons (kDa) (Korkmaz *et al*., 2002). In the prostate, *STEAP1* mRNA and protein expression is significantly elevated, with protein expression particularly high in lymph and bone metastases of prostate cancer (Whiteland *et al*., 2014). *STEAP1* overexpression has also been found in cancers of the breast, bladder, lung and colon and Ewing's sarcoma, yet research is predominantly focussed on its involvement in prostate cancer progression (Gomes *et al*., 2014; Grunewald *et al*., 2012; Lee *et al*., 2016; Xie *et al*., 2019). *In vitro*, *STEAP1* is highly overexpressed in the AR-sensitive prostate cancer cell line LNCaP and overexpressed to a lesser extent in the AR-independent prostate cancer cell lines PC3 and DU145 (Gomes *et al*., 2014).

STEAP1, a membrane-bound channel protein, is implicated in tumour intercellular communication through regulating the transfer of small molecules between neighbouring cells (Ohgami *et al*., 2016). The expression level of *STEAP1* has also been found to be proportionate to Gleason score in prostate cancers, implying STEAP1 overexpression correlates with a more advanced, aggressive disease (Gomes *et al*., 2014). This hypothesis is supported by studies which have shown *STEAP1*-knockdown to reduce tumour proliferation, growth and metastasis in Ewing's sarcomas and lung cancers *in vivo* (Grunewald *et al*., 2012; Zhuang *et al*., 2015). It has been suggested that *STEAP1* promotes tumourigenesis through elevated activity levels of ROS in Ewing's sarcomas and in thyroid epithelial cells (Grunewald *et al*., 2012; Pan *et al*., 2008). STEAP1 is a homologue of NAPDH oxidases, which are frequently overexpressed in cancers and are involved in the production of

cellular ROS (Lambeth *et al*., 2004; Sanchez-Pulido *et al*., 2004; von Rozycki *et al*., 2004). *STEAP1* has also been linked to EMT-related genes, which promote cancer metastasis and invasion (Xie *et al*., 2019). This is thought to occur through the regulation of calcium ion concentration by *STEAP1*, which affects the balance of E-cadherin and N-cadherin, and in turn increase tumour motility and invasiveness (Hazan *et al*., 2004; Xie *et al*., 2019).

The expression of *STEAP1* may also be influenced by a separate but related gene, *STEAP1b* (Gomes *et al*., 2014). *STEAP1b* is located on the same chromosome as *STEAP1*, shares 88% of its amino acid profile with *STEAP1* and encodes for two transcripts; *STEAP1b1* and *STEAP1b2* (Gomes *et al*., 2014). Studies have found that in prostate cancer cells, both *STEAP1* and *STEAP1b2* are overexpressed, whereas *STEAP1b1* has no differential expression when comparing prostate cancer cells and normal prostate epithelial cells (Gomes *et al*., 2014).

1.5.2 STEAP2

STEAP2*,* also known as six transmembrane protein of prostate 1 (STAMP1), is located on chromosome 7q21.13, contains 6 exons and 5 introns, and encodes for a 490 aa long protein with an estimated molecular weight of 56.1 kDa (Gomes *et al*., 2012; Korkmaz *et al*., 2002; Porkka *et al*., 2002). The upregulation of *STEAP2* has recently been suggested to be the result of 42 deleterious non-synonymous single nucleotide polymorphisms (nsSNPs) altering the protein sequence (Naveed *et al*., 2016). STEAP2 is predominantly located to the plasma membrane, and green-fluorescent protein (GFP) labelling revealed STEAP2 as a cell-surface protein (Porkka *et al*., 2002). STEAP2 has been suggested to play a role in protein sorting and secretory pathways, as it shuttles to the Golgi organelle and trans-Golgi network (**Figure 1.5;** Gomes *et al*., 2012; Grunewald *et al*., 2012; Korkmaz *et al*., 2002). *STEAP2* is significantly overexpressed in prostate cancer when compared to normal healthy tissue (Burnell *et al*., 2018; Whiteland *et al*., 2014). Transfection with *STEAP2* in the normal prostate cancer cell line PNT2 resulted in a more aggressive phenotype, with cells gaining an increased migratory potential (Whiteland *et al*., 2014). When *STEAP2* expression was

knocked down using small interfering RNA (siRNA), cancer cell migration and invasion was significantly inhibited, further suggesting a role for *STEAP2* in driving aggressive prostate cancer traits (Burnell *et al*., 2018).

In prostate cancer, overexpression of MMPs -2, -7, -9, -13 and -14 have been found to promote disease progression and proliferation (Kue *et al*., 2002). STEAP2, a molecule whose downstream effectors are MMPs has been found to increase extracellular signal regulated kinase (ERK) signalling and is involved in the endocytotic and secretory pathways (Korkmaz *et al*., 2002; Wang *et al*., 2010). Using these pathways, STEAP2 moves in both directions between the Golgi complex and the plasma membrane, suggesting it may act as a receptor for both endogenous and exogenous ligands, for example lipids and proteins, or play a role in protein regulation (**Figure 1.5;** Gomes *et al*., 2012; Grunewald *et al*., 2012; Korkmaz *et al*., 2002). When down-regulated, *STEAP2* has been found to up-regulate cell cycle inhibitors such as cyclin-dependent kinase inhibitors (CDKIs) and p21, both *in vivo* and *in vitro*, which exerts an effect of tumour growth (Wang *et al*., 2010). This down-regulation also has an effect on proliferation, as apoptosis levels are increased. Knowledge of the exact function of STEAP2 in human prostate cancer tumours is still limited, in particular its effects on migration and invasion. Previous studies did however find that *STEAP2* was in fact up-regulated up to 2.5-fold in prostate tumours when compared to normal glands, indicating that the molecule may play a role in oncogenesis (Korkmaz *et al*., 2002). This overexpression was also confirmed through immunohistochemical analysis of benign and cancerous tissues, which correlated with mRNA expression data (Wang *et al*., 2010). This study did not, however, find a correlation between Gleason score and expression of STEAP2, suggesting the protein acts independently of cancer stage. STEAP2 is also involved in the uptake of iron and copper, acting as a ferrireductase and cupric reductase by reducing Fe^{3+} to Fe^{2+}, and Cu^{2+} to Cu^{+} (**Figure 1.5;** Knutson *et al*., 2007; Ohgami *et al*., 2006). Iron and copper availability in the choroid plexus (where cerebrospinal fluid is synthesised and ions between the blood and cerebrospinal fluid is controlled) and in the gastrointestinal tract, may be regulated by STEAP2 in the enterocytes of the proximal duodenum (Knutson *et al*., 2007).

The overexpression of *STEAP2* in prostate tissue combined with the fact that prostate cancer progression is androgen dependent warrants investigations into the involvement of androgens in the regulation of *STEAP2* expression. *In vitro*, the highest *STEAP2* expression levels have been found in the androgen-sensitive lymph node metastatic prostate cancer cell line LNCaP when compared to the normal prostate epithelial cell line PNT2 (Burnell *et al*., 2018; Whiteland *et al*., 2014). Androgen-dependent CWR22 tumours significantly regressed following castration when grown in mice, regardless of altering the mRNA expression of *STEAP2* (Korkmaz *et al*., 2002). Subsequently, when LNCaP cells were cultured with a synthetic androgen, *STEAP2* expression was not significantly different to untreated cells (Korkmaz *et al*., 2002; Porkka *et al*., 2002). However, a decrease in *STEAP2* expression may be due to another deregulatory mechanism occurring during disease progression as these studies did not find any major genomic changes or mutations (Korkmaz *et al*., 2002; Porkka *et al*., 2002). A partial cell cycle arrest was found at the G_0-G_1 phase, suggesting that *STEAP2* may regulate genes involved in this stage of the cell cycle, as prostate cancer cell proliferation has been seen to increase by *STEAP2* both *in vitro* and *in vivo* (Wang *et al*., 2010). When knocked down, *STEAP2* has been found to increase apoptosis in prostate cancer cells, yet further studies are required to explore the mechanisms behind this effect (Wang *et al*., 2010).

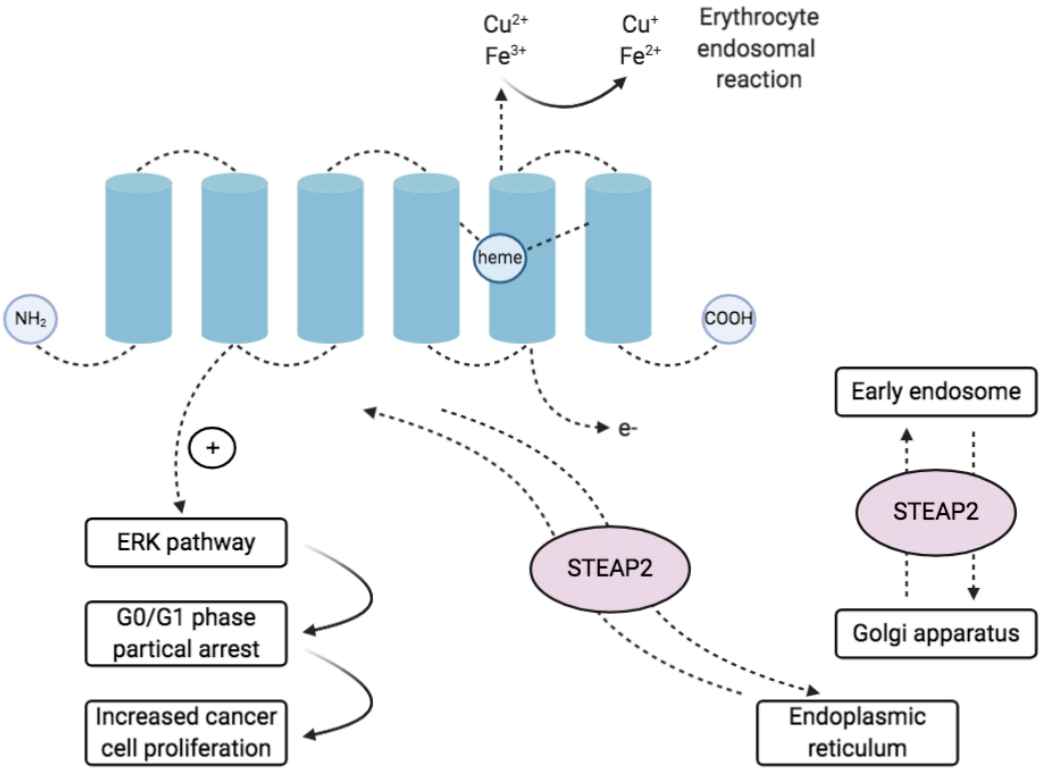

Figure 1.5. Structural overview of STEAP2. STEAP2, like all four members of the STEAP family, comprises of six transmembranes resulting in three extracellular loops. At the N-terminus of STEAP2, a NAD(P)H/FAD domain is present. STEAP2 comprises of 490 aa. Two heme metal binding sites are also present where ferriductase activity takes place. Image adapted from (Gomes *et al*., 2012; Grunewald *et al*., 2012). Created using BioRender.

1.5.3 STEAP3

STEAP3 – also known as tumour-suppressor activated pathway-6 (TSAP6) – is located on chromosome 2q14.2, consists of 6 exons and 5 introns, is composed of 488 aa and has a molecular weight of 50-55 kDa (Ohgami *et al*., 2005; Passer *et al*., 2003). Like other STEAP family members, STEAP3 is localised to the plasma membrane, close to the nucleus and vesicular tubular structures (Amzallag *et al*., 2004). *STEAP3* is highly expressed in haematopoietic tissues and supports physiological functions involved in iron metabolism, and as such has been linked to several types of anaemia, including iron deficiency anaemia and hypochromic microcytic anaemia (Lambe *et al*., 2009; Ohgami *et al*., 2005). In hypochromic microcytic anaemia, an autosomal recessive disorder resulting from a deletion in both *STEAP3* alleles, insufficient iron is supplied to erythrocytes leading to impaired

haemoglobin synthesis, which has been found to be completely reversed once *STEAP3* expression is restored (Ohgami *et al*., 2005).

Overexpression of *STEAP3* mRNA has also been linked to cancers of the lungs, prostate, liver, colon and brain along with myeloid leukaemia (Han *et al*., 2018; Lespagnol *et al*., 2008; Na *et al*., 2020; Passer *et al*., 2003). *STEAP3* has been linked with apoptosis and inhibition of the cell cycle during G_2 – M phase through interactions with Myt1 kinase, a regulator of cyclin-dependent kinase activity and Nix, a mitochondrial proapoptotic protein (Passer *et al*., 2003; Schweers *et al*., 2007). Apoptosis and cell cycle inhibition is also triggered through functional p53-binding sites present in the promotor region of the *STEAP3* gene, which interact with My1 and Nix proteins (Amzallag *et al*., 2004; Lespagnol *et al*., 2008; Ohgami *et al*., 2005; Passer *et al*., 2003; Schweers *et al*., 2007). *In vivo*, p53 activation following induced DNA damage triggered the production of exosomes in a *STEAP3*-dependent manner, suggesting that *STEAP3* modulates protein secretion in exosomes that are no longer required for cell survival (Lespagnol *et al*., 2008). *In vitro*, *STEAP3* became upregulated in response to p53 activation in myeloid leukaemia and breast cancer cell lines, increasing cell death (Lespagnol *et al*., 2008; Passer *et al*., 2003). Cell cycle arrest at the G_0-G_1 phase has also been triggered in colon cancer cells in response to *STEAP3*-knockdown, alongside inhibition of cancer cell proliferation and migration (Na *et al*., 2020).

1.5.4 STEAP4

STEAP4, also known as six transmembrane protein of prostate 2 (STAMP2), is located on chromosome 7q21, contains 5 exons and 4 introns, consists of 495 aa and has an estimated molecular weight of 52 kDa (Korkmaz *et al*., 2005). STEAP4 cellular localisation is similar to that of STEAP2, as it is located in the plasma membrane close to the nuclear region where it co-localises to the Golgi complex and trans-Golgi network (Korkmaz *et al*., 2005). Whilst *STEAP4* is overexpressed in prostate cancer, the main focus of research into *STEAP4* has focussed on its involvement in lipid metabolism due to its overexpression in adipose tissue (Korkmaz *et al*., 2005; Ohgami *et al*., 2006; Zhang *et al*., 2008). As such, *STEAP4* has been implicated in obesity and

obesity-dependent insulin resistance, as its expression becomes downregulated in patients who are obese (Arner *et al*., 2008; Chen *et al*., 2014; Ozmen *et al*., 2016; Qi *et al*., 2015; Qin *et al*., 2010). The involvement of *STEAP4* in obesity has been found to be the result of low-grade inflammation, with *STEAP4* suggested to play a role in other inflammatory disorders (Ozmen *et al*., 2016; Sharma *et al*., 2015). The expression of a *STEAP4* mouse homologue, tumour necrosis factor alpha (TNF-α)-induced adipose-related protein (TIARP) was found to be significantly increased by TNF-α, IL-6 and IL-1B (Arner *et al*., 2008; Inoue *et al*., 2009; Qin *et al*., 2010; Yoo *et al*., 2014). In human adipose tissue, treatment with TNF-α increased the expression of *STEAP4* in a dose-dependent manner, further suggesting its role in inflammatory processes (Qin *et al*., 2010). TNF-α along with STEAP4 has also been found to correlate with rheumatoid arthritis in obese patients, with STEAP4 and CD68+ co-localising in the joints, and *STEAP4* overexpression found in synovial fluid (Inoue *et al*., 2009; Matsumoto *et al*., 2008).

In prostate cancer progression, *STEAP4* plays a vital role in cell viability, proliferation and apoptosis, the latter of which is mediated by caspase-3 and caspase-8 (Qin *et al*., 2010). The role of androgens in the involvement of *STEAP4* upregulation has also been explored and it was found that synthetic androgen induction increased the expression of *STEAP4* mRNA in both a time- and dose-dependent manner (Korkmaz *et al*., 2005). Androgen-insensitive prostate cancer cell lines were also found not to express *STEAP4*, further suggesting *STEAP4* expression is dependent on an active AR being present (Korkmaz *et al*., 2005). *STEAP4* overexpression has also been found to increase prostate cancer cell proliferation, which is thought to be due to interactions between *STEAP4* and focal adhesion kinase (FAK) (Tamura *et al*., 2009). Insufficient activation of FAK when *STEAP4* is inhibited reduced cell growth of prostate cancer cells *in vitro*, suggesting that FAK phosphorylation by *STEAP4* induces a proliferative effect in prostate cancer cells, yet the exact mechanism remains unclear (Tamura *et al*., 2009).

1.5.5 The STEAP family as therapeutic targets

The STEAP protein family present an attractive target for novel therapeutic agents to treat prostate cancer. Given its specific localization to the cell membrane, STEAP1 has been suggested as a tumour-associated antigen, with studies reporting STEAP1 to be an effective antigen for T-cell based immunotherapy (Alves *et al*., 2006; Moreaux *et al*., 2012; Rodeberg *et al*., 2005). STEAP1 has also been the target of specific monoclonal antibodies, which exerted a significant effect on reducing the cell growth of prostate and bladder tumours *in vivo* (Challita-Eid *et al*., 2007). Prostate cancer progression has been inhibited *in vivo* through the immunisation of mice with recombinant DNA and modified vaccinia virus Ankara (MVA) vectors encoding STEAP1 (Krupa *et al*., 2011). These vaccinations significantly reduced tumour burden and proliferation, whilst increasing T-cell infiltration to the prostate tissues (Krupa *et al*., 2011). Furthermore, it has been hypothesised that the survival mechanism of high membranous STEAP1 expression as a result of elevated ROS levels may sensitise cells to radiotherapy (Grunewald *et al*., 2012; Sun *et al*., 2010).

STEAP2 has previously been suggested as a potential drug target for the treatment of advanced prostate cancer due to its overexpression in correlation with high Gleason Score (Burnell *et al*., 2018). Targeting the ECL2 of STEAP2 with anti-STEAP2 monoclonal antibodies found that antibody internalisation was dependent on cholesterol activity, yet the exact mechanisms remain unclear (Hasegawa *et al*., 2018).

Increased STEAP3 expression increases the transcriptional levels of the major histocompatibility complex (MHC) -1 and -2 in exosomes derived from dendritic cells, giving rise to STEAP3 as a potential immunotherapeutic target (Amzallag *et al*., 2004; Machlenkin *et al*., 2005). *In vivo,* an anti-tumour effect was observed when activated autologous cytotoxic T-lymphocyte (CTL) cells were administered subcutaneously to previously induced prostate tumours in mice (Machlenkin *et al*., 2005). STEAP3 has also been suggested as an indicator of disease progression in glioma patients, as its overexpression

activates STAT3-FoxM1 axis signalling and induces mesenchymal transition and promotes transferrin receptor (TfR) expression, which correlates with an invasive phenotype (Han *et al*., 2018).

Targeting STEAP4 with an anti-STEAP4 antibody in preadipocyte cells reduced proliferation and inhibited the cell cycle at G_1-S phase, suggesting that STEAP4 may be a potential target in the clinical management of obesity (Qin *et al*., 2010). In prostate cancer cells *in vitro*, treatment with an anti-STEAP4 monoclonal antibody inhibited cell proliferation (Tamura *et al*., 2009). Collectively, the STEAP family of proteins present an attractive target for therapeutic agents in the treatment of various cancers and other haematological disorders. The FNO-like domain, which is present in STEAP2, STEAP3, and STEAP4 could also be a potential target given its specificity to the STEAP family (Gomes *et al*. 2012).

1.6 Antibodies and their use as therapeutics

1.6.1 Antibody structure

Antibodies have become the most rapidly expanding and evolving class of pharmaceuticals since their identification over one hundred years ago and have been used to treat a variety of human disease, including cancers (Chen *et al*., 2020; Strebhardt & Ullrich, 2008). Antibodies are immunoglobulins, the majority of which used in the clinical management of patients are of the immunoglobulin G (IgG) format and are composed of antigen-binding sites within the variable domain in the heavy chain (VH) and light chain (VL) and constant regions (CH & CL) (Chen *et al*., 2020). Traditional full-length antibodies also consist of Fab fragments which are involved in antigen binding, and Fc fragments which can activate a variety of immunological pathways to trigger cell death (**Figure 1.6**; Chen *et al*., 2020). To reduce the production of human anti-mouse antibodies, antibody genetic engineering technology is used to humanise antibodies which are predominantly generated in mammalian, often murine, cells (Chen *et al*., 2020; Reichert *et al*., 2005).

Cell death is triggered by antibodies through immune-mediated processes including antibody-dependent cellular cytotoxicity (ADCC), antibody-dependent cell phagocytosis (ADCP), complement-dependent cytotoxicity (CDC) and regulation of T-cell activation (Chen *et al*., 2020). Signalling pathway blockade is often the principal mechanism for antibody-based cell killing, which is mediated by the Fc fragments on antibodies through interactions with receptors (FcγRs) expressed on effector cells (Chen *et al*., 2020; Shields *et al*., 2001).

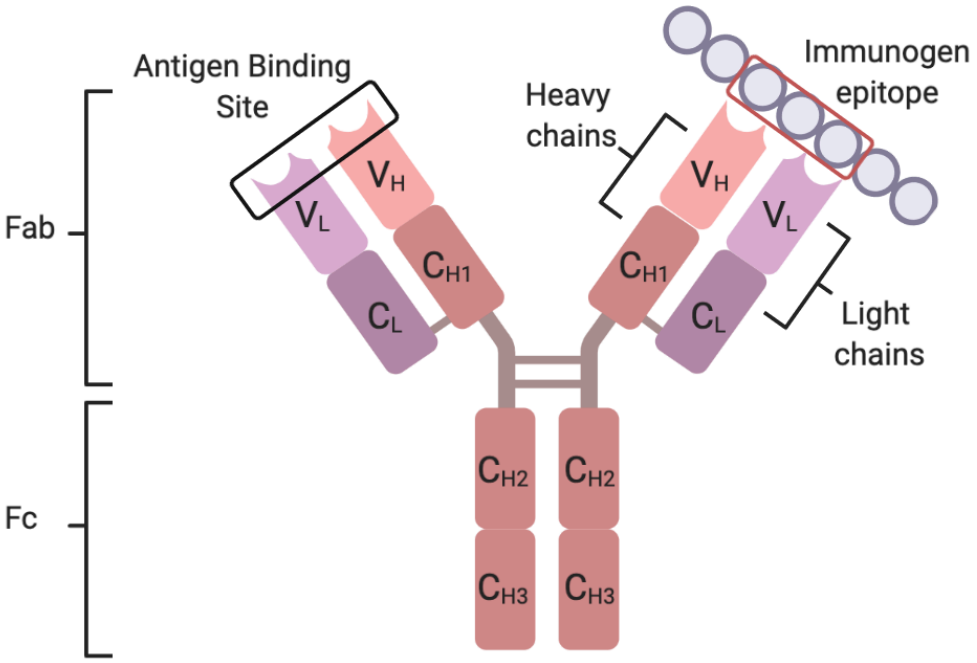

Figure 1.6. Immunoglobulin G (IgG) antibody structure. Fab: antigen fragment binding regions; Fc: constant fragment region; H and L: heavy chain and light chain peptides; V_H and V_L: variable heavy and light chain domains; C_{H1}, C_{H2}, C_{H3} and C_L constant heavy chain and light chain domains. Antigen binding site (black) where the paratope of the antibody binds to the epitope (red) of an immunogen. Adapted from (Chen *et al*., 2020). Created in BioRender.

1.6.2 Polyclonal antibodies

Polyclonal antibodies (pAbs) target multiple epitopes, offering broad strain protection and, unlike monoclonal antibodies (mAbs), are less likely to induce selective resistance (Stiehm *et al*., 2008). pAbs are used to treat a number of diseases, including those caused by viruses, venoms and toxins along with cancers (Stiehm *et al*., 2008; Wang *et al*., 2013). Often higher doses of pAbs are needed to observe a clinical effect as a smaller fraction of antibodies bind the target of interest, with only a low percentage of these triggering the desired result (Wang *et al*., 2013). To overcome this lack of specificity, the development of cocktails of antibodies have been of particular interest which bind multiple non-overlapping epitopes and allow the broad-spectrum activity of a pAb to be combined with the benefits of an engineered mAb (Wang *et al*., 2013). These oligoclonal antibody cocktails have proven effective in the

treatment of some cancers, particularly those with mutated epidermal growth factor (EGF) receptor (EGFR) (Ben-Kasus *et al*., 2009; Demarest *et al*., 2011). Combining two anti-EGFR mAbs (Cetuximab and Panitumumab) was proven effective at inhibiting tumour growth by triggering EGFR internalisation and degradation in pancreatic cancer cells *in vitro* (Ben-Kasus *et al*., 2009). PSA expression has previously been reduced in a clinical trial which studied the effects of treatment with the polyclonal recombinant antibody Bevacizumab delivered in combination with immunotherapy, yet negative effects on dendritic cells were observed suggesting a more selectively targeted approach is required (Rini *et al*., 2006).

1.6.3 Monoclonal antibodies

mAbs are those that originate from the same parent clone and have become increasingly popular in the treatment of various diseases such as cancer, autoimmune disorders and chronic inflammatory disorders due to their high specificity and affinity for targeted antigens (Tsumoto *et al*., 2019; Weiner, 2015). Since the development of the first FDA approved mAb drug OKT3 in 1985, therapeutic mAbs have entered a rapid development phase (Tsumoto *et al*., 2019). Advances in genetic engineering and conjugation technology have allowed for the development of more complex mAbs that include the full-length IgG (Wang *et al*., 2018). These include derivates such as single-chain variable fragments (scFvs), nanoparticle-based antibodies and immunoconjugates (Wang *et al*., 2018). Improvements have also been made to the binding activity, immunogenicity, stability and selectivity of therapeutic mAbs, allowing for increased safety and efficacy in clinical applications (Wang *et al*., 2018). In prostate cancer, a recent study targeting secreted extracellular nicotinamide phosphoribosyltransferase (eNAMPT) with a humanised eNAMPT-neutralising mAb significantly reduced tumour invasiveness both *in vitro* and *in vivo* (Sun *et al*., 2020).

1.6.4 Antibody-Drug Conjugates

Recent advances in antibody-drug conjugates (ADCs) which compose of a humanised antibody and small molecular drug via a chemical linker, have progressed the clinical management of certain cancers (Beck *et al*., 2017;

Zhao *et al*., 2020). The largest class of cytotoxic ADCs in clinical development are auristatin derivatives, including monomethyl analogues monomethyl auristatin E/F (MMAE and MMAF, respectively) (Beck *et al*., 2017). ADCs build upon the specific binding properties of mAbs and selectively bind to receptors on tumour cells, triggering internalisation, usually through the endocytosis pathway (Sievers & Senter, 2013). The chemical linker is then rapidly cleaved, allowing for the release of the cytotoxic drug and subsequent mechanisms of action to be triggered (Diamantis & Banerji, 2016; Sievers & Senter, 2013; Zhao *et al*., 2020). Internalisation is a key element to the cytotoxic effects of an ADC drug, as non-internalised ADCs can exert a bystander effect, inducing cell death by penetrating the membranes of neighbouring cells (Kovtun *et al*., 2006). A clinical trial utilising humanised mAb targeting PSA combined with ADC technology has shown promise in the treatment of prostate cancer, yet neurotoxicity was increased, highlighting the need for further investigations in this emerging field of antibody therapeutics (Milowsky *et al*., 2016).

1.7 CRISPR/Cas9 technology

Clustered regularly interspaced short palindromic repeat (CRISPR) – associated protein 9 (Cas9) is a novel ribonucleic acid (RNA)-guided endonuclease-based genome editing technique (Yi & Li, 2016). The Cas9 endonuclease is precisely guided to target sites by a single-guide RNA (sgRNA) in order to induce double strand breaks (DSBs), which trigger DNA repair processes to produce site-specific genomic modification (Yi & Li, 2016).

The most commonly used CRISPR/Cas9 system consists of three main components; the Cas9 endonuclease, CRISPR RNA (crRNA) and trans-activating crRNA (tracrRNA), and is known as the type II CRISPR/Cas9 system (Jinek *et al*., 2012). To make smaller edits to the genome, the most simple and successful method is the use of single stranded DNA oligonucleotides (ssODNs) as active repair templates in nuclease-mediated genome editing (Bialk *et al*., 2015). To render high-efficiency cleavage of any target sequence, combining the expression of sgRNA and Cas9 has been proven most effective (Jinek *et al*., 2012).

One of the main advantages this RNA guided CRISPR/Cas9 system has over conventional genome editing processes is its ease of use and cost-effective synthesis, as only a short complementary sgRNA is required for DNA targeting (Wei *et al*., 2013). In studies requiring a more high-throughput approach to genome editing, CRISPR/Cas9 can edit multiple different sites simultaneously simply through the use of multiple sgRNAs for various target sequences (Cong *et al*., 2013; Wang *et al*., 2013). One further advantage of CRISPR/Cas9 systems over RNA interference (RNAi) techniques is that fewer off-target effects are encountered as it functions at a DNA level, knocking down or permanently inactivating the gene (Sanchez-Rivera *et al*., 2015).

1.7.1 CRISPR/Cas9 in cancer research

Given the many advantages of CRISPR/Cas9 technology, these systems have proven successful tools in genome editing of cancers, as many involve numerous mutations and therefore require the ability to edit several genes

simultaneously (Chen *et al*., 2015; Hsu *et al*., 2014). In cancer therapeutics, the CRISPR/Cas9 system allows for the direct targeting of cancer cell genomes and is also applicable in the precise engineering of immune cells in cancer immunotherapy (Hsu *et al*., 2014; Shi *et al*., 2017). Cancer progression may be inhibited using CRISPR/Cas9 systems, as genetic alterations may be corrected through the induction of precise loss of function (LOF) and gain of function (GOF) modifications both *in vitro* and *in vivo,* which has the potential to be applied to numerous different cancers (Hsu *et al*., 2014; Yi & Li, 2016). One of the main challenges faced in the development of chemotherapeutic agents is the ability of cancer cells to overcome resistance, which accounts for the main cause of chemotherapy failure. However, CRISPR/Cas9 systems provide the potential to inactivate such genes causing chemotherapeutic resistance, which may subsequently increase the efficacy of chemotherapy (Yi & Li, 2016). This theory has been proven successful in an osteosarcoma cell line, when MDR1, known to confer drug resistance, was efficiently knocked out by targeting of exon 5 by CRISPR/Cas9 (Liu *et al*., 2016). Tang & Shrager, 2019, also overcame drug resistance in EGFR-mutant lung cancers by using CRISPR/Cas9 to target a mutation at position 790, exon 20 which causes a substitution of threonine with methionine (T790M) and is related to resistance to tyrosine kinase inhibitors (TKIs).

1.7.2 CRISPR/Cas9 limitations

The application of CRISPR/Cas9 genome editing systems as a potential future therapeutic option in cancer treatment warrants further investigations to enhance the efficacy of their application, and to develop such systems for clinical use once off-target effects and delivery methods have been addressed. The off-target effect of Cas9-induced DNA cleavage is one of the main hindrances in the universal application of the CRISPR/Cas9 system, and has been studied through a variety of techniques including computational, crystallography and single-cell analysis (Klein *et al*., 2018; Nishimasu *et al*., 2014; Singh *et al*., 2016). The ability of Cas9 to cleave targets with a minor number of mismatches is the result of the genetic sequence of the virus mutating to evade Cas9 nuclease attack (Herai, 2019; Li *et al*., 2019). There have been several suggested approaches to overcome off-target effects by

stabilising on-target binding. One method is to chemically modify the gRNA backbone to incorporate 2′-O-methyl-3′-phosphonoacetate at specific sites of gRNA, or partly replace RNA nucleotides with DNA nucleotides (Ryan *et al*., 2018; Yin *et al*., 2018). Another possible limitation of the CRISPR/Cas9 system is the ability of surviving colonies to contain wild-type (WT) sequences as a result of incomplete CRISPR-based editing (Vento *et al*., 2019). These colonies, referred to as “escaper colonies” are the result of mutations in either the gRNA or Cas9 related genes, or both, leading to the deactivation of the delivered CRISPR system (Vento *et al*., 2019). To prevent the formation of escaper colonies, optimisation of Cas9 endonuclease and gRNA expression is needed, which can be achieved through the use of high-copy number plasmids or stronger gRNA promotors (Guo *et al*., 2019; Wu *et al*., 2019). Despite its limitations and challenges, CRISPR/Cas9 offers a promising genome editing tool which could be implemented in the treatment of a wide variety of cancers.

1.8 The role of androgens in prostate cancer

The androgen family of hormones have long been implicated in prostate development, normal prostate homeostasis, and the development and progression of prostate cancer (Davey & Grossman, 2016). Androgens, of which testosterone (T) is the prototype, are produced primarily by the testes in males with a small amount produced by the adrenal glands (Davey & Grossman, 2016; Lonergan & Tindall, 2011). Androgen regulation is mediated through AR, a ligand-dependent nuclear transcription factor (Davey & Grossman, 2016; Heinlein & Chang, 2004).

1.8.1 Androgen receptor

The human *AR* gene is located on the X chromosome (q11-12) and consists of 8 exons, coding for a protein of 919 aa with a mass of 110 kDa (Davey & Grossman, 2016; Lonergan & Tindall, 2011). *AR* consists of four structurally and functionally distinct domains: a poorly conserved N-terminal domain (NTD), a highly conserved DNA-binding domain (DBD), a moderately conserved ligand-binding domain (LBD) and a short amino acid sequence known as the hinge region, separating the DBD from the LBD (Davey & Grossman, 2016; Heinlein & Chang, 2004 Lonergan & Tindall, 2011).

The cytochrome P450 enzyme, 5α-reductase, converts testosterone to dihydrotestosterone (DHT), and is highly expressed within the prostate (**Figure 1.7;** Lonergan & Tindall, 2011; Schmidt & Tindall, 2011). Both testosterone and DHT can bind to and activate *AR*, with the latter having a greater affinity and therefore activates target genes at lower concentrations than testosterone (**Figure 1.7**; Lonergan & Tindall, 2011; Schmidt & Tindall, 2011). AR is located primarily in the cytoplasm prior to ligand binding, and associates with heat shock proteins (HSP)-56, -70 and -90 (Smith & Toft, 2008). These HSPs are attached to cytoskeletal proteins such as Filament A (FlnA), which modulates the nuclear translocation and transcriptional activity of *AR* through interactions with the hinge region (Loy *et al*., 2003). Once inside the nucleus, *AR* binds to specific recognition sequences known as androgen response elements (AREs) located in the promotor and enhancer regions of

target genes (Dehm & Tindall, 2006). Gene expression is then modulated by the completion of the AR transcriptional complex once co-regulators are recruited by AR in the nucleus (**Figure 1.7**; Dehm & Tindall, 2006).

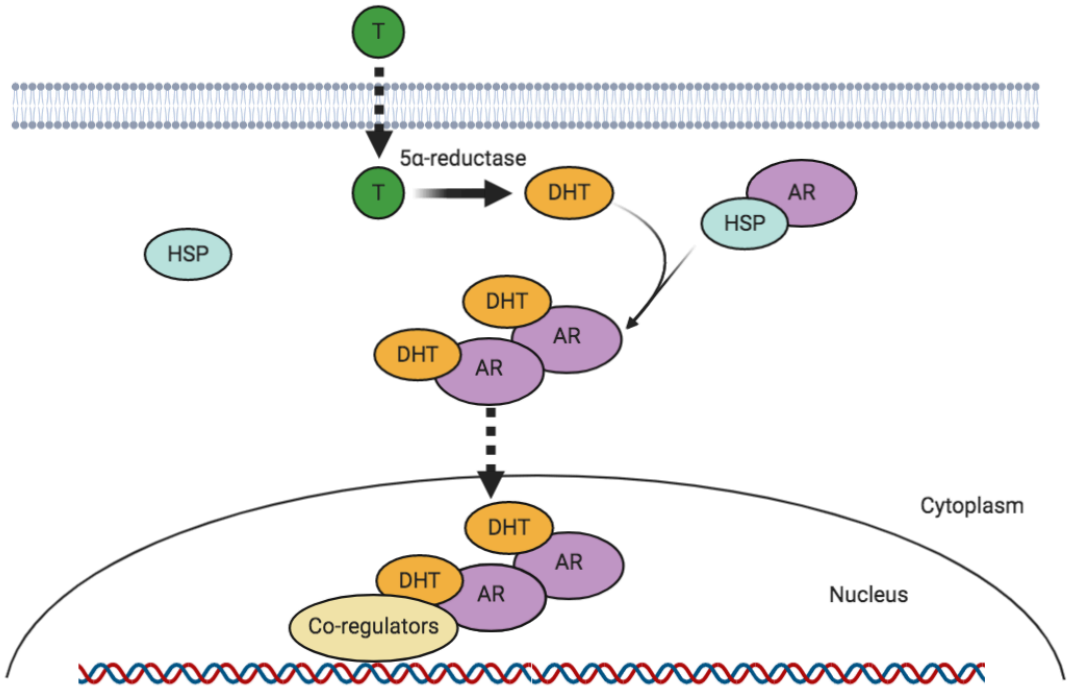

Figure 1.7. Summary of androgen receptor activation in the prostate. Testosterone (T) is converted to dihydrotestosterone (DHT) by 5α-reductase. Androgen receptor (AR) interacts with heat shock proteins (HSP) in the cytoplasm and translocates to the nucleus upon binding to DHT where it recruits co-regulators required for completion of the AR transcriptional complex. Adapted from (Lonergan & Tindall, 2011). Created using BioRender.

Under normal conditions, stromal *AR* signalling promotes cell growth, which is balanced by epithelial *AR* signalling which suppresses basal cell proliferation and maintains differentiated luminal cell survival (Wu *et al*., 2007; Yu *et al*., 2012). However, during the onset of prostate cancer and subsequent disease progression, epithelial *AR* undergoes a malignant switch and begins to stimulate proliferation rather than maintaining differentiation (Dehm & Tindall, 2006; Zhou *et al*., 2015). *AR* activity also acts as a survival mechanism by increasing the ability of prostate cancer cells to evade apoptosis (Dehm & Tindall, 2006). Increased *AR* expression is observed in almost all primary and metastatic prostate cancers regardless of stage or grade, hence its suitability as a target of various prostate cancer therapies through androgen deprivation

(Massard & Fizazi, 2011; Zaffuto *et al*., 2017). *AR* has not been implemented as a clinical prognostic biomarker for prostate cancer due to a lack of reproducible detection methods or defined thresholds (McAllister *et al*., 2019).

Although the exact mechanisms driving this malignant switch remain unclear, several possibilities have been hypothesised including *AR* overexpression, *AR* mutation, and a shift from paracrine to cell autonomous *AR* signalling (Han *et al*., 2005; Lonergan & Tindall, 2011). *AR* and downstream signalling pathways are subject to modifications by various factors including post-translational alterations, methylation and phosphorylation, and are also involved in crosstalk with other signalling pathways such as the PI3K / protein kinase B (Akt) and ERK1/2 pathways (**Figure 1.8**; Górowska-Wójtowicz *et al*., 2017; van der Steen *et al*., 2013).

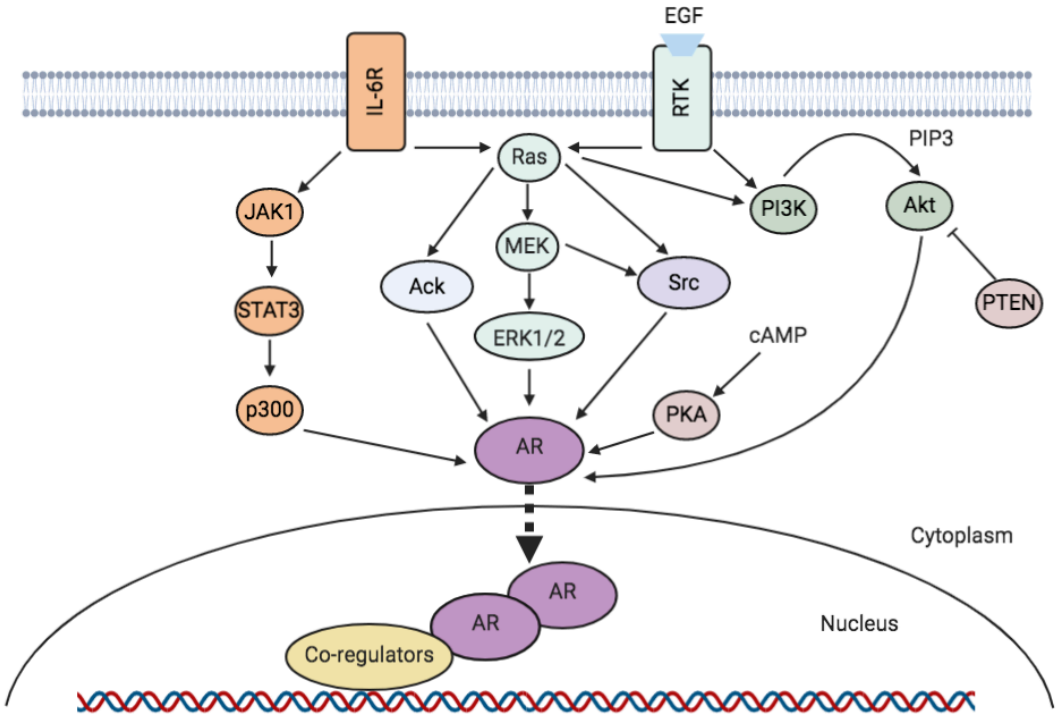

Figure 1.8. Summary of the major androgen signalling pathways in prostate cancer. Androgen receptor (AR) signalling can arise from several non-mutually-exclusive mechanisms including extracellular peptides, epidermal growth factor (EGF) and interleukin-6 (IL-6). Adapted from (Lonergan & Tindall, 2011). Created using BioRender.

1.8.2 Androgen-regulated genes

AR has been linked to the regulation of many genes involved in the onset and progression of prostate cancer. The translation of androgen-responsive genes is regulated through the binding of *AR* to AREs (Heinlein & Chang, 2004; Davey & Grossman, 2016). The most widely studied of these genes is *PSA*, which is used to determine the restoration of *AR* activity post-treatment (Cornford *et al*., 2020; Lipianskaya *et al*., 2014; Scher *et al*., 2004). *AR* is recruited to the enhancer region of *PSA*, increasing its expression through transcriptional activation in the N-terminal domain of *AR* in the nucleus (Dehm & Tindall, 2007). In the enhancer region of *PSA*, AREs recruit other co-activators and transcription factors including histone acetyltransferases, p160 family, mediator and RNA polymerase II (PolII) (Takayama *et al*., 2007; Wang *et al*., 2005). Once activated, *PSA* triggers disease progression by initiating epithelial-mesenchymal transition and cell migration, which is mediated by *PSA* protease activity (Whitbread *et al*., 2006).

Recent studies have found that up to 90% of all prostate cancer overexpress an erythroblast transformation-specific (*ETS*) oncogene, such as *ETS*-related gene (*ERG*), *ETS* translocation variant (*ETV*)-*1*, *ETV5* and *ETV6* (Tomlins *et al*., 2007). Of these, the most common mechanism of overexpression is fusion of the *ETS* gene, usually *ERG*, with the 5'-untranslated region of the highly AR-regulated transmembrane protease serine 2 (*TMPRSS2*) (Tomlins *et al*., 2005 & 2007). *PSA* and *TMPRSS2* overexpression have also been linked to CRPC onset following a gain in function mutation in DHT synthesis allowing for the restoration of circulating androgens in the serum (Chang *et al*., 2013).

Other genes regulated by *AR* activity include FK506 binding protein 5 (*FKBP5*) and G-protein coupled receptor family C group 6 member A (*GPRC6A*) (Febbo *et al*., 2005; Pi & Quarles, 2012). Both genes are implemented in the progression of prostate cancer from localised or locally advanced disease to metastatic disease, playing a vital role in intracellular communication and increased cell proliferation (Dhondt *et al*., 2020 & 2016; Pi & Quarles, 2012). *FKBP5* modulates *AR* function and signalling through the formation of

complexes with HSP90 and HSP70 (Li *et al*., 2011; Ni *et al*., 2010). Like *AR*, *GPRC6A* is also activated through the PI3K/Akt signalling pathway and has therefore been linked to disease progression to CRPC (Pi *et al*., 2015; Zarif & Miranti, 2016). Targeting these genes alongside *AR* may provide novel treatment options for patients with advanced prostate cancer (Zhao *et al*., 2013).

1.9 Thesis aims

At present, the treatment of advanced prostate cancer is often challenging as current therapies present serious adverse effects which impact upon patients' quality of life. To overcome these challenges, the identification of novel biomarkers capable of detecting the progression from early to advanced disease in order to offer more personalised treatment approaches are urgently needed. One biomarker of interest is STEAP2, which has been previously identified within the wider research group at Swansea as being highly expressed in advanced prostate cancer when compared to normal prostate tissue (Burnell *et al*., 2018; Whiteland *et al*., 2014). Research within the group found that *in vitro*, elevated STEAP2 protein expression correlates with an invasive phenotype, and increased levels of cell migration and invasion (Burnell *et al*., 2018). The role of STEAP2 in the metastatic spread of prostate cancer to the bone remains unclear. These aggressive traits in response to elevated STEAP2 expression has been linked with increasing Gleason scores and prostate cancer progression (Whiteland *et al*., 2014). STEAP2 therefore presents an attractive molecular drug target for antibody-based drugs in the treatment of advanced prostate cancer.

The aim of this thesis was to determine whether STEAP2 holds potential as a viable drug target, specifically focusing on targeted STEAP2-knockout by CRISPR/Cas9 engineering. This thesis also aimed to assess the link between *STEAP2* and *AR* in relation to prostate cancer progression. To address these aims, the thesis objectives were to:

1. Develop and optimise a robust method to generate and characterise 3D prostate cancer spheroid models;
2. Develop and optimise CRISPR/Cas9 engineering for STEAP2-knockout to:
    a. Evaluate the impact of STEAP2-knockout on aggressive prostate cancer traits (e.g., cell proliferation, migration and invasion) and;
    b. Assess *AR* gene expression in response to STEAP2-knockout;
3. Select one monoclonal anti-STEAP2 antibody lead candidate to provide

proof-of-concept of STEAP2 as a drug target by:

a. Studying the effect of the anti-STEAP2 monoclonal antibody lead candidate on cell viability in 2D and 3D prostate cancer cell models and;
b. Evaluating STEAP2 receptor internalisation to assess the suitability of the anti-STEAP2 monoclonal antibody lead candidate for use in ADC technology.

Chapter 2

Materials and methods

2.1 Materials and Reagents

2.1.1 Reagents

The reagents used throughout this thesis are detailed in **Table 2.1**

Table 2.1. Reagents used throughout this thesis. DMEM: Dulbecco's Modified Eagle Medium; MTT: 3-(4,5-Dimethyl- 2thiazoyl)-2,5-diphenyl-2H-tetrazolium bromide; HCL: hydrochloride; RIPA: Radioimmunoprecipitation assay; RPMI-1640: Roswell Memorial Park Medium-1640; TEMED: N, N, N', N' Tetramethylenethylenediamine; SDS: Sodium-Dodecyl Sulfate; TRIS: Tris(hydroxymethyl)aminomethane.

Reagent	**Supplier and catalogue number**
Acrylamide/Bis solution 19:1 (30%)	BioRad, USA, #161015
Agarose	Sigma Aldrich, UK, #A6013
Ammonium persulfate (APS)	Sigma Aldrich, USA # 215589
alamarBlue	BioRad, UK, #BUF012A
Bovine serum albumin	Sigma Aldrich, UK, #A2153
Chemiluminescence reagent (ECL)	BioRad, USA, #170-5060
DEPC-treated (RNAse-free) water	Thermo Fisher, USA, #AM9916
DMEM, phenol red-free	Life Technologies, UK, #21063029
Foetal bovine serum	Life Technologies, UK, #10271
Foetal bovine serum (charcoal-stripped)	Sigma Aldrich, USA, #F6765
Formaldehyde, ultra-pure (16%)	Polysciences, USA, #18814-20
Glutamine	Life Technologies, UK, #25030-024
Glycine	Sigma Aldrich, USA, # G8898
Hoechst	Thermo Fisher, UK, #62249
MTT	Sigma Aldrich, UK, #T9281
Miller's LB Broth powder	Sigma Aldrich, USA, #L3152
RIPA buffer	Sigma Aldrich, USA, #R0278

Phosphate-buffered saline	Life Technologies, UK, #10010023
Phosphate-buffered saline 10x	MerckMillipore, USA, #6505
Propidium Iodide	Thermo Fisher, UK, #P1340MP
RPMI-1640	Life Technologies, UK, #31870025
SDS 10%	BioRad, USA, # 1610416
TEMED	Sigma Aldrich, USA, #T9281
Tris-base	BioRad, USA, #1610716
Tris-Glycine (TG) 10x	Sigma Aldrich, USA #T4904
Tris-Glycine-SDS (TGS) 10x	Sigma Aldrich, USA, #T7777
Triton-X 100	Thermo Fisher, UK, #T8787
Trypsin-EDTA	Life Technologies, UK, #25300-062
Tween20	Sigma Aldrich, USA, #P1379

2.1.2 Materials

The material used throughout this thesis are detailed in **Table 2.2**

Table 2.2. Material used throughout this thesis.

Material	**Supplier and catalogue number**
Filter paper	BioRad, USA, #1703956
Flask, T175	VWR, USA, #82050-870
Flask, T25	VWR, USA, #82051-070
Flask, T75	VWR, USA, #82050-854
Foam pads	BioRad, USA, #1703933
Migration culture inserts (2-well)	Ibidi, Germany, #80209
Mini-Protean glass plates, short	BioRad, USA, #165331
Mini-Protean outer glass plates	BioRad, USA, #1651824
Nitrocellulose membrane	BioRad, USA, # 1620115
Petri dish, 100 mm	VWR, USA, #25384-342
Transwell inserts, 8.0 μm pore size	Sigma Aldrich, USA, #CLS3422
6-well plate	VWR, USA, # 734-2323
12-well plate	VWR, USA, #82050-928
24-well plate	VWR, USA, # 734-2325
96-well plate	VWR, USA, #10861-666
μ-slide 8-well chambered slides	Ibidi, Germany, #80826

2.1.3 Equipment

The equipment used throughout this thesis are detailed in **Table 2.3**

Table 2.3. Equipment used throughout this thesis.

Equipment	Supplier and model number
Bacterial incubator	Amerex, USA, GIROMAX 737R
Benchtop centrifuge	VWR, USA, Himac CT6E
Cell culture imaging system	Invitrogen, USA, EVOS XL Core
Cell culture inverted microscope	ZEISS, Germany, AxioCamERC55
Cell culture incubator	MarshallScientific, USA, NU-5510
Centrifuge	ThermoTec, UK, Centra CL3R
Confocal microscope	ZEISS, Germany, LSM710
Electrophoresis cell	BioRad, USA, Mini-PROTEAN Tetra Cell
Heat block	Thermo Fisher, USA, Dry Block Heater
Liquid nitrogen container	Thermo Fisher, UK, Locator JR Plus
Nanodrop spectrophotometer	Thermo Fisher Scientific, UK, ND-1000
Membrane transfer cell	BioRad, USA, Mini Trans-Blot® Cell
Olympus microscope	Olympus, UK, BX51TF
Plate centrifuge	Beckman Coulter, USA, Allegra-X14
Plate reader	BMG Labtech, UK, POLARstar
PowerPac™	BioRad, USA, PowerPac HC
qRT-PCR profiler	Thermo Fisher, USA, QuantStudio™ 12K
Thermal cycler	BioRad, USA, T100 Thermal Cycler
Water bath	Grant, UK, SUB Aqua 18
Western blotting imaging machine	BioRad, USA, ChemiDoc XRS+

2.1.4 Buffers and solutions

Buffers and solutions used throughout this thesis are detailed in **Table 2.4**

Table 2.4. Buffers and solutions. APS: Ammonium persulphate; BSA: Bovine Serum Albumin; MTT: 3-(4,5-Dimethyl-2thiazoyl)-2,5-diphenyl-2H-tetrazolium bromide, NaCl: Sodium chloride; SDS: Sodium-Dodecyl Sulfate; PBS: Phosphate- buffered Saline; PFA: Paraformaldehyde, TRIS-base: tris(hydroxymethyl)aminomethane.

Blocking buffer (3%)	**Transfer buffer**
3.0 g BSA	100 ml of TRIS / Glycine 10x
100 ml of PBS-T	200 ml of methanol
0.22 μm filtered	700 ml of ddH_2O
Stored at 4°C	Stored at room temperature
Triton-X 100 (0.1%)	**Running buffer**
0.1 μl of Triton-X 100	100 ml TRIS / Glycine / SDS 10x
PBS to 100 ml	900 ml ddH_2O
Stored in aliquots at -20°C	Stored at room temperature
PBS-T	**APS (10%)**
100 ml of PBS (10x)	1.0 g APS
900 ml of ddH_2O	1 ml ddH_2O
1 ml of Tween 20	Stored in aliquots at -20°C
PFA (4%)	**MTT (5 mg/ml)**
10 ml of 16% PFA	1 mg of MTT in 200 ml PBS
40 ml of PBS	0.22 μm filtered
Stored in aliquots at -20°C	Stored in aliquots at -20°C
10% SDS	**Miller's LB Broth**
25.0 g SDS	20 g Miller's LB Broth powder
250 ml ddH_2O	800 ml ddH_2O
1.0 M Tris, pH 6.8	**1.5 M Tris, pH 8.8**
30.4 g TRIS-base	45.4 g Tris-base
250 ml ddH_2O, pH 6.8	250 ml ddH_2O, pH 8.8

2.1.5 Computer programs

The computer programs used for analysis throughout this thesis are detailed in **Table 2.5.**

Table 2.5. Computer programs used for analysis.

Program	Supplier and version
BioRender	BioRender, USA, Institution Version
EVOS XL Core software	Invitrogen, USA, Version 1.0.131
ImageJ	ImageJ, USA, Version FIJI 2.0.0.
ImageLab software	BioRad, USA, Version 6.0.1
Zen software	ZEISS, Germany, Version 10

2.2 Cell lines

Cell lines were purchased from American Type Culture Collection ((ATCC), LGC Standard). Human prostate cancer cell lines of different origins (C4-2B, DU145, LNCaP, PC3), human bone stromal cell line (HS5) and human prostate epithelial cell line (PNT2) were utilised throughout this thesis. A representative image of each cell line can be seen in **Figure 2.1**. Details of the origins, and diseased state of each cell line used throughout this thesis can be found in **Table 2.5**.

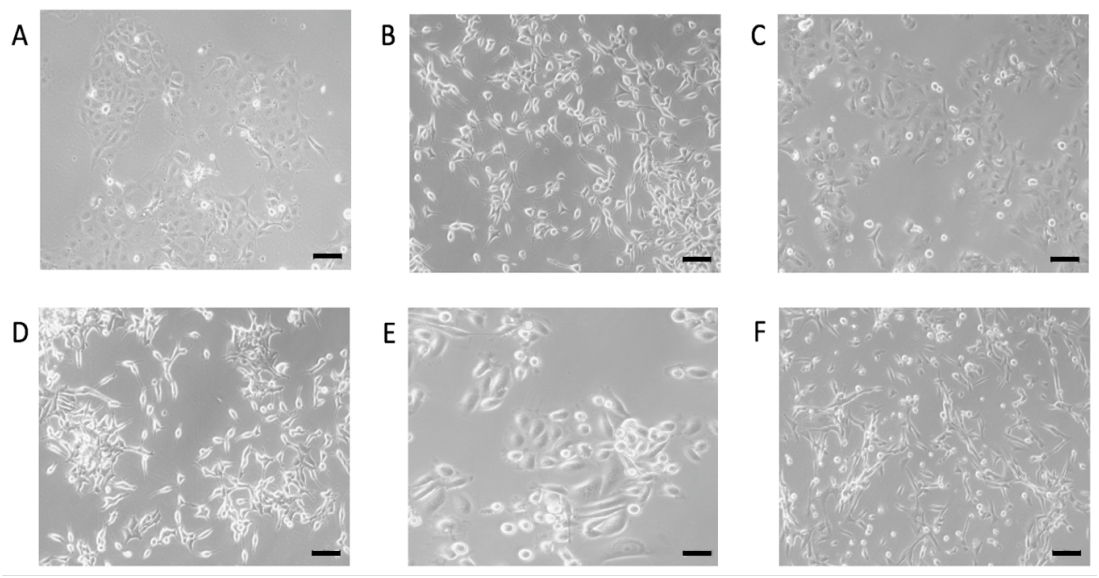

Figure 2.1. Representative images of the cell lines used throughout this thesis. A) Normal, non-cancerous prostate epithelial cells PNT2 were used as a negative control given the low STEAP2 protein expression *in-vitro*. B) LNCaP-derived prostate cancer cell line C4-2B; C) Brain metastatic prostate cancer cell line DU145; D) Lymph node metastatic prostate cancer cell line LNCaP; E) Bone metastatic cancer cell line PC3; F) Human, normal bone stromal cell line HS5 was used in co-culture with prostate cancer cells. Images were acquired with a standard light microscope (AxioCam ERC55, Zeiss, Germany) using a 5x objective. Scale bar = 100 μm.

Table 2.6. Summary of cell lines used throughout this thesis.

Cell line	Species	Origin	Diseased state
LNCaP	Human	Lymph node	Prostate cancer
C4-2B	Human	C4-2 derivative	Prostate cancer
DU145	Human	Brain	Prostate cancer
PC3	Human	Bone marrow	Prostate cancer
PNT2	Human	Prostate epithelia	Normal
HS5	Human	Bone marrow	Normal

2.2.1 LNCaP cell line

Human, prostate cancer cells derived from a lymph node metastases of a 50-year-old male patient (ATCC, USA, #CRL-1470). Cells were sub-cultured at a ratio of 1:3 or 1:6 according to the supplier's recommendations in RPMI-1640 supplemented with 10% FBS, 1% penicillin / streptomycin (P/S) and 1% L-glutamine, all of which were purchased from Gibco, Life Technologies, UK.

2.2.2 C4-2B cell line

Human prostate cancer cells derived from a derivative subline of LNCaP-derived C4-2 cells. (ATCC, USA, #CRL-3315). The LNCaP cell line described in **Section 2.2.1** was co-inoculated into an athymic male nude mouse along with human fibroblasts derived from an osteosarcoma by Thalmann *et al*., in 1994. Following 8 weeks incubation, the mouse was castrated, and after an additional 4 weeks a tumour specimen was removed. The C4 cell line comprises of the *in vitro* cultured cells grown from the tumour removed from the host mouse. To achieve the C4-2 subline, C4 cells were then co-inoculated with osteosarcoma fibroblasts in an already castrated athymic nude male mouse for a further 12 weeks, as previously described, and the C4-2 subline generated from the prostatic epithelial cells cultured from the host's resultant tumour (Thalmann *et al*., 1994 & 2000). Cells were sub-cultured at a ratio of 1:8 or 1:10 according to the supplier's recommendations in DMEM supplemented with 10% FBS and 1% P/S and 1% L-glutamine, all of which were purchased from Gibco, Life Technologies, UK.

2.2.3 DU145 cell line

Human, prostate cancer cells derived from a brain metastases of a 69-year-old male patient (ATCC, USA, #HTB-81). Cells were sub-cultured at a ratio of 1:4 or 1:6 according to the supplier's recommendations in RPMI-1640 supplemented with 10% FBS, 1% P/S and 1% L-glutamine, all of which were purchased from Gibco, Life Technologies, UK.

2.2.4 PC3 cell line

Human, prostate cancer cells derived from a bone metastases of a 62-year-old male patient with grade IV prostate cancer (ATCC, USA, #CRL-1435). Cells were sub-cultured at a ratio of 1:3 or 1:6 according to the supplier's recommendations in RPMI-1640 supplemented with 10% FBS, 1% P/S and 1% L-glutamine, all of which were purchased from Gibco, Life Technologies, UK.

2.2.5 PNT2 cell line

Human, normal prostate epithelial (immortalised). Primary cells were obtained from a 33-year-old male post-mortem. Cells were sub-cultured at a ratio of 1:5 or 1:10 according to the supplier's recommendations in RPMI-1640 supplemented with 10% FBS, 1% P/S and 1% L-glutamine, all of which were purchased from Gibco, Life Technologies, UK.

2.2.6 HS5 cell line

Human, stromal fibroblast cells derived from the bone marrow / stroma of a 30-year-old healthy male patient (ATCC, USA, #CRL-11882). Cells were sub-cultured at a ratio of 1:3 or 1:9 according to the supplier's recommendations in RPMI-1640 supplemented with 10% FBS, 1% P/S and 1% L-glutamine, all of which were purchased from Gibco, Life Technologies, UK.

2.2.7 Cell culture

2.2.7.1 Monolayer cells (2D)

All cell culture was undertaken with the intention to maintain a safe and sterile environment, with cell culture conducted in a biological safety hood with laminar-airflow circulation (Scanlaf Mrs, VWR International Ltd, UK). Prior to use, all materials (culture flasks, plates and pipettes, cell culture media, PBS and trypsin) were disinfected with 70% ethanol. Cells were grown in standard cell culture conditions of 37^{o}C / 5% CO_2 in an incubator (Nuair^{TM} DHD AUTOFLOW CO2 Air-Jacketed Incubator). Cell culture media was obtained from Gibco, Life Technologies, UK.

DU145, HS5, LNCaP, PC3 and PNT2 cells were maintained in Roswell Park Memorial Institute media (RPMI-1640 media, Life Technologies, UK, Cat. 31870025) supplemented with 10% foetal bovine serum (FBS), 1% glutamine, and 1% penicillin/ streptomycin. C4-2B cells were maintained in Dulbecco's Modified Eagle Medium media (DMEM media, Life Technologies UK, Cat. 21063029) supplemented with 10% FBS, 1% glutamine, and 1% P/S. Phenol-red free DMEM media (Life Technologies, UK, Cat. 21063029) supplemented with 10% FBS, 1% glutamine, and 1% P/S was used for microscopical endpoint analysis.

Prior to use, cell culture media, PBS (Gibco, Life Technologies, UK, Cat. 10010023) and trypsin-EDTA were pre-warmed in an incubator (SUB Aqua 18, Grant, UK) set at 37^{o}C. To detach cells from tissue culture flasks, all media was removed, and they were first washed with 5 ml of PBS and 3 ml of trypsin (0.05%; Life Technologies, UK, Cat. 25300-062) was added and cells were incubated in standard cell culture conditions (37^{o}C, 5% CO_2) for 5-10 minutes, incubation times were cell line dependent. 6 ml of fresh media was added to neutralise the trypsin, and the cell suspension was transferred to a 15 ml centrifuge tube, which was centrifuged at 270 g for 5 minutes using a bench-top centrifuge (VWR, Himac CT6E, UK). The old media was discarded, and the cell pellet resuspended in 10 ml of fresh media, and cells split according

to the supplier's recommended ratio. All cells were propagated in standard cell culture conditions (37°C, 5% CO_2) in cell cultured treated T75 flasks (VWR, USA, Cat. 82051-070). Media was replenished every 3 days when required. Once cells had reached 70-80% confluency, cells were sub-cultured according to the supplier's guidelines for each cell line. After 10-15 passages, cells were discarded.

2.2.7.2 Determination of cell numbers

A haemocytometer was used to calculate the number of cells/ml present in the cell solutions. 50 μl of cell suspension (**Section 2.2.7.1**) was pipetted into separate 200 μl Eppendorf tubes; 50 μl of 0.4% trypan blue stain was added to each Eppendorf tube and thoroughly mixed to create a 1:1 dilution. Each chamber of the haemocytometer was loaded with 10 μl of the trypan blue/cell suspension, covered with a glass slide and transferred to an inverted light microscope (AxioCam ERC55, Zeiss, Germany) using a 10X magnification to determine the number of cells present, both total and viable. Cells were counted in the four outer corners of the counting grid of the haemocytometer, and non-viable cells were distinguished as being stained with trypan blue, as opposed to viable cells which remained unstained, as demonstrated in **Figure 2.2.** Each sample was counted once. Only cells touching the top and right lines per corner square were counted. An average was calculated by dividing the total number of cells by four, and this number used to calculate the cell concentration using the following calculations:

Cell density$_f$ (x 10^5 cell/ml) x volume$_f$ (ml) / cell density$_i$ (x 10^5 cell/ml) = cell suspension (ml) + [volume$_f$ (ml) – cell suspension (ml)]

Where: Cell density$_f$ = final cell density (x 10^5 cell/ml); Cell density$_i$ = initial cell density (x 10^5 cell/ml); Volume$_f$ = final volume (ml)

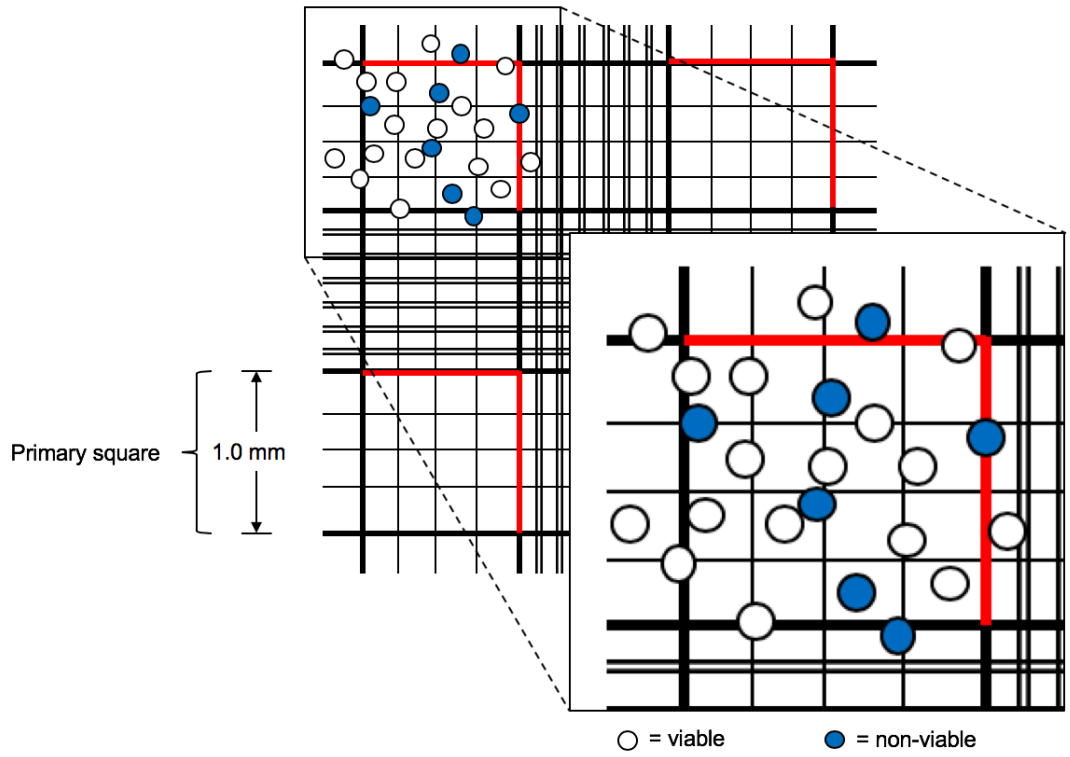

Figure 2.2. Haemocytometer chamber used for cell counting. Schematic diagram of one chamber on a haemocytometer loaded with 10 μl of cell suspension. The cell number located in four corner squares (primary squares) was counted. Inset shows an enlargement of one corner square. Only viable cells (white cells), touching the top and right borders (red) were scored and those that were non-viable (blue cells) were excluded.

2.2.7.3 Growth of 3D spheroids

For miniaturised 3D cultures, 1.5% agarose gel was prepared by adding 0.15 g agarose powder (Sigma Aldrich, UK, Cat. A6013) to 10 ml phenol red free (PRF) DMEM (Life Technologies, UK, Cat.21063029) in the absence of additional supplements and autoclaved at 121°C for 60 minutes and stored at room temperature. As the agarose medium is solid at room temperature, it was briefly microwaved at half power (450 W) for 45 seconds to liquify prior to use. 50 μl of 1.5% agarose / culture medium was added to 96-well plates and left to solidify at room temperature for 15 minutes. Cells were counted as described in **Section 2.2.7.2** and seeded at the required density on top of the solidified agarose in 100 μl PRF media per well, as depicted in **Figure 2.3**. Spheroids were maintained in standard tissue culture conditions. Media was

carefully removed and replenished every 3 days. 3D cultures were maintained for up to 7 days.

Figure 2.3. Side profile of an individual well of a 96-well plate seeded with PCa cells to form spheroids. 96-well tissue culture plates were coated with 50 μl 1.5% agarose which was left to solidify before a cell suspension of prostate cancer cells in 100 μl PRF DMEM was added and incubated in standard tissue culture conditions to form spheroids.

2.2.7.4 Cryopreservation

A 1:9 solution of 1 ml 10% dimethyl sulfoxide (DMSO) and 9 ml FBS was prepared for the routine cryopreservation of cells. Once cells reached 80% confluency, they were detached from tissue culture flasks by the addition of 10 ml trypsin, which was then neutralised by the addition of 6 ml cell culture media. Cells were suspended and transferred to a 15 ml centrifuge tube and centrifuged at 270 g for 5 minutes. The old cell culture media was discarded, and the cell pellet resuspended in DMSO/FBS (1:9) solution. 1 ml of this solution was added per cryo-preservative vial. Vials were transferred into cryo-vessels and stored at -80°C for 24 h and then moved to a -140°C liquid nitrogen container for long-term storage (Locator JR Plus, Thermo Fisher, UK).

2.3 Gene expression

2.3.1 RNA extraction

Cells were grown to 80% confluency, trypsinised and neutralised with RPMI-1640 as described in **Section 2.2.7.1.** Samples were centrifuged, old media discarded, and cell pellets resuspended in 1 ml of TRIzol reagent (Thermo Fisher, USA, Cat. 15596026) in 1.5 ml Eppendorf tubes. 200 μl of chloroform was then added to each sample in a fume hood, samples were shaken and incubated at room temperature for 3 minutes before centrifugation at 270 g for 15 minutes at 4°C. The upper, clear layer (approximately 500 μl) was transferred to a fresh 1.5 ml Eppendorf tube, to which 500 μl isopropanol (100% v/v) was added. Tubes were again shaken and incubated at room temperature for 10 minutes, prior to centrifugation at 270 g for 10 minutes at 4°C. The supernatant was then discarded, 1 ml of ethanol (70% v/v) was added to each tube which was then vortexed and subsequently centrifuged at 6010 g for 5 minutes at 4°C. The supernatant was again discarded, and the pellet left to air dry for 10 minutes. Pellets were then resuspended in 50 μl RNA-free water (Thermo Fisher, USA, Cat. AM9916), and the RNA concentration and quality (A260/280) measured using a Nanodrop machine (Thermo Fisher, ND-1000, USA). RNA with a A260/280 value between 1.8-2.1 was considered acceptable. RNA samples were standardised to 200 ng/μl in RNAse-free water (Thermo Fisher, USA, Cat. AM9916) and kept on ice for immediate cDNA synthesis or transferred to -80°C for long-term storage until needed.

2.3.2 cDNA synthesis

First strand total cDNA was synthesised using a Promega M-MLV Reverse Transcriptase kit (Promega, USA). 20 μl of total RNA (200 ng/μl) obtained from **Section 2.3.1** was pipetted into 200 μl Eppendorf tube. 1 μl of OligodT_{15} (Promega, USA, Cat. C1101) and 1 μl of random hexamer primers (Promega, USA, Cat. C1181) were added to each sample. The tubes were then heated on a heating block (Thermo Fisher, USA, Cat. 88870001) set at 70°C for 5 minutes and cooled immediately on ice. A master mix was prepared from the

reagents detailed in **Table 2.7**, 28.5 μl of which was added to each sample in the 200 μl Eppendorf tubes. Samples were then heated to 37°C using a thermocycler machine (BioRad, T100 Thermal Cycler, USA) and incubated for 60 minutes. The tubes were then heated on a heating block set at 90°C for 10 minutes and cooled immediately on ice for immediate use or transferred to -20°C for storage up to a maximum of 2-weeks.

Table 2.7. Master mix reagents for cDNA synthesis, per sample.

Reagent	**Volume (μL)**
M-MLV 5X Reaction Buffer (Promega, USA, Cat. M5313)	10
10mM dNTPs (Promega, USA, Cat. U1515)	2.5
DNAse free H_2O (Thermo Fisher, USA, Cat. AM9916)	7
M-MLV RT (Promega, USA, Cat. M1701)	1

2.3.3 Quantitative reverse transcriptase polymerase chain reaction

Quantitative reverse transcriptase polymerase chain reaction (qRT-PCR) was carried out to determine the profiles of genes of interest. A BLAST search was performed prior to carrying out each experiment to design unique primer sequences specific to each gene of interest. Pre-validated primers for two housekeeping genes, *β-actin* (NM_001101) and *GAPDH* (NM_002046) were used throughout this thesis, the sequences of which are detailed in **Table 2.8**. All primers were reconstituted and diluted in RNAse free water (Thermo Fisher, USA, Cat. AM9916), to a concentration of 10 mM.

Table 2.8. Sequences of primers utilised in qRT-PCR experiments throughout this thesis. Sequences of primers for the detection of *STEAP1-4, AR, PSA, FKBP5, TMPRSS2* and *GPRC6A,* including housekeeping genes *β-actin* and *GAPDH.*

Gene	Forward primer	Reverse primer
β-actin	CACCATTGGCAATGAGCGGTTC	AGGTCTTTGCGGATGTCCACGT
GAPDH	GTCTCCTCTGACTTCAACAGCG	ACCACCCTGTTGCTGTAGCCAA
STEAP1	CCCTTCTACTGGGCACAATACA	GCATGGCAGGAATAGTATGCTTT
STEAP2	GGTCACTGTAGGTGTGATTGG	ACCACATGATAGCCGCATCTAA
STEAP3	CTCCCCGGAGGTCATCTTTG	TCTTGCTCTGTAGGGTTGCTC
STEAP4	GGCTTTGGGAATACTTGGGTT	TGGACAAATCGGAACTCTCTCC
AR	CCAGGGACCATGTTTTGCC	CGAAGACGACAAGATGGACAA
PSA	GTGTGTGGACCTCCATGTTATT	CCACTCACCTTTCCCCTCAAG
FKBP5	AATGGTGAGGAAACGCCGATG	TCGAGGGAATTTTAGGGAGACT
TMPRSS2	GTCCCCACTGTCTACGAGGT	CAGACGACGGGGTTGGAAG
GPRC6A	CCGGGACATATCATAATTGGAGG	CATTGCCACTGTGACTTCTGT

PowerUp™ SYBR™ Green Master Mix (Thermo Fisher, USA, Cat. A25742) was used for detection of genes of interest by qRT-PCR. 4 μl PowerUp™ SYBR™ Green Master Mix, 1 μl forward primer, 1 μl reverse primer and 2 μl cDNA were pipetted into each well of a 384-well PCR plate (VWR, USA, Cat. 732-3237) in triplicate. Plates were sealed with an adhesive sealing film (BioRad, USA, Cat. MSB1001) and centrifuged using a bench-top plate centrifuge at 8,000 g for 2 minutes (Beckman Coulter, Allegra-X14, USA). Gene profiling was then carried out using an Applied Biosystems™ QuantStudio™ 12K Flex Real-Time PCR System, 384-well block (Thermo Fisher, USA, Cat. 4471134), the conditions for which are detailed in **Table 2.9.**

Table 2.9. Cycling conditions for qRT-PCR.

Step	**Time**	**Temperature (°C)**	**Number of cycles**
Heat activation	5 minutes	95	1
Denaturation	10 seconds	95	40
Annealing	30-40 seconds	55	40
Extension	30 seconds	72	40

2.3.4 qRT-PCR gene expression analysis

Cycle threshold (C_T) values obtained from gene profiling (**Section 2.3.3**) were used to calculate the fold expression changes of each gene of interest, normalised to control cells. An average was taken of the raw C_T values of each experimental sample and each control sample for both genes of interest and the housekeeping genes.

Expression fold change = $2^{-\Delta\Delta C_T}$

Delta (Δ) C_T values were calculated as follows:

GE - HE = ΔCGE

GC - HC = ΔCGC

Where:

GE = Average C_T value of genes of interest in experimental cells

HE = Average C_T value of housekeeping gene in experimental cells

GC = Average C_T value of genes of interest in control cells

HC = Average C_T value of housekeeping gene in control cells

$\Delta CGE - \Delta CGC = \Delta\Delta C_T$

2.4 Cell viability quantification

2.4.1 MTT assay

Cell viability was determined by the 3-(4,5-dimethylthiazol-2-yl)-2,5-diphenyltetrazolium bromide (MTT; Sigma Aldrich, UK, Cat. M5655) reduction assay. The MTT assay, introduced in 1983, is one of the most widely used colourimetric, quantitative biochemical tests for assessing cell viability and proliferation (Mossman, 1983). MTT, a tetrazolium salt, can only be cleaved by active mitochondria present in metabolically active cells, and is therefore a relevant survival assay for distinguishing living cells from dead ones (van Meerloo *et al*., 2011). Upon cleavage by the dehydrogenases in the mitochondria of a live cell, the yellow tetrazolium salt is converted into a blue formazan crystal, with the principle of this assay being that the amount of formazan produced is directly proportional to the number of live, viable cells (**Figure 2.4**; Borra *et al*., 2009; Van Meerloo *et al*., 2011).

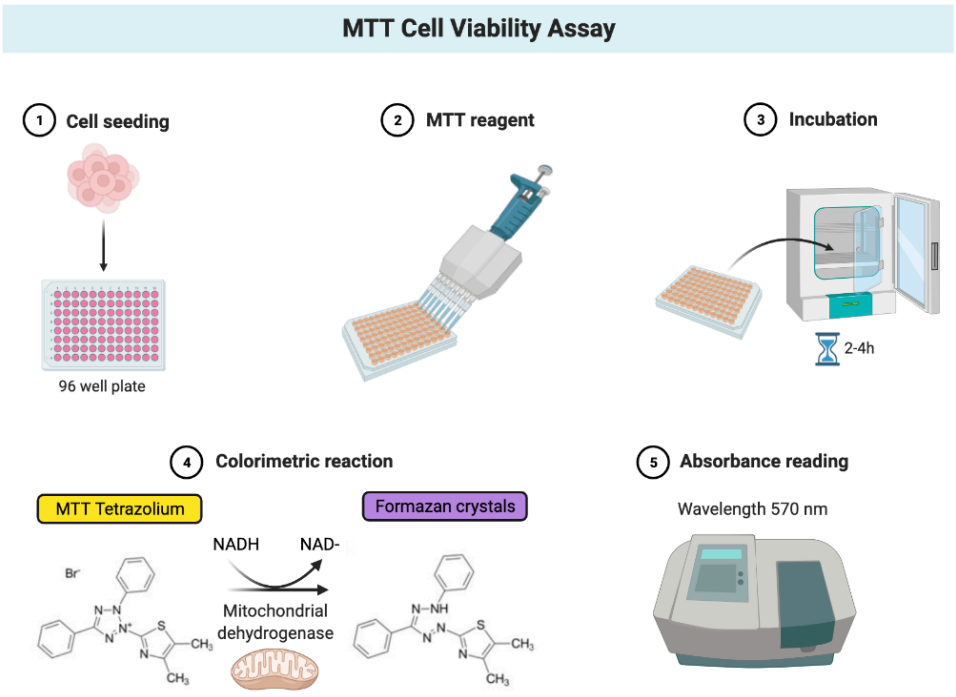

Figure 2.4. Schematic representation of the MTT cell viability assay. Cells are seeded in a 96 well plate, to which the yellow MTT tetrazolium salt is added. Cells are then incubated for 2-4h, during which the yellow MTT salt is reduced to purple formazan crystals by dehydrogenases in the mitochondria of viable cells. Absorbance is then read on a plate reader at 570 nm wavelength. Adapted from (Präbst *et al.*, 2017). Created using BioRender.

Cells were seeded in clear, flat bottomed 96-well plates at a known, cell line dependent density in a volume of 100 µl media per well. Cells were then incubated in standard cell culture conditions until the MTT assay was performed as an end-point analysis of cell viability. MTT solution was prepared by dissolving 5 mg MTT powder in 10 ml PBS, which was then sterile 0.22 µm filtered and stored at 4°C while protected from light. 10 µl MTT stock solution (5 mg/ml) was then added to each well prior to incubating for a further 2 h for 2D cell culture models and 4 h for 3D culture models, in the absence of light. MTT containing medium was then removed, cells were washed in PBS and formazan crystals were solubilised by the addition of 100 µl DMSO per well. Plates were placed on a rocker at room temperature for 15 minutes. Absorbance was read at A = 570 nm using a POLARstar plate reader (POLARstar, BMG Labtech, UK). Cell viability was calculated as a percentage of the control cells. Cell viability experiments were conducted in triplicate unless otherwise stated.

2.4.2 alamarBlue assay for cell viability

The alamarBlue assay was also utilised for cell viability assessments. alamarBlue (blue) is a commercial, resazurin (7-hydroxy-3H-phenoxazin-3-one 10-oxide)-based, fluorogenic redox indicator which is reduced to resorufin (pink), which can be quantified by fluorescence (Borra *et al*., 2009; Nakayama, 1997). This reduction occurs enzymatically when resazurin is taken up by the mitochondria of cells, by nicotinamide adenine dinucleotide phosphate (NADPH) dehydrogenase, which is responsible for the transference of electrons from NADPH and H+ to resazurin, which is subsequently reduced to resorufin (**Figure 2.5**; O'Brien *et al*., 2000; Rampersad *et al*., 2012).

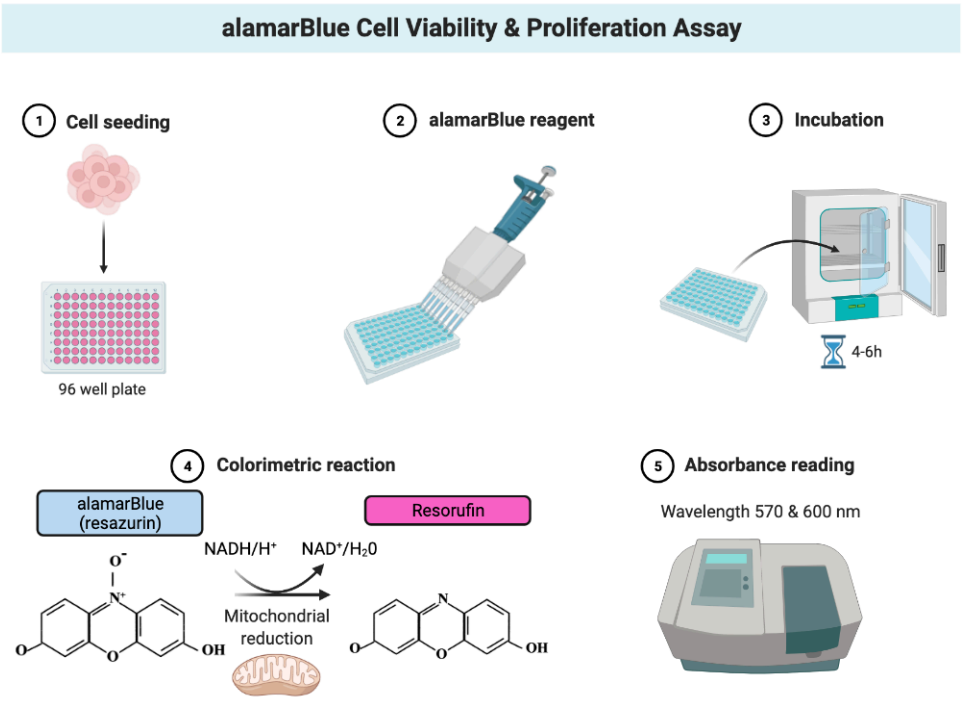

Figure 2.5. Schematic representation of the alamarBlue cell viability and proliferation assay. Cells are seeded in a 96 well plate, to which the blue alamarBlue reagent is added. Cells are then incubated for 4-6h, during which the blue alamarBlue reagent is reduced to pink resorufin by dehydrogenases in the mitochondria of viable cells. Absorbance is then read on a plate reader at wavelengths of 570 and 600 nm. Adapted from (O'Brien *et al*., 2000). Created using BioRender.

Assays were performed in 96-well plates using the commercial resazurin-based dye alamarBlue (BioRad, UK, Cat. BUF012A). Cells were cultured in 96-well plates in 100 μl media per well and left to adhere in standard cell

culture conditions for up to 5 days, until the alamarBlue assay was performed as an end-point analysis of cell viability. Readings were obtained through the application of 10 μl alamarBlue per well, achieving a final concentration of 10% (v/v). After the addition of alamarBlue, cells were further incubated for 4 h for 2D cell culture models and 6 h for 3D models, in standard cell culture conditions in the absence of light. Plates were read using a POLARstar plate reader (POLARstar, BMG Labtech, UK) at A = 570 nm and A = 600 nm. Percentage viability was calculated according to the manufacturer's instructions, using the calculation detailed below and the Molar extinction coefficients (E) for alamarBlue at different wavelengths detailed in **Table 2.10**.

Percentage viability (%) = (O2 x A1) - (O1 x A2) / (O2 x P1) - (O1 x P2) x100

Where:
O1 = molar extinction coefficient (E) of oxidised alamarBlue (Blue) at 570nm
O2= E of oxidised alamarBlue at 600nm
P1 = E of reduced alamarBlue (Red) at 570nm
P2= E of reduced alamarBlue at 600nm
A1 = absorbance of test wells at 570nm
A2 = absorbance of test wells at 600nm
N1 = absorbance of negative control well (media plus alamarBlue but no cells) at 570nm N2 = absorbance of negative control well (media plus alamarBlue but no cells) at 600nm

Table 2.10. Molar extinction coefficients (E) for alamarBlue at different wavelengths.

Wavelength (nm)	Reduced (E)	Oxidised (E)
570	155677	80586
600	14652	117216

2.5 Cell proliferation

2.5.1 alamarBlue assay for cell proliferation

To assess cell proliferation in mono and co-cultured 2D and 3D cells, the alamarBlue assay was conducted in the same manner as when assessing cell viability, as detailed in **Section 2.4.2**. Percentage proliferation was calculated according to the manufacturer's instructions, using the calculation detailed below and the Molar extinction coefficients for alamarBlue at different wavelengths detailed in **Section 2.4.2**, **Table 2.10**. Proliferation assays were conducted in triplicate unless otherwise stated.

Percentage proliferation (%) = (O2 x A1) - (O1 x A2) / (R1 x N2) - (R2 x N1) x10

2.6 Fluorescence microscopy

2.6.1 Sample preparation and staining

2D monolayer and 3D spheroid cultures of prostate cancer cells either as monocultures or as co-cultures with HS5 stromal cells were grown in 96-well tissue culture plates as described in **Section 2.2.7.3**. Once incubated for the desired length of time, cell cultures were carefully washed 3x with PBS and fixed with 4% paraformaldehyde (PFA) for 15 minutes at room temperature. For immunofluorescence labelling, cells were again washed 3 times with PBS then permeabilised with 0.1% Triton-X 100 for 10 minutes at room temperature. Cells were then incubated with primary antibodies, the concentration of which was antibody dependent, in blocking buffer (3% BSA/PBS) overnight at 4^{o}C. Cells were subsequently washed 3x with PBS and incubated with species-specific polyclonal Alexa Fluor-488 secondary antibody (Abcam, UK) and incubated for 2-4 hours in standard cell culture conditions, protected from light. Cells were then washed 3x with PBS, 3x with ddH_2O, and counterstained with the nuclear stain Hoechst prior to imaging (Thermo Fisher, UK).

2.6.2 Confocal microscopy

A confocal laser scanning microscope (LSM710, ZEISS, Germany) was used. To excite green emission fluorochromes (Alexa Fluor-488), the argon-ion was used, to excite blue emission fluorochromes (Hoechst) the diode was used, and to excite red emission fluorochromes the helium-neon light was used (propidium iodide (PI)) **(Table 2.11).** Zen Black software Version 10 was used to process images, and scale bars were based on the known microscope pixel sizes for each objective (μm). The red-blue-green (RBG) setting was used to display coloured images.

Table 2.11. Excitation and emission wavelengths (nm) of each channel used for confocal microscopy and their emission colour. Ex.: excitation wavelength (nm), Em.: emission wavelength (nm); PI; propidium iodide.

Channel	Ex. (nm)	Em. (nm)	Em. colour	Light source
Alexa Fluor-488	488	520	Green	Argon
Hoechst	350	461	Blue	Diode
PI	493	636	Red	Helium neon

2.7 CRISPR/Cas9 genome engineering *in vitro*

2.7.1 Plasmid design

Oligos were designed using BLAST analysis to encode either the whole protein of interest or a variant sequence. Plasmids were then generated from chosen sequences using Sanger QuickPick Knockout gRNA (Sigma Aldrich, USA). Viral blue fluorescent protein (BFP) guide RNA (gRNA; vector: U6-gRNA/PGK-Puro-2A-BFP; Cat. HSANGERV) plasmids were purchased from Sigma Aldrich, USA. PsPAX-2 (Cat. 12260) lentiviral packaging protein and pCMV-vsvg (Cat. 8454) envelope protein were purchased from Addgene, USA.

2.7.2 Plasmid amplification

Knockout, gRNA (Sigma Aldrich, USA, Cat. HSANGERV), PsPAX-2 (Addgene, USA, Cat. 12260) and pCMV-vsvg (Addgene, USA, Cat. 8454)

plasmids were separately streaked onto agar plates and incubated at 37°C, 5% CO_2 in order to form single colonies. Miller's LB broth was prepared in 1 L conical flasks by dissolving 20 g Miller's LB Broth powder (Sigma Aldrich, USA, Cat. L3152) in 800 ml dH_2O, which was then autoclaved at 121°C for 95 minutes and stored at room temperature. After autoclaving, 200 µl ampicillin (Sigma Aldrich, USA, Cat. A0166) was added to each flask of LB broth. Once single colonies had formed (approx. 24 h), colonies were extracted and amplified in each separate flask of Miller's LB Broth and incubated at 37°C with constant agitation for 4 h to amplify. Once the LB broth had turned from transparent to cloudy, each flask was split into 50 ml centrifuge tubes and centrifuged at 10,000 g for 15 minutes. The supernatant was then discarded, and the pellet kept at 4°C for future purification. gRNA (Sigma Aldrich, USA, Cat. HSANGERV) and knockout plasmids were also separately streaked onto agar plates, and incubated at 37°C, 5% CO_2 in order to form single colonies. Single colonies were then selected and added to 3.5 ml of Miller's LB Broth in bacteria tubes and incubated at 37°C with constant agitation overnight (minimum 16 h) to amplify. The following day, amplified plasmids in 3.5 ml LB Broth were added to 10 ml LB Broth in 50 ml centrifuge tubes, and again amplified further at 37°C with constant agitation for 1-2 h. Once amplified, tubes were centrifuged at 10,000 g for 15 minutes. The supernatant was then discarded, and the bacterial cell pellet was kept at 4°C for future purification.

2.7.3 Plasmid DNA purification

DNA from amplified and harvested bacterial plasmids was purified using the NucleoBond Xtra Midi kit and protocol (Macherey-Nagel, USA, Cat. 740410.50). Cell pellets were first thawed at room temperature for 15 minutes prior to being resuspended in resuspension (RES) buffer and RNAse A (kept at 4°C). Resuspended plasmids were combined in one 50 ml centrifuge tube to a total volume 8 ml. 8 ml of lysis (LYS) buffer was then added, and tubes were incubated at room temperature for 5 minutes. Filters were equilibrated by pipetting 12 ml of equilibrating (EQU) buffer to the rim of the column filters, which were placed in 15 ml centrifuge tubes in a rack ready for the collection of lysates. 8ml of blue neutralisation (NEU) buffer was then added to the 50 ml tubes, and the solution was mixed thoroughly by inversion until colourless.

50 ml tubes were then centrifuged at 4,000 g for 15 minutes and the lysate loaded onto the NucleoBond Xtra Column Filters. Once the lysate had filtered through, the rims of the filters were washed with 5 ml EQU buffer. The filter was then removed, and the column washed with 8 ml wash (WASH) buffer. The plasmid was then eluted by adding 5 ml elution (ELU) buffer. 3.5 ml of room temperature isopropanol was then added to precipitate the eluted plasmid DNA and vortexed thoroughly. Tubes were then centrifuged at 4,000 g for 30 minutes at 4^{o}C, after which the supernatant was carefully discarded. 2 ml of room temperature 70% ethanol was added to the pellet, which was again centrifuged at 4,000 g for 5 minutes at room temperature (18-25^{o}C). Ethanol was carefully removed with a pipette tip, and the pellet left to dry at room temperature. The pellet was then reconstituted in 50 μl of Tris-EDTA (TE) buffer (Sigma Aldrich, USA, Cat. 93283) and DNA yield measured using a Nanodrop machine (Thermo Fisher, ND-1000, USA). DNA concentrations of >200.0 ng/μl were considered acceptable. Plasmids were diluted to 200.0 ng/μl in aliquots of 100 μl of TE buffer and stored at -20^{o}C for future use.

2.7.4 Cas9 transfection of HEK293T cells

Cas9 was transfected into HEK293Tcells using polybrene. HEK293T cells were purchased from ATCC (ATCC, USA, #CRL-11268). HEK293T cells are derived from human embryonic kidney cells taken from a foetus. They are a highly transfectable variation of the human embryonic kidney HEK293 cell line and contain the SV-40 T-antigen (ATCC, USA, #CRL-3216). HEK293T cells were seeded at a density of 2x10^{5} cells per well in a 6-well tissue culture plate under standard tissue culture conditions for 24 h prior to transfection. Healthy cells at a confluency of 40-80% are required for successful transfection. After 24 h, a mixture of complete medium with polybrene (Santa Cruz Biotechnology, USA, Cat. sc-134220) was prepared to a final concentration of 5 μg/ml. Original media was removed and this polybrene mix was added at a volume of 1.5 ml per well. Cas9 plasmids were then thawed at room temperature and mixed gently prior to being added to the culture medium. The plate was gently swirled to mix and incubated overnight. The medium containing polybrene was removed and 1.5 ml of complete medium added per

well, without polybrene. Cells were again incubated and routinely sub-cultured until needed.

2.7.5 Preparation of lentiviral particles

3 ml of Opti-MEM media (Thermo Fisher, USA, Cat. 31985070) was added to two separate 15 ml centrifuge tubes. Ps-PAX2 and p-CMV-vsvg vector plasmids were thawed at room temperature and mixed gently before both being added at a ratio of 1p-CMV-vsvg:2Ps-PAX2 to one of the 3 ml aliquots of Opti-MEM, which was then mixed by pipetting and separated into three separate 15 ml centrifuge tubes (1 ml of mix per tube). gRNA and knockout plasmids were all thawed at room temperature, before each being added separately to one of the newly aliquoted 1 ml Opti-MEM/vector mixes, to achieve a ratio of 1p-CMV-vsvg:2Ps-PAX2:3plasmid. 100 μl of lipofectamine 3000 (Thermo Fisher, USA, Cat. L3000015) was added to the second 3 ml aliquot of Opti-MEM, gently pipetted to mix, and incubated for 5 minutes at room temperature. 1 ml of this mix was then added to each of the 1 ml aliquots of Opti-MEM/plasmid, gently pipetted to mix, and incubated for 20 minutes at room temperature.

2.7.6 Lentiviral transfection of knockout plasmids into Cas9-positive HEK293T cells

Cas9-positive HEK293T cells at 50-75% confluency were transfected with knockout plasmids. First, the medium of the HEK293T cells cultured in a 100 mm dish was removed and replaced with 6 ml of DMEM containing 5% FBS only and no other supplements. Dishes were incubated at room temperature for 20 minutes before each of the 2 ml of Opti-MEM/lipofectamine/vector mixes were added to separate dishes, which were then incubated overnight. Medium was replaced with complete DMEM and dishes were again incubated overnight. Medium was collected into a 50 ml tube and 0.45 μm filtered. Complete DMEM was again added to cells, which were incubated and sub-cultured as needed.

2.7.7 Concentrating retroviral knockout stock

The Retro-X Concentrator kit (Clontech, USA, Cat. 631455) was used to concentrate retroviral stocks of STEAP2. The viral supernatant collected from the virus-producing HEK293T cells as described in **Section 2.7.6** was centrifuged at 270 g for 10 minutes to further remove cells and debris following filtration. The clarified supernatant was then transferred to a sterile 15 ml centrifuge tube and made up to achieve 1 volume of Retro-X concentrator with 3 volumes of clarified supernatant, mixed by gentle inversion and incubated overnight at 4^{o}C. The sample was centrifuged at 1,500 g for 45 minutes at 4^{o}C. The supernatant was discarded, and the pellet gently resuspended in 10 ml of complete DMEM, and aliquoted into 1 ml single-use samples which were then stored at -80^{o}C until needed.

2.7.8 Transfection of Cas9 plasmids into wild-type cells

Cas9 (Addgene, USA, Cat. 129727) was transfected into wild-type cells using polybrene. Once at ~50% confluency, wild-type cells were seeded at a density of 2x10^{5} cells per well in a 6-well tissue culture plate under standard tissue culture conditions for 48 and 24 h respectively prior to transfection. A mixture of complete medium with polybrene was prepared to a final concentration of 1 μg/ml. Original media was removed and this polybrene mix was added at a volume of 1 ml per well. Cas9 plasmids were thawed at room temperature and mixed gently prior to being added at a volume of 500 μl per well to the culture medium containing polybrene. The plate was gently swirled to mix and incubated overnight. An additional 1 ml of medium containing polybrene was then added per well, and cells were again incubated until ~50% confluency was reached.

2.7.9 Optimisation of selection antibiotic doses in wild-type cells

A selective antibiotic titration was carried out for each wild-type cell line. Wild-type cells were seeded at a density of 3x10^{5} per well in 6-well plates for 48 h, or until ~70% confluent. Cells were then exposed to a serial dilution of the selection antibiotics blasticidin (Sigma Aldrich, USA, Cat. SBR00022) and puromycin (Sigma Aldrich, USA, Cat. P9620) at 0.625, 1.25, 2.5, 5.0 and 10.0

μg/ml for 120 h. Cells were viewed under the microscope at 48 h and 120 h and any morphological changes were noted to determine toxicity. Based on these results, cell line specific doses of blasticidin and puromycin were chosen for the selection of Cas9-positive cells, and the selection of knockout-positive cells respectively. Medium was replaced with fresh selective antibiotic-containing medium every 3-4 days as needed.

2.7.10 Blasticidin selection of Cas9-activated cells

Cas-9 activated cells were selected via blasticidin selection, with the aim of using a sufficient dose to kill non-transfected cells. Medium containing polybrene was removed from the Cas9-transfected cells obtained in **Section 2.7.9** and replaced with complete medium containing the chosen dose of blasticidin for each cell line, as determined in **Section 2.7.9.** Once ~70% confluency was reached, cells were transferred from the 6-well plates to 100 mm petri dishes and sub-cultured until confluent.

2.7.11 Transfection of knockout plasmids into Cas9-activated cells

gRNA and knockout plasmids were transfected into wild-type cells using polybrene. Once at ~50% confluency, Cas9-activated wild-type cells were seeded at a density of $2x10^5$ cells per well in a 6-well tissue culture plate under standard tissue culture conditions for 24 h prior to transfection. A mixture of complete medium with polybrene was prepared to a final concentration of 1 μg/ml. Original media was removed and this polybrene mix was added at a volume of 1 ml per well. gRNA and knockout plasmids were then thawed at room temperature and mixed gently prior to being added at a volume of 500 μl per well to the culture medium containing polybrene. The plate was gently swirled to mix and incubated overnight. An additional 1 ml of medium containing polybrene was added per well, and cells were again incubated until ~70% confluency was reached. Medium containing polybrene was removed and replaced with complete medium containing the chosen dose of puromycin for each cell line, as determined in **Section 2.7.9.** Once ~70% confluency was reached, cells were transferred from the 6-well plates to 100 mm petri dishes and sub-cultured until confluent.

2.7.12 Isolation and amplification of single knockout clones

To isolate single colonies of positive knockout cells, cells were seeded at a density of 300 cells per plate in 96-well tissue culture plates, in 100 μl media supplemented with the appropriate dose of puromycin. Plates were then incubated for 10-14 days and routinely checked for single colony formations. Once formed, 6 single colonies per cell line, per knockout plasmid were transferred to 24-well tissue culture plates in 0.5 ml of complete medium supplemented with the appropriate dose of puromycin and incubated for a further 7 days. Microscopy was then used to assess morphology of knockout cells in comparison to their wild-type counterparts, and 3 colonies per cell line, per knockout plasmid that most closely resembled wild-type cells were transferred to 6-well tissue culture plates and incubated until ~70% confluent. Western blotting was performed to confirm successful target gene knockout, and stable clones were further expanded and routinely sub-cultured in 100 mm dishes in the same manner as their wild-type counterparts, with the addition of an appropriate dose of puromycin.

2.8 Protein expression

2.8.1 Protein extraction

Once cells had reached ~80% confluency, they were trypsinised, neutralised and centrifuged as described in **Section 2.2.7.1.** Old media was discarded, cells were washed twice in ice-cold PBS, centrifuged again at 270 g for 5 minutes, PBS discarded, and the cell pellet was resuspended in 1 ml of ice-cold radioimmunoprecipitation assay buffer (RIPA; Sigma Aldrich, USA, Cat. R0278). RIPA buffer was supplemented with the addition of one tablet of protease-inhibitor cocktail (Sigma Aldrich, USA, Cat. S8830) which was fully dissolved in 10 ml of buffer. Samples were transferred to pre-cooled 1.5 ml Eppendorf tubes and incubated on ice for 10 minutes. Cells were lysed by pipetting followed by a 10 s vortex and kept on ice for immediate use or transferred to -20^{o}C for long-term storage.

2.8.2 Protein quantification

For protein quantification, a Bradford assay was carried out in a 96-well clear-bottomed plate using the Coomassie based BioRad Protein Assay Kit (BioRad, USA, Cat. 5000002) according to manufacturer's instructions. 10 μl of protein per sample was loaded in duplicate alongside an albumin (BSA) standard series (0 – 2,000 μg/ml), as displayed in **Figure 2.4.**

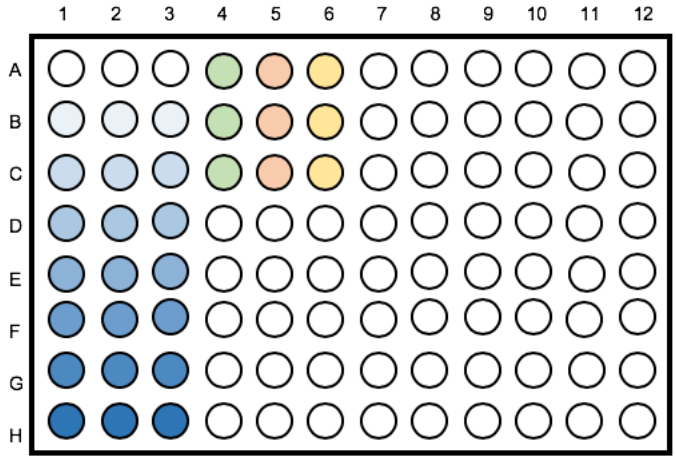

Figure 2.6. The Bradford assay for protein quantification. A 96-well plate containing the protein standard (albumin) with a known concentration range (0 – 2,000 μg/ml) is illustrated in blue. Each standard concentration was loaded in triplicate horizontally from the lowest (0 μg/ml at A1 – A3) to the highest concentration (2,000 μg/ml at H1 – H3). Samples were loaded vertically in triplicate, as illustrated in green, orange and yellow.

The albumin standard (BSA) was prepared according to the supplier's instructions. Absorbance was read at A = 595nm to determine protein concentration using a fluorescence plate reader (POLARstar, BMG Labtech, USA). To calculate the sample loading concentration, a protein standard curve of known concentration plotted against the measured absorbance with the mathematical equation (y = mx + c) was generated. Using the protein standard, a line of best fit was displayed with a minimum r^2 value of 0.95 **(Figure 2.5).** The protein concentration of each sample was calculated using the equation of the line of best fit and adjusted by dilution with RIPA buffer to match the concentration of the sample with the lowest protein concentration.

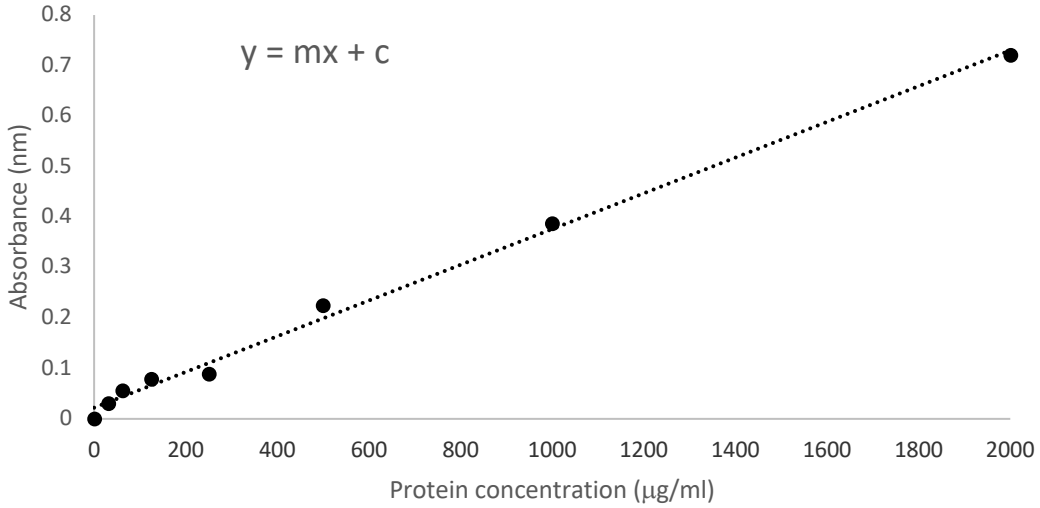

Figure 2.7. Standard curve generated from a Bradford assay for protein quantification showing proteins of a known concentration (μg/ml) against absorbance (nm). Following the Bradford assay for protein quantification a protein standard curve of known concentration 0 – 2,000 μg/ml was plotted against the measured absorbance at A = 595 nm for which the equation y = mx + c is displayed. $r^2 \geq 0.95$.

2.8.3 Sodium-Dodecyl-Sulphate polyacrylamide gel preparation

As STEAP2 has a molecular weight of 56 kDa, a 12% resolving gel was prepared as detailed in **Table 2.12.** Glass plates and plastic well-combs were wiped with 70% ethanol and dried before being assembled into the casting stand. First, the 12% resolving gel was prepared (**Table 2.12**) and pipetted between the glass plates, leaving 2 cm at the top for the stacking gel, and left to solidify at room temperature for 1 h. A small amount of ethanol was pipetted between the glass plates to aid in polymerisation and ensure no bubbles formed at the top of the gel. Once solidified, the ethanol was carefully removed using filter paper and flushed with water. A 4% stacking gel (**Table 2.13**) was prepared and pipetted on top of the resolving gel, before an appropriately sized comb was carefully inserted to prevent bubble formation and the gel was left to solidify at room temperature for an additional 30 minutes. Once polymerised, gels were wrapped in moistened paper towels and placed in

small plastic pouches and stored at 4°C until needed. Gels were used within 7 days of preparation.

Table 2.12. Resolving gel preparation for SDS-PAGE. A 12% resolving gel was prepared using the reagents detailed below. A total volume of 10 ml was prepared for each gel.

Reagent	Volume (ml)
ddH_2O	0.8
30% Acrylamide	4.0
1.5M Tris-HCL, pH 8.8	5.0
SDS 10%	0.15
10% APS	0.1
TEMED	0.01

Table 2.13. Stacking gel preparation for SDS-PAGE. A 4% stacking gel was prepared using the reagents detailed below. A total volume of 5 ml was prepared for each gel.

Reagent	Volume (ml)
ddH_2O	2.1
30% Acrylamide	0.8
1M Tris-HCL, pH 6.8	3.0
SDS 10%	0.15
10% APS	0.06
TEMED	0.006

2.8.4 Sodium-Dodecyl-Sulphate polyacrylamide gel electrophoresis

Proteins were thawed on ice and denatured for 5 minutes using a heating block set at 90°C (Thermo Fisher, USA, Cat. 88870001) and kept on ice until use. One casted gel and one buffer dam (BioRad, USA, Cat. 1653130) for balance were cleaned with 70% ethanol, they were assembled either side of the electrophoresis cassette and clamped into place. The cassette was placed into the buffer chamber and running buffer was first slowly poured in between the gel and buffer dam to remove and bubbles, followed by the rest of the

chamber. The plastic well combs were then carefully removed from the casted gel. A Precision Plus Protein™ Dual Color Standards pre-stained molecular weight ladder (BioRad, USA, Cat. 1610374) was added into well number 1 of the gel, at a volume of 15 μl. Prior to loading onto the gel, 15 μl of each protein sample was mixed with 3 μl of GeneRuler 100 bp DNA Ladder (6X) loading dye (Thermo Fisher, USA, Cat. SM0244) on ice. 15 μl of each of this sample mix was loaded into separate wells of the gel, from well number 2 onwards. To ensure an equal running of the gel, any empty wells were filled with 10 μl of SDS 10% buffer (BioRad, USA, Cat. 1610416). The SDS-PAGE was run at 120 V until the protein samples had all stacked into a horizontal line (approx. 20 minutes). Once the protein samples had entered the resolving gel, the voltage was increased to 150 V for 45 minutes.

2.8.5 Membrane transfer

A Mini Trans-Blot® Cell cassette (BioRad, USA, Cat. 1703931) was prepared as demonstrated in **Figure 2.6.** The central core was placed in the transfer tank and filled with ice whilst the cassette was prepared. First, a sheet of trans-blot filter paper (BioRad, USA, Cat. 1703956) was cut into six pieces approx. 10 cm wide using a guillotine. A plastic transfer tray was filled with transfer buffer and two foam pads (BioRad, USA, Cat. 1703933) and the six pieces of filter paper were soaked in the transfer buffer. A transfer cassette was opened in the tray containing transfer buffer, with the black (negative; -ve) side at the bottom of the tray. One piece of soaked foam padding was placed on top of the back of the cassette, followed by three pieces of filter paper. After the SDS-PAGE, the cassette was carefully opened with a glass-plate opener and the stacking gel removed. The gel was then carefully placed on top of the three pieces of filter paper in transfer buffer to keep moist. A nitrocellulose membrane for protein blotting (BioRad, USA, Cat. 1620115) was manually cut to the desired size to match that of the SDS gel. A small plastic tray was filled with 5 ml of 100% methanol and the nitrocellulose membrane was added for 30 s to activate. Tweezers were used to remove the nitrocellulose membrane and place it on top of the gel, followed by the remaining three pieces of filter paper and then the second piece of foam padding. A roller was used to remove any bubbles before the cassette was clamped together. The transfer tank was

emptied of ice and the cassette was loaded into place. The middle of the cassette was first filled with transfer buffer, followed by the rest of the tank up to the 2 plates mark. Membrane transfer was carried out at 60 V for 150 minutes at room temperature, or overnight at 4°C.

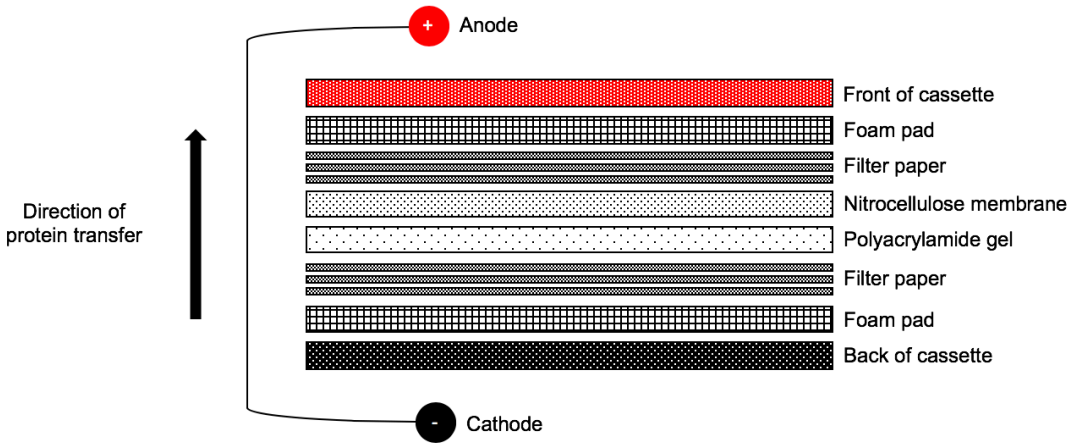

Figure 2.8. Diagram showing the assembly of a transfer cassette assembly utilised for the transfer of proteins from polyacrylamide gel onto a nitrocellulose membrane. From bottom (black; cathode, -ve) to top (red; anode, +ve): One sponge pad is placed at the bottom of the blotting sandwich, followed by three pieces of filter paper, polyacrylamide gel, nitrocellulose membrane, another three pieces of filter paper and another sponge pad on top.

2.8.6 Blocking and antibody incubations

Once the membrane transfer was complete to limit any non-specific binding of the primary antibody, the membrane was placed into a small plastic tray containing 5% blocking buffer (5.0 g milk powder in 10 ml PBS-T) and placed on a plate rocker for 30 minutes at room temperature. The membrane was then washed 3x 5 minutes with PBS-T and cut horizontally dependent on the molecular weight of the protein of interest (**Figure 2.7**). The top right-hand corner of the membrane sections was cut to be able to determine their orientation. Membrane sections were incubated with their respective antibodies for detection of STEAP2 and the house-keeping loading control GAPDH (1:1,000 / 3% BSA) on a plate rocker overnight at 4°C. Membranes were again washed for 3x 5 minutes with PBS-T on a plate rocker to remove any residual primary antibody and incubated with secondary anti-rabbit HRP

antibody (1:5,000 / 5% blocking buffer) for 2 h on a plate rocker at room temperature, or overnight at 4°C.

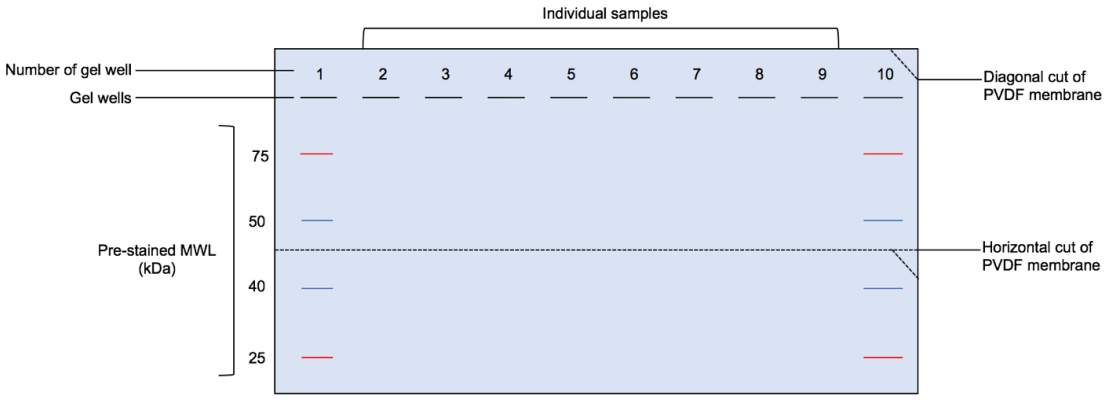

Figure 2.9. Diagram showing the cuts made to the nitrocellulose membrane following membrane transfer prior to antibody incubation. Vertical, short lines = gel wells; numbers = number of gel wells; well 1 + 10 = dual colour precision MWL (kDa) with red and blue short, vertical lines which represent the relevant molecular weight bands for this study. Horizontal line at approx. 45kDa indicates the cut separating STEAP2 (56 kDa) from housekeeping loading control GAPDH (37 kDa). Diagonal line in top-right corner indicates the cuts to determine orientation.

2.8.7 Protein detection and analysis

A 1:1 mix of Clarity ECL Western Substrate reagent (BioRad, USA, Cat. 1705060) was prepared in a 1.5 ml brown Eppendorf tube to keep the solution protected from light, as per the manufacturer's recommendations. After incubation, membranes were washed for 3x 5 minutes with PBS-T on a plate rocker to remove any residual secondary antibody. The membranes were placed onto a Chemisorbs tray and covered with 500 µl of ECL developing solution for 30 s. The ChemiDocXRS+ (BioRad, USA) was used for image acquisition, and ImageLab software, Version 6.0.1 was used for analysis. Membranes were stored in PBS-T at 4°C for up to 3 days to support any future re-probing.

2.9 Cell migration assay

Once cells had reached 80% confluency, media was replaced for 24 h with serum-free cell line specific media. Cells were then trypsinised, resuspended and adjusted to a desired cell concentration. One cell culture insert (IBIDI, Germany, Cat. 80209) was placed in the centre of each well of a 12-well plate, 70 μl of cell suspension was added to each chamber and cells were left to adhere in standard tissue culture conditions for 24 h. Media and inserts were removed following a period of incubation and cells were washed with PBS to remove cell debris, before fresh complete media was applied. The time taken to close the gap created was monitored using an inverted light microscope (Invitrogen, EVOS XL Core, USA) every 24 h until the wound created by the silicone insert had closed. Media was replaced every 3 days. The experiment was conducted in triplicate unless otherwise stated.

2.10 Invasion assay

To investigate the role of various stimuli in mediating invasive cell behaviour, Transwell plate inserts (polycarbonate, 8.0 μm pore size; Sigma Aldrich, USA, Cat. CLS3422) were used. Prior to each invasion assay, cells were trypsinised, resuspended and seeded in 6-well tissue culture plates at a desired density and left to adhere in standard cell culture conditions for 48 h. Cells were then serum starved in serum-free media (SFM) for 24 hours. Prior to seeding cells, 20 μl of GFR Matrigel (1:5 dilution/SFM; Sigma Aldrich, USA, Cat. E1270) was applied to the Transwell insert, one of which was placed in each well of a 12-well tissue culture plate and left to polymerise for 1 hour in standard cell culture conditions. Cells were trypsinised from the 6-well plates, resuspended and adjusted to a desired seeding density and pipetted onto the Matrigel-coated Transwell insert in 250 μl of SFM. Subsequent to the addition of cells, 600 μl of complete media was added to the lower chamber, as depicted in **Figure 2.8**, and the inserts were incubated for 48h in standard cell culture conditions to allow cell invasion to occur. Cell invasion was then quantified by staining with crystal violet (Sigma Aldrich, USA, Cat. V5265). The Transwell inserts were removed, and invaded cells were fixed with 100% methanol for 15 minutes at room temperature and allowed to air dry. They

were then stained with a crystal violet staining solution (0.5% crystal violet in 100% methanol) for 30 minutes to allow for the visualisation of cells. The non-invaded cells on the upper surface of the Transwell inserts were removed with a cotton swab moistened with PBS. The inserts were then washed in purified water and left to air dry for 1 hour. Invaded cells were visualised using an inverted light microscope (Invitrogen, EVOS XL Core, USA) at 10x magnification. Images were taken of different planes of each insert and the experiment was conducted in triplicate unless otherwise stated.

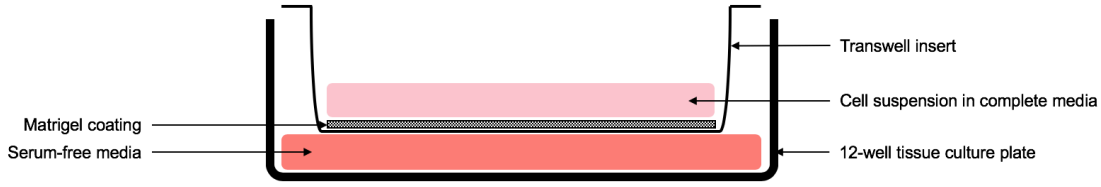

Figure 2.10. Schematic representation of the side profile of a Transwell insert situated in one well of a 12-well tissue culture plate for invasion assays. Transwell plate inserts were coated with Matrigel and left to polymerise in individual wells of a 12-well tissue culture plate. Cells were suspended in serum-free media and added to the top chamber. Complete media was added to the bottom chamber.

2.11 Statistical analysis

Statistical analysis was performed using GraphPad Prism version 8 for iOS. Data was considered statistically significant when a p-value of < 0.05 (*), p-value < 0.01 (**) or a p-value of < 0.001 (***) or p-value < 0.0001 (****) was obtained, which were annotated within the respective figures.

Chapter 3

Development and characterisation of 3D *in vitro* prostate cancer-stromal cell co-culture models

3.1 Introduction

STEAP family members are known to be over-expressed in multiple cancer types, with STEAP2 particularly over-expressed in prostate cancer (see **Chapter 1, Section 1.5.2;** Gomes *et al.,* 2012). Previous studies into the expression of STEAP2 have shown that high protein levels are present in metastatic prostate cancer cell lines (bone metastatic PC3 cells and lymph node metastatic LNCaP calls) in comparison to lower expression levels seen in normal epithelial prostate cells lines such as PNT2 (Burnell *et al.,* 2018; Whiteland *et al.,* 2014). However, such studies have not assessed the gene expression levels of all four *STEAP* family member across multiple metastatic prostate cancer cell lines of different origins.

Two-dimensional, flat, monolayer cell culturing has long been the standard culture method in cancer research since its development in 1907 (Breslin & O'Driscoll, 2013; Harrison *et al*., 1907). The main advantages of 2D cell culture techniques include convenience, low costs and ability to maintain cell viability (Breslin & O'Driscoll, 2016; Duval *et al*., 2017). Cells grown in 2D are able to proliferate at a continuous rate, provided they have the space to do so, and as such provide an easily reproducible platform for *in vitro* drug testing (Breslin & O'Driscoll, 2013 & 2016; Edmonson *et al*., 2014; Lin & Chang 2008). Monolayers of cells also show little variance in cell morphology over time and are able to receive a constant supply of nutrients in the growth medium (Breslin & O'Driscoll, 2013; Duval *et al*., 2017). Furthermore, 2D cell culturing is advantageous when performing high-throughput assays, due to ease of cell harvesting and sub-culturing (Breslin & O'Driscoll, 2013; Duval *et al*., 2017). However, differences between the properties of cells grown in 2D cultures *in*

vitro compared to equivalent cells *in vivo* have been noted (Breslin & O'Driscoll, 2013). A major limitation of 2D monolayer cultures grown on a flat solid surface is their lack of stroma, which is of vital importance when modelling human cancers, particularly prostate cancer, in which the stroma plays a critical role in cancer dissemination and metastatic potential (Chung, 2003; Langley *et al*., 2011; Lovitt *et al*., 2014). Cells grown in 2D cultures also lack the complex architecture present in complex 3D tissues, such as the cell-cell or cell-ECM interactions which are only present in 3D structures (Donglai *et al*., 2017; Gialeli *et al*., 2011; Lovitt *et al*., 2014). Recent advances in cell culturing techniques have highlighted the importance of the tumour microenvironment in cancer development and progression (Nath & Devi, 2016). The tumour microenvironment (TME) is composed of multiple cell types including transformed epithelial cells, cancer-associated fibroblasts (CAFs), tumour infiltrating lymphocytes (TILs), mesenchymal stem cells (MSCs) and endothelial cells (Nath & Devi, 2016; Quail & Joyce, 2013). These various cell types interact with cancer cells and exert an effect on multiple biological characteristics such as proliferation, migration, invasion and resistance to therapeutic agents (Nath & Devi, 2016; Quail & Joyce, 2013; Smith & Kang, 2013). As 2D models therefore fail to fully represent the complex pathophysiology of tumour cells, and in order to overcome the limitations surrounding 2D cell culturing, the concept of tumour spheroids was developed to bridge the gap between *in vitro* and *in vivo* research (Donglai *et al*., 2017; Hirschhaeuser *et al*., 2010; Lovitt *et al*., 2014). Various methods for 3D culture exist, including the use of scaffold-based systems such as Matrigel or Jellagen products, or growth on agarose supports, to provide a platform for cells to grow in a semi-solid matrix. These matrices allow for the influence of external physical factors to be observed on cell growth and signalling (Fong *et al*., 2016; Greiner *et al*., 2012; Muir *et al*., 2006; Thoma *et al*., 2014). Other 3D culture methods include liquid-based approaches such as the hanging drop method or rotation-based culture methods which prevent cell adhesion to a substrate and instead encourage 3D cell cluster formation (Fong *et al*., 2016; Greiner *et al*., 2012; Muir *et al*., 2006; Thoma *et al*., 2014).

Previous studies have successfully generated and maintained 3D cancer cell spheroid structures to create a more physiologically relevant model of assessing cancer traits (Fong *et al*., 2016; Muir *et al*., 2006; O'Connor *et al*., 2007; Sung *et al*., 2008; Zhang *et al*., 2011). Spheroids are spherical cell colonies which self-form spontaneously in environments where cell-cell interaction is superior to the cell-substrate interactions of 2D monolayer cultures (Friedrich *et al*., 2009; Ingram *et al*., 1997; Kunz-Schughart *et al*., 2004). Spheroids provide more relevant physiological tumour models than 2D cell culturing techniques as they naturally mimic avascular tumours and micrometastases, generating more meaningful results (Hirschhaeuser *et al*., 2010; Nath & Devi, 2016). These structures have inherent metabolic and proliferative gradients and share many physiological characteristics with *in vivo* models such as cell-cell and cell-matrix interactions, altered gene expression and signalling pathway profiles, heterogeneity and structural complexity (Friedrich *et al*., 2009; Hirschhaeuser *et al*., 2010; Kunz-Schughart *et al*., 2004; Nath & Devi, 2016). Mechanistic investigations can also be performed to observe molecular and cellular events, allowing for the validation of molecular targets in drug development through the discovery of novel intra- and intercellular signalling networks (Thoma *et al*., 2014). As prostate cancer predominantly metastasises to the bone which is a leading cause for morbidity, a co-culture system of cancerous and bone marrow-derived stromal cells would provide a relevant model for studying aggressive prostate cancer traits (Taichman *et al*., 2007; Sun *et al*., 2007).

PC3 prostate cancer cells and HS5 bone derived stromal cells have been proven to be a successful combination to grow as 3D co-cultures for observing cellular interactions (Windus *et al*., 2013; Zhang *et al*., 2011). Previously, the two cell lines have been co-cultured in 3D models generated on a laminin-rich extracellular matrix (lrECM), which promotes the growth of cancer cells in 3D structures (Lovitt *et al*., 2013 & 2014; Muranen *et al*., 2012; Windus *et al*., 2013). This matrix allowed for investigation of cell-to-cell interactions and crosstalk between the two different cell types, demonstrating the altered expression of certain cellular components by integrins such as E-cadherin. (Windus *et al*., 2013). From this study, it was evident that culturing prostate

cancer and stromal cells in 3D can alter gene and protein expression profiles, yet it remains unknown as to whether such differences between 2D and 3D cultures can aid in the identification of novel drug targets, or sensitivity to chemotherapeutic agents (Lovitt *et al*., 2014; Windus *et al*., 2013). This study solely focussed on androgen-independent prostate cancer cell lines PC3 and DU145, and as such was not representative of an androgen-sensitive prostate cancer model (Windus *et al*., 2013). Therefore, applying 3D cell culture to androgen responsive prostate cancer cell lines in co-culture with bone stromal cells would provide a more representative model of the disease.

Although the advantages of 3D tumour spheroid models have been widely studied, their production does come with its own challenges, mainly surrounding the formation and maintenance of stable, viable models. Some of the main concerns regarding spheroid development are efficiency of consistent and reproducible spheroid formation, control of spheroid size, longevity of spheroid culture, and, where co-culture systems are involved, uniform distribution of different cell types throughout the model (Edmondson *et al*., 2014; Mehta *et al*., 2012; Ryu *et al*., 2019). These challenges are therefore the main hurdles when developing and applying such alternative models in cancer-based research programmes, and highlights the need for developing a robust model for generating viable 3D prostate cancer-bone stromal co-culture spheroids. Work within the wider Swansea research group applied 3D spheroid culture techniques to PC3 prostate cancer cells, providing a proof-of-concept study which will be utilised in this thesis and applied to multiple prostate cancer cell lines and co-culture models (Wang, 2019).

The aim of this chapter was therefore to develop and optimise 3D models of prostate cancer cells, as mono- and co-culture systems with bone stromal cells. This chapter also aimed to determine a platform for analysis of the STEAP signalling molecules through evaluating the expression of STEAP family members across a panel of multiple prostate cancer cell lines not previously assessed. The objectives were to:

1. Determine the expression of STEAP family members in a panel of prostate cancer cell lines;

2. Develop and optimise the growth of 3D prostate cancer models by assessing the effects of varying seeding density on viability over time;
3. Determine cell death in 3D models through fluorescent microscopy;
4. Identify the most appropriate ratio of prostate cancer-stromal cells in co-culture models by assessing viability over time.

3.2 Materials and methods

3.2.1 Cell culture

3.2.1.1 2D monolayer cells

The four prostate cancer cell lines C4-2B, DU145, LNCaP and PC3, the normal epithelial cell line PNT2 and the stromal cell line HS5 were routinely cultured as described in **Chapter 2, Section 2.2.7.1.** For absorbance-dependent endpoint analyses, cells were grown in phenol-red free DMEM supplemented with 10% FBS, 1% L-glutamine and 1% P/S (Thermo Fisher, UK).

3.2.1.2 3D cell spheroids

Cells were counted as described in **Chapter 2, Section 2.2.7.2** and seeded at a desired density onto agarose coated 96-well tissue culture plates, as described in **Chapter 2, Section 2.2.7.3.**

3.2.2 Detection of STEAP family members

3.2.2.1 qRT-PCR

Four prostate cancer cells C4-2B, DU145, LNCaP and PC3 and the normal prostate epithelial cell line PNT2 were cultured to ~70% confluency. RNA was extracted, cDNA synthesised, and qRT-PCR carried out as described in **Chapter 2, Section 2.3**. Cells were probed for all four *STEAP* family members with *GAPDH* as the housekeeping control using the primers detailed in **Chapter 2, Section 2.3.3, Table 2.8**. The results were subsequently analysed as described in **Chapter 2, Section 2.3.4.**

3.2.3 3D Prostate cancer cell spheroid stability and viability over time

3.2.3.1 Measurement of size over time (monoculture 3D spheroids)

Cell suspensions of 2,500, 5,000, 7,500 and 10,000 prostate cancer cells per 100 μl culture media were prepared as described in **Chapter 2, Section 2.2.7.2** and seeded into an agarose-coated 96-well tissue culture plate, as described in **Chapter 2, Section 2.2.7.3.** Every 24 h for 5 days spheroids were imaged using an inverted light microscope (AxioCam ERC55, Zeiss, Germany), and their diameter (μm) measured. Media was replenished every 2-3 days as required. The average size of the spheroids was reported as mean diameter ± standard deviation. Measurements were taken in triplicate.

3.2.3.2 Cell viability (monoculture 3D spheroids)

Cell suspensions of 2,500, 5,000, 7,500 and 10,000 prostate cancer cells per 100 μl culture media were prepared as described in **Chapter 2, Section 2.2.7.2** and seeded into an agarose-coated 96-well tissue culture plate, as described in **Chapter 2, Section 2.2.7.3.** Every 24 h for 5 days, cell viability was assessed by MTT assay as described in **Chapter, 2, Section 2.4**. Absorbance was read at A = 570 nm using a POLARstar plate reader (POLARstar, BMG Labtech, UK). The cell viability assay was performed in triplicate unless otherwise stated.

3.2.3.3 Measurement of size over time (co-culture 3D spheroids)

Prostate cancer cells and HS5 cells were counted as described in **Chapter 2, Section 2.2.7.2** and normalised to ensure the same number of each cell line were present in each cell suspension. Based on the results of microscopy and size over time obtained in **Section 3.2.3,** the most viable initial seeding density was determined for each prostate cancer cell line. Varying ratios of prostate cancer (PCa)-stromal cells – 1PCa:1HS5, 1PCa:2HS5 and 2PCa:1HS5 – were created by mixing the appropriate volume of cells by pipetting. This co-culture mix was seeded onto an agarose-coated 96-well tissue culture plate, as described in **Chapter 2, Section 2.2.7.3,** to the total number of cells per

well determined to be the most viable seeding density for each cell line. Every 24 h for 5 days spheroids were imaged using an inverted light microscope (AxioCam ERC55, Zeiss, Germany), and their diameter (μm) measured. Media was replenished every 2-3 days as required. The average size of the spheroids was reported as mean diameter ± standard deviation. Measurements were taken in triplicate.

3.2.3.2 Cell viability (co-culture 3D spheroids)

Co-culture 3D spheroids of prostate cancer and stromal cells were prepared in various ratios as described in **Section 3.2.3.3** and seeded into an agarose-coated 96-well tissue culture plate, as described in **Chapter 2, Section 2.2.7.3.** The MTT assay has successfully been used to assess the viability of 3D cell spheroid models across a variety of cancer types, including but not limited to; breast, liver and prostate (Abuela *et al*., 2015; Fotakis & Timbrell, 2006; Rhee *et al*., 2001; Risbud *et al*., 2012; Takagi *et al*., 2007). Every 24 h for 5 days, cell viability was assessed by MTT assay as described in **Chapter, 2, Section 2.4**. Absorbance was read at A = 570 nm using a POLARstar plate reader (POLARstar, BMG Labtech, UK). The cell viability assay was performed in triplicate unless otherwise stated.

3.2.3.5 Cell proliferation (co-culture 3D spheroids)

Co-culture 3D spheroids of prostate cancer and stromal cells were prepared in various ratios as described in **Section 3.2.3.3.** Every 24 h for 5 days, cell proliferation was assessed by alamarBlue assay as described in **Chapter, 2, Section 2.5.1**. Absorbance was read at A = 570 nm and A = 600 nm using a POLARstar plate reader (POLARstar, BMG Labtech, UK). The cell proliferation assay was conducted in triplicate unless otherwise stated.

3.2.4 Fluorescent Microscopy

3.2.4.1 Sample preparation and staining for live/dead imaging

Optimal ratios of prostate cancer-stromal cell co-culture models were determined from spheroid size over time measurements and cell viability

assay results and used for subsequent fluorescent microscopy. The following samples were prepared in the absence of light. Co-culture 3D spheroids of prostate cancer and stromal cells were prepared in 96-well tissue culture plates as described in **Section 3.2.3.3.** and incubated to form spheroids. The following antibodies were applied for live/dead cell imaging: nuclear stain Hoechst (1:100, Thermo Fisher, UK) and chromosomal stain propidium iodide (PI; 1:500, BioLegend) Cells were incubated for 15 minutes on a plate rocker at room temperature, protected from light. Staining was carried out 1, 3 and 5 days after seeding.

3.2.4.2 HS5 cell preparation for imaging of stromal cell integration

Approximately 5 x 10^5 HS5 cells were seeded per well of a 6-well tissue culture plate in phenol-red free, serum-free DMEM (Thermo Fisher, UK) for 24 h. Media was replaced with phenol-red free, supplemented DMEM, to which stromal-specific antibody 1 (STRO-1) (1:200, R&D, UK) was added and cells were incubated for 24 h protected from light. Subsequently, cells were washed free of the primary STRO-1 antibody (3 x PBS), and secondary antibody human antibody Alexa Fluor-488 (1:1,000, Abcam, UK) was added in phenol-red free, supplemented DMEM and cells were incubated at room temperature on a plate rocker for 2 h protected from light.

3.2.4.3 Co-culture sample preparation and staining for imaging of stromal cell integration

Co-culture 3D spheroids of prostate cancer and pre-stained stromal cells prepared in **Section 3.2.4.1** were prepared in 96-well tissue culture plates as described in **Section 3.2.3.3.** and incubated to form spheroids. Spheroids were carefully washed (3 x PBS) and fixed with 4% paraformaldehyde (PFA) for 15 minutes at room temperature. For immunofluorescence labelling, cells were again washed (3 x PBS) and permeabilised with 0.1% Triton-X 100 for 10 minutes at room temperature. Hoechst (1:100, Thermo Fisher, UK) was added as a nuclei counterstain. Cells were incubated for 15 minutes on a plate rocker at room temperature, protected from light. Staining was carried out 1, 3 and 5 days after seeding.

3.2.4.4 Fluorescent imaging analysis and image processing

For fluorescent microscopical analysis, a confocal laser scanning microscope (LSM710, ZEISS, Germany) was used (**Chapter 2, Section 2.6**). The analysed channels and emission wavelengths (nm) were blue (405 nm) for the nuclei and red (543 nm) for dead cells. Zen Black software Version 10 was used to process images, and scale bars were based on the known microscope pixel sizes for each objective (μm). The red-blue-green (RBG) setting was used to display coloured images.

3.2.5 Statistical analysis

Statistical analysis was performed using GraphPad Prism version 8 for iOS, using the one-way ANOVA *post-hoc* Dunnett test. Data was considered statistically significant when a p-value of < 0.05 (*), p-value < 0.01 (**) or a p-value of < 0.001 (***) or p-value < 0.0001 (****) was obtained, as annotated within the respective figures.

3.3 Results

The aim of this chapter was to determine the optimal conditions for generating the most viable prostate cancer-stromal cell spheroids in order to develop a platform for subsequent analysis, with relevance to *STEAP2* expression. The aim was addressed by determining the expression levels of *STEAP* family members in four human prostate cancer cell lines in comparison to the normal prostate epithelial cell line PNT2. The properties of four prostate cancer cell lines when cultured as 3D spheroids over time was then evaluated by assessing spheroid size, viability and proliferation, in both mono- and co-culture models.

3.3.1 *STEAP2* is highly expressed in androgen-sensitive prostate cancer cell lines

To determine the expression of the four *STEAP* family members, a panel of human prostate cancer cell lines were screened by qRT-PCR. The normal prostate epithelial cell line PNT2 was used for comparison.

Upon analysis of gene expression of the four *STEAP* family members, *STEAP2* was found to have the highest increase in expression in 3 of the 4 cell lines screened (>2-fold increase). Moreover, the highest levels of *STEAP2* were observed in androgen-sensitive cell lines; LNCaP and C4-2B, which exhibited 264.7-fold and 53.5-fold increases in expression respectively **(Figure 3.1)**. *STEAP1*, *STEAP3* and *STEAP4* all showed a decrease in expression in all prostate cancer cell lines when compared to the normal PNT2 cell line, with the exception of *STEAP1* in LNCaP cells (31.7-fold increase); however, this change in expression did not reach significance. qRT-PCR analysis of *STEAP* family expression therefore demonstrated that *STEAP2* is highly expressed in androgen-sensitive prostate cancer cell lines and thus, could be a viable drug target in prostate cancer.

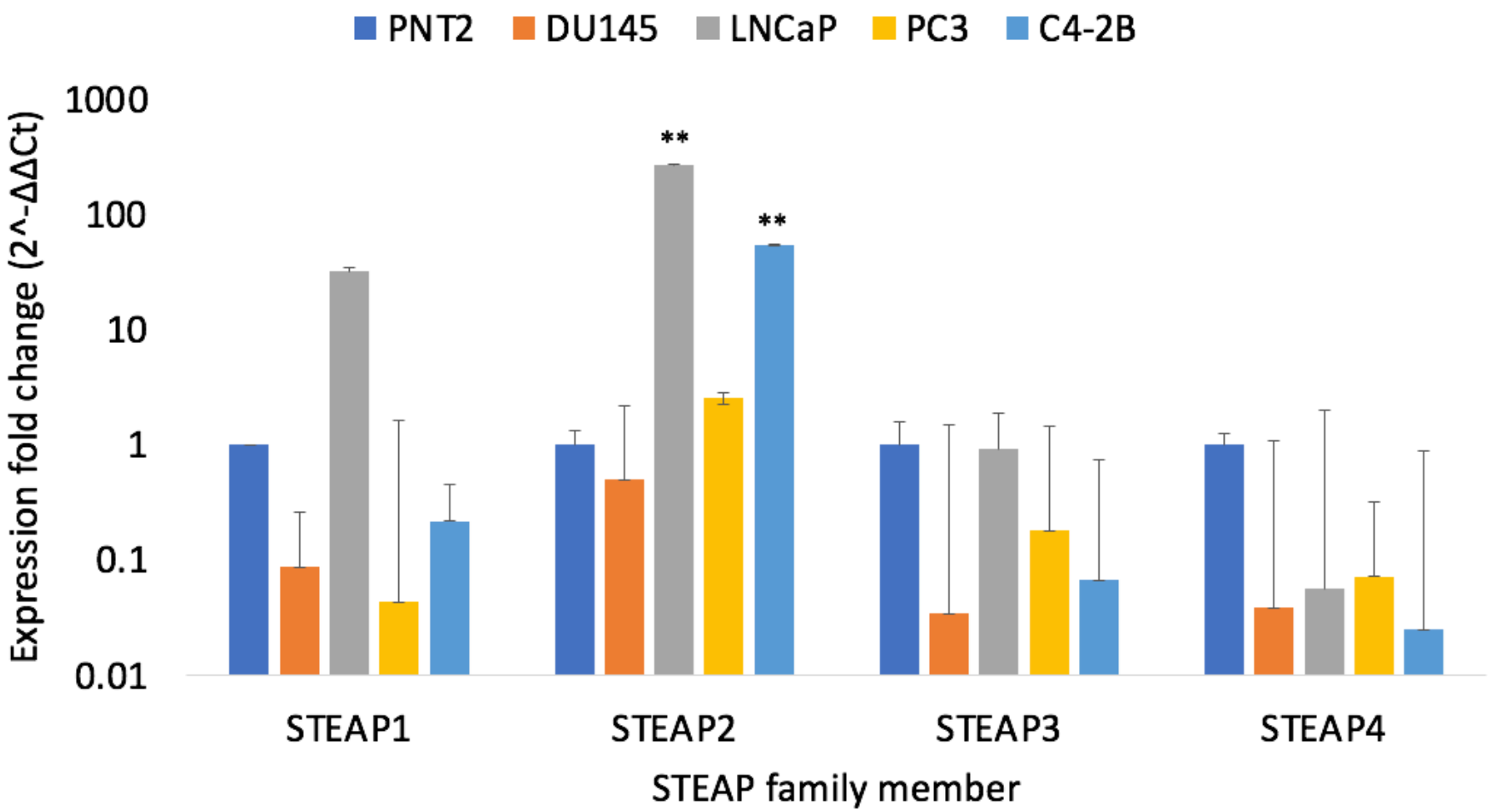

Figure 3.1. Fold changes in *STEAP1-4* gene expression in four human prostate cancer cell lines. qRT-PCR of *STEAP1-4* to establish gene expression levels in four human prostate cancer cell lines. Gene expression fold changes are normalised to the normal prostate epithelial cell line PNT2, which was defined as having an expression value of 1.0. GAPDH was used as the housekeeping gene. An ANOVA post-hoc Dunnett test was performed for statistical analysis. Error bars denote S.E.M. p-value < 0.05 (*), p-value < 0.01 (**). (N = 3).

3.3.2 Development of a 3D *in vitro* monoculture prostate cancer model

3.3.2.1 Size of 3D monoculture prostate cancer spheroids reduces over time

To monitor the effects of culturing prostate cancer cells in 3D on the size of the resultant spheroids over time, the diameter of the spheroids associated with different initial seeding densities were measured over 5 days. To determine the difference in spheroid size over time, spheroids were normalised to spheroids formed on day 1 for each seeding density.

In PC3 cell spheroids, no significant changes in spheroid size were observed at any seeding density until 4 days after seeding, when a significant decrease in the size of spheroids seeded with 7,500 cells per well was seen on days 4 and 5 (-100 μm and -150 μm diameters respectively; $p \leq 0.05$; **Figure 3.2A**). In DU145 cell spheroids, significant decreases in spheroid size were observed across all initial seeding densities from days 2 to 5, with the most significant decreases observed in all spheroids seeded with ≥ 5,000 cells per well on days 4 and 5. The largest decrease in size observed in spheroids seeded with 7,500 cells on day 4, which remained unchanged on day 5 (-300 μm; $p = 0.0001$; **Figure 3.2B**). LNCaP cell spheroids followed a similar growth curve to DU145 cell spheroids, with significant decreases in spheroid size observed across all initial seeding densities from days 3 to 5, with the most significant decreases observed in all spheroids seeded with 7,500 and 10,000 cells per well on day 5 (-300 μm & -150 μm respectively; $p = 0.0001$; **Figure 3.2C**). A significant decrease in spheroid size was observed when comparing C4-2B spheroids seeded with 10,000 cells on day 5 to spheroids on day 1 (-200 μm; $p = 0.0001$; **Figure 3.2D**). These data implied that the optimal initial seeding density to generate stable sized spheroids was cell line dependent (**Figure 3.2**). The optimal seeding density for each cell line was determined as follows; PC3: 10,000 cells per well, DU145: 5,000 cells per well, LNCaP: 10,000 cells per well and C4-2B: 7,500 cells per well.

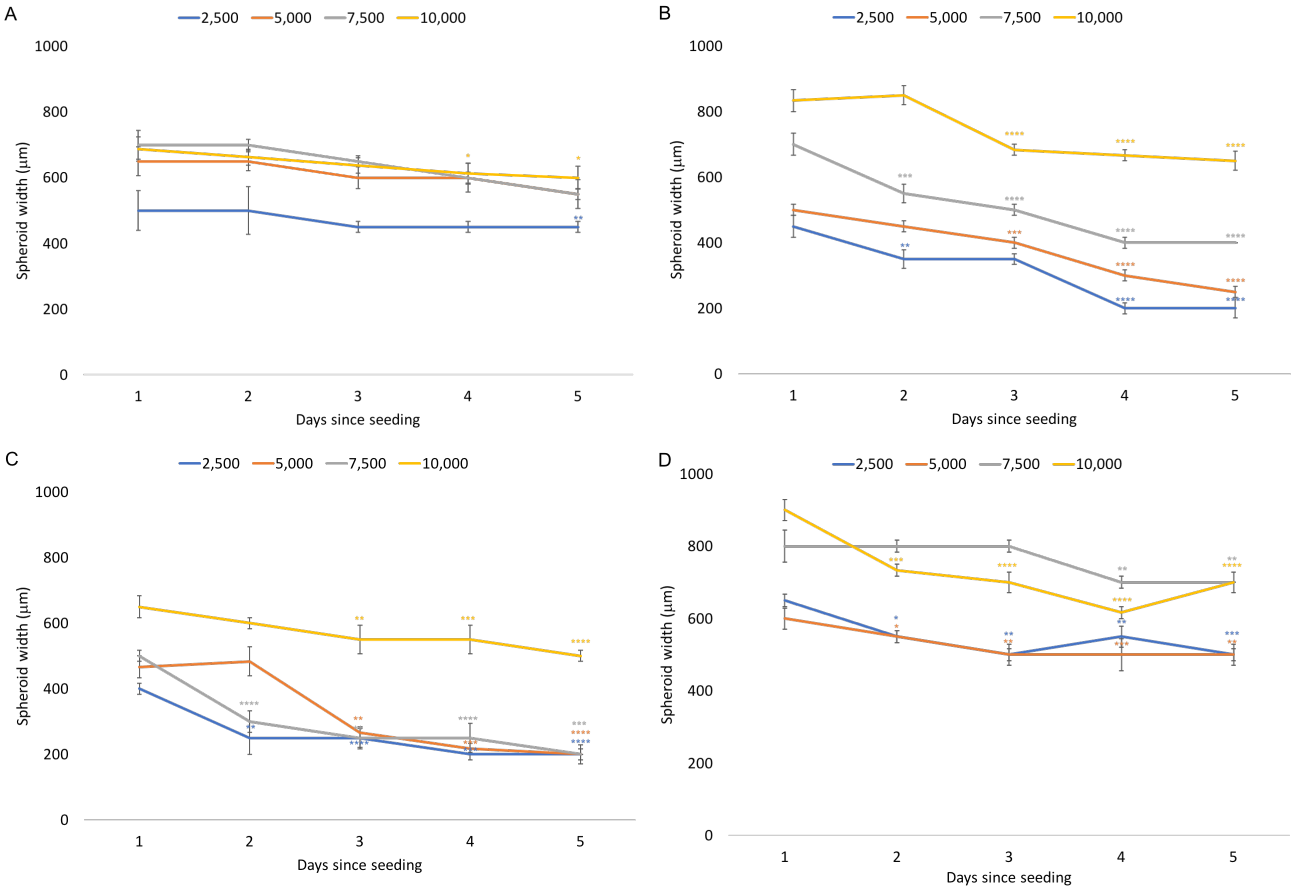

Figure 3.2. Growth curves showing the effects of different initial seeding densities on the size of 3D monoculture prostate cancer cell spheroids over time. A) PC3, B) DU145, C) LNCaP and D) C4-2B prostate cancer cell lines were cultured at various initial seeding densities on agarose coated 96-well flat-bottomed plates to generate cultures of reproducibly sized, single spheroids in each well. The diameter of each spheroid was measured (µm) every day for 5 days. Measurements were taken from images acquired from 3 separate spheroids per cell line, per seeding density using a standard light microscope (AxioCam ERC55, Zeiss, Germany) using a 5x objective. An ANOVA post-hoc Dunnett test was performed for statistical analysis. Error bars denote S.E.M. p-value < 0.05 (*), p-value < 0.01 (**), p-value < 0.001 (***), p-value < 0.0001 (****) (N = 3).

3.3.2.2 Viability of monoculture prostate cancer 2D monolayers and 3D spheroids over time is dependent on initial seeding density

To determine the optimal initial seeding density for generating viable 3D spheroids over 5 days, light microscopy images were taken, and the MTT cell viability assay was used. To determine the difference in spheroid viability over time, spheroids were normalised to spheroids formed on day 1 for each seeding density.

In PC3 cell spheroids, no significant change in the percentage of viable cells was observed over 5 days when cells were seeded at an initial density of 10,000 cells per spheroid. However, a significant decrease in the percentage of viable cells was observed at all lower initial seeding densities, with the most significant decrease observed at 7,500 cells per spheroid on day 2 (50.8%, $p = 0.001$; **Figure 3.3A**). In DU145 cell spheroids no significant decreases in the percentage of viable cells were observed at any initial seeding density at any day across 5 days, yet a significant increase was found at an initial seeding density of 5,000 cells per spheroid (223.7%, $p = 0.05$; **Figure 3.3B**), with the least changes in the percentage of viable cells observed at an initial seeding density of 7,500 cells per spheroid (**Figure 3.3B**). In LNCaP cell spheroids, no significant change in the percentage of viable cells was observed over 5 days when cells were seeded at an initial density of 5,000 cells per spheroid. LNCaP cell spheroids showed a significant decrease in the percentage of viable cells on day 4 when seeded at an initial density of 7,500 (11.1%, $p = 0.05$) and 10,000 cells (11.4%, $p = 0.01$) per spheroid (**Figure 3.3C**). In C4-2B cell spheroids significant decreases were observed in the percentage of viable cells when cells were seeded at initial seeding densities of 7,500 after 2, 3 and 4 days (18.9%, 20.8% and 7.3% respectively, $p \leq 0.05$; **Figure 3.3D**) and 10,000 cells per spheroid, also after 2, 3, 4 and 5 days (9.4%, 14.3%, 10.2% and 10.2% respectively, $p = \leq 0.01$ respectively; **Figure 3.3D**). These data, together with the data on spheroid size (**Section 3.2.2.1**), suggest that the optimal initial seeding densities for each cell line for generating viable spheroids over 5 days are as follows; PC3 – 10,000, DU145 – 7,500, LNCaP – 5,000 and C4-2B – 5,000 cells per well (**Figure 3.3**).

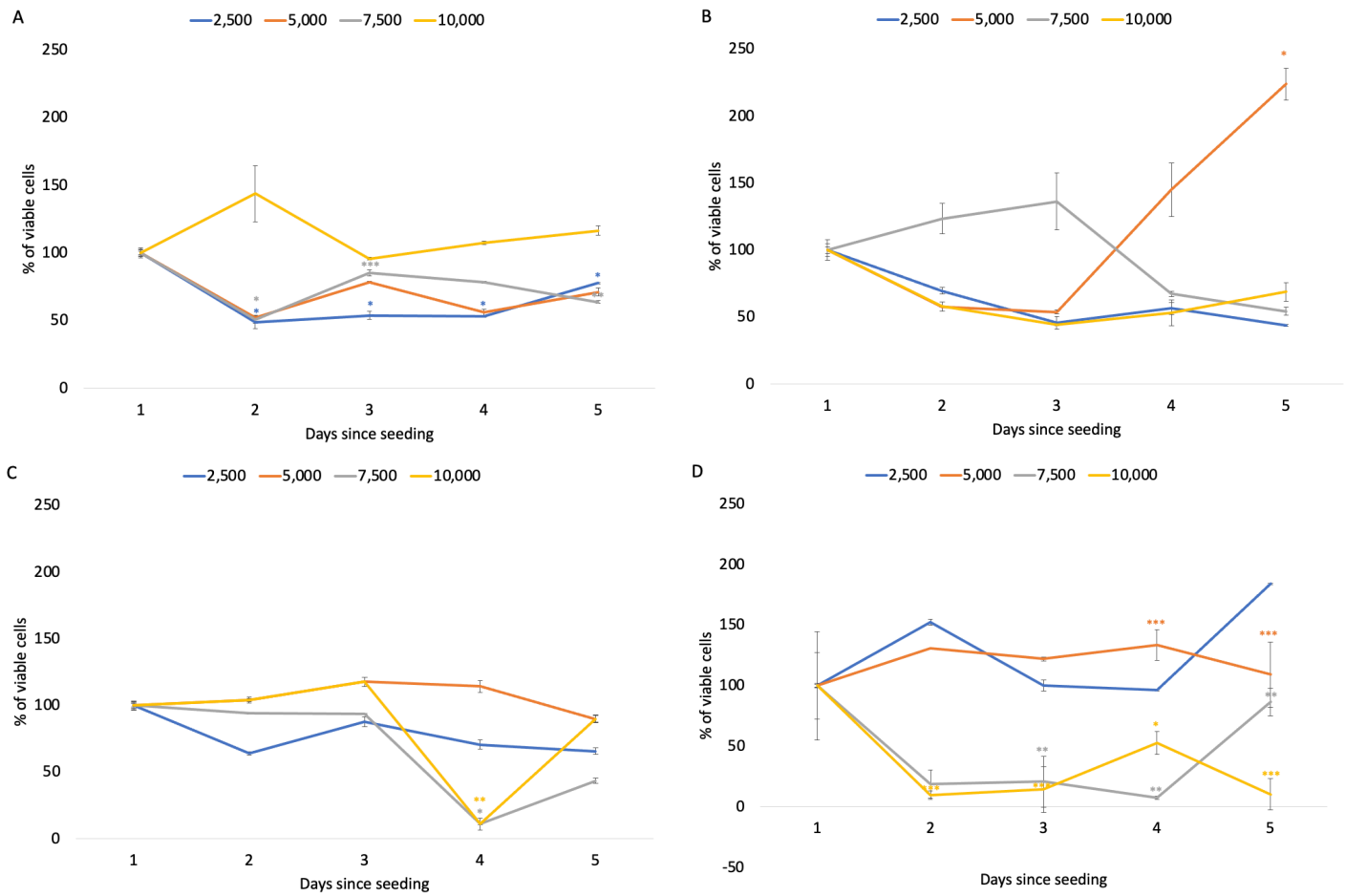

Figure 3.3. Effects of different initial seeding densities on the viability of 3D prostate cancer cell spheroids over time. A) PC3, B) DU145, C) LNCaP and D) C4-2B prostate cancer cells were cultured as 3D spheroids with a range of initial seeding densities. An MTT viability assay was carried out each day for 5 days, with viability calculated as a percentage of day 1 per seeding density, per cell line. An ANOVA post-hoc Dunnett test was performed for statistical analysis. Error bars denote S.E.M. p-value < 0.05 (*), p-value < 0.01 (**), p-value < 0.001 (***), p-value < 0.0001 (****) (N = 3).

Standard light microscopy was used to visualise spheroid formation and monitor size over time. PC3 and C4-2B cells formed uniform spheroids at all initial seeding densities (**Figure 3.4 A & D**). A necrotic core was indicated by a darkening of the centre of each spheroid when visualised under light microscopy, as seen in DU145 cell spheroids seeded with 5,000 and 7,500 cells per well on day 3 (**Figure 3.4B**) and LNCaP cell spheroids seeded with 7,500 cells per well on day 3 (**Figure 3.4C**). A wider range of seeding densities and time points can be found in **Appendix 1, Figure A1. 2.** When combined with the MTT cell viability assay results from **Figure 3.3**, the optimal seeding densities for each cell line were determined as follows; PC3 – 10,000, DU145 – 7,500, LNCaP – 5,000 and C4-2B – 5,000 cells per well (**Figures 3.3 & 3.4**).

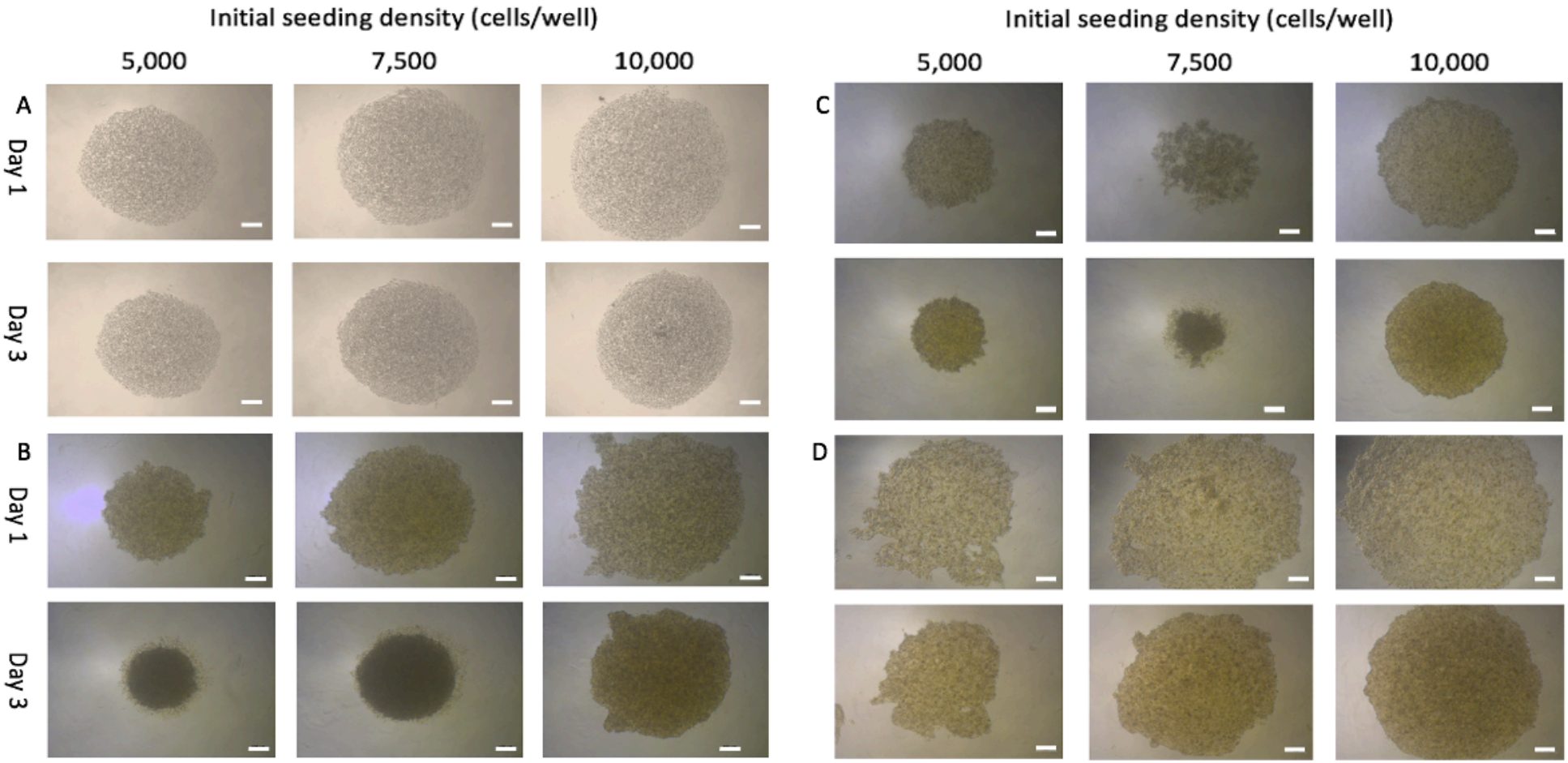

Figure 3.4. Representative light microscopy images of spheroids over time (A) PC3, (B) DU145, (C) LNCaP and (D) C4-2B prostate cancer cells were cultured as 3D spheroids with a range of initial seeding densities. Images were taken 1 and 3 days after seeding and were acquired using a standard light microscope (AxioCam ERC55, Zeiss, Germany) using a 5x objective. Scale bar = 100 μm.

3.3.3 Development of a 3D *in vitro* co-culture prostate cancer-stromal model

3.3.3.1 Size of 3D co-culture spheroids reduces over time

To monitor the effects of culturing prostate cancer cells in co-culture with stromal HS5 cells on spheroid size, the diameter of spheroids of different co-culture ratios – 1PCa:1HS5 (1:1), 2PCa:1HS5 (2:1) and 1PCa:2HS5 (1:2) – was measured over 5 days. To determine the difference in spheroid size over time, spheroids were normalised to spheroids formed on day 1 for each seeding density.

In PC3-HS5 cell spheroids, no significant changes in spheroid were observed at any ratio at any day across 5 days, yet the least changes in size were observed at a 1:1 prostate cancer-stromal cell ratio (**Figure 3.5A**). In DU145-HS5 cell spheroids significant decreases in spheroid size were observed at all ratios on days 3, 4 and 5 ($p \leq 0.05$; **Figure 3.5B**). The only significant increases in spheroid size across all four cell lines were observed in LNCaP cells when spheroids were seeded at a ratio of 2LNCaP:1HS5 cells spheroid after 2 days (+100 μm $p = 0.05$; **Figure 3.5C**). However, in the same cell line, significant decreases in spheroid size were observed when cells were seeded at a ratio of 1LNCaP:2HS5 cells after 3, 4 and 5 days (-150 μm, -183.3 μm & -200 μm respectively, $p \leq 0.05$; **Figure 3.5C**). In C4-2B co-culture spheroids, no significant differences in size were observed over time in spheroids cultured at a 1C4-2B:1HS5 ratio, yet significant decreases in spheroid size were found in spheroids cultured at ratios of both 1C4-2B:2H5 cells at days 3, 4 and 5 (-300 μm, -383.3 μm & -416.7 μm respectively, $p = 0.01$; **Figure 3.5D**) and 2C4-2B:1HS5 cells, also at days 3, 4 and 5 (-233.3 μm, -283.3 μm and -350 μm respectively, $p = 0.01$; **Figure 3.5D**). These data implied that a 1PCa:1HS5 ratio of prostate cancer-stromal cell co-culture spheroids was optimal for all cell lines as this ratio resulted in the most consistently sized spheroids across all cell lines (**Figure 3.5**).

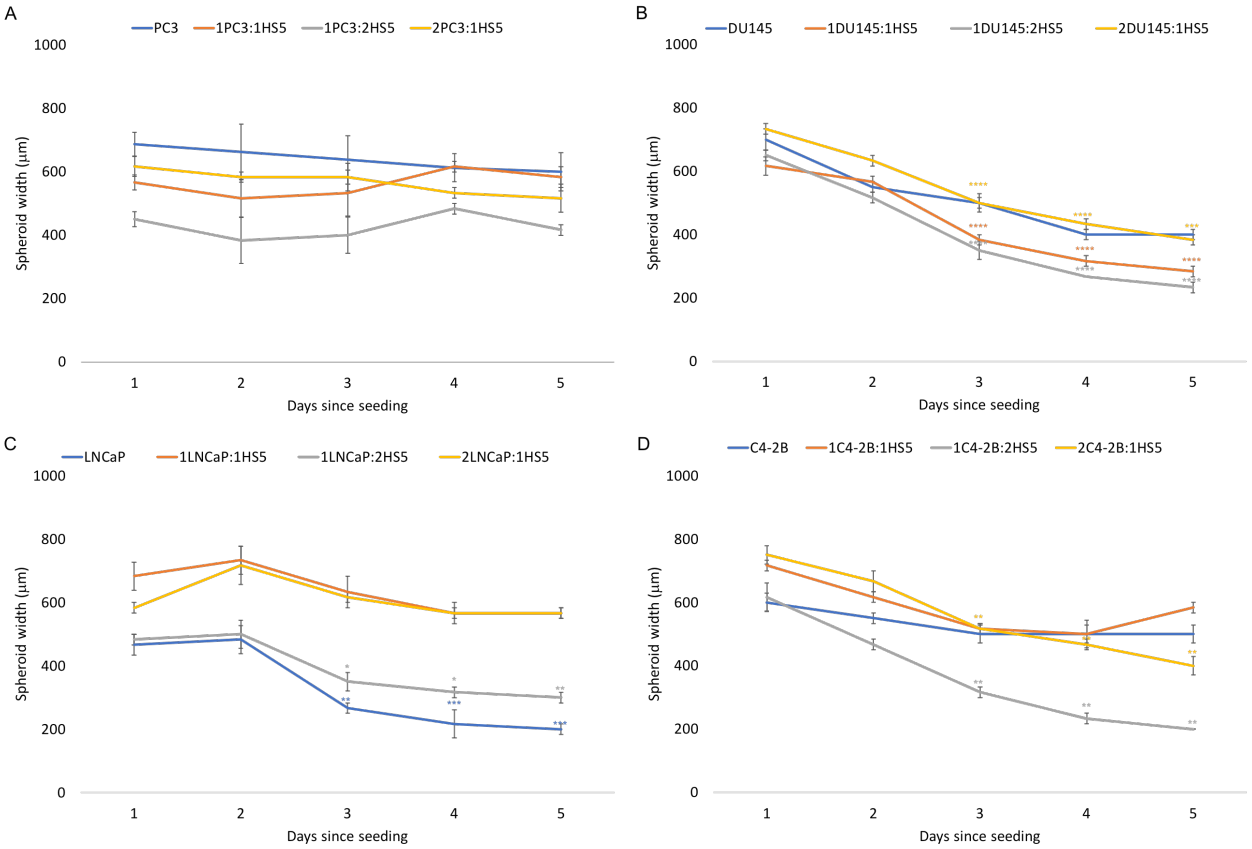

Figure 3.5. Growth curves showing the effects of different ratios of stromal and prostate cancer cells on the size of 3D co-culture spheroids over time. A) PC3, B) DU145, C) LNCaP and D) C4-2B prostate cancer cell lines were cultured with various ratios of HS5 stromal cells on agarose coated 96-well flat-bottomed plates to generate cultures of reproducibly sized, single spheroids in each well. The diameter of each spheroid was measured (µm) every day for 5 days. Ratios of prostate cancer (PCa) to stromal cells were as follows: 1PCa:1HS5 (1:1), 2PCa:1HS5 (2:1) and 1PCa:2HS5 (1:2). Measurements were taken from images acquired from 3 separate spheroids per cell line, per seeding density using a standard light microscope (AxioCam ERC55, Zeiss, Germany) using a 5x objective. An ANOVA post-hoc Dunnett test was performed for statistical analysis. Error bars denote S.E.M. p-value < 0.05 (*), p-value < 0.01 (**), p-value < 0.001 (***), p-value < 0.0001 (****) (N = 3).

3.3.3.2 The ratio of stromal-prostate cancer cells grown as 3D spheroids has little effect on viability over time

To further evaluate the optimal ratio for generating viable prostate cancer-stromal cell spheroids over 5 days, the MTT cell viability assay was used. To determine the difference in spheroid viability over time, spheroids were normalised to spheroids formed on day 1 for each seeding density.

In PC3-HS5 (**Figure 3.6A**), DU145-HS5 (**Figure 3.6B**) and C4-2B-HS5 (**Figure 3.6D**) co-culture spheroids, no significant changes in the percentage of viable cells were observed across all 5 days. In LNCaP-HS5 spheroids, a significant decrease in the percentage of viable cells was found on days 2, 3, 4 and 5 in co-culture spheroids cultured at a 1LNCaP:1HS5 ratio (15.4% 14.3%, 17.8% and 18.0% respectively, $p = 0.0001$; **Figure 3.6C**). The percentage of viable HS5 cells was seen to decrease after day 3, yet no significant changes in the percentage of viable HS5 cells were observed across all 5 days (**Figure 3.6**). These data suggest that the optimal ratios of prostate cancer-stromal cells for generating viable co-culture spheroids over 5 days are as follows: 2PC3:1HS5, 1DU145:1HS5, 2LNCaP:1HS5 and 2C4-2B:1HS5 (**Figure 3.6**).

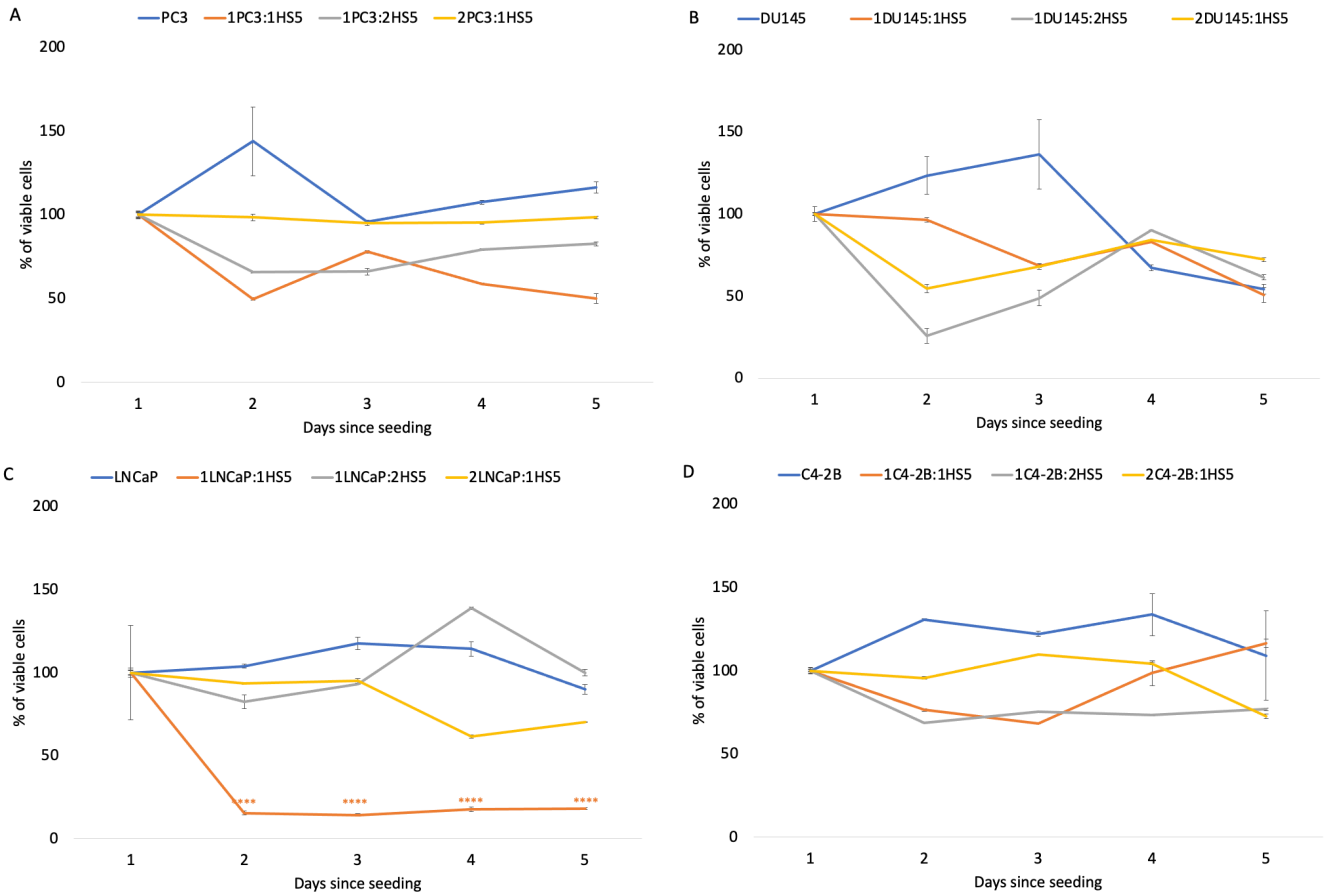

Figure 3.6. Effects of different stromal-prostate cancer cell ratios on the viability of 3D co-culture spheroids over time. A) PC3, B) DU145, C) LNCaP and D) C4-2B prostate cancer cells were cultured with different ratios of HS5 stromal cells as 3D spheroids. An MTT viability assay was carried out each day for 5 days, with viability calculated as a percentage of day 1 per ratio, per cell line. Ratios of prostate cancer (PCa) to stromal cells were as follows: 1PCa:1HS5 (1:1), 2PCa:1HS5 (2:1) and 1PCa:2HS5 (1:2). An ANOVA post-hoc Dunnett test was performed for statistical analysis. Error bars denote S.E.M. p-value < 0.05 (*), p-value < 0.001 (***), p-value < 0.0001 (****) (N = 3).

3.3.3.3 Proliferation assays revealed PC3-stromal spheroids show the most variation over time

To evaluate the impact of prostate cancer-stromal cell ratio on the proliferation of spheroids over 5 days, the alamarBlue cell proliferation assay was used. To determine the difference in spheroid proliferation over time, spheroids were normalised to spheroids formed on day 1 for each seeding density.

The alamarBlue assay demonstrated a highly significant increase in the percentage of proliferating PC3 cells on day 3 both as mono- and co-culture across all ratios ($p \leq 0.001$; **Figure 3.7A**). Significant increases were also observed on days 4 and 5 at ratios of 1PC3:1HS5 (233.7% and 163.2% respectively, $p = 0.05$; **Figure 3.7A**), and 1PC3:2HS5 on days 2, 4 and 5 (109.4%, 199.5% and 148.2% respectively, $p = 0.01$; **Figure 3.7A**). As monoculture spheroids, DU145 cells showed a significant increase in the percentage of proliferating on day 3 (117.3%, $p = 0.01$; **Figure 3.7B**), and in co-culture with HS5 at ratios of 1DU145:1HS5 and 2DU145:1HS5 on day 4 (156.3% and 145.2% respectively, $p = 0.01$; **Figure 3.7B**). LNCaP monoculture spheroids showed a decrease in the percentage of proliferating cells on days 2 and 4 (78.9% and 76.2% respectively, $p \leq 0.05$; **Figure 3.7C**) yet no significant changes in the percentage of proliferating cells were observed in co-culture spheroids. No significant changes in the percentage of proliferating cells of mono- or co-culture C4-2B-HS5 cell spheroids were observed across the 5 days (**Figure 3.7D**), nor were any significant changes in the percentage of proliferating cells of monoculture HS5 cell spheroids observed across the 5 days (**Figure 3.7**). These data suggest that the optimal ratios of prostate cancer-stromal cells for generating proliferating co-culture spheroids over 5 days are as follows: 1PC3:2HS5, 1DU145:1HS5, 2LNCaP:1HS5 and 1C4-2B:1HS5 based on the consistency of cell proliferation rates (**Figure 3.7**).

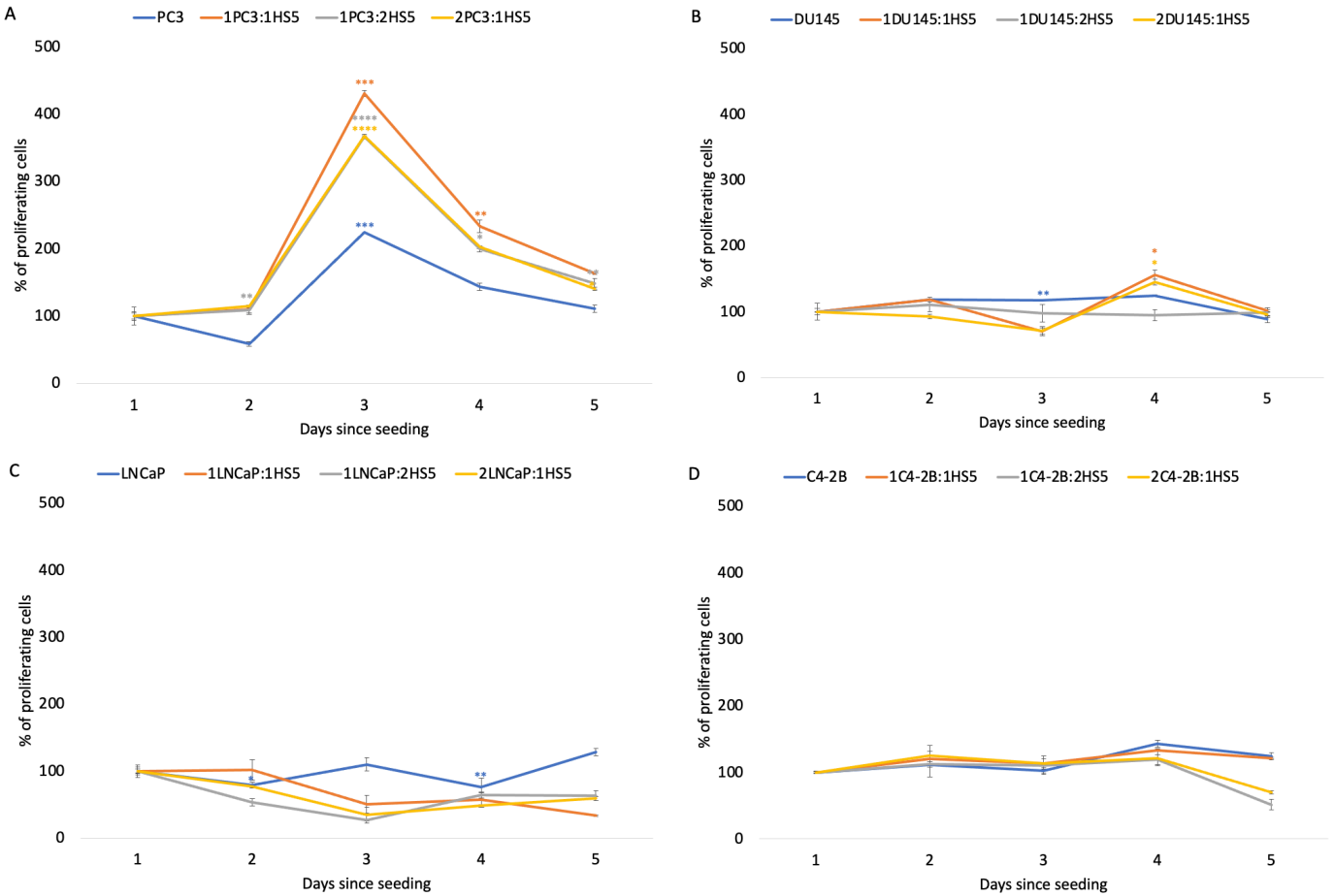

Figure 3.7. Effects of different stromal-prostate cancer cell ratios on the proliferation of 3D co-culture spheroids over time. A) PC3, B) DU145, C) LNCaP and D) C4-2B prostate cancer cells were cultured with different ratios of HS5 stromal cells as 3D spheroids. An alamarBlue proliferation assay was carried out each day for 5 days, with proliferation calculated as a percentage of day 1 per ratio, per cell line. An ANOVA post-hoc Dunnett test was performed for statistical analysis. Error bars denote S.E.M. p-value < 0.05 (*), p-value < 0.001 (***), p-value < 0.0001 (****) (N = 3).

3.3.3.4 Fluorescent imaging indicated high levels of cell death in the cores of spheroids

To evaluate the levels of cell death occurring within cells co-cultured as 3D spheroids, PI stain was used to identify dead cells. PI is a vital stain which can be used to identify dead cells, as the membranes of dead and damaged cells are permeable to PI, whilst those that are intact are impermeable (Kole *et al*., 2016). Staining with PI alongside another stain such as the nucleic dye Hoechst 33342 allows for cells that are considered viable and dead to be visualised simultaneously (Dasiram *et al*., 2017; Liu *et al*., 2012; Oosterhoff *et al*., 2003).

Confocal microscopy demonstrated PI as a strong, red fluorescent signal of varying strength dependent on the cell line (**Figures 3.8 – 11,** illustrate representative images; a z-stack showing PI distribution throughout each spheroid can be found in Appendix 1, **Figures A1. 9 – 12.** In PC3 cells, PI staining was evenly distributed throughout both mono- and co-culture spheroids, which increased in strength over time. PI staining was consistently stronger in co-culture cells, with highest expression observed on day 5 (**Figure 3.8**). DU145 cell spheroids also showed relatively low levels of PI staining which was evenly distributed throughout the spheroid in mono- and co-cultures alike, with the exception of monoculture spheroids imaged on day 5 which showed highly concentrated PI staining in the core of the spheroid (**Figure 3.9**). LNCaP cell spheroids exhibited the highest levels of PI staining across 5 days, in both mono- and co-culture models. PI was evenly distributed throughout all LNCaP cell spheroids, with the highest signal observed on day 5 in both mono- and co-culture spheroids (**Figure 3.10**). C4-2B cell spheroids also showed an even distribution of PI staining throughout all spheroids, with no discrimination between mono- and co-culture models (**Figure 3.11**). Collectively, these images imply that cell death within spheroids is mainly occurring within the core and they also confirmed that cell death increases over time in both mono- and co-culture prostate cancer-stromal cell models. As monocultures, PC3 cells generated the most viable 3D spheroid models over time to be utilised in future experiments, which was also the case when

cultured as co-culture models with HS5 stromal cells. DU145 cells also produced a viable co-culture model for use going forward. Viability was significantly compromised in LNCaP and C4-2B cells both as mono- and co-culture 3D spheroid models, suggesting their use going forward should be restricted to 2D monolayer systems.

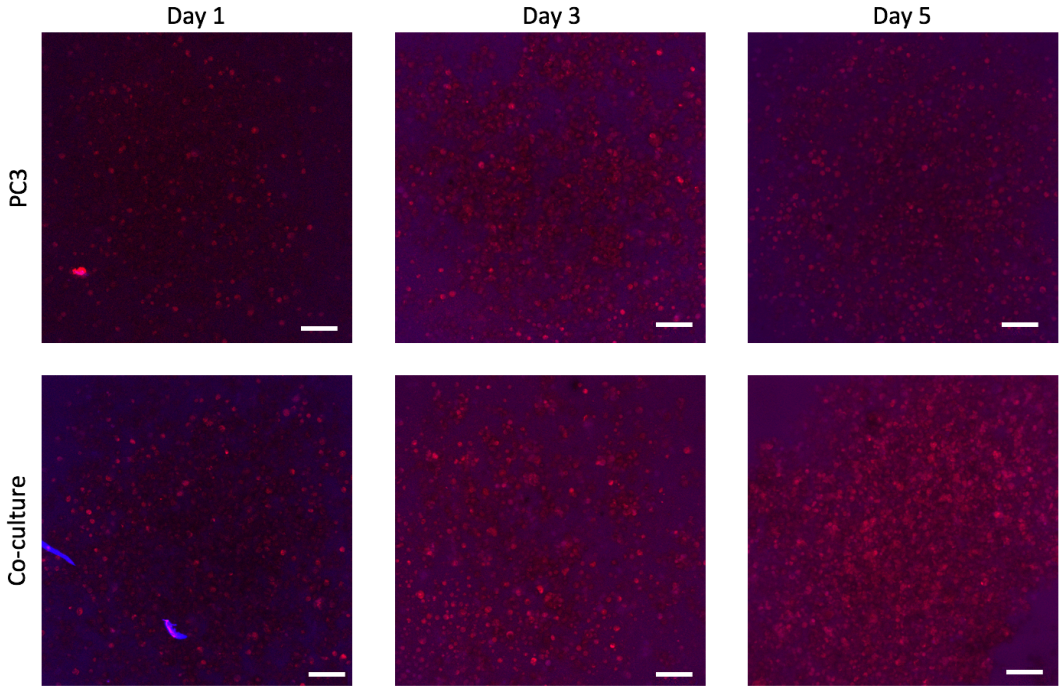

Figure 3.8. PI staining of 3D PC3 co-culture spheroids by fluorescence microscopy shows a decrease in viability over time. PI / Hoechst co-staining of 3D mono- and co-culture spheroids at 10x magnification show an increase in PI uptake in co-culture spheroids, indicative of cell death over time. Scale bar = 100 μm Blue: nuclei; red: dead cells. Images were taken on days 1, 3 and 5 after seeding and were acquired with the Confocal LSM 710 (ZEISS, Germany) (N = 3).

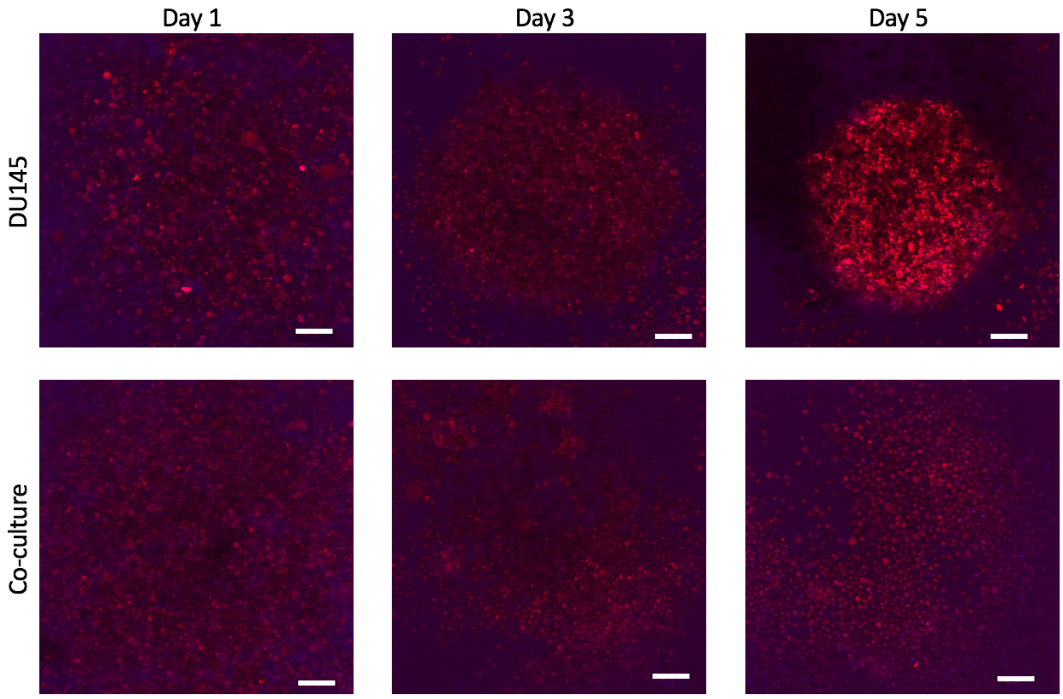

Figure 3.9. PI staining of 3D DU145 co-culture spheroids by fluorescence microscopy shows a decrease in viability over time. PI / Hoechst co-staining of 3D mono- and co-culture spheroids at 10x magnification showing an increase in PI uptake in mono-culture spheroids, indicative of cell death by day 5. Scale bar = 100 μm. Blue: nuclei; red: cell death. Images were taken on days 1, 3 and 5 after seeding and were acquired with the Confocal LSM 710 (ZEISS, Germany) (N = 3).

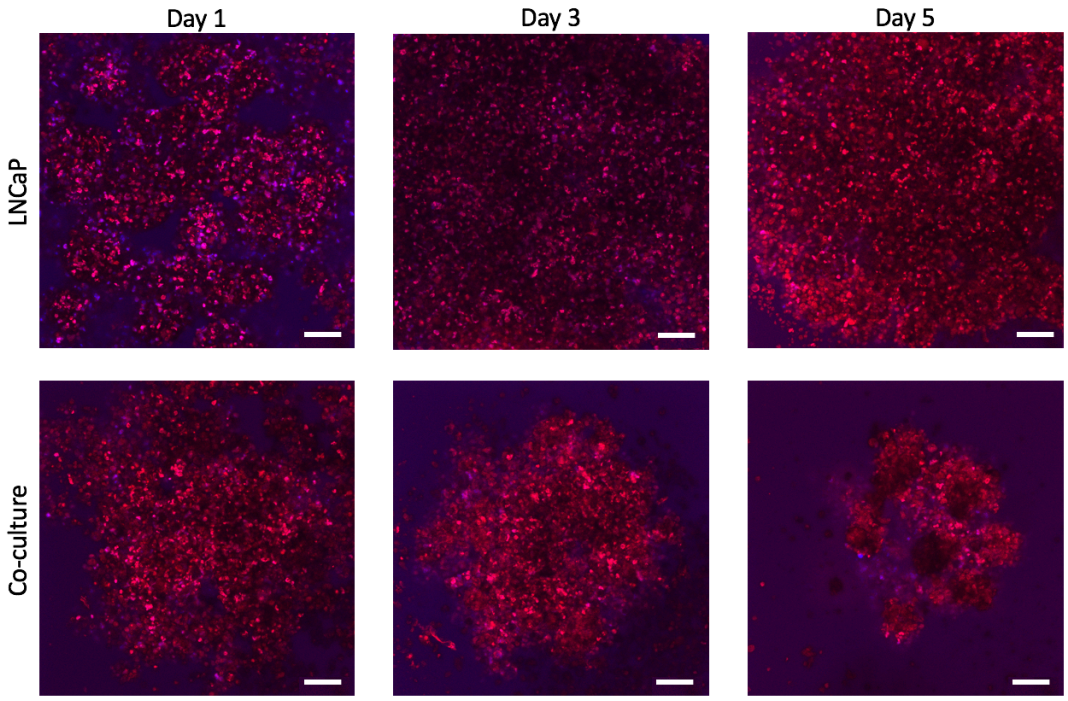

Figure 3.10. PI staining of 3D LNCaP co-culture spheroids by fluorescence microscopy shows a decrease in viability over time. PI / Hoechst co-staining of 3D mono- and co-culture spheroids at 10x magnification showing an increase in PI uptake in both mono- and co-culture spheroids, indicative of cell death. Scale bar = 100 μm. Blue: nuclei; red: cell death. Images were taken on days 1, 3 and 5 after seeding and were acquired with the Confocal LSM 710 (ZEISS, Germany) (N = 3).

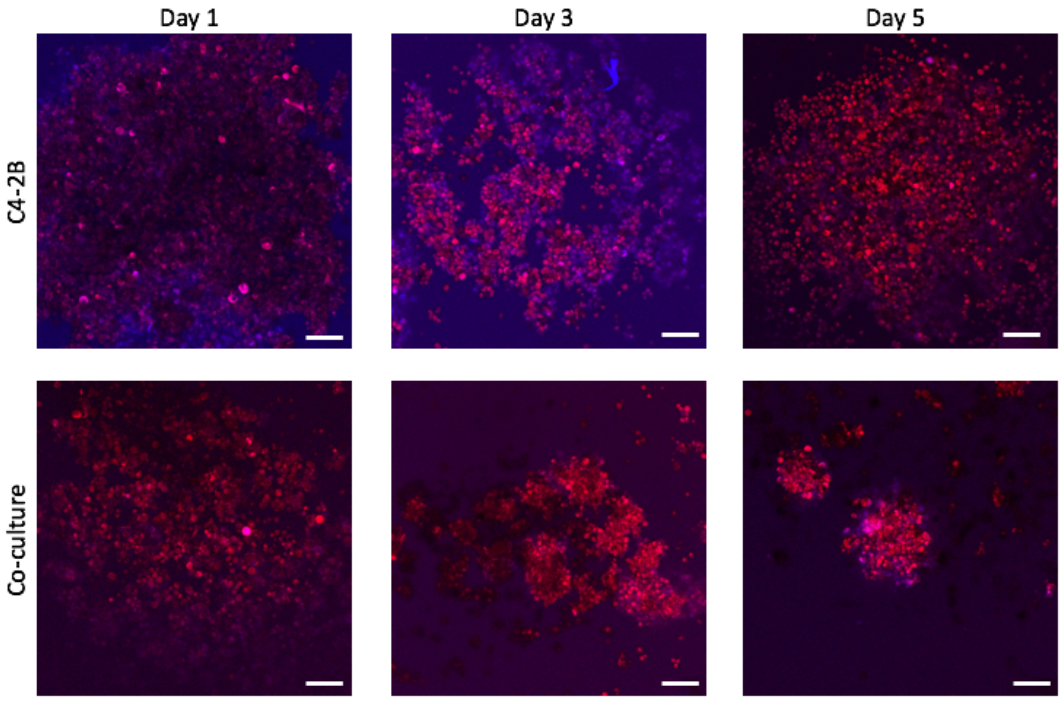

Figure 3.11. PI staining of 3D C4-2B co-culture spheroids by fluorescence microscopy shows a decrease in viability over time. PI / Hoechst co-staining of 3D mono- and co-culture spheroids at 10x magnification showing an increase in PI uptake in both mono- and co-culture spheroids, indicative of cell death. Scale bar = 100 μm. Blue: nuclei; red: cell death. Images were taken on days 1, 3 and 5 after seeding and were acquired with the Confocal LSM 710 (ZEISS, Germany) (N = 3).

3.3.3.5 Fluorescent imaging indicated stromal cells integrate well with androgen-sensitive prostate cancer cells in 3D models

To evaluate the distribution of HS5 stromal cells within 3D co-culture prostate cancer-stromal cell spheroids, the expression of STRO-1 was evaluated. STRO-1 is a monoclonal IgM antibody specific for an undefined cell surface antigen expressed by a small population of adult human bone marrow cells (Gronthos *et al*., 2003; Simmons & Torok-Storb, 1991). Therefore, staining of STRO-1 allowed for differentiation and observation of stromal cells within a 3D structure, using confocal microscopy (Brusnahan *et al*., 2010; McArthur *et al*., 2006; Windus *et al*., 2013). The nucleic counterstain Hoechst 33342 was used to differentiate cells positive for both the nucleic stain and STRO-1 as stromal cells in these models (Windus *et al*., 2013; Xu *et al*., 2009).

Confocal microscopy demonstrated STRO-1 as a strong, green fluorescent signal. Images show that stromal cells were evenly distributed within LNCaP and C4-2B spheroids (**Figure 3.12C & D**, respectively), as opposed to PC3 and DU145 spheroids where STRO-1 staining is predominantly observed at the spheroid periphery and surrounding media (**Figure 3.12A & B**, respectively). These images suggest that the androgen-sensitive prostate cancer cell lines LNCaP and C4-2B form more evenly distributed co-culture spheroids with HS5 cells than the androgen-independent PC3 and DU145 cell lines (**Figure 3.14** where representative images are illustrated; Z-stacks for each spheroid can be found in **Appendix 1, Figure A1.10**).

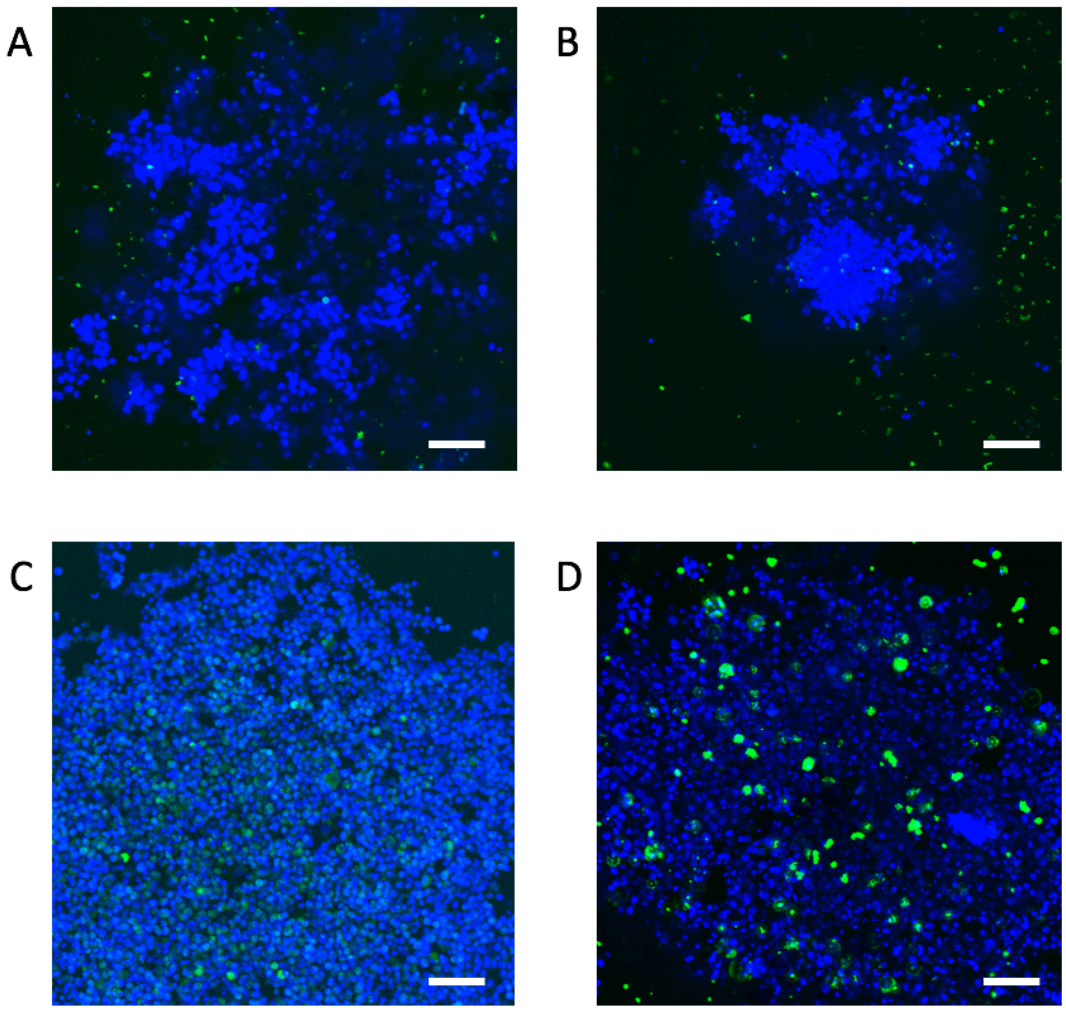

Figure 3.12. Integration of bone stromal (HS5) cells when co-cultured as 3D spheroids with prostate cancer cells. A) PC3, B) DU145, C) LNCaP and D) C4-2B prostate cancer cells were cultured with HS5 stromal cells as 3D spheroids. Confocal microscopy revealed HS5 cells were better integrated into androgen-sensitive prostate cancer cell spheroids (C & D). Scale bar = 100 μm. Blue: nuclei; green: STRO-1 stromal-specific antibody expression. Images were taken 3 days after seeding and were acquired with the Confocal LSM 710 (ZEISS, Germany) (N = 3).

3.4 Discussion

3.4.1 STEAP family gene expression in human prostate cancer cell lines

This chapter aimed to determine the gene expression levels of all four members of the *STEAP* family in a panel of prostate cancer cell lines of different metastatic origins, in order to determine the most appropriate platform to carry forward for subsequent analysis throughout this thesis. Previous studies have predominantly focussed on *STEAP2* expression (Burnell *et al*., 2018; Whiteland *et al*., 2014), however to date, all four *STEAP* family members had not been assessed across all the prostate cancer cell lines studied in this chapter.

STEAP1, the first of the *STEAP* family of genes, is known to play a role in prostate cancer progression through the control of intracellular communication between prostate cancer cells and cancer-associated stromal cells (Yamamoto *et al.,* 2013). In this study, *STEAP1* expression was found to be overexpressed in LNCaP cells, consistent with previous studies (**Figure 3.1**; Challita-Eid *et al*., 2007; Romanuik *et al*., 2010; Whiteland *et al*., 2014), yet down regulated in DU145, PC3 and C4-2B cells when compared to the normal prostate epithelial cell line PNT2. These findings are consistent with previous studies which also found that *STEAP1* gene expression is relatively low in PC3 and DU145 cells, despite previous reports of an overexpression in the STEAP1 protein (Hubert *et al*., 1999; Wang *et al*., 2010).

STEAP2 has been found to be expressed in low levels in normal human prostate tissues, with little to no expression in other normal human tissues (Shyamsundar *et al*., 2005). This expression has then been found to increase when the prostate is in a diseased state (Korkmaz *et al*., 2002; Porkka *et al*., 2002; Wang *et al*., 2010). Previous studies have found *STEAP2* to be most highly expressed in LNCaP cells, with lower but still increased levels recorded in PC3 cells, which correlate with the results of this study (**Figure 3.1**; Gonen-Korkmaz *et al*., 2014; Porkka *et al*., 2002; Whiteland *et al*., 2014). Of the four

prostate cancer cell lines assessed here, DU145 cells were the only cell line to exhibit lower levels of *STEAP2* than the normal cell line PNT2, consistent with previous studies (**Figure 3.1**; Korkmaz *et al*., 2002; Porkka *et al*., 2002). In previous studies, *STEAP2* overexpression has been induced either ectopically or by transfection in DU145 cells to monitor its effects in androgen-independent cells, further suggesting its expression in this cell line is relatively low (Gonen-Korkmaz *et al*., 2014; Wang *et al*., 2010). The highest significant increases in *STEAP2* expression were found in androgen-sensitive prostate cancer cell lines; LNCaP and C4-2B, suggesting that AR signalling may play a role in its expression, hence the inclusion of the androgen-sensitive, LNCaP-derived C4-2B cell line in this study. Whilst the expression of *STEAP2* in this cell line has not previously been investigated, the significant increase in *STEAP2* expression found in this study further suggests that *STEAP2* expression correlates with androgen sensitivity. It is of particular interest that previous studies have also noted that STEAP2 is highly expressed in AR-sensitive cells, warranting further investigations into this link (Gonen-Korkmaz *et al*., 2014; Porkka *et al*., 2002; Wang *et al*., 2010).

STEAP3 gene expression is highly upregulated in haematopoietic tissues and has been known to play a role in iron homeostasis in iron deficiency anaemia (Ohgami *et al*., 2005; Zhang *et al*., 2012). *STEAP3* expression was decreased in all four prostate cancer cell lines (**Figure 3.1**). These results are in line with previous studies, as *STEAP3* has been found to be highly expressed in cell lines originating from other cancer types such as lung and melanomas, when compared to prostate cancer (Grunewald *et al*., 2012). However, an increase in *STEAP3* expression has previously been observed in LNCaP cells by Machlenkin *et al*., who found that LNCaP cells demonstrated specific CTL responses when targeted with CTL epitopes of *STEAP3*. This was not found to be the case in PC3 and DU145 cells, suggesting that *STEAP3* is naturally processed and presented by LNCaP cells (Machlenkin *et al*., 2005).

STEAP4 expression is primarily known to be associated with metabolic disease as opposed to prostate cancer, and therefore the lower levels of *STEAP4* expression observed across the panel of prostate cancer cell lines in

this study is not surprising (Freyhaus *et al*., 2012; Wellen *et al*., 2007). Similarly, low expression levels of *STEAP4* have previously been observed in DU145 and PC3 prostate cancer cells (**Figure 3.1**; Korkmaz *et al*., 2005). *STEAP4* expression has been found to increase in LNCaP cells in a time-dependent manner, which may account for the low levels observed in this study as cells were assessed 48 h after seeding (Korkmaz *et al*., 2005). The same study by Korkmaz *et al*., also reported that *STEAP4* in LNCaP cells was expressed in a cell line dependent manner following treatment with a synthetic androgen, suggesting *STEAP4* expression could be androgen-mediated.

Based on the findings of this study and those carried out previously, of the four family members *STEAP2* was selected for further analysis in this thesis due to its markedly high expression in three of the four prostate cancer cell lines studied (Burnell *et al*., 2018; Whiteland *et al*., 2014). Thus, it was of particular interest to develop a platform for modelling prostate cancer cells known to express high levels of *STEAP2* as viable 3D spheroids.

3.4.2 Size vs viability of prostate cancer cells when cultured in a 3D format

3D tissue models provide a more physiologically relevant *in vitro* system that are more representative of *in vivo* tumours than the same cells cultured as 2D monolayers. Spheroids can be cultured with single cell types (monocultures) to represent localised or locally advanced disease, or with cell types of multiple origins (co-cultures), which are more representative of metastatic, advanced disease. Whilst *in vitro* 3D spheroid models have become more popular in recent years, they still come with limitations such as limited efficiency and reproducibility of spheroid formation, spheroid maintenance, and cell heterogeneity, particularly in 3D co-culture models. Hence the need for a robust method for the reproducible generation of viable spheroid models. A co-culture model of prostate cancer and bone stromal cells is of particular interest given that the predominant site for prostate cancer metastases is the bone. This chapter aimed to determine the most suitable and reproducible method for growing prostate cancer cells as viable 3D spheroid models, as both monocultures and in co-cultures with HS5 stromal cells. The development

of such methods would allow spheroids to be readily established without the need of specialised equipment, with conditions optimised to each individual cell line. Previous work within the group had established a method for culturing prostate cancer cells as 3D spheroid cell models grown on agarose gel; however, this previous work had only focussed on the PC3 prostate cancer cell line (Wang *et al*., 2019). Therefore, this method was applied to other prostate cancer cell lines within this chapter, with the addition of HS5 stromal cells to develop and optimise a prostate cancer-stromal cell co-culture model.

A variety of seeding densities and viability assessments were employed to monitor the growth of a panel of human prostate cancer cell lines in 3D format, as it has previously been found that altering the seeding density can subsequently produce spheroids with a wide range of characteristics (Hurrell *et al*., 2018). Previous work within the group when monitoring the growth characteristics of PC3 cells over a 14-day period found that viability peaked within the first 72 h after seeding and subsequently decreased, hence a decision was made to monitor cells over a 5-day period within this chapter (Wang *et al*., 2019). In this chapter, optimal seeding densities were established such that the viability of tumour spheroids for each cell line tested (regardless of their proliferative potential and cell cycle time) did not fall below 50% by day 5, which was considered appropriate for initiating experimental studies.

Previous studies using experimental measurements and mathematic modelling have found that spheroid size can influence viability, with spheroids larger than 200 μm known to have steep oxygen gradients (Charoen *et al*., 2014; Hirschhaeuser *et al*., 2010; Khaitan & Dwarakanath, 2006). In these spheroids, the centre of the spheroid is starved of oxygen and nutrients, leading to the formation of a necrotic core (Charoen *et al*., 2014; Hirschhaeuser *et al*., 2010; Khaitan & Dwarakanath, 2006). Concurrently, the periphery of the spheroid has been found to be a viable, proliferating zone as it continues to interact with nutrient-rich media (Grimes *et al*., 2014; Hirschhaeuser *et al*., 2010; Riffle *et al*., 2017). Using standard light

microscopy, a necrotic core appears as a darker centre of the spheroid in relation to its periphery (Gong *et al*., 2015; Vinci *et al*., 2012; Zanoni *et al*., 2016). Cell viability increased significantly in spheroids of all cell lines seeded at an initial density of 2,500 cells per well, and the smallest sized spheroids were produced (**Figure 3.3, Appendix 1.1**). However, when visualised with light microscopy, DU145 and LNCaP spheroids with a seeding density of 2,500 cells did exhibit a necrotic core by days 3 and 5 (see **Appendix 1, Figures A2.1B & C**), which correlated with a reduction in viability at this density (**Figure 3.4B & C**). This suggests that as these spheroids still measured > 350 μm, an oxygen gradient may still present (Charoen *et al*., 2014; Hirschhaeuser *et al*., 2010; Khaitan & Dwarakanath, 2006). Previous studies have also noted that the necrotic core increases in size proportionate to the overall size of the spheroid, suggesting that it is relatively small in these models (Riffle *et al*., 2017).

When visualised using light microscopy, PC3 cells cultured as a monoculture were the only cell line to not display a necrotic core under standard light microscopy at any seeding density across 5 days (**Appendix 1, Figure A1.2A**), suggesting that metabolic limitation did not play a role in these models, despite PC3 spheroids measuring > 600 μm (**Figure 3.2A**; Hirschhaeuser *et al*., 2010; Mosaad *et al*., 2018). 10,000 cells per well was chosen as the optimum seeding density for PC3 spheroids as the diameter stayed the most consistent over time, which also correlates with the results from the MTT viability assay, where no significant changes in the viability of these spheroids were observed across 5 days (**Figures 3.3A and 3.4A**). Previous studies measuring the size of cancer cell spheroids over time have found a decrease in spheroid size, which correlates with a decrease in viability, as demonstrated by DU145, LNCaP and C4-2B monoculture spheroids, the size of which continually reduced 3-5 days after seeding (**Figures 3.2B & C;** (Dvir-Ginzberg *et al*., 2003). 7,500 cells per well was chosen as the optimum seeding density for DU145 cells as although they decreased in size more rapidly that spheroids seeded with 10,000 cells per well, when assessed by the MTT assay, their viability remained higher than 50% on all 5 days. In

contrast, the viability of spheroids seeded with 10,000 cells per well dropped below 50% by day 3 (**Figures 3.2B & 3.3B**). 5,000 cells per well was chosen as the optimum seeding density for both LNCaP and C4-2B cells, as this seeding density did not result in any significant decreases in spheroid viability in either cell line across the 5-day culture period (**Figures 3.3C & D**). Initially, the size of the LNCaP spheroids slightly increased 2 days after seeding, which may be due to their longer doubling time of 60 hours (Cunningham & You, 2015). This was also found to be the case with C4-2B cells seeded at 7,500 and 10,000 cells per well (**Figures 3.2D and 3.3D**), yet these spheroids displayed a significant ($p < 0.001$) decrease in both viability and size on days 4 and 5, which when observed under standard light microscopy correlated with a darker core (**Figure 3.4D; Appendix 1, Figure A1.2D**). In higher density spheroids, cellular functions such as the secretion of urea and albumin in hepatocytes, have been found to remain high across up to 7 days of culture in 3D, highlighting the importance of spheroid density on cell viability (Dvir-Ginzberg *et al*., 2003). In prostate cancer cell spheroids this could be assessed through monitoring secretions of PSA, which has been known to increase in the culture supernatant of healthy LNCaP spheroids (Takagi *et al*., 2007).

Morphologically, the cell lines used in this chapter have been known to form spheroids of two distinct phenotypic categories; round (PC3 and DU245) or mass (LNCaP and C4-2B) (Harma *et al*., 2010; Kenny *et al*., 2007). As time progresses, such cell spheroids have been known to undergo metamorphosis to an invasive or stellate phenotype, during which cells dissociate around the periphery of the spheroid (Harma *et al*., 2010). Seeding densities of > 5,000 cells per well resulted in the dissociation of cells from the tightly packed spheroid by day 5 in all cell lines (**Figure 3.4 & Appendix 1; Figure A1.2**) This could explain the discrepancy between an increase in viability shown in DU145 cells on Day 5 (**Figure 3.3B**) and the presence of a necrotic core (**Figure 3.4B & Appendix 1; Figure A1.2B**), as MTT would not have been able to penetrate this core. However, an increase in MTT cleavage by the mitochondria of these readily available and metabolically active dissociated cells may have occurred, in turn increasing the metabolic production of

formazan crystals and therefore influencing the peak in spheroid viability (Borra *et al*., 2009; Van Meerloo *et al*., 2011).

In monoculture, no significant changes were observed in either the size or viability of HS5 cells, with viability remaining high until day 3, suggesting that any impact on spheroid viability is exerted by prostate cancer cells in co-culture models (**Appendix 1, Figures A1.1 & A1.3**; Windus *et al*., 2013). When co-cultured with stromal HS5 cells, the size of spheroids generally decreased over the 5-day period, in a trend matching the monocultured prostate cancer cell line as opposed to the stromal cell line, with LNCaP co-cultures still showing an increase in size on day 2 (**Figure 3.5C**). This downward trend in spheroid size resulted in the formation of denser, and therefore more tightly packed, spheroids over time. Collectively, the viability of monoculture spheroids was higher than that of co-culture spheroids, potentially due to the formation of more compact structures as size decreases, which may not have allowed for MTT to fully penetrate the spheroids when assessing viability (**Figure 3.6**; Lazzari *et al*., 2018).

In co-culture spheroids, the viability of PC3-HS5 models remained high (**Figure 3.6A**). PC3 cells have been known to undergo an EMT *in vitro,* which may be due to a loss of phosphatase and tensin homolg (PTEN) (Dubrovska *et al*., 2009; Harma *et al*., 2010; Windus *et al*., 2013). This loss of PTEN has been found to occur simultaneously with activation of the Akt and PI3K pathway, which has been found to be integral in the maintenance of spheroid viability (Dubrovska *et al*., 2009). PTEN loss has also been found to correlate with an increased sphere-forming ability in PC3 and DU145 cells, along with an increase in tumorigenicity (Dubrovska *et al*., 2009).

The viability of LNCaP cells in co-culture models at a ratio of 2:1 LNCaP:HS5 compared to a 1:1 or 1:2 ratio was higher when assessed by the MTT viability assay and when visualised under standard light microscopy (**Figure 3.6C; Appendix 1, Figure A1.4C**). This could be due to an overexpression of the Bcl-2 antigen which has been found to be expressed on the peripheral layer of LNCaP spheroids (Takagi *et al*., 2007). As these spheroids contain higher

numbers of LNCaP cells compared to the other ratios studied due to the higher seeding ratio of 2 LNCaP: 1 HS5 cells, Bcl-2 expression may also be higher. This could be associated with protecting LNCaP cells from cell death through inhibiting caspases 3 and 7 during apoptosis (Cohen *et al*., 2012; Erdogan *et al*., 2018; Takagi *et al*., 2007). Another possible explanation for these spheroids displaying higher viability than those containing lower numbers of LNCaP cells is an enhanced level of VEGF production (Takagi *et al*., 2007). VEGF production has been found to correlate with the levels of hypoxia present in LNCaP cell spheroids, as it is regulated by hypoxia-inducible transcriptional mediator HIF-1 (Muir *et al*., 2006; Riffle *et al*., 2007). In the spheroids studied here, VEGF could play a role in enabling the survival of the spheroids. For future studies, to assess the degree of hypoxia occurring within a spheroid, the levels of the hypoxic marker micro-RNA (miRNA)-210 could be measured, which have found to be elevated in both prostate cancer cell lines LNCaP, PC3 and DU145 when cultured under hypoxic conditions, and in the serum of prostate cancer patients (Ivan & Huang, 2014; Quero *et al*., 2011). mi-RNA expression has been found to be regulated by HIF-1 in a variety of tumour types through a hypoxia responsive element, including prostate cancers (Huang *et al*., 2009; Porkka *et al*., 2007). Future work should therefore focus on the characterisation of these genes in the 3D prostate cancer cell systems to confirm their hypothesised effect and determine their role in spheroid viability over time.

Many previous studies have employed fluorescent markers to visualise spheroid viability, proliferation and the regionalisation of cells. For example, Ki-67 staining is used to distinguish areas of proliferation, whilst double fluorescent staining using Hoechst 33342 to stains the condensed chromatin in both apoptotic and viable cells, and PI to stain only dead cells (Gomes *et al*., 2016; Laurent *et al*., 2013; Liu *et al*., 2013; Mosaad *et al*., 2018; Vinci *et al*., 2012). Previous studies within the research group had also employed this method in PC3 prostate cancer cells, and found that spheroid viability decreases after 72 h, as visualised by PI staining (Wang *et al*., 2019). This co-staining method differs from the MTT assay used to assess viability as MTT provides a quantitative measurement of metabolic activity and is only cleaved

by the mitochondria of metabolically active cells. PI staining, however, allows for visualisation of cell death by specifically identifying dead cells as it is excluded from intact, viable cells (van Meerloo *et al*., 2011).

The most viable ratios of prostate cancer and HS5 stromal cells were selected for fluorescence imaging based on the results of the MTT viability assay and alamarBlue proliferation assay and were chosen specific to each prostate cancer cell line. As shown in **Figures 3.8 – 3.11**, minimal dead cells were detected by staining with PI on day 1 across all spheroids in mono- and co-cultures, suggesting these spheroids are healthy and viable. As time progressed, an increase in positive PI staining of dead cells was observed on day 3 in LNCaP and C4-2B co-culture models (**Figures 3.10 & 3.11**) yet was not present in PC3 mono- or co-culture models at any point (**Figure 3.8**) and were only observed in DU145 monocultures on day 5 (**Figure 3.9**). On day 5, DU145 monoculture spheroids show the highest levels of PI staining (**Figure 3.9**), consistent with the MTT (**Figure 3.6B**) and alamarBlue (**Figure 3.7B**) assays, which, on day 5, showed the lowest viability and proliferation rates respectively. PC3 cells have previously been found to be viable in 3D co-cultures with osteoblast and endothelial cells across 7 days when visualised with DsRed, which co-localised with viable cells stained with Calcein-AM (Hsiao *et al*., 2009). PI staining was found to be more concentrated at the centre of each spheroid in the present study, further suggesting the development of a central necrotic core and outer proliferating zone (Grimes *et al*., 2014; Hirschhaeuser *et al*., 2010; Riffle *et al*., 2017). Similar patterns of cell death have also been observed when co-staining with Hoechst 33342 and cleaved caspase 3, a marker of apoptosis (Riffle *et al*., 2017; Slee *et al*., 2001). To provide a more quantitative assay, future work may utilise the CellTiterGlo test (Promega), which correlates the absorbance with the cell viability using a simple add and read format. This assay is not dissimilar to the alamarBlue assay and has been successfully implemented in the assessment of 3D spheroid viability (Mosaad *et al*., 2018; Zanoni *et al*., 2015).

3.4.3 Changes in proliferation rate of prostate cancer-stromal cells grown as mono- and co-culture models

The proliferation rates of cells cultured in 2D and 3D are usually different and are often matrix and cell line dependent (Edmondson *et al*., 2014). Compared to cells cultured in 2D, many cell lines display lower proliferation rates when cultured in 3D (Luca *et al*., 2013). Tumour cells which continue to display proliferative capacity under the hypoxic conditions associated with 3D models has been associated with tumour aggression and lower disease-free survival rates (Hoogsteen *et al*., 2005). As the 3D cell spheroids grow, chemical and oxygen diffusion gradients develop across the radius of each individual spheroid, which can influence cellular proliferation and viability (Gomes *et al*., 2016; Mosaad *et al*., 2018; Zanoni *et al*., 2015). alamarBlue was used in this study to assess proliferation rates, as it has successfully been implemented as a tool for tracking proliferation rates in similar 3D models, particularly those using prostate cancer cells (Florczyk *et al*., 2012; Windus *et al*., 2013).

Proliferation rates in 3D models as opposed to their 2D counterparts remain consistently low, as self-assembled spheroids do not experience the same cell tensions found in cells cultured on 2D surfaces, which stimulate proliferation (Khaitan *et al*., 2006). This was found to be the case in this study, with the proliferation rate of 3D spheroids remaining consistently low, with the exception of PC3 cells (**Figure 3.7A**; Mosaad *et al*., 2018). PC3 cells cultured with medium from HS5 cells have previously shown increased invasion and proliferation rates, suggesting secretions of certain growth factors such as granulocyte from stromal cells-colony stimulating factor (G-CSF), GM-CSF, and macrophage-colony stimulating factor (M-CSF) could influence prostate cancer cell metastases (Wang *et al*., 2020). Proliferation rates in PC3-HS5 co-culture spheroids were highest in the 1:1 PC3:HS5 co-culture on day 3, which correlates with the viability data shown previously (**Figure 3.6A**) that indicates the lowest decline in viability also occurred on day 3. These results are consistent with those of Windus *et al*., who found that by day 3, PC3 cells in co-culture spheroids proliferated at significantly higher rates in comparison to HS5 cells and followed a similar pattern to PC3 cells in monocultures. It has

also been demonstrated that PC3 cells are able to survive and proliferate within osteoblast and endothelial cell co-cultures, independently of the other cell types present (Hsaio *et al*., 2009). A 2:1 PC3:HS5 ratio was chosen for PC3 cells in co-culture as this ratio exhibited the most stable viability across the 5-day culture period, and the proliferation rates of all ratios studied followed the same trend, despite variances in viability and therefore a 2:1 PC3:HS5 ratio was deemed the most consistent (**Figures 3.6A and 3.7A**). As the proliferation rates of all co-culture spheroids (regardless of PC3:HS5 ratio) follow the same trend as PC3 monocultures after day 3, it could be suggested that PC3 cells are influencing the proliferative behaviour of HS5 cells (**Appendix 1, Figure A1.5**; Windus *et al*., 2013). Recently, PC3 cells have been found to influence an increase in the proliferative capacity of bone-derived MSCs, thought to be the result of the secretion of pro-inflammatory cytokines from prostate cancer cells (Ridge *et al*., 2017).

For DU145 cells in co-culture, a ratio of 1:1 DU145:HS5 ratio was chosen as, whilst a ratio of 1:1 DU145:HS5 and 2:1 DU145:HS5 both followed similar patterns in spheroid size and proliferation rates (**Figures 3.5B and 3.7B**), the viability profile of spheroids cultured at a 1:1 DU145:HS5 ratio more closely mirrored that of the DU145 cells in monoculture (**Figure 3.6B**). The growth of prostate cancer cells that do not metastasise to the bone, i.e., DU145 cells, are inhibited by BMP-4 (Cooper *et al*., 2003; Lamm *et al*., 2001; Nishimori *et al*., 2012). In co-culture with LNCaP cells, osteoblastic differentiation of bone stromal cells has been noted to be induced by BMP-4 through the production of Sonic hedgehog (Shh) (Nishimori *et al*., 2012; Zunich *et al*., 2009). It has been suggested that the hedgehog signalling pathways in bone development may also play a role in the formation of bone metastases where osteoblast differentiation is induced when Shh-expressing prostate cancer cells activate the signalling pathway in osteoblast progenitor cells (Zunich *et al*., 2009). In these models, proliferation may also be increased through the production of growth factors stimulated by BMP-4, which has been noted in bone stromal cells producing fibroblast growth factor (FGF)-2 and EGF when co-cultured with LNCaP cells (Nishimori *et al*., 2012).

The considerably lower rates of proliferation observed in the non-invasive LNCaP cell line (**Figure 3.7C**) in comparison with the invasive metastatic PC3 cell line (**Figure 3.7A**) suggest that cells in 3D cultures exhibit proliferation rates that mimic those of prostate cancers found *in vivo* (Windus *et al*., 2012). Whilst tumour cells have been known to influence the proliferative potential of stromal cells, proliferation is also known to increase in the bone microenvironment through osteomimicry, the acquisition of bone cell-like properties by tumour cells (Knerr *et al*., 2004; Windus *et al*., 2013). This could explain the increase in proliferation observed when the number of HS5 cells in co-cultures is twice that of LNCaP cells, suggesting that HS5 cells are proliferating at a faster rate than LNCaP cells (**Figure 3.7C**). The viability of LNCaP cells in a 1:1 LNCaP:HS5 co-culture was significantly lower than spheroids seeded with either 2:1 LNCaP:HS5 cells or 1:2 LNCaP:HS5 cells, which may explain the low rates of proliferation observed at this ratio as only viable, proliferating cells would be able to metabolise alamarBlue (Rampersad *et al*., 2012). For LNCaP cells in co-culture, a ratio of 1:2 LNCaP:HS5 cells was chosen as the viability of these spheroids was the most consistent over time, whilst the proliferation profiles of all ratios studied remained similar (**Figures 3.6C & 3.7C**). It has previously been noted that the proliferation rate of C4-2B cell spheroids gradually increases from days 0 – 5, as observed in this study (**Figure 3.9D**; Florczyk *et al*., 2012; Mosaad *et al*., 2018). For C4-2B cells in co-culture, a ratio of 1:1 C4-2B:HS5 was chosen as these spheroids displayed the most consistent size and proliferation rates over time (**Figures 3.5D & 3.7D**) whilst also maintaining a viability of > 60% across all 5 days (**Figure 3.6D**).

As the surface of a spheroid is curved, it has been reported that the surface cells experience higher levels of tension as they can spread over this curved surface, and therefore proliferate at a higher rate than those at the core of the spheroid (Kenny *et al*., 2007; Mosaad *et al*., 2018; Zanoni *et al*., 2015). To assess this theory, other studies have used fluorescent markers such as Ki-67 to determine zones of proliferation within spheroids, and model a gradient of proliferation (Friedrich *et al*., 2007; Kenny *et al*., 2007; Mosaad *et al*., 2018; Vinci *et al*., 2012). Ki-67 is a protein present in all phases of the cell cycle, with

the exception of G_0, and is therefore used as a marker for the growth fraction of a cell population (Riffle *et al*., 2017). In smaller spheroids of < 400 μm, Ki-67 staining has been observed throughout the spheroid, yet once spheroid size exceeds 500 μm, Ki-67 positive cells only become present around the spheroid surface (Riffle *et al*., 2017). This phenotype relates back to the presence of a necrotic core, as larger spheroids (> 500 μm) have previously been characterised by an external proliferating zone surrounding a necrotic core, which resembles the cellular heterogeneity of solid *in vivo* tumours (Charoen *et al*., 2014; Hirschhaeuser *et al*., 2010; Khaitan & Dwarakanath, 2006; Takagi *et al*., 2007). It has also been noted that the thickness of the proliferating zone remains consistent over time, despite the size of the necrotic core increasing in proportion to the size of the spheroid, which may account for the consistent levels of proliferation observed in some spheroids in this study (Riffle *et al*., 2017). Mosaad *et al*., noted a gradual increase in the DNA content of C4-2B spheroids over the first 5 days of culture, suggestive of an increase in proliferation over the first 5 days of culture, which subsequently decreased by day 7, consistent with a reduction in cellular proliferation when visualised by confocal microscopy using Ki67 staining. Further studies should therefore focus on the use of proliferative markers such as Ki67 to visually determine how representative the models generated in this Chapter are of the *in vivo* environment in terms of the formation of proliferative peripheral zones.

Spheroid shape has been known to contribute to proliferation rates, with more spherical, rounded spheroids similar to those generated in this chapter showing slower rates of proliferation due to a reduced distance between each cell and the culture medium (Kenny *et al*., 2007; Mosaad *et al*., 2018; Zanoni *et al*., 2015). It has been found that non-spherical spheroids, which have an irregular morphology and larger surface area for interaction with culture medium, have a wider zone of active cell proliferation (Kenny *et al*., 2007; Mosaad *et al*., 2018; Zanoni *et al*., 2015). In co-culture with HS5 cells, spherical DU145 and PC3 cells spheroids have been found to have proliferative zones around the periphery of each spheroid, visualised when stained with EdU (Windus *et al*., 2013). Staining with EdU, which marks cells

in the S-phase – has also been found to be more restricted to the periphery of spheroids than Ki-67 staining, indicating a failure to progress through S-phase (Riffle *et al*., 2017).

3.4.4 Use of fluorescent markers to distinguish between cell types in 3D prostate cancer-stromal models

In order to distinguish between prostate cancer and stromal cells and to evaluate stromal cell integration within the prostate cancer spheroid models, the human STRO-1 antibody was used as a fluorescent marker specific to stromal cells (Fong *et al*., 2016; Nishimori *et al*., 2012; Ono *et al*., 2007). It was of importance to generate a uniformly distributed co-culture model to assess the impact of prostate cancer-stromal cell interactions on spheroid formation, viability and proliferation. To date, there are no known specific markers for any of the prostate cancer cell lines used in this study, and therefore to visualise all cells a general nucleic stain, Hoechst 33342, was used (Dasiram *et al*., 2017; Liu *et al*., 2012; Oosterhoff *et al*., 2003). This co-staining allowed the identification of cells negative for STRO-1 yet positive for Hoechst 33342 as prostate cancer cells, whilst those both STRO-1 and Hoechst 33342 positive were HS5 stromal cells (Fitter *et al*., 2017; Windus *et al*., 2013).

STRO-1 has previously been used to co-stain PC3-HS5 and DU145-HS5 prostate cancer and stromal cell 3D co-culture models (Windus *et al*., 2013). Here, when co-cultured with PC3 cells, minimal STRO-1 staining was observed, and therefore it could be suggested that PC3 cells are altering the proliferative behaviour of HS5 cells when compared to their monoculture counterparts (**Figure 3.12A**; Windus *et al*., 2013). In this study, HS5 cells were located primarily around the outer regions of the spheroid when co-cultured with DU145 cells (**Figure 3.12B**), with a distinct absence of cells in the inner region when visualised by Z-stacks (see **Appendix A1.10B**). A similar pattern was noted by Windus *et al*., who reported that HS5 cells seeded in co-culture 3D models with DU145 cells retained their characteristic phenotype and rarely formed cell-cell interactions. Immunostaining of these models found that in co-cultures, E-cadherin was upregulated when compared to monocultures of both prostate cancer and stromal cell spheroids, further suggesting the induction of

an EMT (Windus *et al*., 2013). Evidence of a switch to EMT has been found to initiate the release of cancer cells from their organ of origin, which also correlates with an increase in proliferation in co-culture models as opposed to monocultures, as observed in PC3 and DU145 co-cultures in this study (**Figure 3.7A & B**; Gravdal *et al*., 2007; Putzke *et al*., 2011; Trimboli *et al*., 2008; Windus *et al*., 2013). In co-culture models with LNCaP and C4-2B cells, STRO-1 staining of HS5 cells was more pronounced (**Figure 3.12C & D**), with stromal cells integrated with the prostate cancer cells throughout the spheroids (see **Appendix A1.10C & D**). As C4-2B cells were derived from a bone metastasis of the LNCaP parental line, they exhibit a higher affinity for cell-cell interactions with stromal cells (Sobel *et al*., 2005; Windus *et al*., 2013). Positive STRO-1 staining of HS5 cells was observed towards the centre of the spheroid in co-culture with C4-2B cells (**Figure 3.12D)**, suggesting HS5 cells have a higher affinity to interact with bone-derived metastatic prostate cancer cells (Windus *et al*., 2013). This effect has recently been reported in bone-derived MSCs which showed a significantly increased chemoattraction towards bone metastasis-derived PC3 cells in comparison to non-metastatic 22Rv1 cells or brain metastasis-derived DU145 cells (Ridge *et al*., 2017).

To establish communications between metastasising cancer cells and surrounding bone stromal cells, it is important to determine how cancer cells exit the vasculature once in the bone marrow. Two chemokines of particular interest in the trafficking of prostate cancer cells to the bone, which are involved in the C-X-C (CXC) motif, are CXC receptor 4 (CXCR4) and CXC ligand 12 (CXCL12) (Sun *et al*., 2010; Taichman *et al*., 2002; Windus *et al*., 2012). CXCL12, also known as stromal cell-derived factor-1 (SDF1), is expressed by stromal cells in target organs of prostate cancer metastasis such as the bone, brain and lymph (Taichman *et al*., 2002). CXCR4, the receptor of CXCL12, has been found to be highly expressed by all four prostate cancer cell lines used in this chapter, both in 2D and 3D models, consistent with a metastatic phenotype (Taichman *et al*., 2002; Windus *et al*., 2012). Colonisation of tumour cells to the bone is thought to be the result of co-operative signalling between CXCR4 and CXCL12, establishing interactions between tumour and stromal cells (Schneider *et al*., 2011; Taichman *et al*.,

2002). CXCL12 has also been demonstrated as a chemoattractant of both PC3 and C4-2B cells to stromal cells (Cooper *et al*., 2003). To determine the use of the CXCL12/CXCR4 pathway in the models used in this chapter, immunostaining for each chemokine could be employed. It has previously been demonstrated that CXCR7, another CXCL12 receptor, is highly expressed in 3D PC3 models co-cultured with HS5 cells in areas where STRO-1 expression was also increased (Windus *et al*., 2013). In the bone microenvironment, integrin signalling through alpha-v-beta-3 (αvβ3) on tumour cells has been known to promote tumour metastasis and proliferation (Schneider et al., 2011). In metastatic prostate cancer cells, CXCR4 ligation has been reported to increase αvβ3 expression and subsequently increase aggressiveness (Sun et al., 2007). αvβ3 is an essential integrin for the adherence and migration of prostate cancer cells to the bone matrix in the early stages of bone metastasis, assisting cells with interactions with bone stromal cells, osteoblasts, osteoclasts and the bone matrix itself (Nakamura *et al*., 2007). To further evaluate the effect co-culturing prostate cancer cells with bone stromal cells has on tumour aggressiveness, it would be of interest to characterise changes in the expression of genes known to be involved in cell-cell communication and disease progression, such as CXCR4 and CXCL12. This information would assist in determining the mechanisms driving prostate progression to the bone and may help identify novel drug targets to inhibit this process.

3.5 Conclusion

3D co-culture spheroid models can be used to mimic the tumour microenvironment, exhibiting populations of cells that are viable and proliferating in niches similar to those seen in solid tumours. The data generated in this chapter provides strong evidence for the successful generation of viable 3D monoculture prostate cancer cell spheroids, which will be used as a platform for subsequent experiments in this thesis. This chapter provides a comprehensive, simple method for yielding reproducible 3D prostate cancer spheroid models that recapitulate *in vitro* some of the key characteristics of *in vivo* tumours, whilst also providing a platform for imaging and quantitative analysis. Data here also suggests that this method is capable of producing viable 3D co-culture prostate-cancer stromal cell spheroids models. The androgen-sensitive prostate cancer cell lines LNCaP and C4-2B provide the most relevant model for assessing the effects of altering and monitoring *STEAP2* expression, whilst also proving capable of forming evenly distributed co-culture spheroids that remain viable over time.

Chapter 4

Impact of exposure to anti-STEAP2 mono- and poly-clonal antibodies on prostate cancer cell properties and androgen-regulated responses

4.1 Introduction

STEAP2 has been identified as a potential drug target in the treatment of prostate cancer (see **Chapter 1; Section 1.5.2**; Burnell *et al*., 2018; Whiteland *et al*., 2014). Studies to date have highlighted the potential for viable therapeutic antibodies against STEAP2 in the treatment of advanced prostate cancer (Burnell *et al*., 2018; Nguyen-Chi, 2020; Whiteland *et al*., 2014). The use of antibodies in the treatment of various diseases, including cancer, has rapidly expanded over recent years (see **Chapter 1, Section 1.6;** Chen *et al*., 2020; Strebhardt & Ullrich, 2008). Antibodies target a specific sequence on antigens and induce cell death through an immune-mediated signalling cascade (see **Chapter 1, Section 1.6;** Chen *et al*., 2020; Shields *et al*., 2001). pAbs target multiple epitopes and are associated with more off-target adverse effects, whereas mAbs specifically target single epitopes. This allows for mAbs to be delivered at lower doses than pAbs whilst inducing less off-target side effects (Wang *et al*., 2013).

STEAP2 holds potential as a therapeutic target for antibody-based treatments due to its transmembrane location and correlation with prostate cancer progression (see **Chapter 1, Section 1.5.5**; Burnell *et al*., 2018). Specific targeting of STEAP2 may allow for promoting prostate cancer cell death, whilst preserving healthy cells from the toxic off-target side-effects posed by many current therapies (Sikkeland *et al*., 2016). Given that STEAP2 has six transmembrane helices and three extracellular loops (ECLs), work within the research group has previously identified these loops as accessible targets for

mAbs (Grunewald *et al*., 2012; Nguyen-Chi, 2020). A commercially available pAb was also identified by previous members of the group as a lead candidate that is highly specific to membranous STEAP2, targeting the third extracellular loop (ECL3) (Nguyen-Chi, 2020).

Whilst anti-STEAP2 pAbs and mAbs have been found to be effective at decreasing cell viability in 2D monolayers of prostate cancer cells, it currently remains unknown whether such agents have the potential to induce cell death in 3D prostate cancer cell models (Hasegawa *et al*., 2018; Nguyen-Chi, 2020). This is an important consideration because, while 2D cells have the advantage of low costs and simplicity of use during the early stages of drug development, they lack the complex physiology and heterogeneity presented in tumour tissues (Hirschhaeuser *et al*., 2010). 3D culture models allow for cell-cell interactions to occur in a manner that is more representative of the *in vivo* system, allowing for evaluation of interaction between the drug and tissue in a more realistic test system (Hirschhaeuser *et al*., 2010; Kunz-Schughart *et al*., 2004; Thoma *et al*., 2014). To date, anti-STEAP2 antibodies have not been applied to 3D prostate cancer models, and hence the 3D models generated in **Chapter 3** provide a platform for interrogation with anti-STEAP2 pAbs and mAbs in this Chapter.

A potential approach to reducing off-target toxicity would be to enhance the specificity of drugs through the use of ADCs (see **Chapter 1, Section 1.6.4**; Tarcsa *et al*., 2020). ADCs allow for drugs to be transported into cells by utilising the ability of mAbs to specifically target tumour-specific cell surface biomarkers (Tarcsa *et al*., 2020). To enable drug delivery to cells, receptor internalisation must be triggered, which for STEAP2 to be considered for use in ADC technology would occur upon the highly specific binding of the mAb to STEAP2 (Hasegawa *et al*., 2018; Tarcsa *et al*., 2020). Cell death is then achieved by lysosomal enzymes degrading the ADC-receptor complex and subsequently releasing the cytotoxic payload (Kamath & Iyer, 2015; Tarcsa *et al*., 2020). As it is currently unclear whether STEAP2 becomes internalised upon the application of mAbs, the suitability of anti-STEAP2 mAbs with ADC technology also remains unknown (Hasegawa *et al*., 2018).

Previous work within the wider Swansea research group has focussed on assessing the viability of PC3 prostate cancer cells in response to a commercially available anti-STEAP2 pAb, and the generation of anti-STEAP2 mAbs (Nguyen-Chi, 2020). However, such antibodies have not been applied to a wide range of prostate cancer cell lines to compare the responses of androgen-sensitive and androgen-independent cell lines, nor have they been applied to 3D spheroid models. To date, the effects of targeting STEAP2 with pAbs and mAbs on downstream genes associated with prostate cancer progression has not been studied, and therefore the effect of targeting STEAP2 on *AR* expression is also currently unknown. This is of interest when developing a potential therapeutic agent to treat prostate cancer, as the disease is largely androgen-regulated and therefore any changes in *AR* expression may affect disease progression (see **Chapter 1, Section 1.8**; Gonen-Korkmaz *et al*., 2014; Myung *et al*., 2013; Tanner *et al*., 2011). Overexpression of *STEAP2* has been linked with increased cell proliferation via the ERK/MAPK signalling pathways, resulting in a more aggressive phenotype leading to enhanced cell migration and invasion (Gomes *et al*., 2012). The MAPK signalling pathway is also linked with resistance to androgen therapy, and it is therefore of interest to determine links between *STEAP2* and *AR* expression with regards to identifying novel therapeutic targets in the treatment of prostate cancer (Jia *et al*., 2013; Li *et al*., 2019).

The aim of this Chapter was to assess the suitability of STEAP2 as a therapeutic target. This aim was addressed through the following objectives:

1. To identify a lead anti-STEAP2 mAb candidate capable of significantly reducing cell viability in a panel of prostate cancer cell lines from a panel of anti-STEAP2 mAbs previously generated within the wider Swansea research group;
2. To evaluate the impact of anti-STEAP2 mono- and polyclonal antibodies on the viability of 3D prostate cancer spheroids;
3. To evaluate the impact of an anti-STEAP2 pAb on the gene expression of *AR* and androgen-regulated genes;

4. To assess the ability of an anti-STEAP2 monoclonal antibody to trigger STEAP2 receptor internalisation in order to determine the suitability for use with ADC technology.

4.2 Materials and methods

4.2.1 Cell culture

4.2.1.1 2D monolayer cells

The four prostate cancer cell lines C4-2B, DU145, LNCaP and PC3 and the normal prostate epithelial cell line PNT2 were routinely cultured as described in **Chapter 2, Section 2.2.7.1.** For absorbance-dependent endpoint analyses, cells were grown in phenol-red free DMEM supplemented with 10% FBS, 1% L-glutamine and 1% P/S (Thermo Fisher, UK).

4.2.1.2 3D cell spheroids

Cells were counted as described in **Chapter 2, Section 2.2.7.2** and seeded at a desired density onto agarose coated 96-well tissue culture plates, as described in **Chapter 2, Section 2.2.7.3.**

4.2.2 Exposure of 2D monolayers and 3D spheroids to STEAP2 antibodies

4.2.2.1 Polyclonal STEAP2 antibody treatment

A commercially available anti-STEAP2 polyclonal antibody (stock concentration 1 mg/ml) was used within this Chapter (Aviva Systems Biology, OASG06901). Approximately 10,000 cells per well in a 96-well were cultured for 24 h before 24 h exposure to the anti-STEAP2 polyclonal antibody treatment in triplicate.

4.2.2.2 Monoclonal STEAP2 antibody treatment

Three anti-STEAP2 monoclonal antibodies were previously developed by group members in conjunction with Antibody Production Services, the concentrations of which can be found in **Table 4.1** (Nguyen-Chi, 2020). Approximately 10,000 cells per well in a 96-well were cultured for 24 h before

24 h exposure to the anti-STEAP2 monoclonal antibodies treatment in triplicate.

Table 4.1. Stock concentrations of anti-STEAP2 mAbs.

mAb #	Target	Stock concentration (mg/ml)
1	Linear	2.0
2	Linear	1.3
3	Linear	1.8

4.2.2.3 Cell viability quantification

Monolayers of prostate cancer cells were cultured in 96-well plates as described in **Section 4.2.1.1,** whilst 3D prostate cancer cell spheroids were generated in 96-well plates as described in **Section 4.2.1.2.** Cells were exposed to anti-STEAP2 antibodies as described in **Sections 4.2.2.1 & 4.2.2.2**. The MTT cell viability assay was used following treatment with either poly- or monoclonal anti-STEAP2 antibodies, as described in **Chapter 2, Section 2.4.1.** Absorbance was read at A = 570 nm using a fluorescence plate reader (POLARstar, BMG Labtech, UK). The cell viability experiments were conducted in triplicate.

4.2.3 Detection of *AR* and *AR*-regulated genes in prostate cancer cells following treatment with STEAP2 antibodies

PC3, DU145, LNCaP and C4-2B cells were treated with anti-STEAP2 polyclonal antibody as described in **Section 4.2.2.1**. Treated cells were harvested, RNA was extracted, cDNA synthesised, and qRT-PCR performed as described in **Chapter 2, Section 2.3**. Cells were probed for the detection of *AR* and its downstream targets; *PSA*, *FKBP5*, *TMPRSS2*, and *GPRC6A*, with *GAPDH* as the housekeeping control, using the primers detailed in **Chapter 2, Section 2.3.3, Table 2.8.** The results were subsequently analysed as described in **Chapter 2, Section 2.3.4.**

4.2.4 Receptor internalisation

4.2.4.1 Slide preparation

In an 8-well chamber slide (Ibidi, Germany), cells were seeded in 300 µl serum-free media for 48 h at 37°C/ 5% CO_2 receptor internalisation was carried out. Once cells had reached 80% confluency, old serum-free media was discarded, cells were washed with PBS and the treatment was added in complete media. Slides were initially incubated on ice for 30 minutes prior to incubation at 37°C/ 5% CO_2 for the desired time (0, 3, 12 or 24 h) to allow for receptor internalisation. Following the desired incubation time, the chamber was washed with PBS and fixed with PFA (Polysciences, USA, Cat. 18814-20) for 20 minutes at room temperature. Chambers were washed with PBS and cells were permeabilised with 0.1% Triton-X 100 (Sigma Aldrich, UK, Cat. T8787) for 5 minutes at room temperature. Chambers were washed with PBS and cells were blocked with 3% BSA (Sigma Aldrich, UK, Cat. A2153) for 1 hour at room temperature. Chambers were washed with PBS and incubated with secondary Alexa-Fluor 488 antibody (1:200, Invitrogen, UK) in 3% BSA overnight at 4°C blocked from light. The secondary antibody was removed, and cells washed with PBS. Nuclei were counterstained with 4',6-diamidino-2-phenylindole (DAPI) (Vectorlabs, UK, Cat. H-1200). Images were acquired with the confocal LSM 710 microscope (Zeiss, Germany) at a 63x zoom magnification. The experiment was conducted in duplicate unless otherwise stated.

4.2.4.2 Fluorescent imaging analysis and image processing

For fluorescent microscopical analysis, a confocal laser scanning microscope (LSM710, ZEISS, Germany) was used (**Chapter 2, Section 2.6**). The analysed channels and emission wavelengths (nm) were blue (405 nm) for the nuclei and red (543 nm) for internalised STEAP2-receptor mAb. The secondary goat anti-mouse anti-IgG antibody (1:1,000, Invitrogen, UK) was used to detect the primary antibodies. Zen Black software Version 10 was used to process images, and scale bars were based on the known microscope

pixel sizes for each objective (μm). The red-blue-green (RBG) setting was used to display coloured images.

4.2.5 Statistical analysis

Statistical analysis was performed using GraphPad Prism version 8 for iOS, using the one-way ANOVA *post-hoc* Dunnett test. Data was considered statistically significant when a p-value of < 0.05 (*), p-value < 0.01 (**) or a p-value of < 0.001 (***) or p-value < 0.0001 (****) was obtained, which were annotated within the respective figures. Confocal microscopy for receptor internalisation studies was conducted through acquisition of three images at three different fields of view per test sample as qualitative analysis.

4.3 Results

The aim of this Chapter was to evaluate the impact of a commercially available anti-STEAP2 polyclonal antibody, along with three anti-STEAP2 monoclonal antibodies, on the viability of prostate cancer cells grown as both 2D monolayers and 3D spheroids, as determined by the MTT assay. The impact of the anti-STEAP2 polyclonal antibody on *AR* and androgen-regulated gene expression was then assessed by qRT-PCR. Finally, this Chapter aimed to address the potential of a selected anti-STEAP2 monoclonal antibody for use with ADC technology, by assessing receptor internalisation by confocal microscopy.

4.3.1 Anti-STEAP2 pAb substantially reduces cell viability in four prostate cancer cell lines in 2D

In order to determine the ability of a commercially available anti-STEAP2 polyclonal antibody to induce cell death in 2D prostate cancer cells, the MTT cell viability assay was utilised. Four prostate cancer cell lines were exposed to three different doses of anti-STEAP2 polyclonal antibody ranging from 25, 50 and 75 μg/ml of pAb for 24 h before the assay was conducted (**Figure 4.1**). All doses induced significant reductions in the percentage of viable cells in PC3, DU145 and LNCaP cells (**Figures 4.1**). However, only > 50% cell death was achieved in LNCaP cells treated with 50 and 75 μg/ml anti-STEAP2 pAb, as indicated by the calculated IC_{50} values (**Table 4.2;** AAT Bioquest Inc., 2020). The largest reduction in the percentage of viable cells was observed in LNCaP cells at the highest pAb dose of 75 μg/ml (-63.4%, $p < 0.0001$; **Figure 4.1C**). In C4-2B cells, only the highest dose of 75 μg/ml induced a significant reduction in cell viability (-19.2%, $p < 0.05$); **Figure 4.1D**). Interestingly, in PC3 cells, reduction in the number of viable cells did not occur in a dose-dependent manner, with an initial decrease in the percentage of viable cells of -28.5% when treated with 25 μg/ml anti-STEAP2 pAb, which plateaued across the range of doses ($p < 0.01$; **Figure 4.1A**). These data suggest that in the interest of conserving the drug, increasing the dose in PC3 cells is not warranted.

Overall, these data suggest that 75 μg/ml anti-STEAP2 pAb substantially decreases the cell viability of all four prostate cancer cell lines.

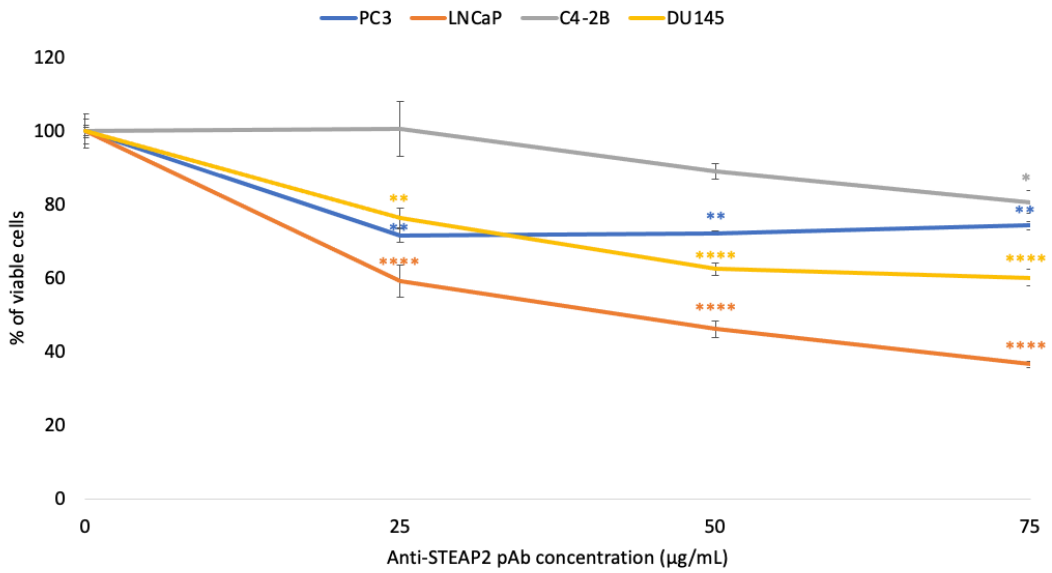

Figure 4.1. Effect of anti-STEAP2 pAb on prostate cancer cell viability. PC3, LNCaP, C4-2B and DU145 prostate cancer cells were treated with increasing concentrations of anti-STEAP2 pAb. After 24 h treatment, cell viability was assessed by the MTT assay. An ANOVA post-hoc Dunnett test was performed for statistical analysis. Error bars denote S.E.M. p-value < 0.01 (**), p-value < 0.001 (***), p-value < 0.0001 (****) (N = 3).

Table 4.2. IC_{50} values of the anti-STEAP2 pAb determined by the results of the MTT cell viability assays displayed in Figure 4.1. Calculated using AAT Bioquest Inc. *Quest Graph™ IC50 Calculator* (AAT Bioquest Inc., 2020).

	PC3	DU145	LNCaP	C4-2B
pAb (μg/ml)	120	124	40	144

4.3.2 Anti-STEAP2 pAb does not substantially reduce cell viability in two prostate cancer cell lines in 3D

Following the results of **Section 4.3.1**, it was of interest to assess the impact of the same commercially available anti-STEAP2 polyclonal antibody on reducing the percentage of viable cells in 3D prostate cancer spheroids, again using the MTT cell viability assay. To represent a low STEAP2 expression model, PC3 cells were chosen, whilst LNCaP cells were selected to represent a high STEAP2 expression model. 3D spheroids were exposed to the same three different doses ranging from 25, 50 and 75 μg/ml of pAb for 24 h before the assay was conducted (**Figure 4.2**). Neither of the doses induced significant reductions in the percentage of viable cells in either cell line (**Figure 4.2**). Interestingly, the pAb exposure did reduce the percentage of viable cells in a dose dependent manner in 3D PC3 cell spheroids, with the greatest reduction observed at a dose of 75 μg/ml (-28.0%; **Figure 4.2**). These data suggest that to significantly induce a reduction in 3D spheroid viability, higher doses of anti-STEAP2 pAb may be needed than those that are able to reduce viability in a 2D cell culture system.

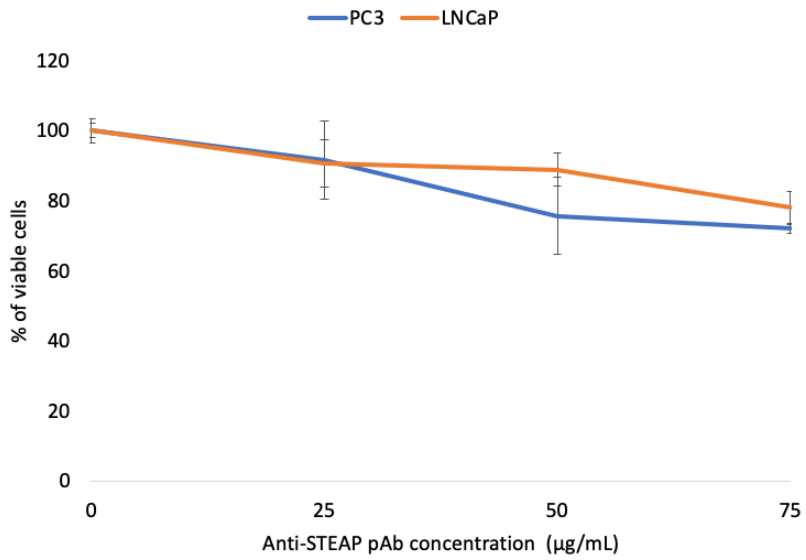

Figure 4.2. Effect of Anti-STEAP2 pAb on 3D prostate cancer spheroid viability. PC3 and LNCaP prostate cancer cells were grown as 3D spheroids treated with increasing concentrations of anti-STEAP2 pAb. After 24 h treatment, cell viability was assessed by the MTT assay. An ANOVA post-hoc Dunnett test was performed for statistical analysis. Error bars denote S.E.M. p-value < 0.01 (**), p-value < 0.001 (***), p-value < 0.0001 (****) (N = 3).

4.3.3 Anti-STEAP2 pAb increases the expression of *AR* in androgen-sensitive prostate cancer lines

AR plays a vital role in prostate progression and therefore it was of interest to explore *AR* expression following exposure to anti-STEAP pAb. Four prostate cancer cell lines were exposed to three different doses of anti-STEAP pAb ranging from 25, 50 and 75 μg/ml of pAb for 24 h before RNA was extracted, cDNA synthesised, and qRT-PCR conducted.

LNCaP and C4-2B are both androgen-sensitive cell lines, whilst PC3 and DU145 are androgen-independent. Whilst the results did not reach statistical significance, 75 μg/ml of pAb increased *AR* expression in PC3 and DU145 cells (3.8- and 5.6-fold respectively; **Figure 4.3**). *AR* was found to be highly and significantly overexpressed in C4-2B cells exposed to pAb doses of 25 and 50 μg/ml (28.6- and 28.9-fold respectively, $p < 0.01$; **Figure 4.3**), yet this was not found to be significant at the highest dose of 75 μg/ml (13.5-fold; **Figure 4.3**). pAb exposure increased *AR* expression in a dose dependent manner in LNCaP cells, inducing a 332905.6-fold increase at 75 μg/ml pAb ($p < 0.0001$; **Figure 4.3**). These data suggest that anti-STEAP2 pAb exposure significantly increases *AR* expression in androgen-sensitive but not androgen-independent cell lines. On the basis of these results, qRT-PCR was further utilised to explore the impact of anti-STEAP2 pAb treatment on the expression of four genes downstream of *AR*: *PSA, FKBP5, TMPRSS2* and *GPRC6A* in LNCaP and C4-2B cells.

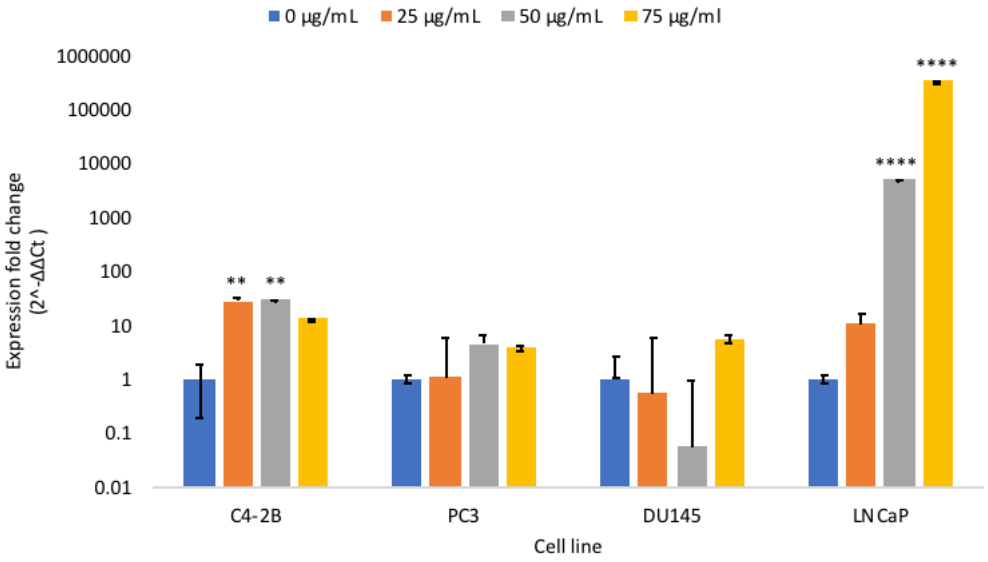

Figure 4.3. Effect of anti-STEAP2 pAb on *AR* expression in prostate cancer cells. Fold changes in *AR* gene expression in a panel of human prostate cancer cell lines treated with anti-STEAP2 pAb as compared to untreated cells. An ANOVA post-hoc Dunnett test was performed for statistical analysis. *GAPDH* was used as the housekeeping gene. Error bars denote S.E.M. p-value < 0.01 (**), p-value < 0.001 (***), p-value < 0.0001 (****) (N = 3).

4.3.4 Anti-STEAP2 pAb increases the expression of androgen-related genes in androgen-sensitive prostate cancer lines

Section 4.3.3 demonstrated that AR is significantly overexpressed in the androgen-sensitive cell lines LNCaP and C4-2B cells following anti-STEAP2 pAb treatment. Following these results, the gene expression of four androgen-regulated genes – *PSA, FKBP5, TMPRSS2* and *GPRC6A* – were quantified in response to anti-STEAP2 pAb treatment by qRT-PCR in LNCaP and C4-2B cells. Untreated cells were used for comparison.

Upon gene expression analysis of the four androgen-regulated genes, the highest overexpression was found in C4-2B cells treated with the lowest dose of pAb of 50 μg/ml, which induced a significant increase in *TMPRSS2* expression ($1.9x10^{10}$-fold, $p < 0.001$; **Figure 4.4B**). *PSA* was also significantly increased at all three doses of pAb exposure, the lowest of which (25 μg/ml) induced the highest fold increase in expression (197.7-fold, $p < 0.01$; **Figure 4.4B**). In LNCaP cells, a significant increase in *FKBP5* expression was induced following exposure to both 50 and 75 μg/ml pAb (1128.0- and 469.0-fold respectively, $p < 0.0001$; **Figure 4.4A**). *GPRC6A* overexpression was also significant following exposure to 75 μg/ml pAb in LNCaP cells (95495.5-fold, $p < 0.05$; **Figure 4.4A**). qRT-PCR analysis of *PSA, FKBP5, TMPRSS2* and *GPRC6A* expression therefore demonstrated that all four genes are overexpressed following pAb exposure in androgen-sensitive cell lines.

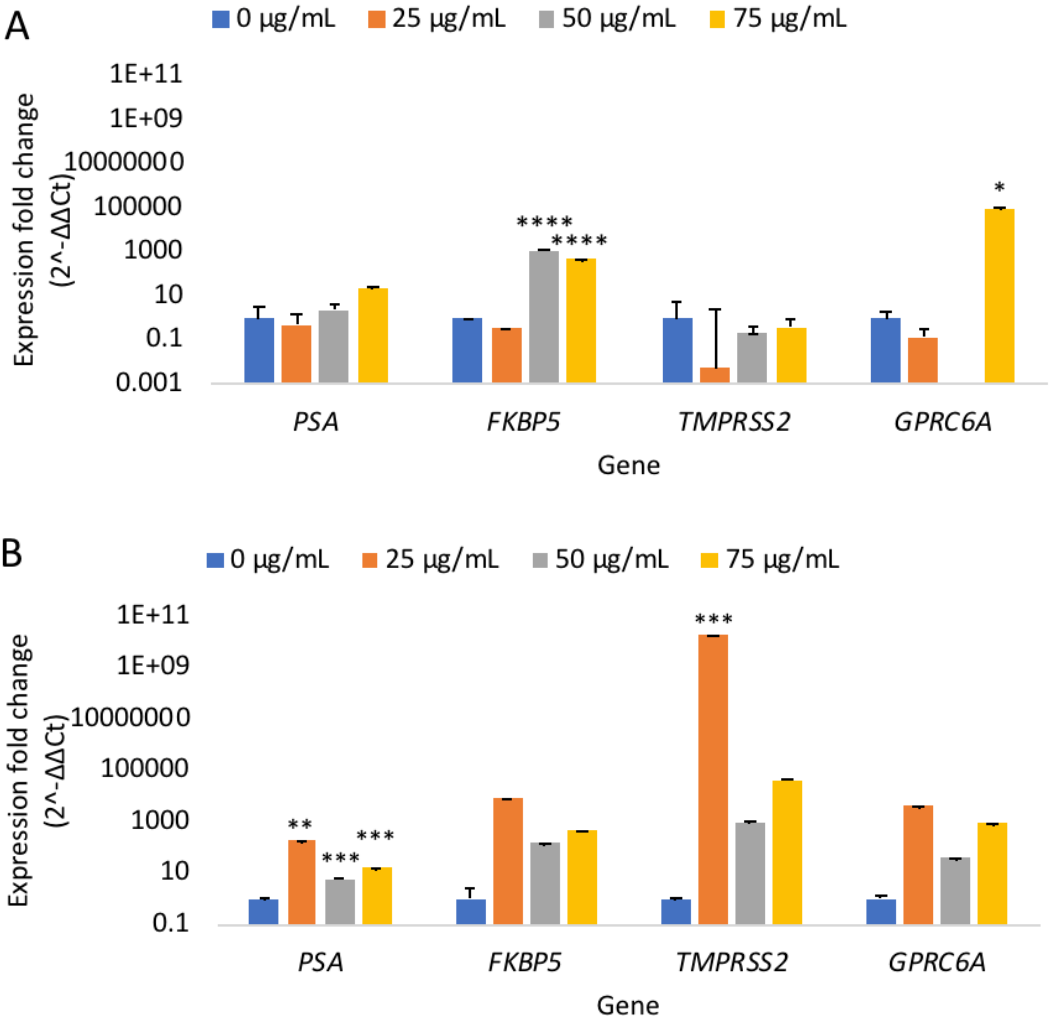

Figure 4.4. Effect of anti-STEAP2 pAb on *AR* regulated genes in androgen-sensitive prostate cancer cells. Fold change in expression of *PSA, FKBP5, TMPRSS2* and *GPRC6A* genes in LNCaP (A) and C4-2B (B) prostate cancer cells treated with anti-STEAP2 pAb as compared to untreated cells. An ANOVA post-hoc Dunnett test was performed for statistical analysis. *GAPDH* was used as the housekeeping gene. Error bars denote S.E.M. p-value < 0.01 (**), p-value < 0.001 (***), p-value < 0.0001 (****) (N = 3).

4.3.5 Anti-STEAP2 mAbs substantially reduce cell viability in four prostate cancer cell lines in 2D

Whilst pAbs are effective at inducing cell death, they target multiple epitopes of the target antigen and therefore offer reduced specificity compared to mAbs which target single epitopes. mAbs also have the potential to be used in ADC technology whereas pAbs are therefore less suitable. Hence, it was of interest to utilise the MTT cell viability to assess the toxicity of a panel of three anti-STEAP2 monoclonal antibodies in 2D prostate cancer cells. Four prostate cancer cell lines were exposed to doses of anti-STEAP2 monoclonal antibodies ranging from 31.25 to 1,000 μg/ml of mAb for 24 h before the assay was conducted (**Figure 4.5**).

In PC3 cells, the lower doses of 31.25, 62.5 and 125 μg/ml mAb2 increased the percentage of viable cells by +49.1%, +53.6% and +42.8% respectively ($p \leq 0.05$; **Figure 4.5A**). In PC3 cells only the highest dose of 1,000 μg/ml of all three mAbs significantly reduced the percentage of viable cells, with mAb2 inducing the biggest reduction of -71.8% ($p < 0.001$; **Figure 4.5A**). In LNCaP cells, mAb3 did not induce a significant reduction in the percentage of viable cells at any dose, yet both mAb1 and mAb2 significantly reduced the percentage of viable cells at doses between 250 – 1,000 μg/ml (**Figure 4.5B**). The most significant reduction in the percentage of viable LNCaP cells of -84.7% was observed in cells treated with 1,000μg/ml mAb2 ($p < 0.001$; **Figure 4.5B**). C4-2B cells were the most responsive to treatment with all three mAbs, with all doses significantly reducing the percentage of viable cells (**Figure 4.5C**). In C4-2B cells, the biggest reduction in the percentage of viable cells of -89.9% was induced by mAb2 at a dose of 1,000 μg/ml ($p < 0.0001$; **Figure 4.5C**). Finally, DU145 was the only cell line to exhibit a significant reduction in the percentage of viable cells in response to all doses of mAb3 (**Figure 4.5D**). However, as with the previous three cell lines, the greatest reduction in the percentage of viable cells was following treatment with 1,000 μg/ml of mAb2 (-81.8%, $p < 0.0001$; **Figure 4.5D**). Based on these data, mAb2 was selected to be carried forward for further analyses within this Chapter as this antibody

induced cell death at lower doses across all four cell lines (**Figure 4.5; Table 4.3**).

Table 4.3. IC_{50} values of each anti-STEAP2 mAb determined by the results of the MTT cell viability assays displayed in Figure 4.5. Calculated using AAT Bioquest Inc. *Quest Graph™ IC50 Calculator* (AAT Bioquest Inc., 2020).

	PC3	**DU145**	**LNCaP**	**C4-2B**
mAb1 (μg/ml)	510	289	566	57
mAb2 (μg/ml)	650	441	248	42
mAb3 (μg/ml)	770	235	1,028*	189

*estimation from extrapolated data provided for comparison purposes

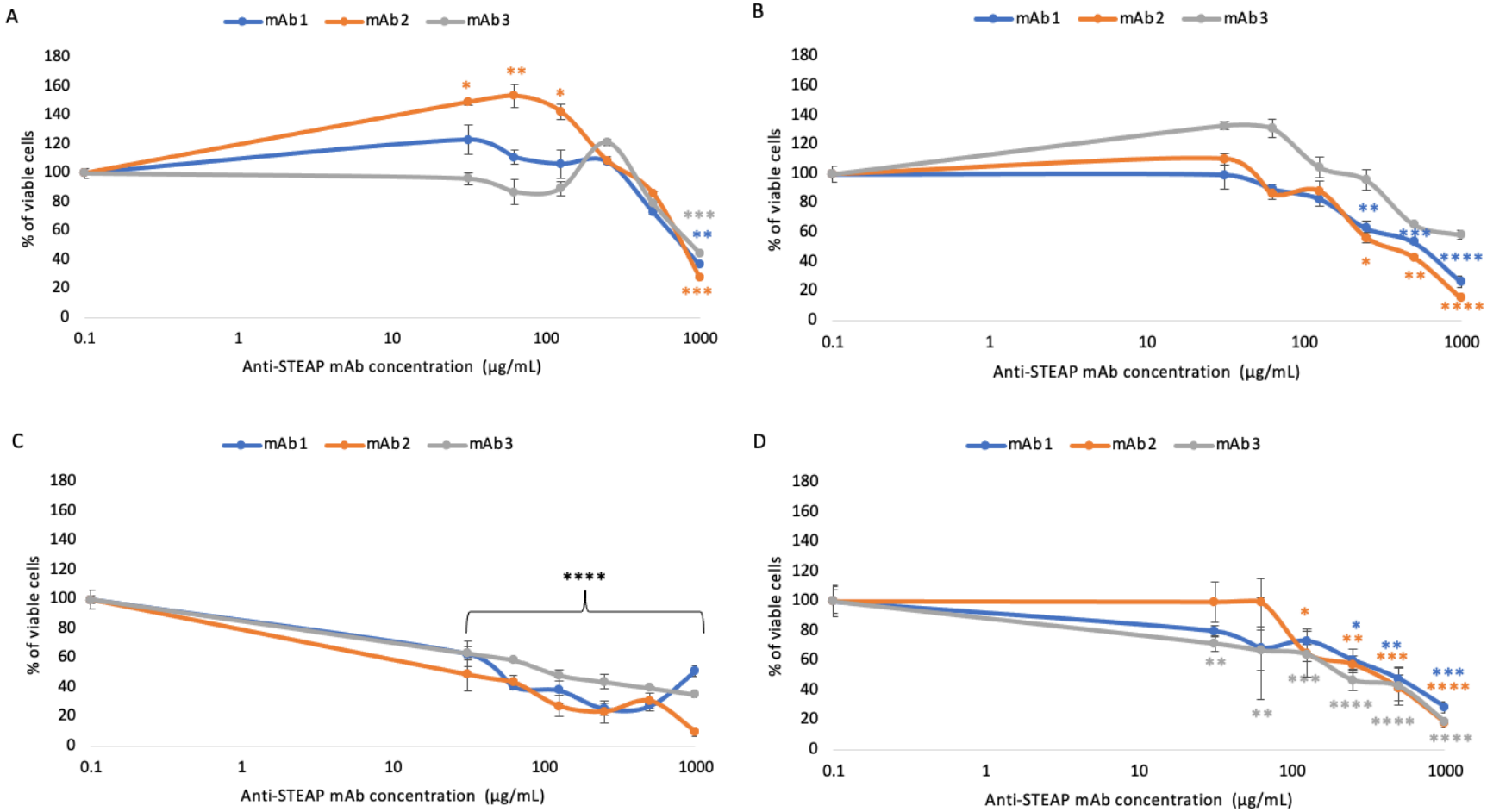

Figure 4.5 Effect of three anti-STEAP2 mAbs on 2D prostate cancer cell viability. PC3 (A), LNCaP (B), C4-2B (C) and DU145 (D) prostate cancer cells were treated with increasing concentrations of anti-STEAP2 mAbs. After 24 h treatment, cell viability was assessed by the MTT assay. An ANOVA post-hoc Dunnett test was performed for statistical analysis. Error bars denote S.E.M. p-value < 0.01 (**), p-value < 0.001 (***), p-value < 0.0001 (****) (N = 3).

4.3.6 Anti-STEAP2 mAbs substantially reduce cell viability in two prostate cancer cell lines in 3D

Based on the results of **Section 4.3.5**, mAb2 was selected to be carried forward for assessing cell viability in 3D prostate cancer cell spheroids. PC3 and LNCaP cells were chosen to represent one low and one high STEAP2 expression model respectively (see **Chapter 3, section 3.3.1**). 3D spheroids were left to form for 24 h before being exposed to doses of anti-STEAP2 mAb2 ranging from 31.25 to 1,000 μg/ml of mAb2 for 24 h before the assay was conducted (**Figure 4.6**).

As in 2D cells (**Figure 4.5A**), the percentage of viable PC3 spheroids initially increased at doses between 31.25 – 125 μg/ml mAb2 (**Figure 4.6**). Only the highest mAb2 dose of 1,000 μg/ml induced a significant reduction in the percentage of viable PC3 spheroids (-68.5%, $p < 0.001$; **Figure 4.6**). LNCaP spheroids were more susceptible to mAb2 treatment, with doses between 62.5 – 1,000 μg/ml all inducing significant reductions in the percentage of viable spheroids (**Figure 4.6**). Interestingly, a dose of 250 μg/ml reduced the percentage of viable LNCaP spheroids the most (-88.2%, $p < 0.0001$; **Figure 4.6**). As such, increasing the dose of mAb2 in LNCaP spheroids did not continue to reduce the percentage of viable spheroids, with doses of 500 and 1,000 μg/ml mAb2 reducing viability by -87.3% and -78.1% respectively ($p \leq 0.001$; **Figure 4.6**). Therefore, in the interest of conserving the drug, in LNCaP spheroids increasing the dose of mAb2 above 250 μg/ml would not be warranted, whilst in PC3 spheroids viability decreased in a dose dependent manner. These data, combined with that of **Section 4.3.5**, suggest that prostate cancer spheroids with higher STEAP2 expression are more susceptible to mAb2 treatment than those with low STEAP2 expression (**Figures 4.5 & 4.6**).

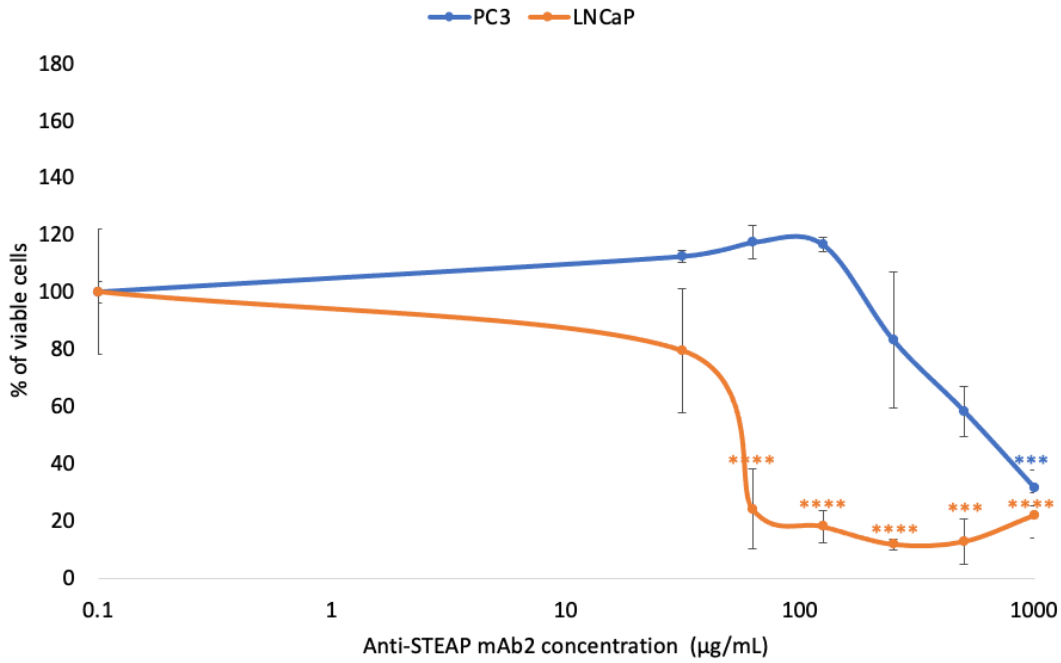

Figure 4.6. Effect of Anti-STEAP2 mAb2 on 3D prostate cancer spheroid viability. PC3 and LNCaP prostate cancer cells were grown as 3D spheroids treated with increasing concentrations of anti-STEAP2 mAb2. After 24 h treatment, cell viability was assessed by the MTT assay. An ANOVA post-hoc Dunnett test was performed for statistical analysis. Error bars denote S.E.M. p-value < 0.01 (**), p-value < 0.001 (***), p-value < 0.0001 (****) (N = 3).

4.3.7 Anti-STEAP2 mAb2 triggers STEAP2 receptor internalisation in both a time and dose dependent manner

To visualise cell surface STEAP2 prior to evaluating receptor internalisation, the fluorescent signal of STEAP2 was activated through conjugation with Alexa-488 (green), whilst cell nuclei were counterstained with DAPI (blue). This represented time point 0 h (see **Figures 4.7 – 4.9**). PC3, LNCaP and C4-2B cells were exposed to anti-STEAP2 mAb2 for 3, 12 and 24 h to observe STEAP2 receptor internalisation (**Figures 4.7 – 4.9** respectively, where representative images are shown; additional images from the second replicate can be found in **Appendix 2, Figures A2.1 – A2.3**). Anti-STEAP2 mAb2 doses that induced a significant reduction in cell viability were selected for future use in this Chapter (**Figure 4.5**).

STEAP2 receptor internalisation became more evident in all three cell lines in a time- and dose-dependent manner. In PC3 cells, STEAP2 receptor internalisation was observed as early as 3 h post incubation and was fully internalised by 24 h (**Figure 4.7)**. At 24 h, prominent STEAP2 staining (green) was evenly distributed in PC3 cells exposed to 100 and 200 μg/ml (**Figure 4.7**). In PC3 cells, a dose of 500 μg/ml did not trigger as prominent receptor internalisation at either time point (**Figure 4.7**). In LNCaP cells, some STEAP2 receptor internalisation was visible at 0 h, prior to incubation with anti-STEAP2 mAb, and increased in a dose-dependent manner (**Figure 4.8**). A lack of STEAP2 receptor internalisation was visible following exposure to 200 μg/ml in LNCaP cells at either time point, suggesting this dose was too high and therefore saturated cells (**Figure 4.8**). Both 50 and 100 μg/ml mAb2 triggered STEAP2 receptor internalisation from as early as 3 h, with 50 μg/ml triggering a more even distribution (**Figure 4.8**). In C4-2B cells, receptor internalisation was also triggered as early as 3 h post incubation with all three anti-STEAP2 mAb2 doses and was most evenly distributed following 12 h exposure to 50 μg/ml mAb2 (**Figure 4.9**).

These data suggest that STEAP2 receptor internalisation is triggered following exposure to lower doses of anti-STEAP2 mAb2 in LNCaP and C4-2B cells

than in PC3 cells. Anti-STEAP2 mAb2 also triggered STEAP2 receptor internalisation in a shorter time frame in LNCaP and C4-2B cells than in PC3 cells. Together, these data suggest that anti-STEAP2 mAb2 holds potential for use in ADC technology in cells with high STEAP2 expression.

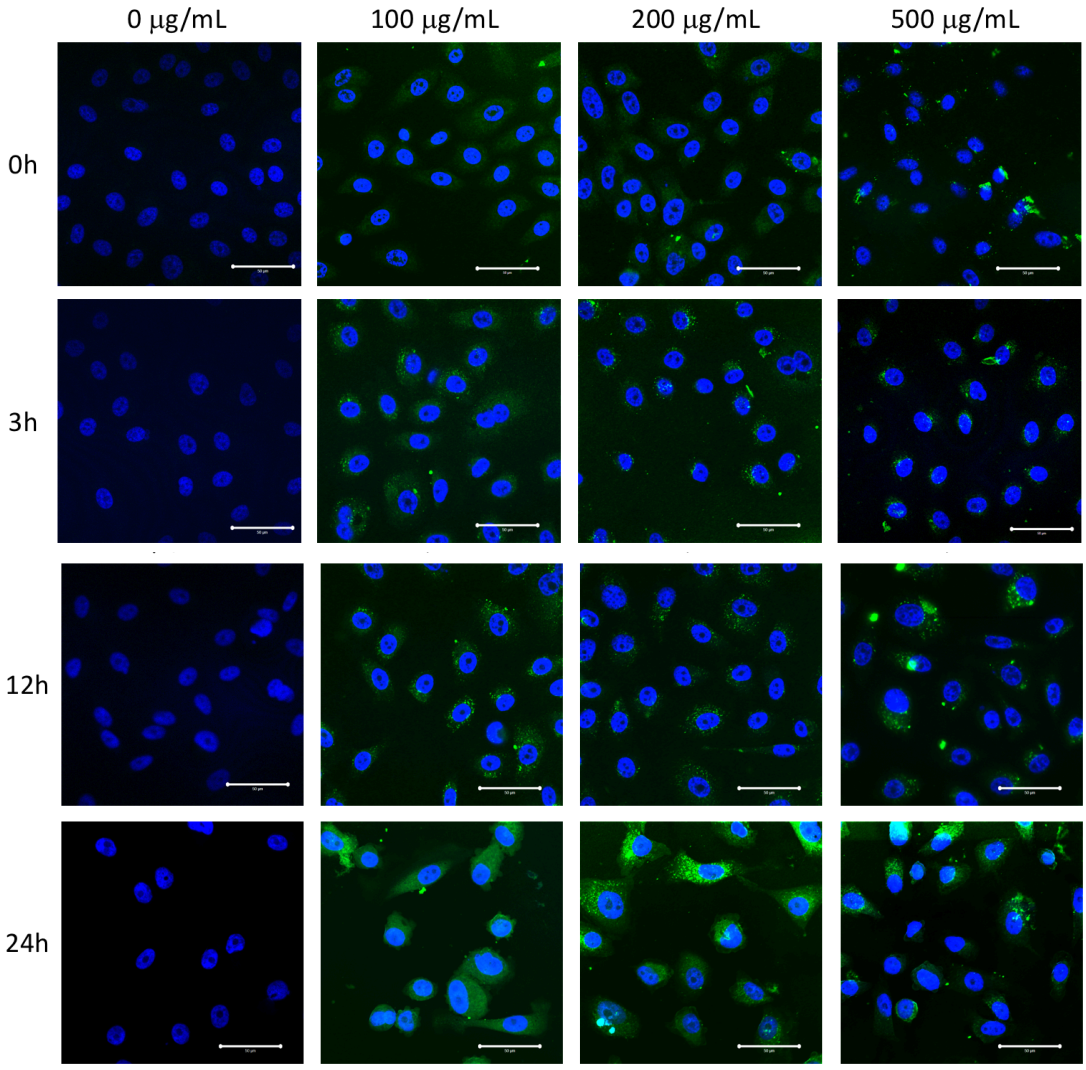

Figure 4.7. Anti-STEAP2 mAb2 exposure triggers STEAP2 receptor internalisation in PC3 cells. PC3 cells were exposed to anti-STEAP2 mAb2 for 0, 3, 12 and 24h at doses of 0, 100, 200 and 500 μg/ml. 0h: cell surface STEAP2 was visualised before receptor internalisation. 3h & 12h: STEAP2 receptor internalisation was initiated. 24h: fully internalised STEAP2 was evident. Blue: nuclei; green: STEAP2. Images were acquired with a Confocal LSM 710 with a 63x zoom objective (ZEISS, Germany). Scale bar = 50 μm. (N = 2).

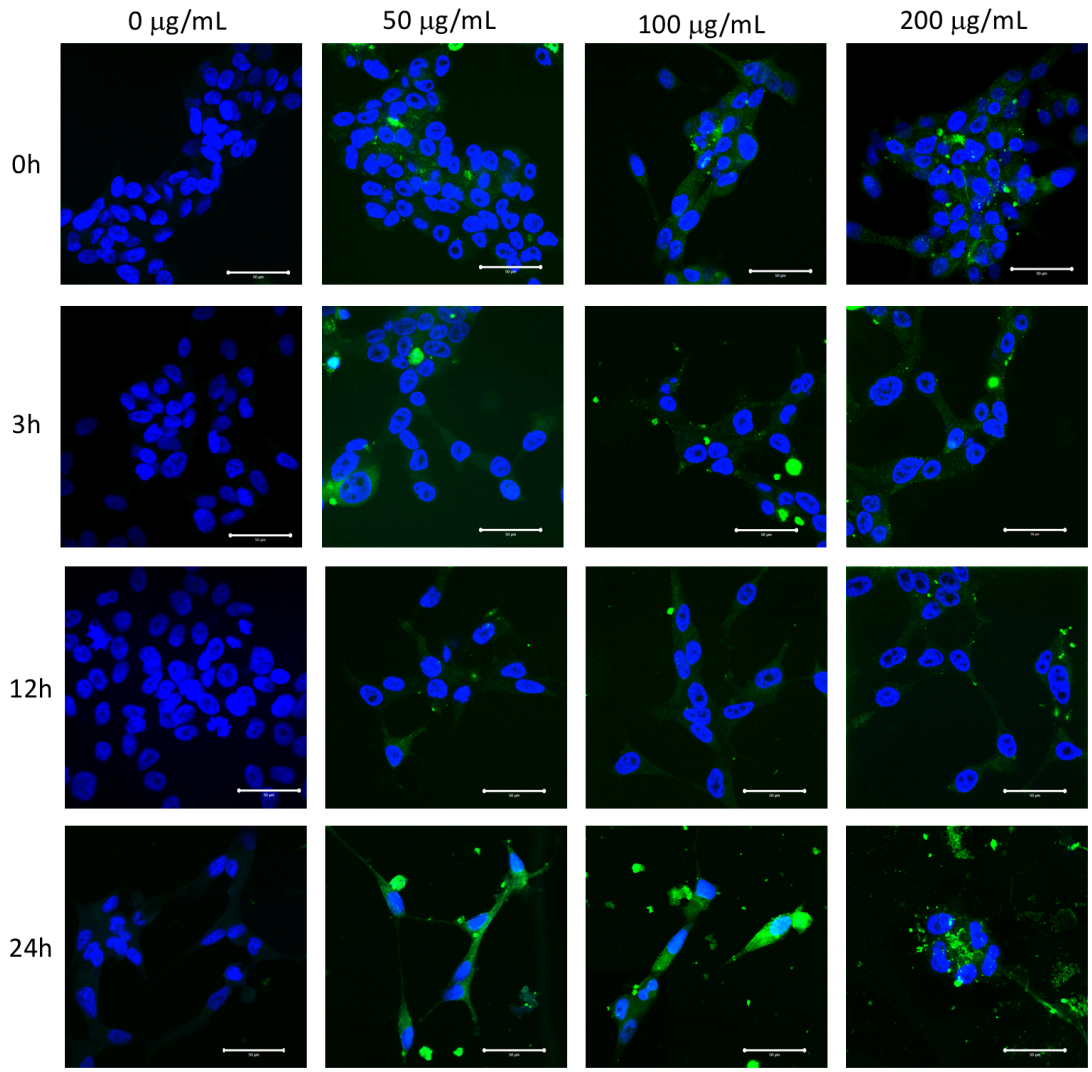

Figure 4.8. Anti-STEAP2 mAb2 triggers STEAP2 receptor internalisation in LNCaP cells. LNCaP cells were exposed to anti-STEAP2 mAb2 for 0, 3, 12 and 24h at doses of 0, 50, 100 and 200 μg/ml. 0h: cell surface STEAP2 was visualised before receptor internalisation. 3h & 12h: STEAP2 receptor internalisation was initiated. 24h: fully internalised STEAP2 was evident. Blue: nuclei; green: STEAP2. Images were acquired with a Confocal LSM 710 with a 63x zoom objective (ZEISS, Germany). Scale bar = 50 μm. (N = 2).

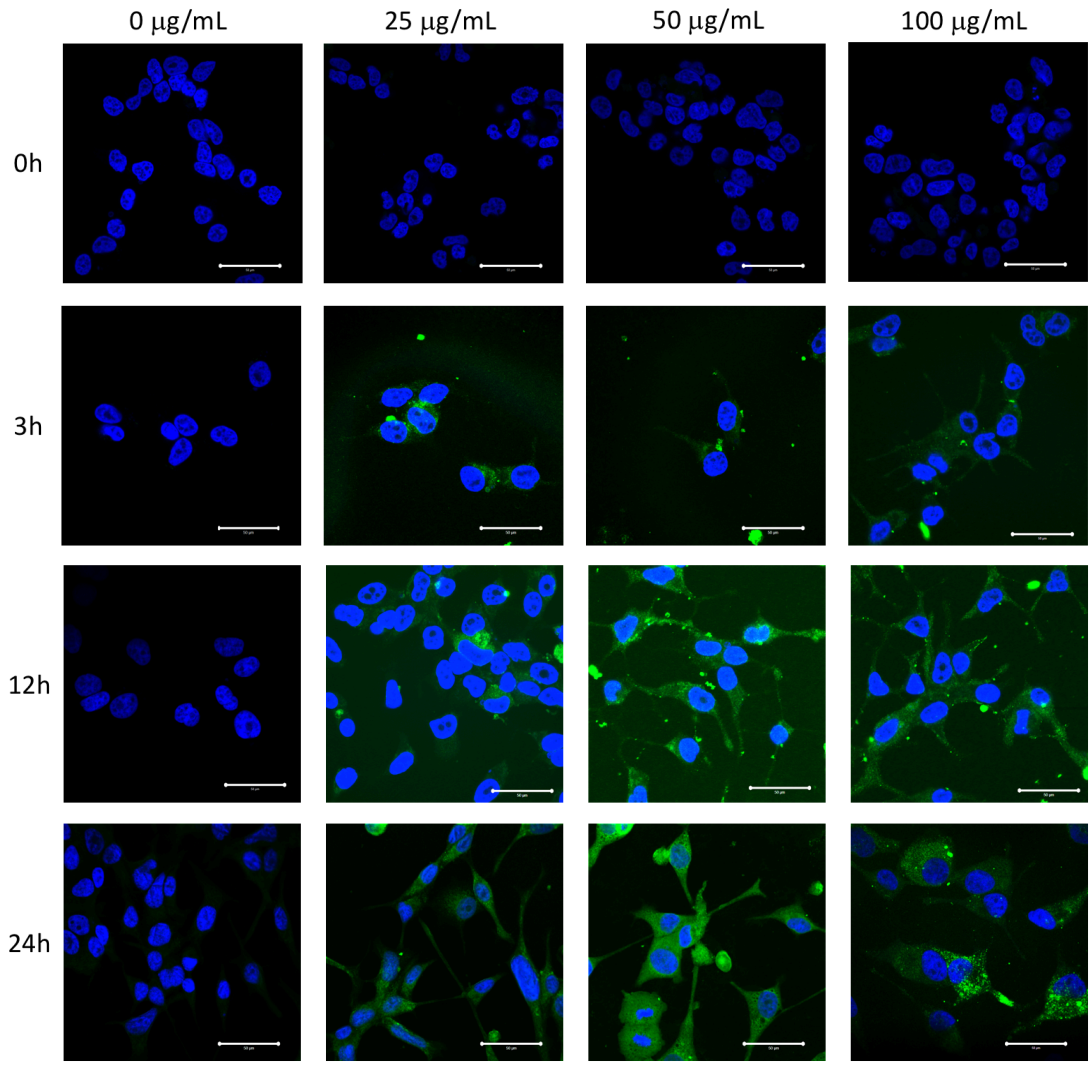

Figure 4.9. Anti-STEAP2 mAb2 triggers STEAP2 receptor internalisation in C4-2B cells. C4-2B cells were exposed to anti-STEAP2 mAb2 for 0, 3, 12 and 24h at doses of 0, 25, 50 and 100 μg/ml. 0h: cell surface STEAP2 was visualised before receptor internalisation. 3h & 12h: STEAP2 receptor internalisation was initiated. 24h: fully internalised STEAP2 was evident. Blue: nuclei; green: STEAP2. Images were acquired with a Confocal LSM 710 with a 63x zoom objective (ZEISS, Germany). Scale bar = 50 μm. (N = 2).

4.4 Discussion

This Chapter aimed to determine the ability of a commercially available anti-STEAP2 pAb, and previously developed anti-STEAP2 mAbs on reducing cell viability in a panel of prostate cancer cell lines. To do so, viability assays were conducted to evaluate whether treatment with the pAb or mAbs could induce significant cell death in a panel of human prostate cancer cell lines. Assays were first conducted in 2D monolayers in order to identify which cell lines responded to treatment, with chosen cell lines carried forward for culture as 3D spheroid models to assess viability in response to anti-STEAP2 antibody treatment in more physiologically relevant models. The results demonstrated that the commercial pAb significantly reduced cell viability in all four cell lines (**Figure 4.1**), yet this was not the case in 3D PC3 and LNCaP spheroid models (**Figure 4.2**). This Chapter also aimed to evaluate the effect of anti-STEAP2 pAb treatment on the expression of *AR* and androgen-regulated genes. qRT-PCR analysis found that *AR* increased in a dose-dependent manner following pAb treatment of AR-sensitive LNCaP and C4-2B cells (**Figure 4.3**). The expression of four androgen-regulated genes – *PSA, FKBP5, TMPRSS2* and *GPRC6A* – also increased in LNCaP and C4-2B cells following pAb treatment (**Figure 4.4**). Furthermore, all three mAbs significantly reduced cell viability in all four prostate cancer cell lines (**Figure 4.5**). Viability assays aimed to identify a lead mAb candidate to carry forward to evaluate STEAP2 receptor internalisation, a key property that underpins its suitability for use in ADC technology. mAb2 was selected following its ability to significantly reduce cell viability in both PC3 and LNCaP cells (**Figure 4.5**) as 2D monolayer and 3D LNCaP cell spheroid models (**Figure 4.6**). Receptor internalisation of cell surface STEAP2 was triggered upon anti-STEAP2 mAb2 binding (**Figures 4.7 – 4.9**). Together these data highlight STEAP2 as a potential therapeutic target in the treatment of prostate cancer, including use in ADC technology, yet its effects on inducing an androgen response warrant further investigation.

4.4.1 Cell viability following STEAP2 antibody treatment

The ability of a drug to induce targeted cell death is an essential property when evaluating its suitability as a potential therapeutic agent in the treatment of cancer (Kepp *et al*., 2011; Liu *et al*., 2011). To determine whether anti-STEAP2 pAb and mAbs triggered cell death in prostate cancer cells, MTT cell viability assays were conducted. Treatment with anti-STEAP2 pAb and mAbs triggered significant cell death in all four prostate cancer cell lines as 2D monolayers, whilst mAb2 triggered significant cell death in LNCaP cells grown as 3D spheroids.

Upon cell death, the apoptotic cascade is triggered, yet it is unclear which of the apoptotic pathways STEAP2 is involved in (Wang *et al*., 2010). As STEAP2 is localised to the cell membrane, it has been suggested that the extrinsic apoptosis pathway may be affected by STEAP2 (Wang *et al*., 2010). During the extrinsic apoptosis pathway, the signalling of cell surface receptors initiates a cascade, ultimately resulting in cell death through the formation of the death-inducing signalling complex (DISC) (Dickens *et al*., 2012; Wang *et al*., 2010). STEAP2 may exert its effect on this pathway by decreasing the stability of the DISC (Wang *et al*., 2010). It has also been suggested that STEAP2 may play a role in the intrinsic apoptosis pathway, as cells with STEAP2-knockdown have been found to undergo apoptosis in the absence of induction of the extrinsic apoptosis pathway through transcription factors (Sayers, 2011; Wang *et al*., 2010). STEAP2 is localised to the Golgi, and as such may interact with and affect the function of an anti-apoptotic proteins such as the Golgi anti-apoptotic protein, which has been found to inhibit apoptosis through modulation of intracellular calcium fluxes (De Mattia *et al*., 2009). The endocytic trafficking of cell surface receptors that influence receptor signalling, essential for cell growth or apoptosis, may also be influenced by STEAP2 (Wang *et al*., 2010).

LNCaP cells were found to have the highest naturally occurring levels of *STEAP2* expression (see **Chapter 3, Section 3.3.1**), and in this Chapter, 3D LNCaP cell spheroids where susceptible to anti-STEAP2 mAb induced cell

death (**Figure 4.5B**). Previously STEAP2-knockdown has also been found to increase the sensitivity of LNCaP cells to tumour necrosis factor–related apoptosis-inducing ligand (TRAIL)-induced apoptosis (Wang *et al*., 2010). Other drugs that trigger TRAIL-induced apoptosis in prostate cancer include the anthracycline doxorubicin (Kelly *et al*., 2002; Wu *et al*., 2002). TRAIL-induced apoptosis is often the result of caspase-3, -6 and -8 mediated cell death (Dickens *et al*., 2012; Nimmanapalli *et al*., 2001; Sayers, 2011; Wu *et al*., 2002). Caspase-8 mediated apoptotic cell death has also been linked to DISC formation in response to TRAIL signalling receptors triggering the extrinsic pathway of apoptosis (Dickens *et al*., 2012). Furthermore, targeting other members of the STEAP family with mAbs has been found to trigger caspase-dependent apoptosis (Qin *et al*., 2010 & 2011; Tanaka *et al*., 2012).

A study by Fong *et al*., 2014 showed that 3D prostate cancer cells grown as patient derived xenograft (PDX) models do show an increased resistance to chemotherapeutic agents compared to standard culture methods. This suggests that genetic differences between human and cell culture models may alter treatment responses (Fong *et al*., 2014). As noted previously, cells which display higher STEAP2 expression levels such as LNCaP and C4-2B cells were more susceptible to anti-STEAP2 antibody treatment than cell lines with lower STEAP2 expression levels (see **Chapter 3, Section 3.3.1; Figures 4.1, 4.5B & 4.5C**). Due to time limitations in the current study plan, it was not possible to quantify STEAP2 expression levels in 3D spheroid models. This will be an interesting piece of future work that is required to support a comparison of STEAP2 levels in the 3D models versus their 2D counterparts, to determine the role of STEAP2 expression on the differences in cell death observed between 2D and 3D models.

3D models are more representative of tumours *in situ* as they display key characteristics, such as a hypoxic core and extensive ECM, particularly in stromal co-culture models, allowing for a more realistic assessment of drug penetration (Thoma *et al*., 2014). A possible explanation for the observed lower cell death levels induced in 3D models treated with anti-STEAP2 pAb in comparison to 2D cells is the capability of the drug to fully penetrate the

spheroid (Lazzari *et al*., 2018). It would therefore be warranted to also measure cell death by fluorescent microscopy with a viability dye such as PI to observe the location of any changes in spheroid viability, as the observed cell death may only be occurring around the periphery of the spheroid (Hirschhaeuser *et al*., 2010; Riffle *et al*., 2017). Future work could also utilise fluorescently tagging of the anti-STEAP2 antibodies in order to observe their capability at penetrating through the spheroid. In order to inhibit cell growth in 3D spheroid models, higher doses of antibodies may be required to induce the same levels of cell death as those administered in 2D systems. Whilst all doses above 62.5 μg/ml triggered significant cell death in LNCaP spheroids, only the highest dose of 1,000 μg/ml significantly reduced the viability of PC3 spheroids. Previous studies have found that higher concentrations of drugs are needed to induce cell death in 3D versus 2D models, as cells at the core of the spheroid can still survive despite higher drug concentrations (Mehta *et al*., 2012; Sarisozen *et al*., 2014; Zoetemelk *et al*., 2019). A similar observation has been made with colorectal cancer cell spheroids, where it was reported that an 8-times greater dose of drug was required to achieve the same level of cell death in 3D models compared to 2D monolayers (Sarisozen *et al*., 2014). This not only suggests that the drug may not be able to fully penetrate PC3 spheroids in the present study, but also that the MTT dye may only be metabolised by cells at the periphery of the spheroid (Borra *et al*., 2009; Van Meerloo *et al*., 2011). As demonstrated in **Chapter 3, Section 3.3.2**, PC3 cells formed more dense spheroids with a visibly noticeable necrotic core when compared to LNCaP spheroids, further warranting the use of fluorescent imaging such as PI to visually evaluate cell death in these model (Gong *et al*., 2015; Vinci *et al*., 2012; Zanoni *et al*., 2016).

Whilst anti-STEAP2 monoclonal antibodies have not yet been widely studied, targeting other STEAP family members has induced promising tumour growth inhibition both *in vitro* and *in vivo* (Barroco-Ferreira *et al*., 2018; Challita-Eid *et al*., 2007). Two anti-STEAP1 monoclonal antibodies specific to STEAP1 extracellular loops successfully inhibited STEAP1-mediated intercellular communication and transport *in vitro*, and significantly reduced the growth of

prostate cancer xenografts *in vivo* (Challita-Eid *et al*., 2007). STEAP1 and STEAP2 share similar expression profiles in *in vitro* cell lines (see **Chapter 3, Section 3.3.1**). STEAP1 and STEAP2 both act as ion transporter channels, and as such the effects of STEAP1 on intercellular communication have been attributed to the regulation of adhesion or gap junction activity, through modulation of calcium influx (Jørgensen *et al*., 2003). Another STEAP family member, STEAP3, has been found to be associated with promoting communication between neighbouring cells through exosome secretion (Yu *et al*., 2006). Cell-cell communication plays a vital role in the progression of prostate cancer, as it allows for the exchange of small molecules such as nutrients and metabolites required to support tumour growth and progression (Edlund *et al*., 2004; Maia *et al*., 2018). The ability of anti-STEAP2 mAb2 to inhibit cell growth warrants further investigations into its effects on intercellular communication, which may provide a link between STEAP2 and intercellular ion transport.

Like STEAP1, STEAP2 also contains a heme-binding domain known as the ACRATA (Sanchez-Polido *et al*., 2004). This ACRATA domain is also present in a structurally related family which includes STEAP family members, the bacterial Nox family, and the oxidoreductase family YedZ (Ohgami *et al*., 2005 & 2006; Sanchez-Polido *et al*., 2004). Electron transfer may be supported through this heme-binding function, which has been found to affect cell growth and metabolism in Nox proteins, and electron transport across membranes in both Nox and STEAP proteins (Oosterheert *et al*., 2020; Yamada *et al*., 2004). It would therefore be of interest in the future to evaluate the role of the ACRATA domain when cell death is induced in response to anti-STEAP2 antibody exposure.

Collectively the data in this Chapter suggest that anti-STEAP2 poly- and monoclonal antibodies successfully inhibit cell growth in 2D monolayers, whilst only mAb2 impacted upon the viability of 3D LNCaP spheroids.

4.4.2 Androgen responses following STEAP2 antibody treatment

Treatment of cells with anti-STEAP2 pAb induced significant increases in *STEAP2* expression in androgen-sensitive LNCaP and C4-2B cells in a dose-dependent manner. These two cell lines also display the highest baseline levels of STEAP2 expression (see **Chapter 3, Section 3.3.1**). To date, it remains unclear whether *STEAP2* and *AR* expression are linked, yet STEAP2 expression has been suggested to be androgen regulated as it is more highly expressed in androgen-sensitive prostate cancer cell lines including LNCaP and CWR22Rv1 (Chen *et al*., 2010; Gomes *et al*., 2012; Porkka *et al*., 2002; Xu *et al*., 2001).

Prostate cancer is a largely androgen-regulated disease, with androgen being the primary molecule to stimulate prostate cancer progression through promoting proliferation and inhibiting apoptosis upon binding to and activation of *AR* (Buchanan *et al*., 2002; Heinlein & Chang, 2004). As such any changes to androgen expression may be significant for patients and can trigger unfavourable changes, affect treatment responses and trigger metabolic changes (Mitsuzuka & Arai, 2018). AR signalling in prostate cancer stimulates malignant growth through binding of the ligand domain of circulating testicular androgens with testosterone and DHT (Askew *et al*., 2007; Tan *et al*., 2015). ADT with therapeutic agents such as docetaxel and more recently enzalutamide remains the gold standard in the treatment of prostate cancer, however many tumours develop androgen independence and resistance, often through an *AR* mutation (Guo *et al*., 2009; Nelson & Shah, 2019). Of these mutations, those in androgen receptor splice variant 7 (*ARv7*) as a result of alternate splicing of the AR transcript are most prevalent and have been linked to treatment resistance and hormone refractory disease (Dehm *et al*., 2008; Nakazawa *et al*., 2014; Scher *et al*., 2018; Qu *et al*., 2015). *ARv7* lacks the ligand-binding domain of *AR* yet retains transcriptional activity, allowing for *ARv7* to act as a constitutively active AR protein independent of binding with DHT (Hu *et al*., 2009; Qu *et al*., 2015). Drugs which target AR disrupt DHT-dependent *AR* signalling, and as such *ARv7* signalling would not be inhibited

(Chan *et al*., 2012). Therefore, future work should employ qRT-PCR to determine whether the observed increases in *AR* expression were of the full-length gene or one of its variants.

The substantially significant increase in AR receptor expression observed in response to anti-STEAP2 pAb treatment of androgen-sensitive cells could be the result of a switch to androgen-independence. When nsSNPs were evaluated in STEAP2, 42 alterations were found (Naveed *et al*., 2016). Of these, a mutation in H316R replaced amino acids histidine with arginine at position 316, disturbing the domain and interactions with metal ions, subsequently destroying its function (Naveed *et al*., 2016). In human AR when a nsSNP results in the replacement of arginine 773 with histidine, androgen insensitivity develops which confers resistance to androgen targeting (Prior *et al*., 1992). More recent studies have found that androgen resistance as a result of such mutations is due to disruption of N- and C-terminal interactions in the AR ligand binding domain (Jaaskelainen *et al*., 2006; McPhaul, 2016).

In prostate cancer, MMPs are known to regulate disease progression, in particular MMPs -2, -7, -9, -13 and -14 (Brehmer *et al*., 2003; Daja *et al*., 2003; Morgia *et al*., 2005). *STEAP2* has been found to increase ERK signalling, the downstream effectors of which are MMPs (Wang *et al*., 2010). This upregulation of ERK has been hypothesised to promote an invasive phenotype through the stimulation of the transcription factor activating protein-1 (AP-1), which may then activate MMPs -2, -7, -9, -13 and -14 (Whiteland *et al*., 2014). *AR* expression has also been found to increase MMP-9 signalling in the promotion of prostate cancer metastasis (Hu *et al*., 2015). Therefore, the increase in *AR* expression in response to anti-STEAP2 pAb treatment is potentially worrying for patients as it may induce a more invasive phenotype and warrants further investigations into the signalling pathways involved (Hu *et al*., 2015; Whiteland *et al*., 2014).

The expression of *AR* target genes is modulated by the binding of *AR* to AREs in the genome, or through interactions with other transcription factors bound to specific recognition sites on target genes (Davey & Grossman, 2016;

Heinlein & Chang, 2004; Wang *et al*., 2005). AREs are involved in regulating the transcription of androgen-responsive genes (Davey & Grossman, 2016; Heinlein & Chang, 2004). In prostate cancer progression, *AR* promotes the expression of specific target genes, of which *PSA* expression is the most widely studied and correlates with increased *AR* expression and metastatic disease (Baek *et al*., 2012; Lipianskaya *et al*., 2014). *PSA* expression is triggered through transcriptional activation in the N-terminal domain of *AR* in the nucleus (Dehm & Tindall, 2007). AREs in the promotor and enhancer regions of PSA have been found to recruit numerous co-activators and transcription factors including histone acetyltransferases, p160 family, mediator and RNA polymerase II (PolII) (Takayama *et al*., 2007; Wang *et al*., 2005). STEAP2 has also been found to contain an AR-binding site (ARBS) in intron 3 (Takayama *et al*., 2007). Moderate histone acetylation and PolII recruitment was observed in ARBS-4 located in intron 3 of STEAP2 in response to the synthetic androgen R1881 (Takayama *et al*., 2007; Wang *et al*., 2005).

Another member of the STEAP family, STEAP4, has been found to contain an androgen-dependent cis-regulator element in the 5' flanking sequence of the gene, thought to be involved in ARE binding (Sak *et al*., 2007). STEAP2 and STEAP4 share structural similarities as the six transmembrane domains of STEAP2 and STEAP4 are both flanked by a large N-terminal and a short C-terminal domain (Korkmaz *et al*., 2005). The 5' gene region of the *STEAP4* gene was found to induce androgen-dependent promotor activity in androgen-sensitive but not androgen-independent cell lines, increasing the expression of androgen-regulated genes including *PSA* (Sak *et al*., 2007). The expression of *STEAP4* has also been found to be androgen-mediated through the expression of the haematological and neurological expressed 1 (*HN1*) gene, which in prostate cells down-regulates PI3K-dependent Akt activation (Varisli *et al*., 2011 & 2012). The downregulation of *STEAP4* and *PSA* was found to correlate with *HN1* overexpression which induced *AR* degradation, suggesting *HN1* may be involved in the increased *AR* and *PSA* expression observed in this Chapter (Varisli *et al*., 2012). It would therefore be of interest going forward to assess *HN1* expression in anti-STEAP2 pAb treated cells.

PSA contributes to disease progression through its protease activity, which induces epithelial-mesenchymal transitions and cell migration (Whitbread *et al*., 2006). The response elements of *PSA* and nuclear factor kappaB (NFκB) are located at the *AR* promotor region, suggesting that *AR* expression may be affected by NFκB (Zhang *et al*., 2004). The progression of prostate cancer from androgen dependence to androgen independence has been linked with the activation of Akt and NFκB in LNCaP cells *in vitro* and mouse models *in vivo* (Kikuchi *et al*., 2003; Murillo *et al*., 2001). Together this suggests that inhibition of NFκB may hold potential as a targeted pathway in the inhibition of prostate cancer progression (Gonen-Korkmaz *et al*., 2014; Sun *et al*., 2010). *STEAP2* expression has been found to correlate with androgen stimulation and NFκB signalling in LNCaP cells, suggesting a potential mechanism behind the increase in *AR* and *PSA* expression observed in anti-STEAP2 pAb treated LNCaP cells in this Chapter (**Figures 4.3 & 4.4A**; Gonen-Korkmaz *et al*., 2014).

Other target genes implicated in the progression of prostate cancer which are regulated by AR include *FKBP5, TMPRSS2* and *GPRC6A* (Febbo *et al*., 2005; Pi & Quarles, 2012; Tomlins *et al*., 2005). The expression of all three genes increased in response to anti-STEAP2 pAb treatment in both LNCaP and C4-2B (**Figure 4.4**). *TMPRSS2* expression has also been found to increase alongside *PSA* in CRPC following a gain in function mutation in DHT synthesis (Chang *et al*., 2013). In this Chapter, *TMPRSS2* expression was also observed alongside an increase in *PSA* expression in C4-2B cells treated with anti-STEAP2 pAb (**Figure 4.4B**). High transcript levels of *TMPRSS2* have been observed alongside high levels of *STEAP2* in CRPC, further suggesting that *STEAP2* is an androgen-regulated gene (Ylitalo *et al*., 2017). Interestingly, patients with high levels of *STEAP2* and *TMPRSS2* also presented with higher serum *PSA* levels and were determined as having AR-driven CRPC (Ylitalo *et al*., 2017).

Similar to *PSA, FKBP5* and *TMPRSS2* have also been found to be increased in extracellular vesicle (EV)-rich prostate cancers, and their expression has been found to decrease in response to treatment either via a radical

prostatectomy or radiation (Dhont *et al*., 2020). In EV-rich prostate cancers, *FKBP5* and *TMPRSS2* play a vital role in intracellular communication, implying that the increase observed in this Chapter may be compromising for patients as increased intracellular communication may aid in the formation of metastases (Dhondt *et al*., 2020 & 2016). The overexpression of *PSA, FKBP5* and *TMPRSS2* and another *STEAP* family member *STEAP1* has also been found to increase following androgen stimulation by R1881 in androgen-independent PC3 cells, suggesting that anti-STEAP2 pAb may act as an androgen stimulant in this Chapter (Marques *et al*., 2011). *PSA, FKBP5* and *TMPRSS2* have been suggested to hold potential as markers predictive of treatment outcome, as their expression has been found to decrease in response to successful treatment of prostate cancer (Shaw *et al*., 2016). Their overexpression in response to anti-STEAP2 pAb treatment may therefore be indicative of an androgen-mediated response and potential onset of CRPC (Chang *et al*., 2013; Shaw *et al*., 2016; Ylitalo *et al*., 2017).

The triggering of *GPRC6A* overexpression would also be of concern for the patient, as *GPRC6A* activation has been found to increase cell proliferation (Pi & Quarles, 2012). The effects of *AR* are mediated by *GPRC6A*, and as such its overexpression observed in this Chapter could signal a switch to CRPC through the activation of PI3K/Akt signalling pathways responsible for AR-independent disease progression (Pi *et al*., 2015; Zarif & Miranti, 2016). Overexpression of *GPRC6A* has also been found to promote epithelial-mesenchymal transitions leading to prostate cancer progression, particularly to the bone as *GPRC6A* is a ligand for osteocalcin and has been identified as a marker of prostate cancer metastasis (Liu *et al*., 2016; Pi & Quarles, 2012; Suva *et al*., 2011). A further concern regarding the overexpression of *GPRC6A* in response to anti-STEAP2 pAb treatment is its involvement in ERK signalling, which has been found to increase upon *GPRC6A* activation (Ye *et al*., 2017). As *STEAP2* is also involved in the ERK signalling pathway, it would be of interest to further explore the crosstalk between *GPRC6A* and *STEAP2* (Gomes *et al*., 2012; Wang *et al*., 2010; Ye *et al*., 2017).

Future studies are required to extend this work, utilising qRT-PCR to evaluate *AR* levels post treatment with anti-STEAP2 mAb2 in 2D and 3D PC3 and LNCaP monolayer and spheroid models to determine whether the reduction in viability of 3D models affects *AR* expression. Androgen-sensitive C4-2B cells grown in 3D models as compared to their 2D counterparts have been found to express lower levels of *AR* and *PSA*, whilst the opposite was observed in androgen-independent 22Rv1 cells (Xu *et al*., 2019). It would also be of interest to assess the expression of the four androgen-regulated genes in response to anti-STEAP2 pAb treatment in androgen-independent cell lines. Together, the data presented here suggests anti-STEAP2 pAb treatment may have concerning knock on effects for the patient in terms of increased *AR* and *AR*-mediated gene expression, warranting further investigations into the mechanisms driving this increase.

4.4.3 Receptor internalisation following anti-STEAP2 mAb2 treatment

STEAP2 receptor internalisation was induced upon treatment with anti-STEAP2 mAb in PC3, LNCaP and C4-2B cells, with lower doses triggering internalisation in androgen-sensitive cell lines (**Figures 4.7 – 4.9**). It was of importance to study STEAP2 receptor internalisation following anti-STEAP2 mAb2 treatment to evaluate the potential of mAb2 to be utilised in conjunction with ADC technology. ADCs utilise highly specific mAbs to link potent chemotherapeutic agents in order to target tumour-specific antigens on the surface of cancer cells (Kamath & Iyer, 2015; Tarcsa *et al*., 2020). Cell killing is achieved through ADC binding with the receptor on the target disease cell, which becomes internalised and releases the active drug payload (Tarcsa *et al*., 2020). ADCs are of particular interest as off-target or systemic side effects can be limited through their increased specificity and targeted, localised killing of diseased cells compared to the administration of standard chemotherapeutic agents (Kamath & Iyer, 2015; Tarcsa *et al*., 2020). For an ADC to be viable, factors such as target antigen, antibody, conjugation technology and payload must all be considered as they have the potential to affect the efficacy and toxicity of the drug (Kamath & Iyer, 2015; Tarcsa *et al*., 2020).

To date, studies into the precise subcellular localisation and the intracellular site of STEAP2 function remain unclear. STEAP2 localises to the plasma membrane and numerous cytoplasmic structures of unknown identity in DU145 cells; it co-localises with trans-Golgi network markers and early endosomes in COS-1 cells, and also co-localises with transferrin and the transferrin receptor in the endosomes of HEK293T cells (Korkmaz *et al*., 2002; Ohgami *et al*., 2006; Porkka *et al*., 2002). When developing ECL2 mAb targeting of STEAP2, Hasegawa *et al*., characterised the location of STEAP2 to the juxtanuclear Golgi region and endosome-like puncta. They also reported transient cell surface localisation of STEAP2 to be dependent on the local membrane cholesterol levels (Hasegawa *et al*., 2018). The internalisation of metal-containing molecules such as heme, iron and copper may be facilitated by cell surface STEAP2 (Korkmaz *et al*., 2005). The metalloreductase activity of STEAP2 in STEAP2-transfected HEK293T cells was also suppressed at the cell surface, suggesting that whilst STEAP2 is broadly distributed its activity could be regulated in a conformation and localisation dependent manner (Hasegawa *et al*., 2018). Previous studies within the wider Swansea research group have also identified STEAP2 to be localised to the cell membrane prior to internalisation, yet this work was limited to PC3 cells, hence the need for its application to a wider range of prostate cancer cells within this Chapter (Nguyen-Chi, 2020).

In this Chapter, STEAP2 was found to be specifically localised to the cell membrane in PC3 cells (**Figure 4.7**), however some internal STEAP2 was detected in LNCaP and C4-2B cells at the 0 h timepoint prior to incubation with anti-STEAP2 mAb2 (**Figures 4.8 & Figures 4.9**). Cells at all timepoints were exposed to anti-STEAP2 mAb2 for 30 minutes on ice to keep the temperature of samples at around 4^{o}C prior to incubation at 37^{o}C for either 3, 12 or 24 h, or in the case of the 0 h cohort immediately fixed and stained. This 30-minute period allows for uniform and evenly distributed mAb binding, as receptor internalisation becomes triggered once samples are incubated and the temperature is raised to 37^{o}C (Vainshtein *et al*., 2015). However, the slight internalisation observed in LNCaP and C4-2B cells at 0 h suggests that this could be sufficient time for anti-STEAP2 mAb internalisation to be triggered.

STEAP2 may also be involved in fatty acid metabolism, as it was found to be one of nine genes reported to be associated with resistance to lovastatin, a statin traditionally used for lowering serum cholesterol levels (Savas *et al*., 2011). This resistance is thought to be the result of a SNP in intron 2 of STEAP2 which may be used to predict resistance to lovastatin (Savas *et al*., 2011). This resistance was found to decrease in response to silencing of elongation factor for RNA Polymerase II (ELL)-associated factor 2 (*EAF2*), an androgen-response gene also involved in the inhibition of cell growth and induction of apoptosis, further suggesting a role of androgen-mediated STEAP2 regulation (Hahn *et al*., 2007; Savas *et al*., 2011).

Doses of anti-STEAP2 mAb2 below the calculated IC_{50} value for each cell line were chosen to ensure significant cell death did not occur during the full 24-hour incubation period (**Figure 4.5; Table 4.3;** AAT Bioquest Inc., 2020). Maintenance of high cell viability before and during the incubation period is critical in ensuring receptor internalisation is not affected by the cytotoxic effects of the antibody (Hasegawa *et al*., 2018). In this Chapter, lower doses of anti-STEAP2 mAb triggered receptor internalisation in androgen-sensitive LNCaP and C4-2B cells, further suggesting androgen plays a role in the effects of STEAP2. STEAP2 is more naturally abundant in these cell lines (see **Chapter 3, Section 3.3.1**), which may suggest a reason for the faster internalisation observed in LNCaP and C4-2B cells in comparison to PC3 cells. Higher concentrations of anti-STEAP2 mAb2 appeared to saturate the cells, as depicted by the pooling of strong fluorescent signals after 12 h incubation at mAb2 doses greater than 100 μg/ml in LNCaP and C4-2B cells, and 500 μg/ml in PC3 cells (**Figures 4.7 – 4.9**). This saturation may reduce the maximal uptake capacity of the cells due to complete occupation of binding sites (Rhoden *et al*., 2012). If the STEAP2 binding sites of the cells become fully saturated and no longer capable of internalising the monoclonal antibody, a binding site barrier may be produced which may lead to a cytotoxic bystander effect inducing cell death of antigen-negative cells (Rhoden *et al*., 2012). This may be overcome through the incorporation of ADC technology, which would allow for more specific target receptor internalisation, as ADCs are clinically

administered at their maximum tolerated dose in order to overcome receptor saturation (Li *et al*., 2016; Khera *et al*., 2018; Tarcsa *et al*., 2020; Singh *et al*., 2020). For mAb2 to translate clinically, it would also be of interest to determine its effects on the metalloreductase function of STEAP2. Previously, an ECL2-targetting mAb did not trigger uncontrollable metalloreductase activity in prostate cancer cells, which was suggested as a desired property of a potential therapeutic STEAP2 target, as the function of STEAP2 which is expressed at lower levels in other cell types throughout the body would be left unaffected (Hasegawa *et al*., 2018).

To determine the suitability of anti-STEAP2 mAb2 for use in ADC technology, more information regarding STEAP2 localisation would be required. It would have been beneficial to fluorescently label the Golgi network to determine the site of STEAP2 localisation upon receptor internalisation; which should be the focus of future work. Such future studies aimed at determining whether STEAP2 had internalised to specific acidic cell components, would need to use a pH amine dye conjugate to confirm whether internalisation to the endosomes and lysosomes had occurred. Here, the presence of proton pumps creates an acidic environment (pH 4.5 – 5.5) for the degradation of endocytosed macromolecules (Nath *et al*., 2016).

Together, the data presented in this Chapter suggest anti-STEAP2 mAb2 triggers receptor internalisation within 3 h in androgen-sensitive LNCaP and C4-2B cells, and within 12 h in androgen-independent PC3 cells. Thus, anti-STEAP2 mAb2 may hold potential for use with ADC technology in clinical translation as a therapeutic target for the treatment of prostate cancer.

4.5 Conclusion

The data presented in this Chapter provides strong evidence for the potential of both a commercially available anti-STEAP2 pAb and anti-STEAP2 mAb for the development of novel therapies to treat prostate cancer. This Chapter also identified a lead mAb candidate (mAb2) which shows potential for use in ADC technology following the successful triggering of receptor internalisation. Both the pAb and mAb2 target ECL3, suggesting targeting the ECL3 reduces prostate cancer cell viability, both in 2D monolayers and 3D spheroids. However, the anti-STEAP2 pAb significantly increased *AR* expression, along with the expression of androgen-regulated genes associated with the progression of prostate cancer. Together, the anti-STEAP2 mAb lead candidate (mAb2) holds potential for future clinical translation as an ADC for the treatment of prostate cancer, however further investigations into its effect on androgen responses are needed.

Chapter 5

Design and development of CRISPR/Cas9 engineering for the knockout of *STEAP2* in prostate cancer cell lines and its effects on aggressive prostate cancer traits

5.1 Introduction

Members of the *STEAP* family of genes are known to be over expressed in a variety of cancer types, with *STEAP2* particularly over expressed in prostate cancer (see **Chapter 1, Section 1.7**; Gomes *et al.,* 2012). When compared to the normal prostate epithelial cell line PNT2, high protein expression of *STEAP2* has been found in the metastatic prostate cancer cell lines PC3 and LNCaP, which are derived from bone and lymph node metastases, respectively (Burnell *et al.,* 2018; Whiteland *et al.,* 2014). Such studies suggest that an increase in *STEAP2* expression leads to a more aggressive cancer phenotype, with cell proliferation, migration and invasion higher in cells with elevated *STEAP2* levels, suggesting that *STEAP2* may promote prostate cancer progression (Burnell *et al.*, 2018; Wang *et al.*, 2010; Whiteland *et al.*, 2014). When assessed as a potential therapeutic target through gene knockdown and transfection, previous studies have shown that *STEAP2* provides promise in reducing these aggressive prostate cancer traits (Burnell *et al.*, 2018; Korkmaz *et al.*, 2002; Ohgami *et al.*, 2006; Wang *et al.*, 2010; Whiteland *et al.*, 2014).

Previous studies have altered *STEAP2* expression through gene knockdown using siRNA (Burnell *et al*., 2018). However, the use of siRNA comes with limitations, including variability in the degree of knockdown that can be achieved, which can often differ across experiments (Boutros & Ahringer,

2008). Additionally, siRNA induces a transient knockdown effect, and as such may not be sustained over time (Boutros & Ahringer, 2008). Given these limitations, in the present Chapter, gene-knockout using CRISPR/Cas9 engineering technology will be explored to achieve a more efficient, longer term knock-out of *STEAP2* expression. Clustered randomly interspaced short palindromic repeats / caspase-9 (CRISPR/Cas9) genome editing technology has gained popularity in recent years as a versatile editing tool which has been widely utilised in a variety of cell types and organisms, both *in vitro* and *in vivo*, resulting in efficient gene disruption and gene modification (see **Chapter 1, Section 1.7**; Chen *et al.,* 2019; Yuen *et al.,* 2017). The CRISPR/Cas9 system is comprised of an sgRNA and DNA endonuclease Cas9, with sgRNA directing Cas9 to specific, targeted DNA sequences to induce site-specific cuts in double stranded DNA (**Figure 5.1A**; Jiang & Doudna, 2017).

Once the targeted DNA sequence is cleaved by Cas9, DSBs are made in the genome sequence of interest and are located at approximately three nucleotides before the proto-spacer adjacent motif (PAM) region (Doudna & Charpentier, 2014; Li *et al*., 2020). The repair of these DSBs can be initiated by either non-homologous end joining (NHEJ) or homology-directed repair (HDR) (**Figure 5.1B**; Hsu *et al*., 2014). Of these repair mechanisms, HDR is less frequently initiated and uses donor DNA templates to precisely repair the DSB for gene modification with low efficiency (Jiang & Doudna, 2017). NHEJ often dominates as a repair mechanism for gene disruption and loss-of-function mutations with high frequency, yet regularly results in frameshift mutations due to the generation of insertion or deletion mutations (indels) near the Cas9 cleavage site (Sanchez-Rivera *et al.,* 2015; Sander & Joung, 2014). By taking advantage of these DSB repair pathways, specific gene disruption, deletion, correction and insertion can be achieved (Doudna & Charpentier, 2014). Novel changes to the CRISPR/Cas9 system can also be made by fusing either wild-type or engineered mutant Cas9 with other functional ligands or protein domains, allowing for specific gene labelling, activation, silencing, enhanced specificity or even single base editing of DNA and RNA (Wang *et al*., 2017). By simply altering the sgRNA sequence and respective expression of different sgRNAs, the CRISPR/Cas9 system can retarget new DNA

sequences, introducing multiple DSBs, and therefore allows for a more sophisticated gene editing system (Li *et al.*, 2020).

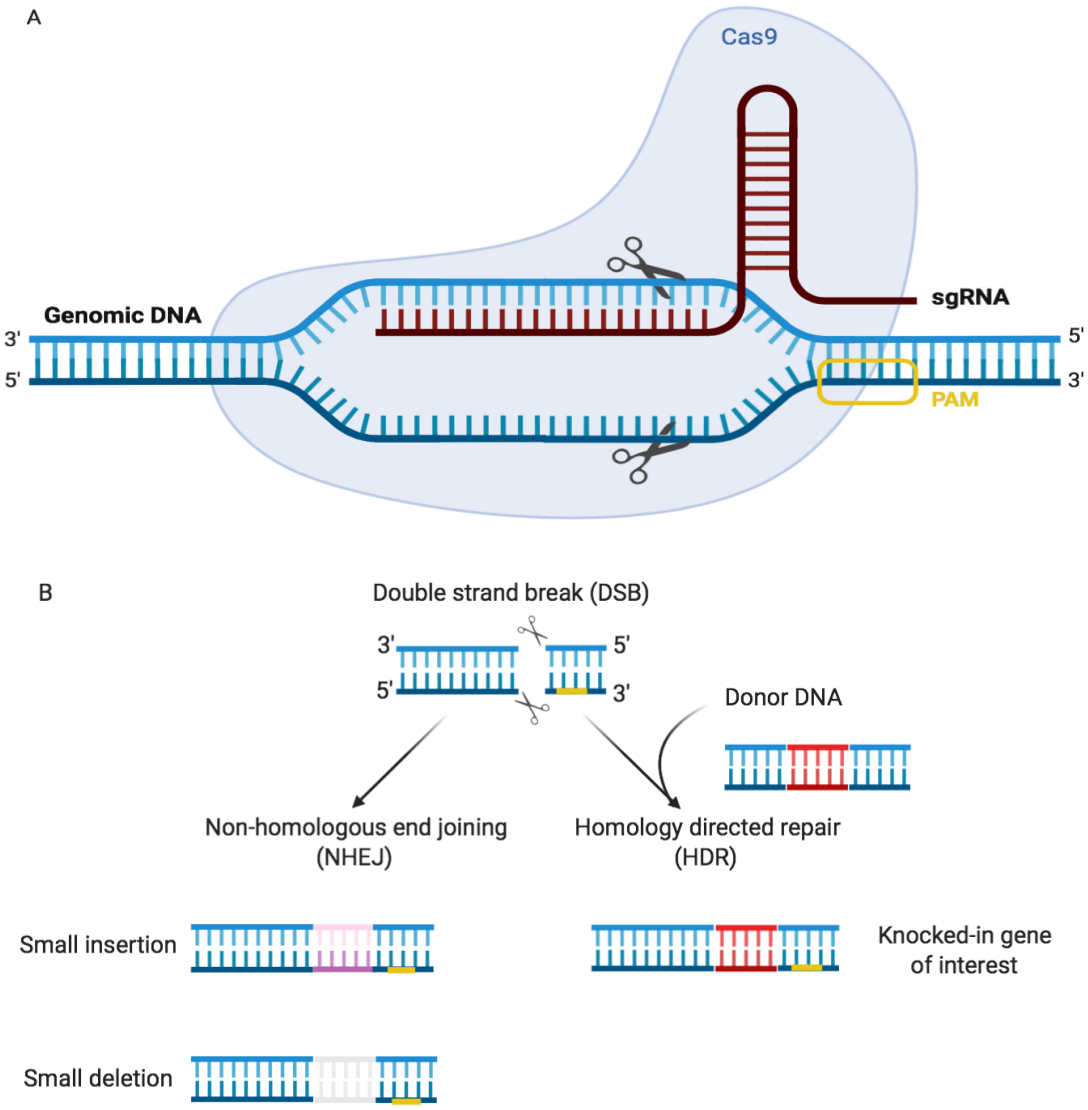

Figure 5.1. The mechanisms of CRISPR/Cas9-mediated genome editing. (A) The Cas9 nuclease is guided to specific genomic sequences by the sgRNA. Double strand breaks (DSBs) are introduced close to the PAM region by the Cas9 nuclease. (B) Two DNA repair pathways can be induced to repair DSBs; the NHEJ pathway which results in small random insertions or deletions for gene knockout, or the HDR pathway which results in the insertion of a homologous donor template at the site of the DSBs for gene knock-in. Adapted from (Chen *et al.*, 2019). Created using BioRender.

In order for CRISPR/Cas9 system to successfully be used as a genome editing tool, sgRNA with the Cas9 protein complexed in the nucleus is required (Glass *et al*., 2018). For this to be achieved, the Cas9 can be introduced by either protein, mRNA, or DNA (plasmid or viral genome) formats (Glass *et al*., 2018). Using these approaches, the sgRNA can either be *in vitro* transcribed (IVT) RNA, chemically synthesised, or encoded in viral genomes to be expressed directly by the target cell (Glass *et al*., 2018). A delivery system is necessary as one of the main challenges in the CRISPR/Cas9 system is that neither the protein nor the nucleic acid components can bypass the physical and chemical barriers of the target cells and tissues without assistance (Glass *et al*., 2018; Li *et al*., 2020). To allow for the intracellular delivery of CRISPR/Cas9 components, physical (e.g., micro-injection or electroporation), viral (e.g., retrovirus or lentivirus), and non-viral (e.g., lipids or inorganic particles) carrier methods have been developed (Hansen-Bruhn *et al*., 2018; Kim *et al*., 2014; Tang *et al*., 2017). Of these options, viral carriers are often preferred as they support the stable delivery of CRISPR/Cas9 components into cells and are advantageous as they pose low immunogenicity, low risk of carcinogenesis and serotype-associated target cell specificity (Kotterman & Schaffer, 2014). Adeno-associated viruses (AAVs) are the most widely applied and studied delivery viral vector. Whilst efficiently infecting cells, the virus provokes little to no innate or adaptive immune response or associated toxicity, allowing viral vectors to successfully deliver CRISPR/Cas9 particles to target sites (Daya & Burns, 2008; Lino *et al*., 2018).

Several open access, freely available online tools exist to facilitate the design and production of plasmids for gene knockout (Ran *et al*., 2013). These tools take a genomic sequence of interest and identify suitable target sites, with the aim of minimizing identical genomic matches or near-matches, to help prevent cleavage away from target sites, and therefore reduce any off-target effects (Bauer *et al*., 2015; Ran *et al*., 2013). When using such tools, it is essential to ensure that the guide sequences consist of a 20-mer protospacer sequence upstream of the PAM region at the genomic recognition site (Bauer *et al*., 2015; Ran *et al*., 2013). The system also provides a scoring system for the off-target potential of a similar sequence in the genome, allowing for the selection

of optimal sites (Hodgkins *et al*., 2015; Shen *et al*., 2014). Lentiviral CRISPR/Cas9 can be used to infect a wide variety of mammalian cells through the co-expression of a mammalian codon-optimised Cas9 nuclease in conjunction with a sgRNA to facilitate genome editing (Sanjana *et al*., 2014; Shalem *et al*., 2014).

The therapeutic potential of CRISPR technology lies in the fact that the targeted cleavage activity of the Cas9 protein can be guided via synthetic sgRNA, allowing a wide variety of genomic sequences to be targeted (Li *et al*., 2020). CRISPR/Cas9 is a rapidly evolving field of genetic engineering that has been successfully developed for the knockdown of many well studied genes involved in cancer progression. For example, CRISPR/Cas9 mediated knockout of hypoxia-inducible factor-1α (HIF-1α) has been found to supress metastasis in pancreatic cancer cells whilst targeted knockout of EGFR has been reported to limit proliferation in glioma cells, showing promise for the application of CRISPR/Cas9 genome editing technology as a novel tool in cancer therapeutics (Huang *et al*., 2017; Li *et al*., 2019).

Several studies have recently successfully utilised CRISPR/Cas9 systems in prostate cancer research. A study by Zhen *et al.*, in 2017 designed an aptamer-liposome-CRISPR/Cas9 chimera-based system to combine the efficient delivery and modified flexibility of the model. This study investigated A10, an RNA aptamer which is reported deliver therapeutic CRISPR/Cas9-gRNA to target polo-like kinase 1, which plays a role in the survival of prostate cancer cells and binds specifically to the cell surface receptor of prostate specific membrane antigen (PMSA) (Troyer *et al*., 1997). This study used LNCaP cells *in vitro* and male nude mice for *in vivo* work and used RT-PCR to assess the successful gene knockdown of A10 in mRNA. It was concluded that modified A10 in the chimeras mediated cell type-specific binding to human prostate specific membrane antigen (PSMA) and suggested that CRISPR/Cas9 systems may be applicable to more widespread therapeutic approaches using nucleic acid drugs (Zhen *et al*., 2016).

A more recent study by Ye *et al*. in 2017 used CRISPR/Cas9 to edit the endogenous *GPRC6A* gene, which is increased in human prostate cancer cell lines (LNCaP and PC3) and human prostate cancer tumours (Pi & Quarles, 2012). Cell proliferation and chemotaxis had previously been found to increase when *GPRC6A* is activated, and the gene also plays a role in prostate cancer progression as it was found to promote epithelial-mesenchymal transitions (Liu *et al*., 2016; Pi & Quarles, 2012). Removal of *GPRC6A* expression using siRNA-mediated knockdown had previously been found to inhibit the migration and invasion of prostate cancer cells (Pi & Quarles, 2012). One of the ligands of *GPRC6A* is osteocalcin, which is released into circulation by activated osteoblasts and can be used as both a marker and therapeutic target of prostate cancer metastasis (Suva *et al*., 2011). *In vitro*, it was found that editing the endogenous *GPRC6A* gene inhibited the osteocalcin activation of ERK, Akt and mTOR signalling pathways, which subsequently inhibited cell proliferation and migration. This recent study also found that CRISPR/Cas9 deletion or endogenous modification of *GPRC6A* in prostate cancer xenograft models altered the response to osteocalcin and subsequent disease progression (Ye *et al*., 2017). This study therefore suggested that *GPRC6A* and osteocalcin may collectively provide therapeutic targets for the suppression of prostate cancer progression (Ye *et al*., 2017). CRISPR/Cas9 engineering therefore offers multiple benefits in both providing new knowledge on the mechanisms and signalling pathways underlying carcinogenesis, whilst also offering the potential for future use as a therapeutic tool in the treatment of a variety of cancers.

Previous work within the wider Swansea research group successfully used siRNA knockdown to reduce transient levels of *STEAP2*, however such a reduction is neither stable nor permanent unlike that offered by CRISPR/Cas9 engineering (Burnell *et al*., 2018). The aims of this Chapter were to identify if CRISPR/Cas9 knockout could successfully knockout *STEAP2* expression and determine whether such knockout of *STEAP2* could reduce aggressive prostate cancer traits. To achieve this aim, the Chapter was therefore divided into the following objectives:

1. To design and develop CRISPR/Cas9 technology for *STEAP2* knockout in LNCaP and C4-2B prostate cancer cells *in vitro.*
2. To evaluate the impact of *STEAP2* knockout in LNCaP and C4-2B prostate cancer cells on aggressive prostate cancer traits, including cell proliferation, migration and invasion.
3. To evaluate the impact of *STEAP2* knockout on the gene expression of *AR*, and the androgen-regulated genes *PSA, FKBP5, TMPRSS2* and *GPRC6A.*

5.2 Methods

5.2.1 Cell culture

The human prostate cancer cell lines LNCaP and C4-2B, and the normal prostate epithelial cell line PNT2 were utilised in this Chapter, and are described in **Chapter 2, Section 2.2.1, 2.2.2 & 2.7.4.** Wild-type (^{WT}) LNCaP cells (LNCaP^{WT}) and wild-type C4-2B cells (C4-2B^{WT}) cells were routinely cultured and maintained as described in **Chapter 2, Section 2.2.7.1.** The selection antibiotic puromycin was used to select for *STEAP2* knockout (^{KO}) positive cells. LNCaP knock-out (LNCaP^{KO}) cells were maintained in complete RPMI media supplemented with 0.625 µg/ml puromycin, whilst C4-2B knock-out (C4-2B^{KO}) cells were maintained in complete RPMI media supplemented with 1.25 µg/ml puromycin. These doses were utilised following a serial dilution implemented to determine the optimum dose for each cell line (see **Chapter 2, Section 5.2.3.5**). HEK293T cells were maintained in DMEM supplemented with 10% FBS, 2% L-glutamine and 1% P/S. HEK293T cells were routinely sub-cultured at a ratio of 1:3 or 1:8 as per the supplier's recommendations.

5.2.2 Detection of *STEAP2* in a panel of prostate cancer cell lines

Four human prostate cancer cells C4-2B, DU145, LNCaP and PC3 and the normal human prostate epithelial cell line PNT2 were cultured to ~70% confluency. RNA was extracted, cDNA synthesised, and qRT-PCR performed as described in **Chapter 2, Section 2.3**. qRT-PCR for *STEAP2*, with *GAPDH* as the housekeeping control, involved the use of primers detailed in **Chapter 2, Section 2.3.3, Table 2.8**. The results were subsequently analysed as described in **Chapter 2, Section 2.3.4.**

5.2.3 Design and optimisation of CRISPR/Cas9 engineering for *STEAP2* knockout

The Welcome Trust Sanger Institute Genome Editing (WGE) database was used for plasmid design, which is based on successfully arrayed lentiviral CRISPR knockout libraries and provides a highly interactive tool for the visualisation of all possible CRISPR and paired Cas9 sites (Metzakopian *et al*., 2017). CRISPR/Cas9 engineering was developed, optimised and utilised for the knockout of *STEAP2* from LNCaP and C4-2B prostate cancer cells, using the method outlined in **Chapter 2, Section 2.7.**

5.2.3.1 Plasmid design

gRNA, PsPAX-2 lentiviral packaging protein and pCMV-vsvg envelope protein were purchased as described in **Chapter 2, Section 2.7.1.** Two *STEAP2* oligonucleotides were designed using BLAST analysis to encode for either the complete protein (*STEAP2* plasmid #1) or a *STEAP2* transcript variant (*STEAP2* plasmid #2), as shown in **Table 5.1**. Plasmids were generated from chosen sequences using Sanger QuickPick Knockout gRNA (Sigma Aldrich, USA).

Table 5.1. Sequences of gRNA and *STEAP2* plasmids utilised in CRISPR/Cas9 targeted knockout of *STEAP2.*

Plasmid	Sequence
gRNA	CGCGATAGCGCGAATATATT
STEAP2 #1	AATATTCAAGCGCGACAAC
STEAP2 #2	GGAATGAAATTCAACTGGC

5.2.3.2 Plasmid amplification and purification

Both *STEAP2* plasmids, BFP gRNA control, (Sigma, USA), *PsPAX-2* (Sigma, USA) and *pCMV-vsvg* (Sigma, USA) plasmids were separately amplified and purified following the methods outlined in **Chapter 2, Section 2.7.2 & 2.7.3**. Purified plasmid pellets were reconstituted in 50 μl of TE buffer and DNA yield measured. The DNA yields outlined in **Table 5.2** were then diluted to 200.0

ng/μl in aliquots of 100 μl of TE buffer and stored at -20 °C for future use throughout this Chapter.

Table 5.2. Quantification of bacterial plasmid DNA. The amplified and purified plasmid DNA generated in Section 5.2.3.2 was quantified for use throughout this Chapter.

Plasmid	Concentration (ng/μl)
PsPAX-2	2189.1
pMCV-vsvg	2339.7
BFP gRNA control	457.8
STEAP2 plasmid #1	398.2
STEAP2 plasmid #2	470.1

5.2.4 CRISPR/Cas9 knockout of *STEAP2*

5.2.4.1 Cas9 transfection of HEK293T cells

Cas9 was transfected into HEK293Tcells using polybrene, as described in **Chapter 2, Section 2.7.4**.

5.2.4.2 Preparation of lentiviral particles

Lentiviral particles were prepared using Opti-MEM media and lipofectamine, as described in **Chapter 2, Section 2.7.5**.

5.2.4.3 Lentiviral transfection of *STEAP2* plasmids into Cas9-positive HEK293T cells

Cas9-positive HEK293T cells were transfected with *STEAP2* knockout plasmids, as described in **Chapter 2, Section 2.7.6.**

5.2.4.4 Concentrating lentiviral STEAP2 stock

The Retro-X Concentrator kit (Clontech, USA, #631455) was used to concentrate lentiviral stocks of STEAP2 as described in **Chapter 2, Section 2.7.7** using the viral supernatant collected from the virus-producing HEK293T cells as described in **Section 5.2.3.2.**

5.2.4.5 Transfection of Cas9 plasmids into LNCaP and C4-2B wild-type cells

Cas9 was transfected into wild-type LNCaP and C4-2B wild-type cells using polybrene, following the method detailed in **Chapter 2, Section 2.7.8**. Once at ~50% confluency, LNCaP and C4-2B wild-type cells were seeded at a density of $2x10^5$ cells per well in a 6-well tissue culture plate under standard tissue culture conditions for 48 and 24 h respectively prior to transfection. A mixture of complete medium with polybrene was prepared to a final concentration of 1 μg/ml. Original media was removed and this polybrene mix was added at a volume of 1 ml per well. Cas9 plasmids were thawed at room temperature and mixed gently prior to being added at a volume of 500 μl per well to the culture medium containing polybrene. The plate was gently swirled to mix and incubated overnight. An additional 1 ml of medium containing Polybrene was added per well, and cells were again incubated until ~50% confluency was reached.

5.2.4.6 Optimisation of selection antibiotic doses in wild-type cells

A selective antibiotic titration (see **Chapter 2, Section 2.7.9**) was carried out for each wild-type cell line. C4-$2B^{WT}$ and $LNCaP^{WT}$ cells were seeded at a density of $3x10^5$ per well in 6-well plates for 48 h and 72 h respectively. Cells were exposed to a serial dilution of the selection antibiotics blasticidin and puromycin (Sigma, USA) at 0.625, 1.25, 2.5, 5.0 and 10.0 μg/ml for 120 h. Cells were viewed using standard light microscopy (Invitrogen, EVOS XL Core, USA) at 48 h and 120 h and any morphological changes were noted to determine toxicity, as described in **Tables 5.3 & 5.4.** Based on these results 0.625 μg/ml and 2.5 μg/ml blasticidin was used for the selection of Cas9-positive LNCaP and C4-2B cells respectively (**Tables 5.3 & 5.4**). 0.625 μg/ml and 1.25 μg/ml puromycin were used to maintain *STEAP2*-positive $LNCaP^{KO}$ and C4-$2B^{KO}$ cells respectively (**Tables 5.3 & 5.4**). Medium was replaced with fresh selective antibiotic-containing medium every 3-4 days as needed.

Table 5.3. Changes in viability of LNCaP^{WT} and C4-2B^{WT} cells following exposure to puromycin.

Dose (μg/ml)	48 h	120 h
0.625	Some survival of both cell lines	No survival of either cell line
1.25	Some C4-2B^{WT} survival, no LNCaP^{WT} survival	No survival of either cell line
2.5	No survival of either cell line	No survival of either cell line
5.0	No survival of either cell line	No survival of either cell line
10.0	No survival of either cell line	No survival of either cell line

Table 5.4. Changes in viability of LNCaP^{WT} and C4-2B^{WT} cells following exposure to blasticidin.

Dose (μg/ml)	48 h	120 h
0.625	Both cell lines healthy	Some C4-2B^{WT} survival, no LNCaP^{WT} survival
1.25	Both cell lines healthy	Some C4-2B^{WT} survival, no LNCaP^{WT} survival
2.5	Both cell lines healthy	No survival of either cell line
5.0	Some LNCaP^{WT} survival, C4-2B^{WT} healthy	No survival of either cell line
10.0	LNCaP^{WT} mostly dead, C4-2B^{WT} healthy	No survival of either cell line

5.2.4.7 Transfection of *STEAP2* plasmids into Cas9-activated LNCaP and C4-2B cells

STEAP2 knockout and gRNA plasmids were transfected into wild-type LNCaP and C4-2B cells using polybrene, as outlined in **Chapter 2, Section 2.7.11**. Once at ~50% confluency, Cas9-activated LNCaP and C4-2B cells were seeded at a density of $2x10^5$ cells per well in a 6-well tissue culture plate under standard tissue culture conditions for 48 and 24 h respectively prior to transfection. A mixture of complete medium with polybrene was prepared to a final concentration of 1 μg/ml. Original media was removed and this polybrene mix was added at a volume of 1 ml per well. *STEAP2* plasmids #1 and #2, and gRNA plasmids, were thawed at room temperature and mixed gently prior to being added at a volume of 500 μl per well to the culture medium containing polybrene. The plate was gently swirled to mix and incubated overnight. An additional 1 ml of medium containing polybrene was added per well, and cells were again incubated until ~70% confluency was reached. Medium containing polybrene was removed and replaced with complete medium containing the chosen dose of puromycin for each cell line, as determined in **Section 5.2.3.5**. Once ~70% confluency was reached, cells were transferred from the 6-well plates to 100 mm petri dishes and sub-cultured until confluent.

5.2.4.8 Isolation and amplification of single *STEAP2* knockout clones

Single *STEAP2* knockout clones were isolated and amplified as outlined in **Chapter 2, Section 2.7.12**. To isolate single colonies of positive *STEAP2* knockout cells, cells were seeded at a density of 300 cells per plate in 96-well tissue culture plates, in 100 μl media supplemented with the appropriate dose of puromycin. Plates were incubated for 10-14 days and routinely checked for single colony formations. Once formed, 6 single colonies per cell line, per *STEAP2* plasmid were transferred to 24-well tissue culture plates in 0.5 ml of complete medium supplemented with the appropriate dose of puromycin and incubated for a further 7 days. Microscopy was used to assess morphology of knockout cells in comparison to their wild-type counterparts, and 3 colonies per cell line, per *STEAP2* plasmid that most closely resembled wild-type cells were transferred to 6-well tissue culture plates and incubated until ~70%

confluent. Western blotting was performed to confirm successful target gene knockout, and stable clones were further expanded and routinely sub-cultured in 100 mm dishes in the same manner as their wild-type counterparts, with the addition of an appropriate dose of puromycin. These expanded colonies are annotated herein as depicted in **Figure 5.2** to distinguish between *STEAP2* knockout plasmid, colony number and cell line.

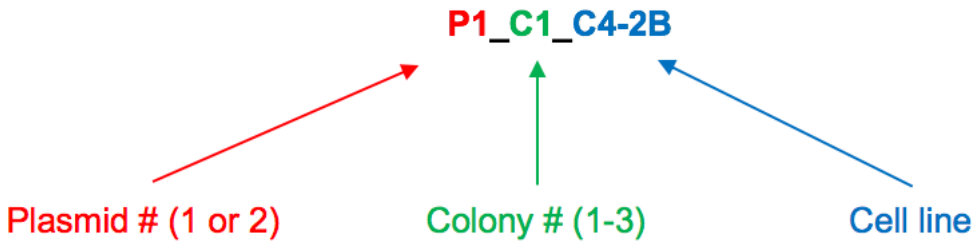

Figure 5.2. Annotation of single colonies of knockout cells. Schematic representation of the system used to annotate expanded colonies of knockout cells dependent on *STEAP2* knockout plasmid, colony number and cell line.

5.2.5 Confirmation of STEAP2 knockout by Western blotting

5.2.5.1 Protein extraction and quantification

Protein was extracted from expanded single knockout colonies as described in **Chapter 2, Section 2.8.1** and quantified using a Bradford assay for protein quantification as described in **Chapter 2, Section 2.8.2.**

5.2.5.2 Blocking and antibody incubations

Western blotting was conducted as described in **Chapter 2, Section 2.8.** Membranes were first probed overnight at 4°C with anti-STEAP2 (1:1,000, Sigma, US). After washing 3x in PBST, the secondary rabbit anti-IgG-HRP antibody was applied at 1:5,000 for 1 h at room temperature to detect STEAP2 protein expression. The membranes were washed, stripped, washed and blocked for 1 h in 5% BSA at room temperature **(Chapter 2, Section 2.8.6)** before cutting (**Figure 5.3**) prior to specific antibody staining for STEAP2 and the loading control GAPDH.

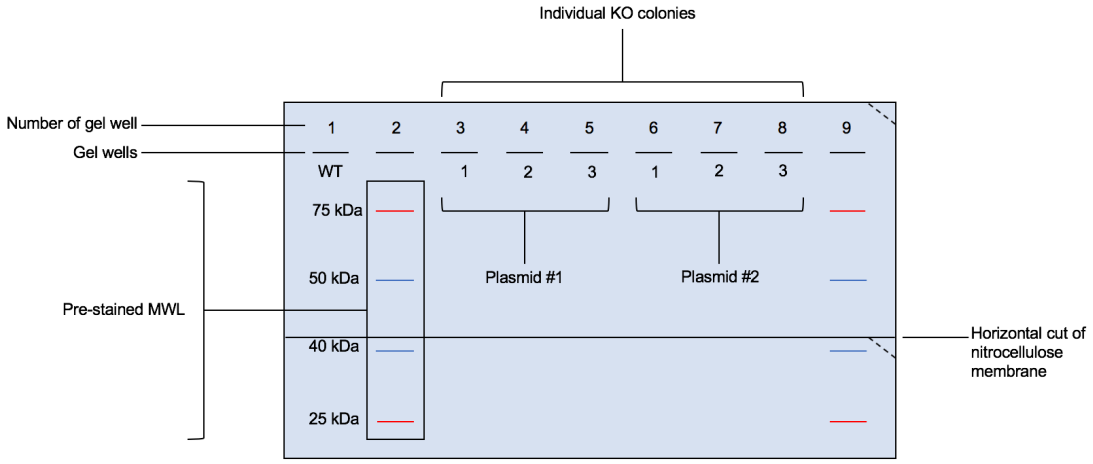

Figure 5.3. Diagram showing the cuts made to the nitrocellulose membrane following membrane transfer prior to antibody incubation. Vertical, short lines = gel wells; numbers = number of gel wells; well 1 + 10 = dual colour precision MWL (kDa) with red and blue short, vertical lines which represent the relevant molecular weight bands for this study. Membrane was cut into two pieces indicated by the horizontal lines. Horizontal line at approx. 45kDa indicates the cut separating STEAP2 (56 kDa) from housekeeping loading control GAPDH (37 kDa). Cell lysates from the WT (high STEAP2 expression) and KO (no STEAP2 expression) cell lines were utilised. Diagonal line in top-right corner indicates the cuts to determine orientation.

5.2.5.4 Protein detection analysis

Images were acquired and analysed as described in **Chapter 2, Section 2.8.7.** Protein quantification of STEAP2 was carried out every 5th passage of cells to ensure a stable knockout had been achieved.

5.2.6 Assays to study the effect of *STEAP2* knockout on aggressive cancer traits

5.2.6.1 Cell viability quantification

Cell suspensions of desired cell numbers were prepared as described in **Chapter 2, Section 2.2.7.2** and seeded in 100 µl culture media in 96-well tissue culture plates. To assess cell viability in STEAP2-knockout cells, the commercial resazurin-based dye alamarBlue assay (BioRad, UK, Cat. BUF012A), was performed as described in **Chapter 2, Section 2.4.2.** Viability was assessed in knockout cells and compared to that of wild-type cells every 24 h for 5 days. Viability assays were conducted in triplicate unless otherwise stated.

5.2.6.2 Cell proliferation

Cell suspensions of desired cell numbers were prepared as described in **Chapter 2, Section 2.2.7.2** and seeded in 100 μl culture media in 96-well tissue culture plates. The alamarBlue assay was used to assess cell proliferation in STEAP2-knockout cells, as described in **Chapter 2, Section 2.5.1.** The alamarBlue assay offers a more simplistic, one-step *in vitro* assay for cell viability and proliferation and was applied in this Chapter due to the more fragile nature of knockout cells compared to their wild-type counterparts (Squatrito *et al*., 1995). Proliferation was assessed in knockout cells and compared to that of wild-type cells every 24 h for 5 days. Proliferation assays were conducted in triplicate unless otherwise stated.

5.2.6.3 Cell migration assay

Migration assays were carried out as described in **Chapter 2, Section 2.9**. After C4-2B and LNCaP cells had reached ~80% confluency, medium was replaced for 24 h with serum-free DMEM and RPMI-1640 medium respectively. Cells were trypsinised, resuspended and adjusted to a desired cell concentration, as described in **Chapter 2, Section 2.2.7.2**. One cell culture insert (IBIDI, Germany, Cat. 80209) was placed in the centre of a well of a 12-well plate, and 70 μl cell suspension was added per chamber adhered for 24 h (C4-2B) or 48 h (LNCaP) in standard tissue culture conditions. $LNCaP^{WT}$ and $LNCaP^{KO}$ cells were incubated for 72 h prior to the removal of the silicone inserts, whilst $C4\text{-}2B^{WT}$ and $C4\text{-}2B^{KO}$ cells were incubated for 48 h. Media and inserts were removed, and cells were washed with PBS to remove cell debris, before fresh media was applied. The time taken to close the gap created was monitored using an inverted light microscope (Invitrogen, EVOS XL Core, USA). Media was replaced every 3 days. The migration assay was conducted in triplicate unless otherwise stated.

5.2.6.4 Invasion assay

Invasion assays were carried out as described in **Chapter 2, Section 2.10**. 48 h prior to each invasion assay, cells were harvested and seeded in 6-well plates at a density of 3×10^5 cells/ml and left to adhere in standard cell culture

conditions. Cultures were serum starved in SFM for 24 hours. Prior to seeding cells, 20 μl of GFR Matrigel (1:5 dilution/SFM; Corning) was applied to the Transwell insert and polymerised for 1 hour in standard cell culture conditions. Cells were harvested with trypsin and adjusted to a desired seeding density in a volume of 250 μl SFM. Prior to the addition of cells, 600 μl of serum containing media was added to the lower chamber. LNCaP^{WT} and LNCaP^{KO} cells were incubated for 72 h prior to staining, whilst C4-2B^{WT} and C4-2B^{KO} cells were incubated for 48 h in standard cell culture conditions to allow for cell invasion to occur. Cell invasion was quantified through staining with crystal violet. Invaded cells were fixed with 100% methanol for 15 minutes at room temperature and allowed to air dry. They were stained with crystal violet staining mixture (0.5% crystal violet in 20% methanol) for 30 minutes to allow visualisation of cells. The non-invaded cells on the upper surface of the Transwell insert were removed with a cotton swab moistened in media. The inserts were washed in purified water and left to air dry for 1 hour. Invaded cells were visualised using a standard light microscope at 10x magnification (Invitrogen, EVOS XL Core, USA). Images were taken of different planes of each insert and the invasion assay was conducted in triplicate unless otherwise stated.

5.2.7 Detection of *AR* and downstream targets in *STEAP2* knockout LNCaP and C4-2B cells

LNCaP^{WT}, LNCaP^{KO}, C4-2B^{WT} and C4-2B^{KO} cells were cultured to ~70% confluency. RNA was extracted, cDNA synthesised, and qRT-PCR performed as described in **Chapter 2, Section 2.3**. Cells were probed for the detection of *AR* and its downstream targets; *PSA*, *FKBP5*, *TMPRSS2* and *GPRC6A*, with *GAPDH* as the housekeeping control, using the primers detailed in **Chapter 2, Section 2.3.3, Table 2.8.** The results were subsequently analysed as described in **Chapter 2, Section 2.3.4.**

5.2.8 Statistical analysis

Statistical analysis was performed using GraphPad Prism version 8 for iOS. The one-way ANOVA *post-hoc* Dunnett test and an unpaired t-test were used, as detailed in each figure. Data was considered statistically significant when a

p-value of < 0.05 (*), p-value < 0.01 (**) or a p-value of < 0.001 (***) or p-value < 0.0001 (****) was obtained, which were annotated within the respective figures.

5.3 Results

The initial focus of this Chapter was to optimise and develop CRISPR/Cas9 technology for the successful targeted *STEAP2* knockout in LNCaP and C4-2B prostate cancer cells *in vitro*. Following this, the work within the current Chapter was aimed at evaluating the impact of CRISPR/Cas9 knockout of *STEAP2* on the aggressive traits of LNCaP and C4-2B prostate cancer cells. This aim was addressed by evaluating the following properties of LNCaP^{KO} and C4-2B^{KO} cells in comparison to their wild-type counterparts: cell viability, proliferation, migration and invasion. Finally, this chapter also aimed to determine whether targeted *STEAP2* knockout influenced the expression levels of *AR* and the androgen-associated genes *PSA, FKBP5, TMPRSS2* and *GPRC6A.* This was achieved through qRT-PCR analysis of these genes in LNCaP^{KO} and C4-2B^{KO} cells in comparison to their wild-type counterparts.

5.3.1 STEAP2 gene and protein expression is upregulated in androgen-sensitive prostate cancer cell lines

As demonstrated in **Chapter 3, Section 3.3.1,** of the four *STEAP* family members, *STEAP2* gene expression was highest in androgen-sensitive human prostate cancer cell lines. Additionally, western blotting was carried out to determine if the STEAP2 protein expression levels in C4-2B and LNCaP prostate cancer cell lines, were increased in the same manner as the *STEAP2* gene expression levels. The normal prostate epithelial cell line PNT2 was used for comparison.

In **Chapter 3, Section 3.3.1**, *STEAP2* was found to have the highest increase in expression in all 4 of the cell lines screened, as determined by a >2-fold increase in fold expression. Moreover, the highest and most significant overexpression levels of *STEAP2* were observed in the androgen-sensitive cell lines LNCaP and C4-2B, which exhibited 264.7-fold and 53.5-fold increases in expression respectively ($p \leq 0.001$; **Figure 5.4A**). The data is presented again in this Chapter for comparison purposes with STEAP2 protein expression. STEAP2 protein levels in LNCaP and C4-2B cells were also evaluated to determine whether the *STEAP2* overexpression was translated

at a protein level, as determined by Western blot analysis (**Figure 5.4B).** On the basis of these results, the cell lines LNCaP and C4-2B were carried forward throughout this chapter.

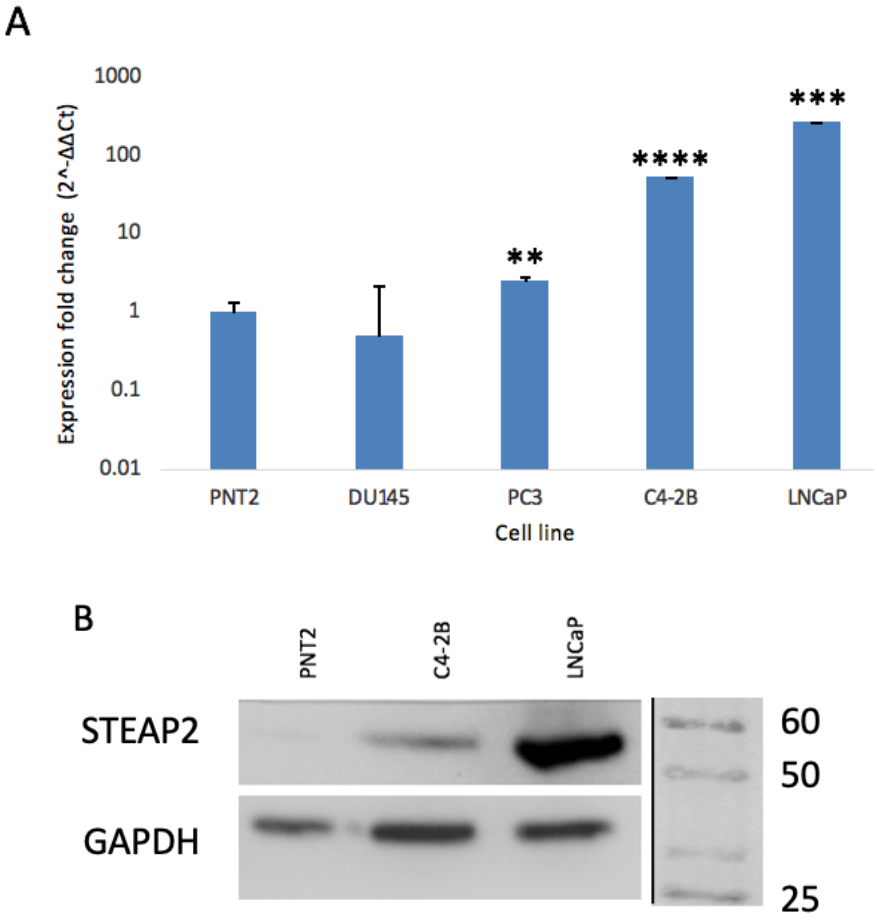

Figure 5.4. STEAP2 is highly expressed in androgen-sensitive prostate cancer cell lines. (A) Fold changes in *STEAP2* gene expression in a panel of human prostate cancer cell lines as compared to the normal prostate epithelial cell line PNT2. An ANOVA post-hoc Dunnett test was performed for statistical analysis. Error bars denote S.E.M. p-value < 0.01 (**), p-value < 0.001 (***), p-value < 0.0001 (****) (N = 3). (B) Western blot analysis of STEAP2 protein expression in LNCaP and C4-2B prostate cancer cell lines (Loading control = GAPDH, Black lines represent where the western blot image has been edited for clarity).

5.3.2 Development of CRISPR/Cas9 technology for *STEAP2* knockout in androgen-sensitive prostate cancer cells *in vitro*

5.3.2.1 CRISPR/Cas9 engineering successfully knocks out *STEAP2* from LNCaP and C4-2B cell colonies

Two *STEAP2* knockout plasmids were designed using the WGE database and BLAST analysis to encode for the full length STEAP2 protein (plasmid #1) and a STEAP2 transcript variant (plasmid #2). Plasmids were expanded, purified and quantified prior to lentiviral transfection into LNCaP^{WT} and C4-2B^{WT} cells. Single colonies of LNCaP^{KO} and C4-2B^{KO} cells were then expanded, and protein lysates collected. In order to confirm whether STEAP2 had successfully been knocked out of the expanded colonies of LNCaP^{KO} and C4-2B^{KO} cells following CRISPR/Cas9 engineering, Western blotting was performed. LNCaP^{WT} and C4-2B^{WT} cells were used as positive controls exhibiting high levels of STEAP2 protein expression. Protein lysates from three individual colonies per cell line, per STEAP2 plasmid were assessed, with GAPDH used as a loading control.

Upon analysis of STEAP2 protein expression, all expanded colonies of LNCaP^{KO} cells exhibited a complete ablation of STEAP2 expression in comparison to their wild-type counterparts (**Figure 5.5A**). In C4-2B^{KO} cells, CRISPR/Cas9 knockout of STEAP2 was also successful in all expanded colonies, with the exception of P1_C3_C, which displayed some, albeit reduced, STEAP2 protein expression in comparison with their wild-type counterparts (**Figure 5.5B**). The protein expression of GAPDH loading control was consistent across all colonies, demonstrating that similar quantities of protein lysates were present across all samples (**Figure 5.5**). Based on these results, all six colonies from both cell lines were carried forward for cell viability assessment. STEAP2 protein expression was periodically assessed to ensure stable knockout of STEAP2 was achieved in order to confidently determine that any subsequent results were the result of STEAP2 knockout (see **Appendix 3, Figure A3. 1**).

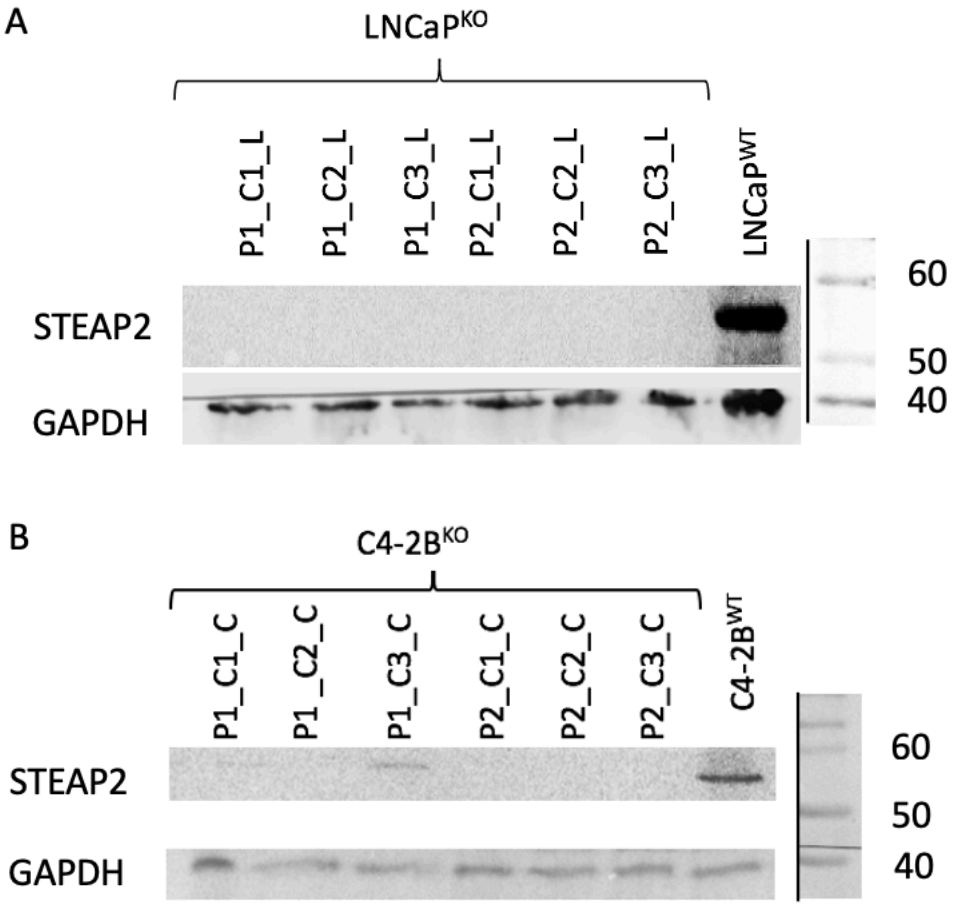

Figure 5.5. STEAP2 protein expression analysis by Western blotting. Protein lysates were taken from LNCaP^{WT} and LNCaP^{KO} cells (A) and C4-2B^{WT} and C4-2B^{KO} cells (B). LNCaP^{WT} cells (A) and C4-2B^{WT} cells (B) represent high STEAP2 levels. Three individual colonies per STEAP2 plasmid of LNCaP^{KO} and C4-2B^{KO} cells to determine STEAP2 knockout efficiency. STEAP2: approx. 56 kDa; GAPDH: approx. 37 kDa. (Loading control = GAPDH, Black lines represent where the western blot image has been edited for clarity).

5.3.2.2 Optimisation of viable *STEAP2* knockout prostate cancer cell colonies

To determine the optimal expanded cell colony from each cell line to carry forward for further analysis, the viability of all colonies was assessed by the alamarBlue viability assay. Cell viability was measured every 24 h after seeding, with the aim of selecting a colony with consistent viability over time. Colonies were maintained until cell viability dropped below half that of their wild-type counterparts. Cell viability was measured as a percentage of viable cells present in the population.

In LNCaP^{KO} cells, the percentage of viable cells varied across colonies. Colony P1_C1_L was the only one to display a significant increase in the percentage of viable cells (+11%, $p < 0.05$; **Figure 5.6A**). Whilst the percentage of viable cells did increase in colony P1_C1_L, it was of concern that this could be the result of an unstable *STEAP2* knockdown. Only LNCaP^{KO} colony P2_C1_L showed a significant decrease in the percentage of viable cells by day 3 (-35%, $p < 0.01$; **Figure 5.6A**). LNCaP^{KO} colony P1_C3_L exhibited the least changes in the percentage of viable cells in comparison to LNCaP^{WT} cells, as shown by a percentage of viable cells of 49% in comparison to 51% displayed by LNCaP^{WT} cells on day 3. In P1_C2_L, although a decrease in the percentage of viable cells in comparison to LNCaP^{WT} cells was observed, this remained the most consistent over the 3-day period (**Figure 5.6A**). However, in C4-2B^{KO} cells, a significant reduction in the percentage of viable cells was observed at every time point from as early as 24 h **(Figures 5.6B).** By Day 5, the C4-2B^{KO} colony P2_C3_C exhibited the largest significant decrease in the percentage of viable cells (-33%, $p < 0.0001$; **Figure 5.6B**). C4-2B^{KO} colony P1_C2_C exhibited the lowest decreases in the percentage of viable cells across all 5 days, as shown by a percentage of 63% in comparison to 80% displayed by C4-2B^{WT} cells on day 3. Based on these results, LNCaP and C4-2B knockout colonies were chosen as P1_C2_L and P1_C2_C respectively, as depicted by the red circles shown in **Figure 5.6** and expanded for use throughout this chapter; they are herein referred to generically as LNCaP^{KO} and C4-2B^{KO} respectively. These colonies were chosen as it was important to select colonies from the same knockout plasmid

in order for comparisons to be made throughout this Chapter. Plasmid #1 encoded for the full length STEAP2 protein and was therefore the preferred method for complete *STEAP2* knockout.

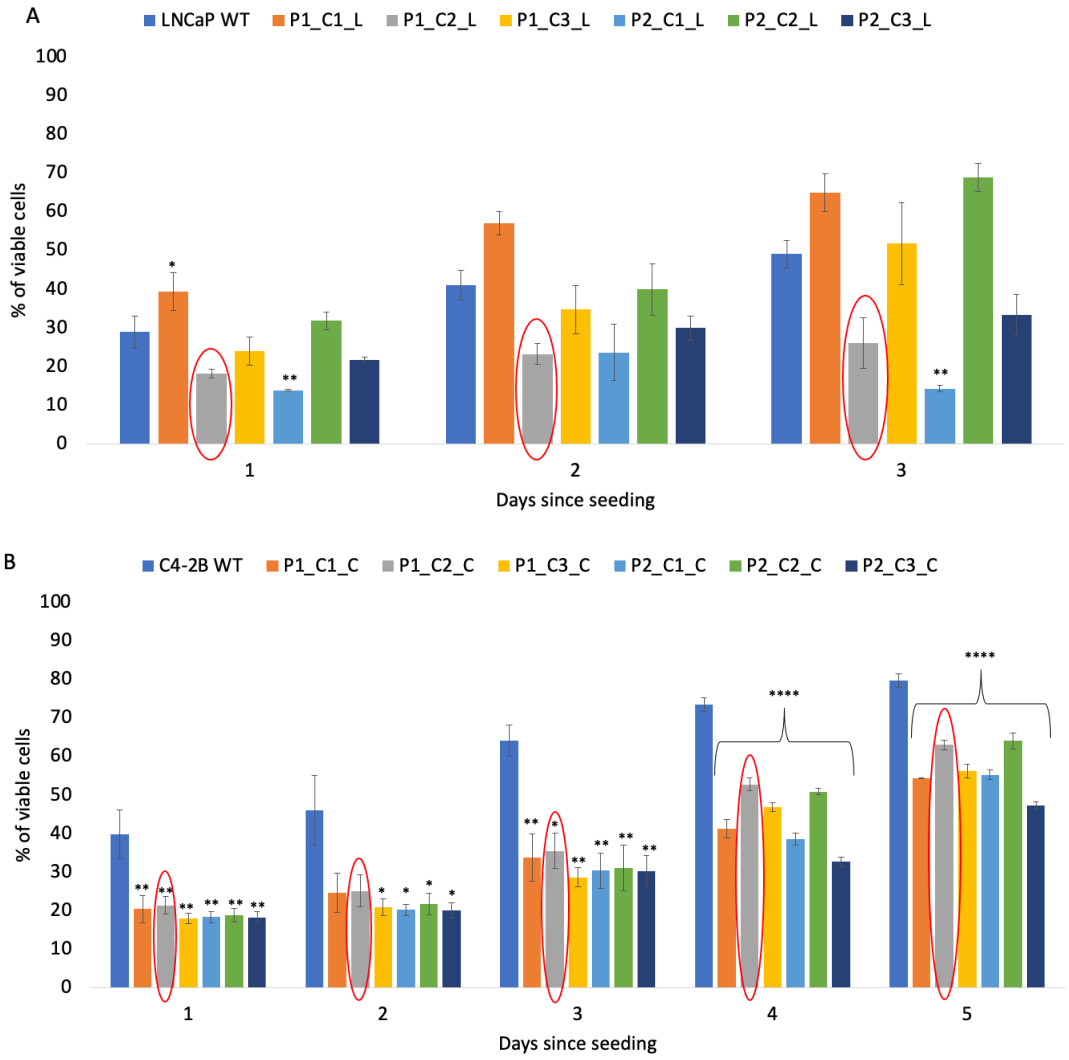

Figure 5.6. *STEAP2* knockout decreases cell viability. Quantification by the alamarBlue assay of the percentage of viable cells in individual LNCaP^{KO} (A) and C4-2B^{KO} (B) cell colonies. Red circles indicate colonies carried forward. An ANOVA post-hoc Dunnett test was performed for statistical analysis. Error bars denote S.E.M. p-value < 0.05 (*), p-value < 0.01 (**), p-value < 0.001 (***), p-value < 0.0001 (****) (N = 3).

5.3.3 Analysis of aggressive prostate cancer traits in response to *STEAP2* knockout in androgen-sensitive prostate cancer cells

5.3.3.1 *STEAP2* knockout reduces cell proliferation and migration

In order to evaluate the impact of CRISPR/Cas9 knockout of STEAP2 from LNCaP and C4-2B cells on cell proliferation, the alamarBlue cell proliferation assay was performed. Based on the percentage of viable cells of each cell line over time as shown in **Section 5.3.2.2**, the assay was carried out every 24 h after seeding for a total of either 3 days (LNCaP) or 5 days (C4-2B), as after this time cell growth began to significantly slow for each cell line. The percentage of proliferating cells was normalised to cells on day 1 to determine the difference in proliferation rate over time.

In LNCaP^{KO} cells, the percentage of proliferating cells was significantly reduced on day 3 (-48%, $p < 0.05$; **Figure 5.7B,**). The percentage of proliferating C4-2B^{KO} cells was also consistently and significantly reduced across all 5 days and was lowest on day 5 (-53%, $p < 0.0001$; **Figure 5.7B**). Based on these data, it can be suggested that *STEAP2* knockout significantly reduces the proliferative capacity of androgen-sensitive prostate cancer cell lines.

To further evaluate the potential of CRISPR/Cas9 knockout of *STEAP2* on reducing aggressive characteristics of LNCaP and C4-2B cells, the cell migration assay was carried out. To do so, cells were cultured in separate chambers of a silicone tissue culture plate insert. The insert was removed once cells had reached ~80% confluency (24 h after seeding of C4-2B cells or 48 h after seeding of LNCaP cells), and cells were imaged every 24 h for 5 days.

In LNCaP cells, whilst the wound gap was not completely closed in wild-type cells by day 5 (**Figure 5.8A**), *STEAP2* knockout had completely inhibited migration of LNCaP^{KO} cells (**Figure 5.8B**). In C4-2B cells, the wound gap had

entirely closed between days 3 and 5 in C4-2B^{WT} cells (**Figure 5.8C**), suggesting that they migrate at a faster rate than LNCaP^{WT} cells. In contrast, in C4-2B^{KO} cells, inhibition in cell migration was still observed on day 5 as the wound gap remained fully open (**Figure 5.8D**). These data indicate that *STEAP2* knockout leads to a complete inhibition of the migratory capacity of both LNCaP^{KO} and C4-2B^{KO} cells (**Figure 5.8**, where representative images are shown; additional images from the second replicate can be found in **Appendix 3, Figure A3.4**).

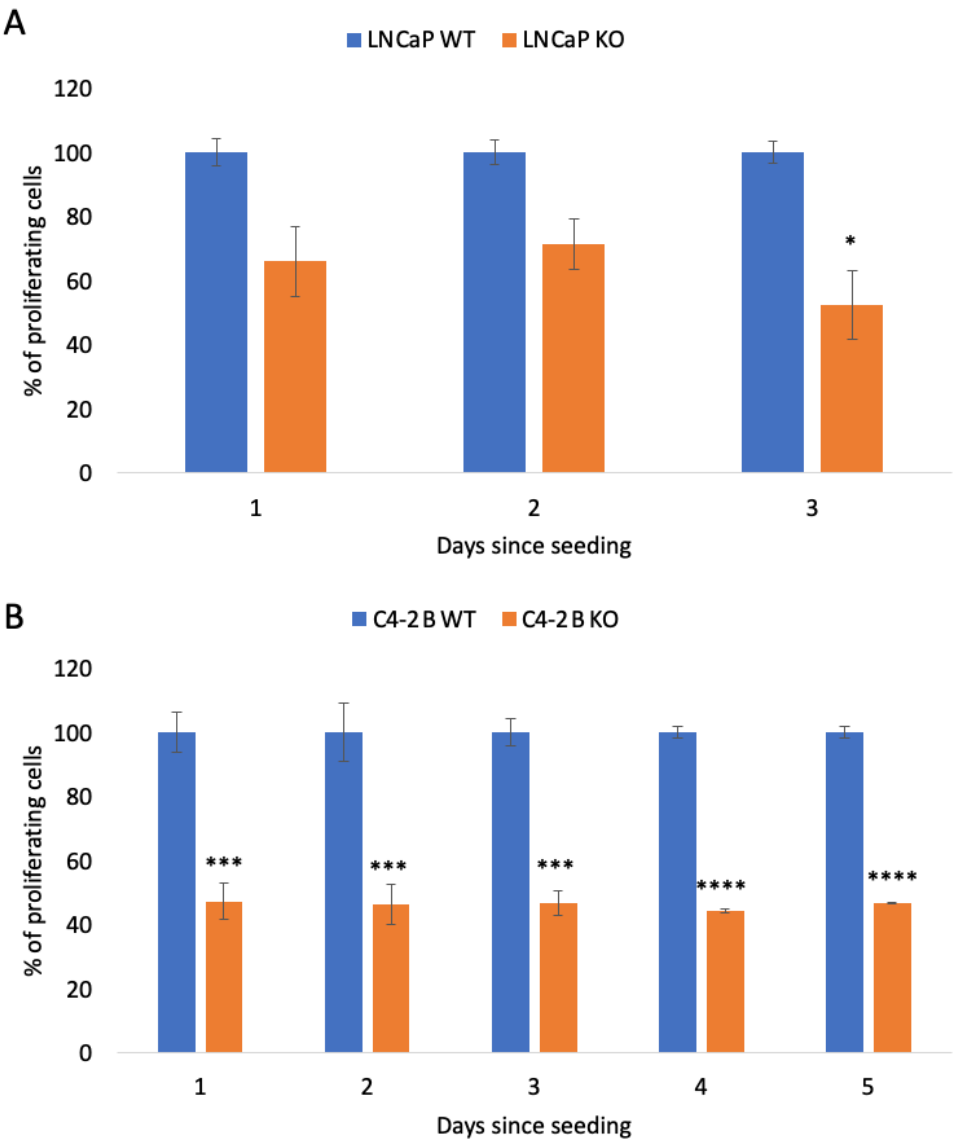

Figure 5.7. *STEAP2* knockout significantly reduces cell proliferation. Quantification by alamarBlue assay of the percentage of proliferating cells in LNCaP^{KO} (A) and C4-2B^{KO} (B) cells in comparison to their wild-type counterparts. An ANOVA post-hoc Dunnett test was performed for statistical analysis. Error bars denote S.E.M. p-value < 0.05 (*), p-value < 0.01 (**), p-value < 0.001 (***), p-value < 0.0001 (****) (N = 3).

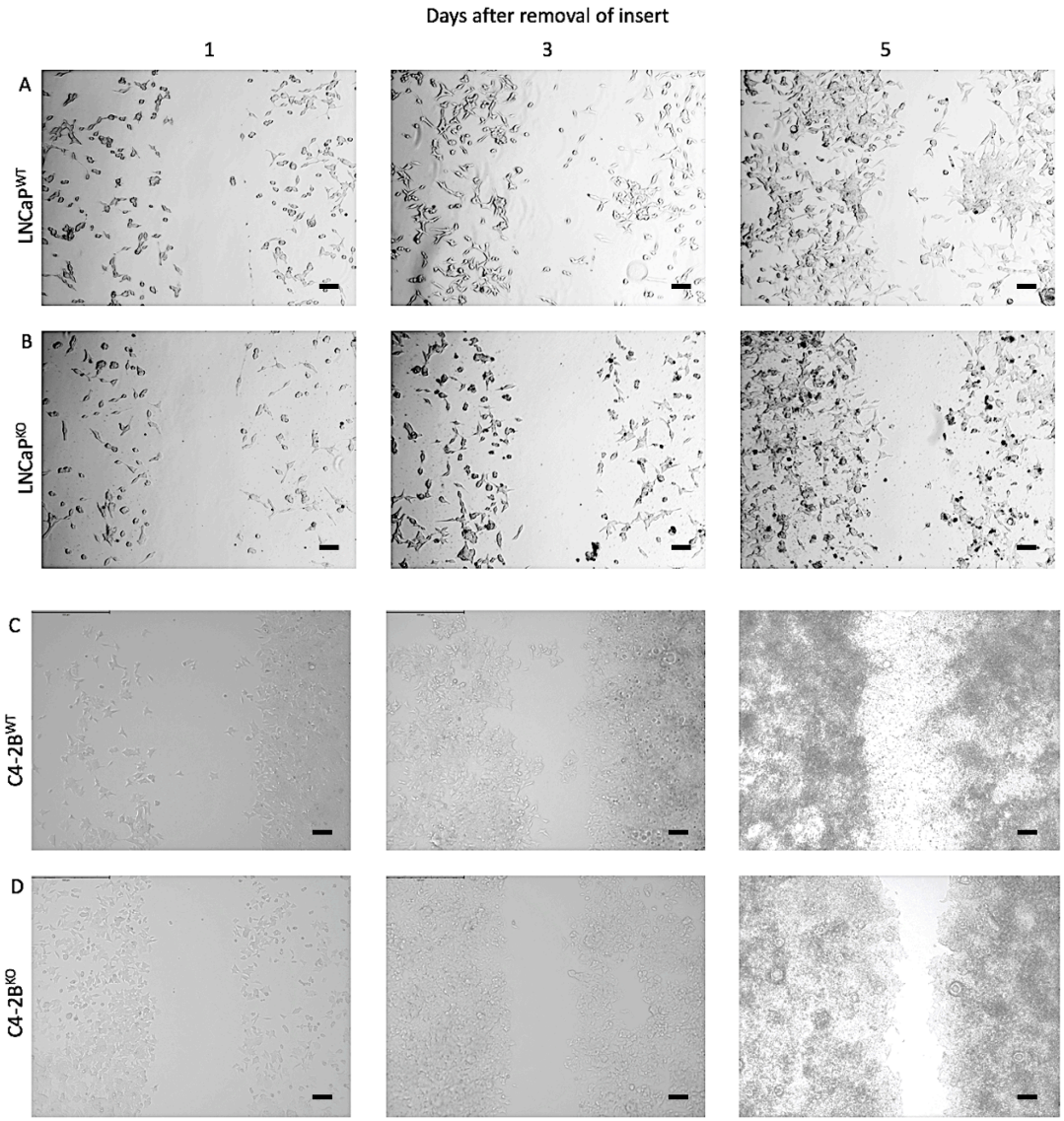

Figure 5.8. *STEAP2* knockout decreases the migratory potential of LNCaP and C4-2B cells. Each panel represents A) LNCaP^{WT}, B) LNCaP^{KO} cells and C) C4-2B^{WT}, D) C4-2B^{KO} cells. Time points at which the images were taken: 0 days, 3 days and 6 days. Wild-type LNCaP and C4-2B cells were used as positive controls. Images were acquired using an inverted light microscope with a 10x objective (Invitrogen, EVOS XL Core, USA). Scale bar = 100 μm. (Illustrated are representative images; the experiment was however conducted in triplicate with biological replicates, N = 3).

5.3.3.2 *STEAP2* knockout reduces cell invasion in LNCaP and C4-2B cells

The cell invasion assay was performed to evaluate whether targeted knockout of *STEAP2* using CRISPR/Cas9 engineering had an effect on inhibiting cancer cell invasion. To do so, the bottom of a culture plate-insert was coated with Matrigel (as per manufacturer's instructions) and to stimulate the ability of cancer cells to invade through this ECM, FBS served as a chemoattractant. Cells were grown in the top layer of the insert, and as such only those with invasive potential were capable of crossing the Matrigel barrier.

The results illustrated in **Figure 5.9** demonstrate that the invasive potential of LNCaP and C4-2B cells is significantly inhibited with *STEAP2* knockout with only 3.0% and 4.1% of LNCaP^{KO} and C4-2B^{KO} cells respectively, invading through the ECM as compared to the equivalent wild-type cells ($p < 0.001$; **Figure 5.9E**). These data, along with the results presented in **Sections 5.3.3.1 & 5.3.3.2**, suggest that *STEAP2* knockout substantially reduces aggressive cancer traits in LNCaP and C4-2B cells (**Figure 5.9**, where representative images are shown; additional images from the second replicate can be found in **Appendix 3, Figure A3.5**).

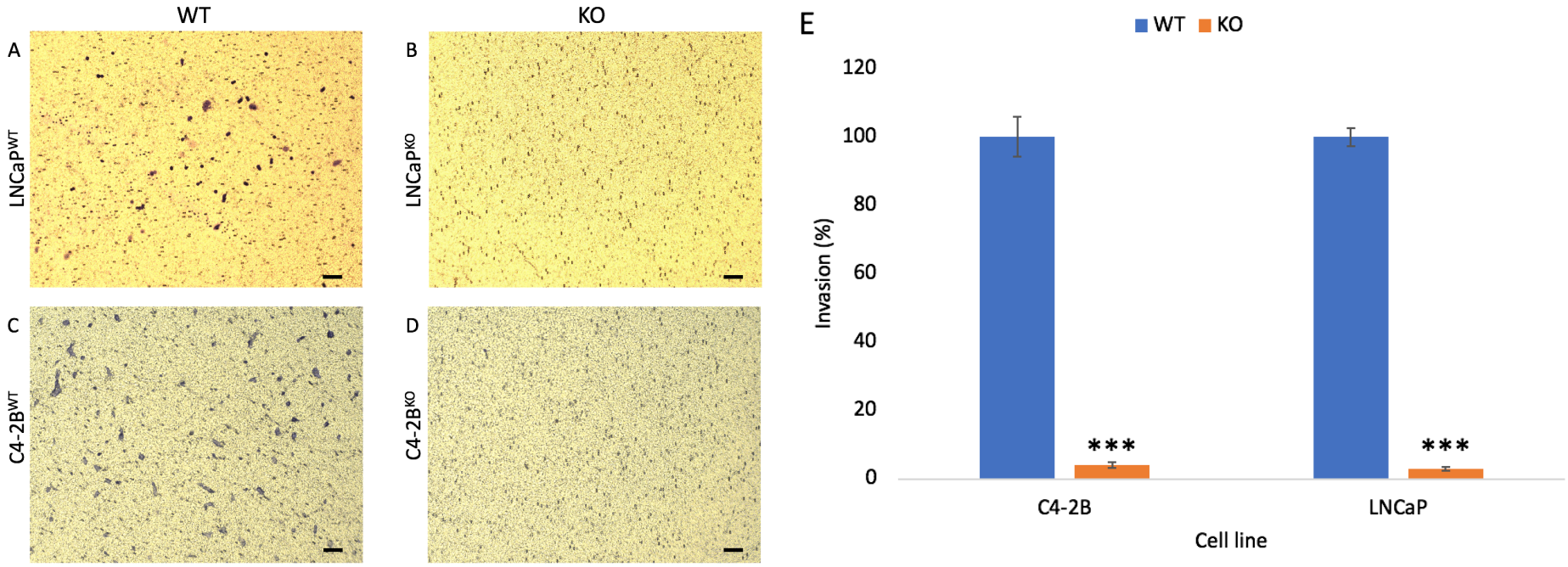

Figure 5.9. *STEAP2* knockout reduces the invasive potential of LNCaP and C4-2B cells. Images of stained cells were taken to give a visual representation of invasion. Each panel represents A) LNCaP^{WT}, B) LNCaP^{KO} cells and C) C4-2B^{WT}, D) C4-2B^{KO} cells. LNCaP^{WT} and C4-2B^{WT} cells show invasive potential. STEAP2 knockout in LNCaP^{KO} and C4-2B^{KO} cells reduces invasive capacity. Invaded cells were stained with crystal violet. Images were taken 48 h (C4-2B) and 72 h (LNCaP) after seeding. E) The number of stained cells that had invaded through the Transwell insert were counted and calculated as a percentage of the wild-type control. An unpaired t-test was performed for statistical analysis. Error bars denote S.E.M. p-value < 0.05 (*), p-value < 0.01 (**), p-value < 0.001 (***), p-value < 0.0001 (****). Images were taken with an inverted light microscope at a 10x objective (Invitrogen, EVOS XL Core, USA). Scale bar = 100 μm. Illustrated are representative images; the experiment was however conducted in triplicate with biological replicates, N = 3).

5.3.4 The impact of CRISPR/Cas9 knockout of *STEAP2* on the expression of *AR* and androgen-regulated genes in androgen-sensitive prostate cancer cells

5.3.4.1 *STEAP2* knockout increases the expression of *AR* and androgen-regulated genes

LNCaP and C4-2B are both androgen-sensitive prostate cancer cell lines. Following the results of **Chapter 4, Section 4.3.3** which found that *AR* gene expression increased in response to STEAP2 polyclonal antibody treatment, this chapter explores *AR* expression in response to *STEAP2* knockout by qRT-PCR.

No significant change in AR expression was observed in LNCaP^{KO} cells (+0.1-fold; **Table 5.5**). However, in contrast, AR was found to be highly and significantly overexpressed in C4-2B^{KO} cells, which exhibited a 38.9-fold increase in expression ($p \leq 0.0001$; **Table 5.5**). On the basis of these results, the impact of *STEAP2* knockout on the expression of three genes regulated by AR; *PSA, FKBP5* and *TMPRSS2* in LNCaP^{KO} and C4-2B^{KO} cells was assessed.

Chapter 4, Section 4.3.4 found that the expression of three out of four genes known to influence *AR* expression – *PSA, FKBP5* and *TMPRSS2* – increased in response to STEAP2 polyclonal antibody treatment in both LNCaP and C4-2B cells, whilst *GPRC6A* expression was undetectable. Following these results, the gene expression of the same four *AR* downstream genes were quantified in response to *STEAP2* knockout by qRT-PCR in LNCaP and C4-2B cells. Wild-type cells were used for comparison.

Upon analysis of gene expression of the four AR downstream genes, *TMPRSS2* was found to be significantly overexpressed in both LNCaP^{KO} and C4-2B^{KO} cells, which exhibited 274.9-fold and 92953.2-fold increases in expression respectively **(Table 5.5)**. *PSA* and *FKBP5* all showed an increase

in expression in LNCaP^{KO} cells when compared to LNCaP^{WT} cells, displaying 49.7-fold and 582.3-fold increases in expression respectively (**Table 5.5**). *PSA* and *FKBP5* expression in C4-2B^{KO} cells (**Table 5.5**), and GPRC6A expression in either LNCaP^{KO} or C4-2B^{KO} cells was undetermined (**Table 5.5**). qRT-PCR analysis of *PSA, FKBP5, TMPRSS2* and *GPRC6A* expression therefore demonstrated that *TMPRSS2* is highly expressed in *STEAP2* knockout androgen-sensitive prostate cancer cell lines and thus, could warrant further investigations into its role in AR expression and aggressive cancer traits.

Table 5.5. *STEAP2* knockout increases the expression of *AR* and androgen-regulated genes. Fold changes in the gene expression of *PSA*, *FKBP5*, *TMPRSS2* and *GPRC6A* in LNCaP and C4-2B *STEAP2* knockout cell lines as compared to their wild-type counterparts. An ANOVA post-hoc Dunnett test was performed for statistical analysis. GAPDH was used as the housekeeping gene. "Undetectable" indicates that no gene expression of this gene was recorded. p-value < 0.01 (**), p-value < 0.001 (***), p-value < 0.0001 (****) (N = 3).

	Expression fold change (2^-ΔΔCt)	
Gene	**C4-2B^{KO}**	**LNCaP^{KO}**
AR	+38.9****	+0.1
PSA	Undetectable	+48.7***
FKBP5	Undetectable	+581.3***
TMPRSS2	+92953.2***	+274.9***
GPRC6A	Undetectable	Undetectable

5.4 Discussion

This chapter aimed to design, optimise and successfully employ CRISPR/Cas9 engineering for targeted *STEAP2* knockout. The aim of this chapter was also to determine whether targeted *STEAP2* knockout could reduce aggressive cancer traits in androgen-sensitive prostate cancer cells, by assessing cell viability, proliferation, migration and invasion in response to targeted *STEAP2* knockout. The results demonstrated that CRISPR/Cas9 engineering had resulted in successful *STEAP2* knockout, and such targeted *STEAP2* knockout resulted in significant reductions in cell proliferation and viability. Cell migration and invasion was also inhibited by *STEAP2* knockout.

5.4.1 Optimisation and development of CRISPR/Cas9 technology for *STEAP2* knockout in androgen-sensitive prostate cancer cells *in vitro*

CRISPR/Cas9 technology has the ability to induce complete gene knockout, as opposed to the transient gene knockdown offered by siRNA silencing (Boutros & Ahringer, 2008; Tuladhar *et al*., 2019). siRNA silencing has previously been used to target *STEAP2 in vitro*, however only a 50% reduction in protein expression was reported, highlighting the need for a more efficient genome engineering tool (Burnell *et al*., 2018). The expression of *STEAP2* and other family members has previously been evaluated in a panel of prostate cancer cells (see **Chapter 3, Section 3.3.1**). Based on the gene expression profiles, LNCaP and C4-2B cells were selected for *STEAP2* knockout, as their high *STEAP2* gene expression levels were mirrored when evaluating STEAP2 protein levels, which for LNCaP, correlates with observations reported in the scientific literature (**Figure 5.4B**; Whiteland *et al*., 2014).

CRISPR/Cas9 knockout efficiency is primarily determined by protein expression, as opposed to gene expression, as clones may display a strong attenuation of mRNA expression due to nonsense-mediated decay, but not complete ablation of protein expression (Ramlee *et al*., 2015; Tuladhar *et al*., 2019). In this study, *STEAP2* was successfully knocked out of all expanded colonies in both cell lines (**Figure 5.5**), and therefore all six knockout colonies

from each cell line were carried forward for subsequent cell viability assays. Successful targeted knockdown of *STEAP2* by lentiviral particles created in HEK293T cells was achieved as once viral particles with specific tropism were created, they were able to infect the target cells in the same way as a native viral particle would, allowing for the persistent presence of CRISPR/Cas9 components and ultimately a long-term knockout of *STEAP2* (Lino *et al*., 2018). One of the main challenges of CRISPR/Cas9 technology is the generation of stable knockout clones (Lino *et al*., 2018).

In order to ensure that the results of any subsequent assays were due to *STEAP2* knockout and not reduced cell viability, it was essential that knockout colonies with no significant changes in viability when compared to wild-type cells were selected. Based on the alamarBlue viability assay results (**Figure 5.6**) and the morphology of parental cells (see **Appendix 3, Figures A3.2 & 3**), *STEAP2* knockout plasmid #1 was found to be successful in generating *STEAP2* knockout positive cells which displayed similar behaviour patterns and morphological profiles to their wild-type counterparts. *STEAP2* knockout plasmid #1 encoded for the complete STEAP2 protein, whereas plasmid #2 encoded for a *STEAP2* transcript variant (see **Section 5.2.3.1**). Plasmid #1 is part of a collection of full-length cDNA clones generated by the Mammalian Gene Collection project, whereas plasmid #2 encodes the longest *STEAP2* isoform (RefSeq, 2008). Therefore plasmid #1 was chosen for targeted knockout of the complete, full length STEAP2 protein. CRISPR/Cas9 targeted *STEAP2* knockout significantly reduced cell viability in half of the LNCaP^{KO} cell colonies (**Figure 5.6A**), and all of the C4-2B^{KO} cell colonies. Generating stable knockout colonies remains to be a challenge in CRISPR/Cas9 engineering, and as such the increases observed in the viability of LNCaP^{KO} colonies P1_C1_L, P1_C3_L and P2_C2_L to similar levels to LNCaP^{WT} may suggest these colonies have not sustained their *STEAP2* knockout, and as such *STEAP2* expression may have returned to basal levels (Giuliano *et al*., 2019; Lino *et al*., 2018). Previous studies show that *STEAP2* knockdown via targeted siRNA increases the number of apoptotic events in prostate cancer cells, which may account for the decreases in viability observed here (Wang *et al*., 2010). In LNCaP cells in which *STEAP2* expression had been knocked down,

Wang *et al*., found that the CDKI p21 was upregulated, which was also found to be the case when cells were grown as xenografts, suggesting *STEAP2* plays a role in the negative regulation of the cell cycle during G_1 and S phase (Bertoli *et al*., 2013; Wang *et al*., 2010). As the pathways by which *STEAP2* influence cell viability remain unclear, future work would be required to explore this in more detail.

5.4.2 The impact of CRISPR/Cas9 knockout of *STEAP2* on aggressive prostate cancer traits

STEAP2 has previously been found to be involved in cellular proliferation in prostate cancer cells (Gomes *et al*., 2012; Wang *et al*., 2010). Here, CRISPR/Cas9 targeted *STEAP2* knockout significantly reduced proliferation of LNCaP^{KO} and C4-2B^{KO}, which was sustained over a 3- and 5- day period, respectively (**Figure 5.7**). The role of *STEAP2* in cell proliferation has previously been explored by Wang *et al*., who found that when *STEAP2* was overexpressed in COS-7 normal monkey kidney fibroblast cells, an increase in cell proliferation rate occurred (Wang *et al*., 2010). In the same study, *STEAP2* was ectopically expressed in DU145 prostate cancer cells, which resulted in ERK activation in response to EGF, the expression of which was increased in response to *STEAP2* (Wang *et al*., 2010). Once ERK becomes phosphorylated, a variety of transcription factors become activated upon the translocation of ERK into the nucleus, including AP-1, which has canonical sequences with MMPs -1, -3, -7, -9, -11 and -13 (Dhillon *et al*., 2007; Gong *et al*., 2014). The role of *STEAP2* in cellular proliferation has previously been found to be co-ordinated through the activation of the ERK pathway, which when activated by *STEAP2* induces this partial cell cycle arrest in the G_0-G_1 phase of the cell cycle in cancer cells, and in turn increases cell proliferation and tumour progression (Gomes *et al*., 2012; Wang *et al.,* 2010).

When the expression of *STEAP2* has been knocked down by the presence of *STEAP2* siRNA, the proliferation of LNCaP cells was found to significantly decrease, yet no changes in cellular morphology were observed (Wang *et al*., 2010). Studies into the changes in the distribution of the cell cycle of LNCaP cells transfected with *STEAP2* siRNA found that there was a significant

increase in the percentage of cells in G_1 phase, which corroborated with a decrease in cells in the S phase, suggesting that loss of *STEAP2* results in a partial cell cycle arrest in G_0-G_1 (Wang *et al*., 2010). When monitoring the proliferation of cells transfected with *STEAP2* siRNA using the proliferative marker Ki67, Wang *et al*., found that Ki67 was significantly downregulated by day 4 in LNCaP cells transfected with *STEAP2* siRNA, further confirming the proliferative influence of *STEAP2* expression. Therefore, in this Chapter, an absence of *STEAP2* expression may have led to a decrease in cell proliferation as the ERK pathway would not become activated by *STEAP2*, and in turn the partial arrest at G_0-G_1 observed in previous studies may have occurred (Wang *et al*., 2010). The results in this Chapter further confirm that *STEAP2* inhibition significantly reduces cell proliferation, as demonstrated by previous studies (Burnell *et al*., 2018; Wang *et al*., 2010). This reduction in proliferation may be the result of an inability to progress through G_0-G_1 phase of the cell cycle (Wang *et al*., 2010). However, as the exact mechanisms by which *STEAP2* knockout reduces proliferation were not assessed, future work should involve the use of flow cytometry to further understand the impact this has on the distribution of the cell cycle in comparison to wild-type cells.

An essential mechanism in the progression of prostate cancer is the ability of cells to migrate to distant sites to form metastases (Rycaj & Tang, 2017). *STEAP2* has previously been hypothesised to be involved in promoting cancer cell migration, thus enhancing prostate cancer progression (Burnell *et al*., 2018; Whiteland *et al*., 2014). In this Chapter the hypothesises posed was that complete gene knockout of *STEAP2* from prostate cancer cells using CRISPR/Cas9 technology will significantly inhibit cancer cell migration. Indeed, the data generated through use of the proliferation assay demonstrated that *STEAP2* knockout significantly reduced proliferation in both cell lines (**Figure 5.7**). Furthermore, it was found that migration of *STEAP2* knockout cells was impaired in comparison to their wild-type counterparts (**Figure 5.8**). These results confirm those of previous studies which indicate that *STEAP2* plays a role in the migration of prostate cancer cells (Burnell *et al*., 2018; Whiteland *et al*., 2014).

In the first study to demonstrate the potential influence of *STEAP2* in non-cancerous cells, the normal prostate cancer epithelial cell line PNT2 was transfected to overexpress *STEAP2*, which induced cell migration at a faster rate than wild-type cells (Whiteland *et al*., 2014). siRNA technology has previously been utilised to knock-down *STEAP2* in the prostate cancer cell line PC3, which significantly decreased the cell migratory potential (Burnell *et al*., 2018). As the primary function of *STEAP2* is to act as a receptor for iron and copper uptake, when absent a lack of iron and copper metabolism may occur, resulting in the suppression of intracellular pathways such as ERK/MAPK (Gomes *et al*., 2012; Grunewald *et al*., 2012; Knutson, 2007). As previously suggested, the lack of activation of the ERK pathway due to *STEAP2* knockout may also inhibit the migratory potential of LNCaP^{KO} and C4-2B^{KO} cells as observed in the present study (Burnell *et al*., 2018; Wang *et al*., 2010).

One of the principal ways of reducing cancer progression is to inhibit cell motility, and subsequently reduce cell migration and invasion (Palmer *et al*., 2011). When downregulated, another member of the *STEAP* family, *STEAP4*, has been found to significantly increase ROS via iron reductase activity (Jin *et al*., 2015; Scarl *et al*., 2017). Whilst ROS increases are often associated with an increase in mutations and disease progression, the induction of excessive ROS activity in prostate cancer cells has been found to reduce tumour cell motility and metastasis through the inhibition of epithelial-mesenchymal transitions (Das *et al*., 2014; Lim et al., 2005). Apoptosis was also found to increase in response to elevated ROS, as a result of caspase-3 and -9 activation and cytochrome-c release (Das *et al*., 2014). Similar to *STEAP4, STEAP2* also contains a N-terminal oxidoreductase domain with a nicotinamide adenine di-nucleotide phosphate (NADPH) binding motif, which can serve as an electron donor for transmembrane electron transport of iron and copper (Grunewald *et al*., 2012; Knutson, 2007; Scarl et al., 2017). An increase in iron uptake has been found to increase ROS and promote carcinogenesis, suggesting targeting iron metabolism may be a potential therapeutic approach in the treatment of some cancers (Bystrom *et al*., 2014; Jung *et al*., 2019). Therefore, it could be suggested that the decrease in migration observed in this chapter could be the result of *STEAP2* knockout

inducing an increase in ROS activity through impaired iron reductase activity. However, as this connection between ROS and *STEAP2* remains unclear, further studies would be warranted to explore this theory further which may include the use of fluorescent microscopy to determine the intercellular localisation of ROS in *STEAP2*-knockout cells compared to their wild-type counterparts (Das *et al*., 2014). It would also be of interest to assess mRNA iron levels using markers such as Tfr1 in *STEAP2*-knockout and wild-type cells alongside monitoring ROS to suggest a mechanism underlying any changes in ROS activity (Jung *et al*., 2019).

Similar to migratory capacity, the invasion potential of PC3 cells has been found to substantially decrease following the gene knock-down of *STEAP2* using siRNA technology (Burnell *et al*., 2018). In addition, when the normal prostate epithelial cell lines PNT2 has previously been transfected with a *STEAP2* plasmid in order to overexpress the gene, cells gained the ability to invade through the extracellular matrix (Whiteland *et al*., 2014). Furthermore, work within the group has demonstrated that *STEAP2* is involved in promoting prostate cancer invasion through treatment with mono- and polyclonal anti-STEAP2 antibodies (Nguyen-Chi *et al*., 2020). The data presented in this chapter indicates that *STEAP2* may play a substantial role in the invasive potential of LNCaP and C4-2B cells, which was significantly reduced in both cell lines by 97.0% and 95.9% respectively (**Figures 5.9E**).

An important step in the progression of prostate cancer is the ability to degrade the ECM, for which MMPs are often required (Gialeli *et al*., 2011). Whilst the exact mechanism of how *STEAP2* is involved in promoting cancer cell invasion is not yet fully understood, previous studies have found that siRNA gene knockdown of *STEAP2* significantly reduces the expression of MMPs needed to degrade the ECM (Burnell *et al*., 2018). In particular, MMPs-3, - 7, -10 and -13 have been identified as downstream targets of *STEAP2* associated with driving invasion (Burnell *et al*., 2018). Increases in MMP expression in prostate cancer have been suggested to promote cancer progression by the NFκB signalling pathway (Chen *et al*., 2013; Nguyen *et al*., 2014). The NFκB

signalling pathway has been found to contribute to an overexpression of the receptor activator of nuclear factor kappa- β (RANK) ligand (RANKL) (Xing & Boyce, 2005). *RANKL* is associated with prostate cancer invasion and progression to form bone metastases (Wright *et al*., 2009). It would therefore be interesting to culture the *STEAP2* knockout cells generated in this chapter as 3D spheroid models, as developed in **Chapter 3**, to assess the role of *STEAP2* on prostate cancer-bone stromal cell interactions.

The reduction in invasive potential of *STEAP2* knockout cells observed in this study could be the result of a decrease in MMP expression by the NFκB signalling pathway, however further work would be required to determine how *STEAP2* knockout alters this pathway. Together, the data presented in this chapter provides evidence that *STEAP2* plays an important role in the progression of androgen-sensitive prostate cancer cells as the ability of both LNCaP and C4-2B to proliferate, migrate and invade was significantly decreased when *STEAP2* expression was knocked out. Whilst the key mechanism behind how *STEAP2* knockout inhibits cell migration remains unknown, the data presented here implies that *STEAP2* could provide a novel therapeutic target for inhibiting prostate cancer migration and metastasis.

5.4.3 The impact of CRISPR/Cas9 knockout of *STEAP2* on the expression of *AR* and androgen-regulated genes in androgen-sensitive prostate cancer cells

Androgen plays a vital role in the regulation of normal development of the prostate gland (Heinlein & Chang, 2004; Davey & Grossman, 2016; Rokhlin *et al*., 2005). *AR* has been widely studied in association with aggressive prostate cancer traits, particularly in LNCaP cells and their derivatives, which are androgen-sensitive prostate cancer cell lines (Gonen-Korkmaz *et al*., 2014). To date, previous studies have determined that *STEAP2* expression may be regulated by *AR*, yet the mechanisms behind this remain unclear (Gomes *et al*., 2012). Following the results of **Chapter 4, Section 4.3.3** which found that *AR* gene expression increased in response to STEAP2 polyclonal antibody

treatment, this chapter found that the expression of *AR* was significantly increased in C4-2B^{KO} cells, but not LNCaP^{KO} cells (**Table 5.5**).

As suggested in **Section 5.4.2.1**, the decrease in proliferation observed in LNCaP^{KO} and C4-2B^{KO} cells may be the result of a lack of *EGF*-induced ERK pathway activation (Wang *et al*., 2010). The transcriptional activity of *AR* has also been known to be activated by EGF, through increasing the expression of *AR* co-activators in prostate cancer cells (Gregory *et al*., 2004; Kaarbo *et al*., 2007). Although changes in *AR* levels in LNCaP^{KO} cells did not reach significance, for a lack of *EGF* activation by *STEAP2* to influence *AR* activity, *AR* expression levels would be expected to decrease in response to *STEAP2* knockout. Therefore, to further explore the role of *STEAP2* in the activation of the ERK pathway, it would be suggested to assess *EGF* expression levels in *STEAP2* knockout cells.

AR expression may be elevated in C4-2B^{KO} cells as a result of p21 upregulation, as p21 has been found to form a complex with cyclin D3, CDK4 and caspase-2 (Migita *et al*., 2012). As previously noted, p21 has been reported to increase in response to *STEAP2* knock down (Wang *et al*., 2010). Caspase-2, a pro-apoptotic protease, is localised to the Golgi apparatus, mitochondria, cytoplasm and nucleus, and is a direct target of *AR* in androgen-sensitive prostate cancer cells (Migita *et al*., 2012; Rokhlin *et al*., 2005). Despite the significant increase in *AR* expression exhibited by C4-2B^{KO} cells, cell proliferation, migration and invasion were substantially reduced, indicating that this increase in *AR* expression does not induce a more invasive phenotype in C4-2B^{KO} cells. An increase in caspase-2 in *STEAP2* knockout cells could provide a mechanism for both the observed decrease in cell viability yet concurrent increase in *AR* expression, and warrants further studies to determine caspase-2 and p21 expression (Migita *et al*., 2012; Wang *et al*., 2010).

To further explore the increase in AR expression exhibited by C4-2B^{KO} cells, additional work was carried out to assess the levels of four key genes known to influence *AR* expression; *PSA, FKBP5*, *TMPRSS2* and *GPRC6A* (Velasco

et al., 2004; Wright *et al*., 2003; Zarif & Miranti, 2016). Following the results of **Chapter 4, Section 4.3.4** which found that the gene expression of all four genes increased in response to STEAP2 polyclonal antibody treatment, this chapter found that the expression of *PSA* and *FKBP5* was significantly increased in LNCaP^{KO} cells, but not C4-2B^{KO} cells (**Table 5.5**), yet *TMPRSS2* expression was significantly increased in both cell lines (**Table 5.5**). *GPRC6A* expression was undetected in both *STEAP2* knockout cell lines (**Table 5.5**).

PSA is known to be regulated by *AR* at a transcriptional level, and previous studies have found *PSA* to become localised to the nucleus in response to androgen stimulation (Kaarbo *et al*., 2007; Migita *et al*., 2012; Saxena *et al*., 2012). Like STEAP2, PSA is also localised to the Golgi apparatus (Saxena *et al.,* 2012). In this study, *PSA* was found to be significantly expressed in LNCaP^{KO} cells, yet no expression was determined in C4-2B^{KO} cells, despite the latter displaying a significant increase in *AR* expression (**Table 5.5**). In androgen-sensitive cells, inhibition of mTOR has also been noted to increase transcriptional activation of *AR* and subsequently increase the expression of *AR* target genes such as *PSA*, whilst inhibiting total *AR* levels through the PI3K/Akt pathway (Cinar *et al*., 2005; Kaarbo *et al*., 2007). *PSA* has also been found to be overexpressed through the induction of IL-6 via activation of the EGF signalling pathway, which may account for the increase in *PSA* expression observed in LNCaP^{KO} cells (Zhu & Kyprianou, 2008). Activation of the EGF signalling pathway may also increase ERK activation, which under androgen-independent conditions has been found to contribute to an increase in PSA levels (Franco *et al*., 2003). MAPK and *AR* signalling crosstalk has been implicated in IL-6 induced transcriptional activity of *AR* in LNCaP cells, as previous studies have found *PSA* expression to decrease when MAPK inhibition repressed the IL-6 stimulated expression of *PSA* (Lin *et al*., 2001).

FKBP5 functions as a steroid receptor and is involved in the modulation of AR function and signalling, through the formation of a complex with the heat shock proteins Hsp90/Hsp70 (Li *et al*., 2011; Ni *et al*., 2010). Previous studies have found *FKBP5* expression to be induced through the activation of *AR*, and the protein has been found to physically interact with *AR* in LNCaP cells

(Ratajczak *et al*., 2003; Febbo *et al*., 2005; Velasco *et al*., 2004). In this chapter, *FKBP5* was found to be significantly expressed in LNCaP^{KO} cells, yet *AR* expression was unchanged (**Table 5.5**). *FKBP5* has been found to be constitutively overexpressed in LNCaP cells which also have increased levels of endogenous *PSA* (Febbo *et al*., 2005). Unlike *PSA*, the *FKBP5* locus is more complex and lacks a consensus *AR* binding site in its proximal locator, and *AR* binding has been localised to an enhancer in the fifth intron of the *FKBP5* gene (Kang *et al*., 2004; Magee *et al*., 2006). The transcriptional cofactor cAMP response element-binding protein (CBP) has been found to interact with *AR* when inducing *PSA* upregulation yet promotes *FKBP5* overexpression through the regulation of histone acetylation, which remains unaffected by androgens (Magee *et al*., 2006). Therefore, the increase in *FKBP5* expression observed in LNCaP^{KO} cells could be a result of an indirect communication between CBP and the proximal *FKBP5* promoter region, independent to *AR* expression (Magee *et al*., 2006). Further studies should explore whether an increase in the *FKBP5* intron-5 enhancer is observed in *STEAP2* knockout cells.

TMPRSS2 has previously been characterised as an androgen-regulated gene (Wright *et al*., 2003; Yu *et al*., 2010). In this chapter, *TMPRSS2* expression was found to increase in both LNCaP^{KO} and C4-2B^{KO} cells, with an exceptionally high increase observed in C4-2B^{KO} cells (**Table 5.5**). Gene fusions commonly occur in prostate cancers, with *TMPRSS2-ERG* one of the most widely studied (Navaei *et al*., 2017). Overexpression of TMPRSS2 has been known to increase gene fusion with *ERG*, resulting in prostate cancer development, consistent with the development of an invasive prostate cancer phenotype (Tomlins *et al*., 2008). Previous studies have found that overexpression of *AR* can initiate *TMPRSS2-ERG* gene fusion by inducing the proximity of *TMPRSS2* and *ERG* genomic loci, and in turn promoting a more invasive prostate cancer phenotype (Hermans *et al*., 2006; Zong *et al*., 2009). In prostate cancer cells where *FKBP5* is also overexpressed, as observed here in LNCaP^{KO} cells, *TMPRSS2-ERG* gene fusion is also present (Tomlins *et al.,* 2005; Yu *et al.,* 2010). However, data here suggests that *STEAP2* knockout reduces the invasive potential of both LNCaP and C4-2B cells,

despite a notable increase in *TMPRSS2* expression. As *TMPRSS2* is commonly known to undergo fusion to *ERG*, future work may involve further characterisation of this gene fusion in *STEAP2* knockout cells in order to provide a potential mechanism for *STEAP2* in the progression of prostate cancer.

GPRC6A is a nutrient sensing receptor that has been found to regulate prostate cancer growth and progression (Liu *et al*., 2016; Pi & Quarles, 2012). *GPRC6A* has been found to indirectly mediate the effects of *AR* in prostate cancer progression (Zarif & Miranti, 2016). Here, *GPRC6A* expression was not detected by qRT-PCR in either LNCaP^{KO} or C4-2B^{KO} cells, despite previously being upregulated in both cell lines in response to STEAP2 polyclonal antibody treatment (see **Chapter 4; Section 4.3.4**). In previous studies, overexpression of *GPRC6A* has been found to increase cell proliferation, whilst its knockdown has been reported to inhibit migration and invasion of prostate cancer cells (Liu *et al*., 2016; Pi & Quarles, 2012; Ye *et al*., 2017). Therefore, the lack of *GPRC6A* expression noted here may provide a mechanism for the observed reduction in aggressive prostate cancer traits, as *GPRC6A* knockdown has also been found to inhibit activation of ERK signalling, which, could provide a mechanism for the reduction in cell proliferation in response to *STEAP2* knockout (Wang *et al*., 2010; Ye *et al*., 2017). As *GPRC6A* is the only currently known receptor for osteocalcin, in future it would be interesting to monitor the expression levels of *GPRC6A* in *STEAP2* knockout cells grown as 3D co-cultured models, as generated in **Chapter 3**, to determine whether *GPRC6A* is involved in suppressing prostate cancer-bone stromal cell interactions (Suva *et al*., 2011; Pi *et al*., 2016; Ye *et al*., 2017).

MMPs -3, -7 and -10 have been reported to increase when S*TEAP2* is overexpressed (Burnell *et al*., 2018). Whilst these increases in MMP expression in prostate cancer have been suggested to promote cancer progression by the NFκB signalling pathway, inhibition of the NFκB pathway is also known to suppress *AR* transcription, indicating crosstalk mechanisms between *AR*, MMPs and NFκB (Chen *et al*., 2013; Harada *et al*., 2001; Nguyen

et al., 2014). This crosstalk between *AR* and NFκB signalling is thought to be the result of TNF-α binding to its cell surface receptor (TNFR), which results in the translocation of NFκB to the nucleus (Chopra *et al*., 2004; Rokhlin *et al*., 2005). In LNCaP cells, long-term exposure to TNF-α resulted in androgen hypersensitivity, yet no overall change in levels of total *AR*, as observed here in LNCaP^{KO} cells (Harada *et al*., 2001). *STEAP2* levels have been found to significantly increase by TNF-α induction in response to NFκB silencing, suggesting NFκB may provide a targeted pathway in the inhibition of prostate cancer progression via *STEAP2* knockout (Gonen-Korkmaz *et al*., 2014).

Upregulation of *PSA, FKBP5* and *TMPRSS2* in LNCaP^{KO} cells despite no significant increase in *AR* levels may suggest a potential *AR* bypass pathway and pro-survival mechanism for *STEAP2* knockout cells. It has previously been found that certain growth factors are able to crosstalk with the *AR* signalling pathway, resulting in an increase in the expression of *AR* target genes in the absence of androgens (Marques *et al*., 2010; Zhu *et al*., 2008). One of these is the aforementioned IL-6, which has also been found to promote androgen synthesis in prostate cancer cells through enhancing the transcription of aldo-keto reductase family-1 member-C3 (*AKR1C3*) which is involved in androgen biosynthesis (Chun *et al*., 2009). IL-6 has been found to play a vital role in the transition of hormone-dependent prostate cancers to castrate resistance, notably through the activation of AR (Nguyen *et al*., 2013). IL-6 is not naturally secreted by hormone-sensitive prostate cancer cell lines, such as LNCaP and C4-2B, and when exogenously expressed was found to inhibit growth in these cell lines, as observed in this Chapter (Nguyen *et al*., 2013; Okamoto *et al*., 1997). IL-6 therefore poses a potential mechanism for the overexpression of androgen regulated genes as observed in LNCaP^{KO} cells where levels of androgen itself remains unchanged, and therefore warrants further studies in the future.

Future studies should focus on exploring the mechanism underlying the role of *STEAP2* knockout in the increase in *PSA, FKBP5* and *TMPRSS2* expression yet unchanged *AR* expression, that were observed in LNCaP^{KO}

cells. In prostate cancer cells with low levels of *AR* expression, cells have been found to carry the T877A *AR* mutation, which allows for a bypass of the *AR* signalling pathway, yet cells may continue to overexpress *AR*-regulated genes, which may account for the increase in *PSA, FKBP5* and *TMPRSS2* levels exhibited by LNCaP^{KO} cells (Marques *et al*., 2010). It may also be of interest to explore the effects of inhibitors of androgen and its target genes on *STEAP2* knockout cell survival, to determine whether *STEAP2* has the potential to be administered in combination therapy.

5.5 Conclusion

The data generated in this chapter provides strong evidence that *STEAP2* could potentially be a viable therapeutic target in the treatment of prostate cancer for future clinical translation. CRISPR/Cas9 targeted *STEAP2* knockout resulted in a promising decrease in several aggressive prostate cancer traits, suppressing cell proliferation, migration and invasion. Gene expression analysis of *AR* and its regulated genes found that *STEAP2* knockout initiates an increase in expression of key genes in the progression of prostate cancer, despite *STEAP2* knockout inhibiting cell proliferation, migration and invasion; however, the mechanisms behind this remain unclear. Therefore, targeting *STEAP2* in androgen-sensitive prostate cancer cells may warrant further investigations into combination therapy along with pre-existing androgen therapy approaches. The involvement of androgens in *STEAP2* expression also warrants further studies, such as how *STEAP2* levels are affected when androgen is depleted. Overall, the data presented in this chapter provides further evidence that *STEAP2* presents a novel therapeutic target in the treatment of prostate cancer.

Chapter 6

The impact of androgen depletion on aggressive prostate cancer traits and androgen-regulated genes

6.1 Introduction

Prostate cancer is largely an androgen regulated disease, and therefore many studies have explored how expression of *AR* is linked to disease progression (see **Chapter 1, Section 1.8**; Gonen-Korkmaz *et al*., 2014; Myung *et al*., 2013; Tanner *et al*., 2011). Prostate cancer cell lines are often characterised as being androgen-sensitive, which applies to LNCaP and C4-2B cells, or androgen-independent, including PC3 and DU145 cells (Chlenski *et al*., 2001; Guo *et al*., 2006; Traish *et al*., 2009).

Androgen ablation remains the most common primary therapy in men with both locally advanced and metastatic prostate cancer (Fong *et al*., 2014; Harris *et al*., 2009). However, approximately 20% of men display treatment resistance due to the development of androgen-independent clones which promptly become fatal due to an increased invasive potential and more rapid disease progression (Crawford *et al*., 2017; Nyquist *et al*., 2013). Clinically, once tumours become resistant to ADT, CRPC develops, the drivers of which are currently undetermined (Crawford *et al*., 2017; Qin *et al*., 2014). One of the major challenges in these resistant prostate cancers is understanding the molecular pathways that are androgen-regulated, and determining specific biomarkers linked to castrate resistance (Pfeil *et al*., 2004; Karantanos *et al*., 2015).

AR, a member of the steroid hormone receptor family, binds to specific DNA sequences and in doing so mediates the physiological effects of androgens, producing AREs (Davey & Grossman, 2016; Heinlein & Chang, 2004). AREs are involved in regulating the transcription of androgen-responsive genes

(Heinlein & Chang, 2004). Prostate growth and function are modulated by androgens through the metabolism of testosterone into 5-alpha-dihydrotestosterone (5α-DHT) by the enzyme 5α reductase (Heinlein & Chang, 2004; Traish *et al*., 2009). Interactions between AREs and the AR hormone complex result in molecular activation and transformation of the ligand-bound AR complex (see **Chapter 1, Section 1.8, Figure 1.6**; Davey & Grossman, 2016; Heinlein & Chang, 2004; Traish *et al*., 2009).

AR is also known to affect the expression of a variety of genes also linked to the progression of prostate cancer, including but not limited to *PSA*, *FKBP5*, *TMPRSS2*, and *GPRC6A* (Velasco *et al*., 2004; Wright *et al*., 2003; Zarif & Miranti, 2016). Knowledge of a link between STEAP2 and androgen dependence is currently limited, and as such this present chapter will explore the effect of androgen depletion on *STEAP2* expression, and the expression of the androgen-regulated genes *PSA, FKBP5, GPRC6A* and *TMPRSS2* (Gomes *et al*., 2012).

Standard culture conditions of prostate cancer cell lines use culture medium that is supplemented with FBS, which contains testosterone and provides the cells with androgens (Cao *et al.,* 2009; Fiandalo *et al*., 2018; Sikora *et al.*, 2016). To deprive cells of androgens, media supplemented with androgen-free serum, such as that which has been stripped of androgens using charcoal to create charcoal-stripped serum (CSS), is often used (Fiandalo *et al*., 2018; Sedelaar *et al*., 2009). One of the drawbacks of using CSS is that composition can vary batch-to-batch, which can subsequently impact upon the reproducibility of experiments (Sikora *et al*., 2016). SFM may therefore provide an alternative to CSS supplemented media, yet studies have shown no variation between the viability and responsiveness of cells grown in SFM compared to cells grown in CSS (Fiandalo *et al*., 2018). Charcoal-stripped dextran-treated (CDT) FBS has also been used to deprive cells of androgens, however, has been reported to significantly alter the behaviour, particularly the adherence, of prostate cancer cells and subsequently produce erroneous results (Song & Khera *et al*., 2014). CDT is best used in experiments involving the study of AR ligands, whereas CSS provides the optimal conditions for

assessing cell behavioural patterns in response to androgen depletion (Fiandalo *et al*., 2018; Song & Khera *et al*., 2014). Androgen inhibition can also be targeted with drugs, the most commonly used being the hormone therapeutic agent enzalutamide which blocks translocation of AR to the nucleus by competitively binding with the testosterone / DHT receptor on AR (Scher *et al*., 2012). In this chapter, androgen depletion was achieved through cell culture in CSS-supplemented phenol-red free medium to allow gene expression and functional cellular changes to be assessed.

Given that a link between *STEAP2* and *AR*-dependent growth has not previously been explored, the aims of this Chapter were to identify if androgen depletion by growth in CSS could reduce aggressive prostate cancer traits, and in turn effect the expression of genes known to impact upon prostate cancer progression. To achieve this aim, the Chapter was therefore divided into the following objectives:

1. To evaluate the impact of androgen depletion on cell viability, proliferation, migration and invasion in androgen-sensitive and androgen-independent prostate cancer cells
2. To evaluate the impact of androgen depletion on the expression of *STEAP2* and the androgen regulated genes *PSA, FKBP5, TMPRSS2* and *GPRC6A* in androgen-sensitive and androgen-independent prostate cancer cells.
3. To evaluate the impact of androgen depletion on cell viability and proliferation in STEAP2 knockout androgen-sensitive prostate cancer cells

6.2 Materials and methods

6.2.1 Cell culture

The prostate cancer cell lines PC3, LNCaP and C4-2B used in this chapter are described in **Chapter 2, Section 2.2.1, 2.2.2 & 2.7.4** and were routinely cultured and maintained as described in **Chapter 2, Section 2.2.7.1.** STEAP2-knockout LNCaP and C4-2B cells were generated as described in **Chapter 5, Section 5.2.3**. LNCaP^{KO} and C4-2B^{KO} cells were maintained in puromycin-supplemented RPMI and DMEM media respectively, as described in **Chapter 5, Section 5.2.4.8.**

6.2.2 Androgen depleted conditions

To strip cells of androgens and other growth hormones present in normal cell culture media, CSS (Sigma Aldrich, US, Cat. F6765) was used, as described in **Chapter 2, Section 2.2.6**. Phenol-red free RPMI-1640 (Life Technologies, UK, Cat. 31870025) was supplemented with 10% CSS, 1% L-glutamine and 1% P/S for the growth of LNCaP cells. Phenol-red free DMEM (Life Technologies UK, Cat. 21063029) was supplemented with 10% CSS and 1% P/S for the growth of C4-2B cells. To achieve androgen depletion, cells were first thawed following cryopreservation (see **Chapter 2, Section 2.2.1.5**) and centrifuged at 270 g for 5 minutes using a bench-top centrifuge (VWR, Himac CT6E, UK). Cryopreservation media was discarded, and the cell pellet resuspended in cell line appropriate media supplemented with CSS. Cells were sub-cultured as normal following the supplier's recommendations as detailed in **Section 2.1.5** for a minimum of three passages before being used for various assays.

6.2.3 Assays to study the effect of androgen depletion on aggressive cancer traits

6.2.3.1 Cell viability quantification

Cell suspensions of desired cell numbers were prepared as described in **Chapter 2, Section 2.2.7.2** and seeded in 100 μl culture media in 96-well tissue culture plates. Cells were cultured in either 10% FBS-supplemented media or 10% CSS-supplemented media as described in **Section 6.2.2**. Every 24 h for 5 days, cell viability was assessed by the MTT assay as described in **Chapter 2, Section 2.4.1**. The alamarBlue assay was also used to assess cell viability as described in **Chapter 2, Section 2.4.2** in the STEAP2-knockout cells generated in **Chapter 5**. The cell viability assay was performed in triplicate unless otherwise stated.

6.2.3.2 Cell proliferation

Cell suspensions of desired cell numbers were prepared as described in **Chapter 2, Section 2.2.7.2** and seeded in 100 μl culture media in 96-well tissue culture plates. Cells were cultured in either 10% FBS-supplemented media or 10% CSS-supplemented media as described in **Section 6.2.2**. Every 24 h, proliferation was assessed by the alamarBlue assay as described in **Chapter 2, Section 2.5.1**. Proliferation of cells grown in androgen-depleted media were compared to that of cells grown in androgen-positive conditions. The cell proliferation assay was conducted in triplicate unless otherwise stated.

6.2.3.3 Cell migration assay

Migration assays were carried out as described in **Chapter 2, Section 2.9**. After PC3, C4-2B and LNCaP cells had reached ~80% confluency, medium was replaced for 24 h with serum-free, phenol-red free RPMI-1640 (PC3 and LNCaP) or serum-free, phenol-red free DMEM (C4-2B) medium. Cells were trypsinised, resuspended and adjusted to a desired cell concentration, as described in **Chapter 2, Section 2.2.7.2**. One cell culture insert (IBIDI, Germany, Cat. 80209) was placed in the centre of a well of a 12-well plate,

and 70 μl cell suspension was added per chamber. Cells were left to adhere for 24 h in standard tissue culture conditions. Media and inserts were removed, and cells were washed with PBS to remove cell debris, before fresh media was applied, supplemented with either 10% FBS to represent AR-positive (+ve) or androgen replete conditions, or 10% CSS to represent AR-negative (-ve) conditions or androgen deplete conditions. The time taken to close the gap created was monitored using an inverted light microscope (AxioCam ERC55, Zeiss, Germany) every 24 h for 5 days. Media was replaced every 3 days. The migration assay was conducted in triplicate unless otherwise stated.

6.2.3.4 Invasion assay

Invasion assays were carried out as described in **Chapter 2, Section 2.10**. To investigate the role androgen depletion plays in mediating invasive cell behaviour, prior to the addition of cells to the Matrigel coated Transwell insert, 600 μl of media containing either 10% FBS (AR +ve) or 10% CSS (AR -ve) was added to the lower chamber. Cells were incubated for 48 h in standard cell culture conditions to allow for cell invasion to occur. Cell invasion was quantified through staining with crystal violet, as described in **Chapter 2, Section 2.10**. Invaded cells were visualised using a standard light microscope at 10x magnification (AxioCam ERC55, Zeiss, Germany Images were taken of different planes of each insert and the invasion assay was conducted in triplicate unless otherwise stated.

6.2.4 Detection of STEAP2 gene and protein expression in androgen-depleted cells

6.2.4.1 Detection of *STEAP2* gene expression in androgen-depleted cells

PC3, LNCaP and C4-2B cells were cultured to ~70% confluency in media supplemented with either 10% FBS (AR +ve conditions) or 10% CSS (AR -ve conditions). RNA was extracted, cDNA synthesised, and qRT-PCR performed as described in **Chapter 2, Section 2.3**. Cells were probed for the detection of *STEAP2*, with *GAPDH* as the housekeeping control, using the primers

detailed in **Chapter 2, Section 2.3.3, Table 2.8.** The results were subsequently analysed as described in **Chapter 2, Section 2.3.4.**

6.2.4.2 Detection of STEAP2 protein expression in androgen-depleted cells

6.2.4.2.1 Protein extraction and quantification

Protein was extracted from PC3, LNCaP and C4-2B cells as described in **Chapter 2, Section 2.8.1,** following culture in media supplemented with either 10% FBS (AR +ve conditions) or 10% CSS (AR -ve conditions). Protein quantification was carried out using a Bradford assay for protein quantification as described in **Chapter 2, Section 2.8.2.**

6.2.4.2.2 Blocking and antibody incubations

Western blotting for STEAP2 detection was conducted as described in **Chapter 2, Section 2.8 and Chapter 5, Section 5.2.5.**

6.2.4.2.3 Protein detection analysis

Images were acquired and analysed as described in **Chapter 2, Section 2.8.7.**

6.2.5 Detection of androgen-regulated genes in androgen-depleted cells

PC3, LNCaP and C4-2B cells were cultured to ~70% confluency in media supplemented with either 10% FBS (AR +ve conditions) or 10% CSS (AR -ve conditions). RNA was extracted, cDNA synthesised, and qRT-PCR performed as described in **Chapter 2, Section 2.3**. Cells were probed for the detection of the androgen-regulated genes; *PSA*, *FKBP5*, *TMPRSS2* and *GPRC6A*, with *GAPDH* as the housekeeping control, using the primers detailed in **Chapter 2, Section 2.3.3, Table 2.8.** The results were subsequently analysed as described in **Chapter 2, Section 2.3.4.**

6.2.6 Statistical analysis

Statistical analysis was performed using GraphPad Prism version 8 for iOS. The one-way ANOVA *post-hoc* Dunnett test and an unpaired t-test were used, as detailed in each figure. Data was considered statistically significant when a p-value of < 0.05 (*), p-value < 0.01 (**) or a p-value of < 0.001 (***) or p-value < 0.0001 (****) was obtained, which were annotated within the respective figures.

6.3 Results

The focus of this Chapter was to determine the effects of androgen-depletion on aggressive prostate cancer traits. This aim was addressed by evaluating the following properties of androgen-depleted PC3, LNCaP and C4-2B cells, in comparison to their androgen-replete counterparts; cell viability, proliferation, migration and invasion. Following this, the next objective within this Chapter was to determine whether androgen-depletion influenced *STEAP2* gene and protein expression in androgen-depleted PC3, LNCaP and C4-2B cells, in comparison to their androgen-replete counterparts, which was assessed through qRT-PCR and Western blots. Additionally, to determine whether androgen-depletion influenced the expression of the androgen-associated genes *PSA, FKBP5, TMPRSS2* and *GPRC6A,* their transcriptional levels were assessed by qRT-PCR analysis in PC3, LNCaP and C4-2B cells. Finally, cell viability and proliferation assays were used to determine whether androgen-depletion impacted STEAP2-knockout LNCaP and C4-2B cells.

6.3.1 Androgen depletion reduces the viability of LNCaP and C4-2B cells over time

To evaluate the effect of androgen depletion on cell viability over time, the MTT cell viability assay was used. MTT response was used to assess the metabolic activity of the cells, with MTT absorbance values proportionate to the number of viable cells present. To determine the difference in the number of cells capable of metabolising MTT over time, MTT absorbance values were compared to those of cells on day 1 for each cell line and growth condition.

The MTT assay revealed that the absorbance of androgen-sensitive prostate cancer cell lines LNCaP and C4-2B remained consistent over time when grown in CSS supplemented media (AR-), whilst that of their counterparts grown in FBS-supplemented media (AR+) significantly increased. On day 5, AR+ LNCaP cells showed a significant increase in MTT absorbance (+0.67 nm, $p < 0.0001$; **Figure 6.1B**), whilst there was no significant difference in the MTT absorbance of AR- LNCaP cells (+0.247 nm; **Figure 6.1B**). AR+ C4-2B cells showed a significant increase in MTT absorbance (+0.728 nm, p <

0.0001; **Figure 6.1C**) on day 5, whilst the AR- C4-2B cells showed no significant change at this time point (-0.011 nm; **Figure 6.1C**). AR+ PC3 cells and AR- PC3 cells showed similar changes in viability over time as shown by an increase in MTT absorbance of +0.292 nm and +0.204 nm on day 5 respectively ($p < 0.001$; **Figure 6.1A**). Based on these data, it can be suggested that growth under androgen depleted conditions reduces the capability of androgen-sensitive prostate cancer cell lines to metabolise MTT in comparison to growth under normal conditions. The MTT response of androgen-sensitive prostate cancer cell lines LNCaP and C4-2B was much more pronounced than that of the androgen-independent cell line PC3, suggesting that the availability of androgens in the growth medium significantly impacts upon the viability of cells sensitive to androgen.

6.3.2 Androgen depletion reduces the proliferation of PC3, LNCaP and C4-2B cells over time

To evaluate the effect of androgen depletion on the percentage of proliferating cells over time, the alamarBlue cell proliferation assay was used. To determine the difference in the percentage of proliferating cells over time, cells were normalised to cells on day 1 for each cell line and growth conditions.

The alamarBlue cell proliferation assay revealed a significant increase in the percentage of proliferating cells all three cell lines; PC3, LNCaP and C4-2B over time when grown in FBS-supplemented media (AR+) and CSS-supplemented media (AR-). On day 5, AR+ PC3 cells showed an increase in the percentage of proliferating cells (+64.8%, $p < 0.0001$; **Figure 6.2A**), whilst AR- PC3 cells showed a higher increase in the percentage of proliferating cells than their AR+ counterparts (+98.8%, $p < 0.05$; **Figure 6.2A**). Similarly, on day 5, AR+ C4-2B cells showed an increase in the percentage of proliferating cells (+58.7%, $p < 0.0001$; **Figure 6.2C**), whilst their AR- counterparts showed a higher increase in the percentage of proliferating cells (+125.4%, $p < 0.05$; **Figure 6.2C**). In AR- LNCaP cells, the percentage of proliferating cells was also increased by day 5 (+101.3%, $p < 0.0001$; **Figure 6.2B**) yet was lower than their AR+ counterparts (+207.9%, $p < 0.05$; **Figure 6.2B**). Based on these data, it can be suggested that androgen depletion has little effect on the

proliferative capacity of prostate cancer cell lines over time when compared to growth under normal conditions.

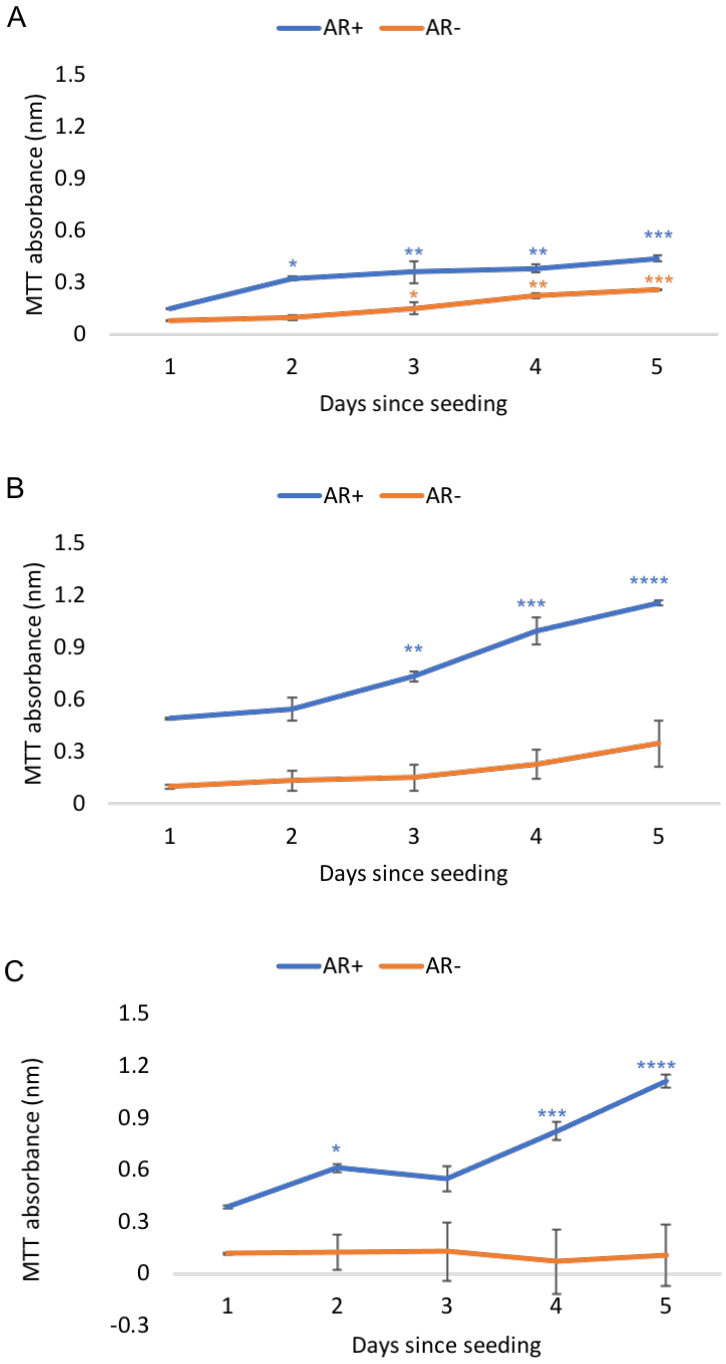

Figure 6.1. Effect of growth in charcoal stripped FBS on MTT absorbance. PC3 (A), LNCaP (B) and C4-2B (C) prostate cancer cells were grown in either FBS-supplemented media (AR+) or CSS-supplemented media (AR-). Every 24 h, cell viability was assessed by MTT assay. An ANOVA post-hoc Dunnett test was performed for statistical analysis comparing MTT absorbance on each day after seeding to cells on day 1. Error bars denote S.E.M. p-value < 0.05 (*), p-value < 0.01 (**), p-value < 0.001 (***), p-value < 0.0001 (****) (N = 3).

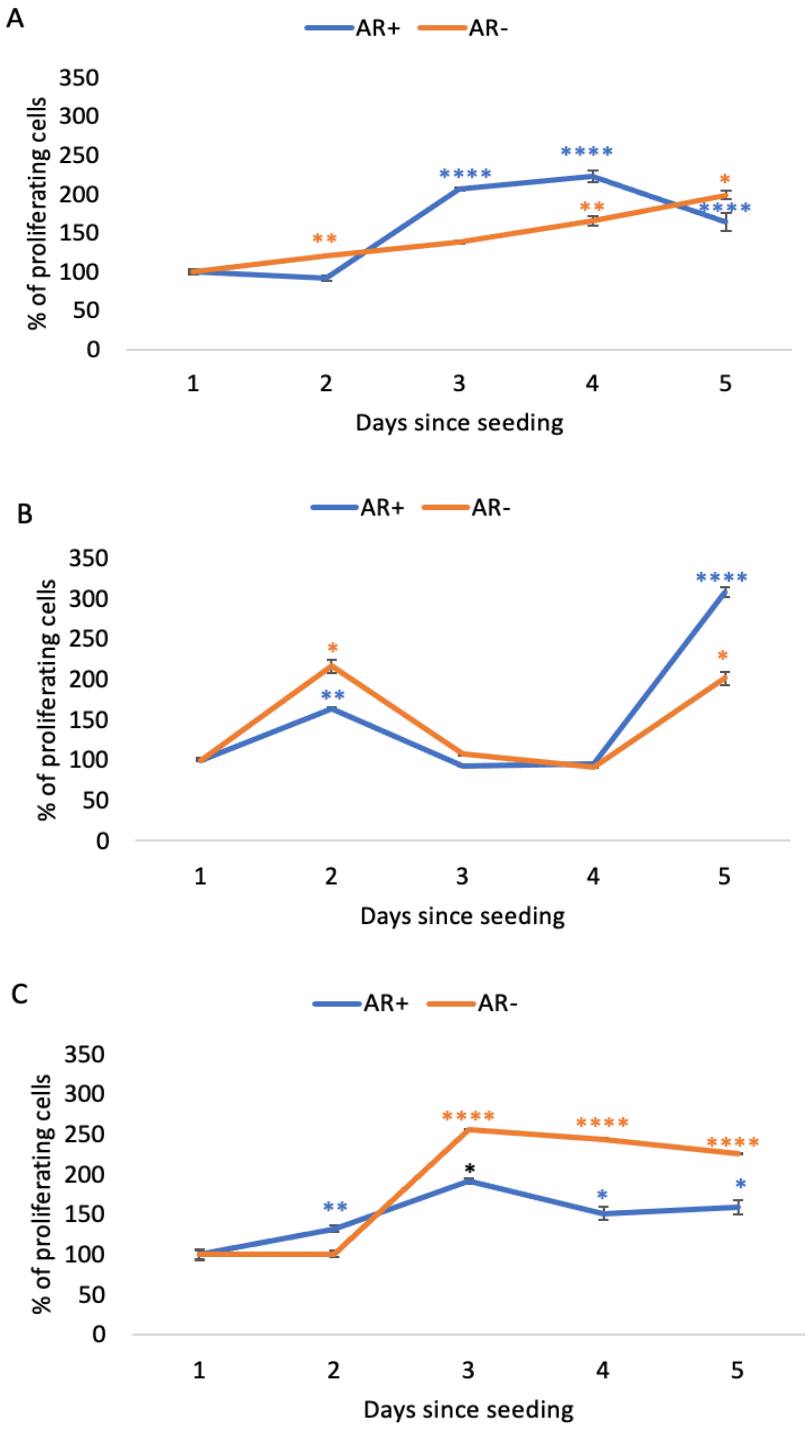

Figure 6.2. Effect of growth in charcoal stripped FBS on cell proliferation. PC3 (A), LNCaP (B) and C4-2B (C) prostate cancer cells were grown in either FBS-supplemented media (AR+) or CSS-supplemented media (AR-). Every 24 h, cell proliferation was assessed by alamarBlue assay. An ANOVA post-hoc Dunnett test was performed for statistical analysis comparing the proliferation rate of cells each day after seeding with that of cells on day 1. Error bars denote S.E.M. p-value < 0.05 (*), p-value < 0.01 (**), p-value < 0.001 (***), p-value < 0.0001 (****) (N = 3).

6.3.3 Androgen depletion inhibits cell migration in PC3, LNCaP and C4-2B prostate cancer cells

To further evaluate the potential of androgen depletion on reducing aggressive characteristics of PC3, LNCaP and C4-2B cells, the cell migration assay was carried out. To do so, cells were cultured in separate chambers of a silicone tissue culture plate insert. The insert was removed after 24 h and cells were imaged every 24 h for 5 days.

In all three cell lines, the wound gap was completely closed in cells grown in FBS-supplemented media (AR+) by day 5 (**Figure 6.3A, 6.3C & 6.3E**). Androgen-depletion through growth in CSS-supplemented media (AR-) had completely inhibited migration of LNCaP and C4-2B cells as the wound gap remained fully open by day 5 (**Figure 6.3D & 6.3F**). Cell migration was somewhat inhibited in PC3 cells as shown by the partial closing of the wound gap by day 5 (**Figure 6.3B**). These data suggest that androgen-depletion leads to a complete inhibition of the migratory capacity of the androgen-sensitive prostate cancer cell lines LNCaP and C4-2B, and partially inhibits the migratory capacity of androgen-independent PC3 cells (**Figure 6.3**; where representative images are shown; additional images from the second replicate can be found in **Appendix 4, Figure A4.1**).

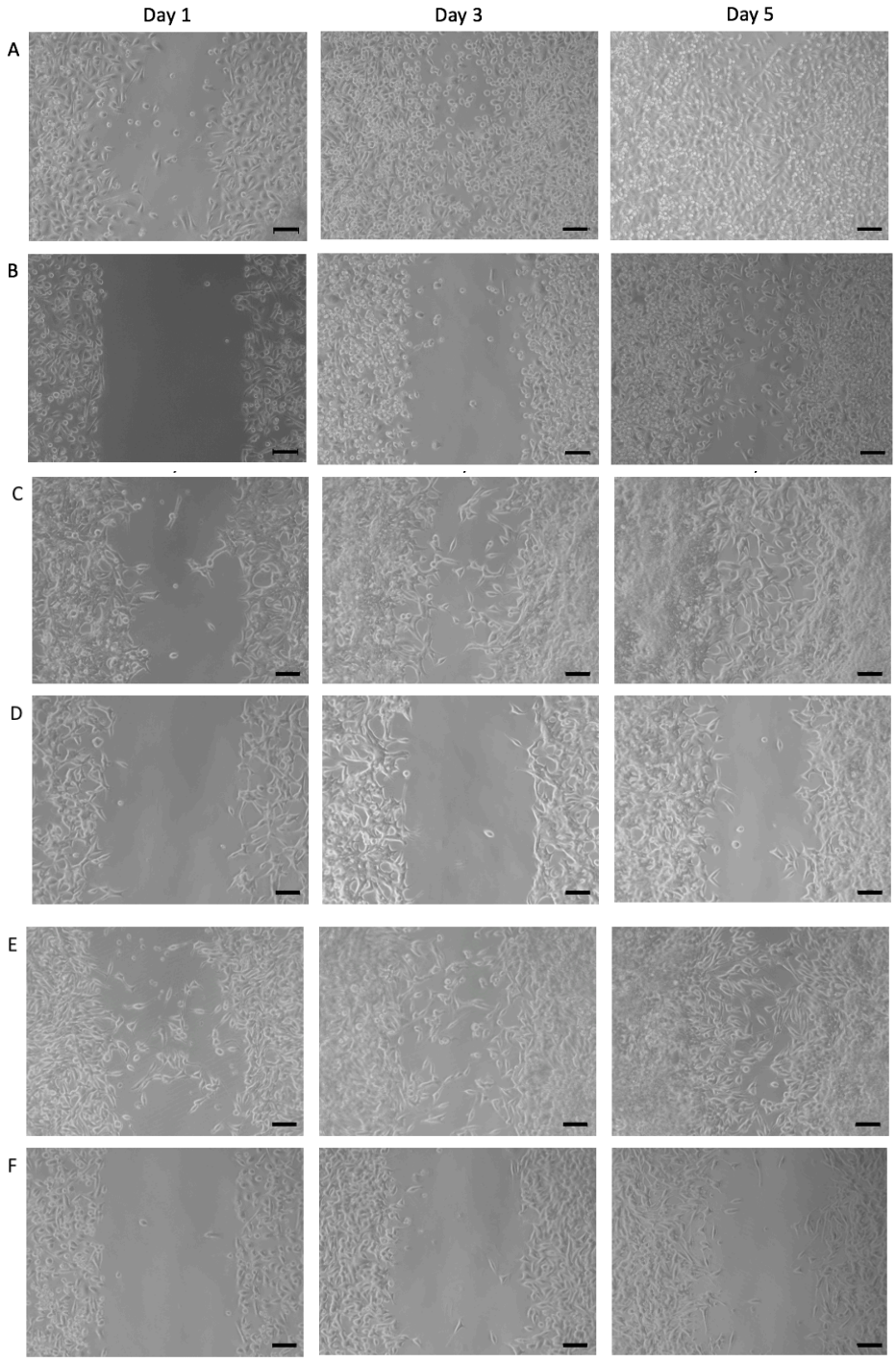

Figure 6.3. Androgen depletion by charcoal stripped FBS decreases the migratory potential of PC3, LNCaP and C4-2B cells. Time points at which the images were taken: 0 days, 3 days and 5 days. PC3 (A), LNCaP (C) and C4-2B (E) cells cultured in FBS-supplemented media (AR+). Androgen depleted PC3 (B), LNCaP (D) and C4-2B (F) cells were cultured in CSS-supplemented media (AR-). Images were acquired using an inverted light microscope with a 10x objective (AxioCam ERC55, Zeiss, Germany). Scale bar = 50 μm. (Illustrated are representative images; the experiment was however conducted in triplicate with biological replicates, N = 3).

6.3.4 Androgen depletion reduces cell invasion in PC3, LNCaP and C4-2B prostate cancer cells

The cell invasion assay was performed to evaluate whether androgen depletion by growth of cells in CSS had an effect on inhibiting prostate cancer cell invasion. To do so, the bottom of a culture plate-insert was coated with Matrigel (as per manufacturer's instructions), and to stimulate the ability of cancer cells to invade through this ECM, FBS and CSS served as chemoattractants. Cells were grown in the top layer of the insert, and as such only those with invasive potential were capable of crossing the Matrigel barrier.

The results illustrated in **Figure 6.4** (where representative images are shown; additional images from the second replicate can be found in **Appendix 4, Figure A4.2**). demonstrate that the invasive potential of LNCaP and C4-2B cells is significantly inhibited when cultured in androgen depleted conditions. When compared to cells grown in FBS-supplemented media, 35.4% of androgen depleted PC3 cells invaded through the ECM (**$p < 0.01$; Figure 6.4G**). In androgen-sensitive cells, invasion was lower with 18.9% of LNCaP cells and 7.4% of C4-2B cells invading through the ECM ($p < 0.001$; **Figure 6.4G**). These data, along with the results presented in **Sections 6.3.1 & 6.3.3**, suggest that androgen depletion substantially reduces aggressive cancer traits most predominantly in the androgen-sensitive cells, LNCaP and C4-2B.

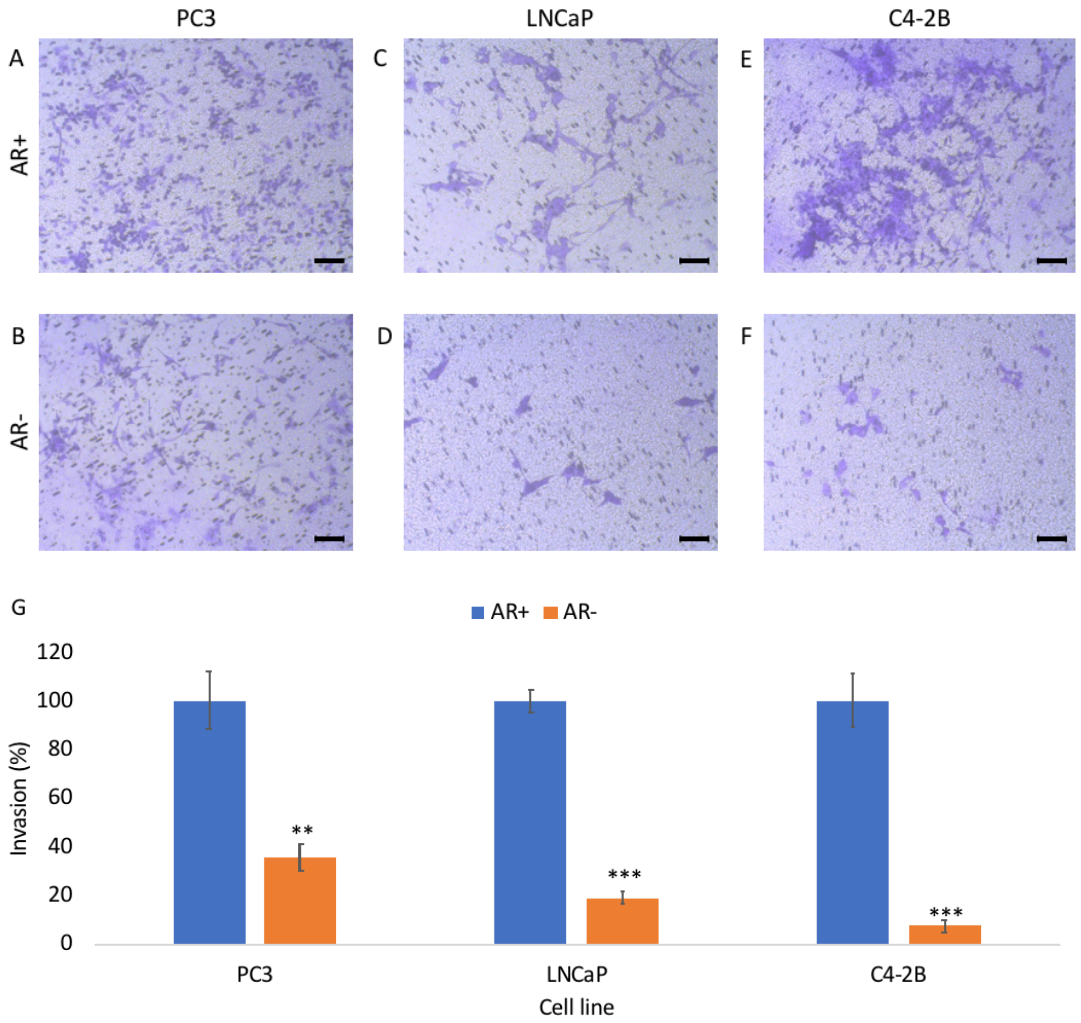

Figure 6.4. Androgen depletion reduces the invasive potential of PC3, LNCaP and C4-2B cells. Images of stained cells were taken to give a visual representation of invasion. PC3 (A), LNCaP (C) and C4-2B (E) cells cultured in FBS-supplemented media (AR+). Androgen depleted PC3 (B), LNCaP (D) and C4-2B (F) cells were cultured in CSS-supplemented media (AR-). Each panel represents A) PC3 AR+, B) PC3 AR- C) LNCaP AR+ D) LNCaP AR-, E) C4-2B AR+ and F) C4-2B AR-. AR+ cells show invasive potential. Invaded cells were stained with crystal violet and images were taken 48 h after seeding. G) The number of stained cells that had invaded through the Transwell insert were counted and calculated as a percentage of the AR+ control for each cell line. An unpaired t-test was performed for statistical analysis. Error bars denote S.E.M. p-value < 0.05 (*), p-value < 0.01 (**), p-value < 0.001 (***), p-value < 0.0001 (****). Images were taken with an inverted light microscope at a 10x objective (AxioCam ERC55, Zeiss, Germany). Scale bar = 50 μm. (Illustrated are representative images; the experiment was however conducted in triplicate with biological replicates, N = 3).

6.3.5 The impact of androgen depletion on the expression of STEAP2 in PC3, LNCaP and C4-2B prostate cancer cells

6.3.5.1 Androgen depletion increases *STEAP2* expression in androgen-sensitive prostate cancer cells

LNCaP and C4-2B are both androgen-sensitive prostate cancer cell lines. Following the results of **Chapter 4, Section 4.3.3** which found that *AR* gene expression increased in response to STEAP2 polyclonal antibody treatment, this chapter explores AR expression in response to STEAP2 knockout by qRT-PCR.

No significant change in *STEAP2* expression was observed in androgen-depleted PC3 cells (0.96-fold; **Figure 6.5A**). However, in contrast, *STEAP2* was found to be highly and significantly overexpressed in both LNCaP and C4-2B androgen-depleted cells, which exhibited 98.0- and 13.2-fold increases in expression respectively ($p \leq 0.01$; **Figure 6.5A**). When STEAP2 protein expression was observed by Western blot analysis, STEAP2 was found to be elevated in both C4-2B and LNCaP androgen-depleted cells yet remained unchanged in androgen-depleted PC3 cells (**Figure 6.5B**).

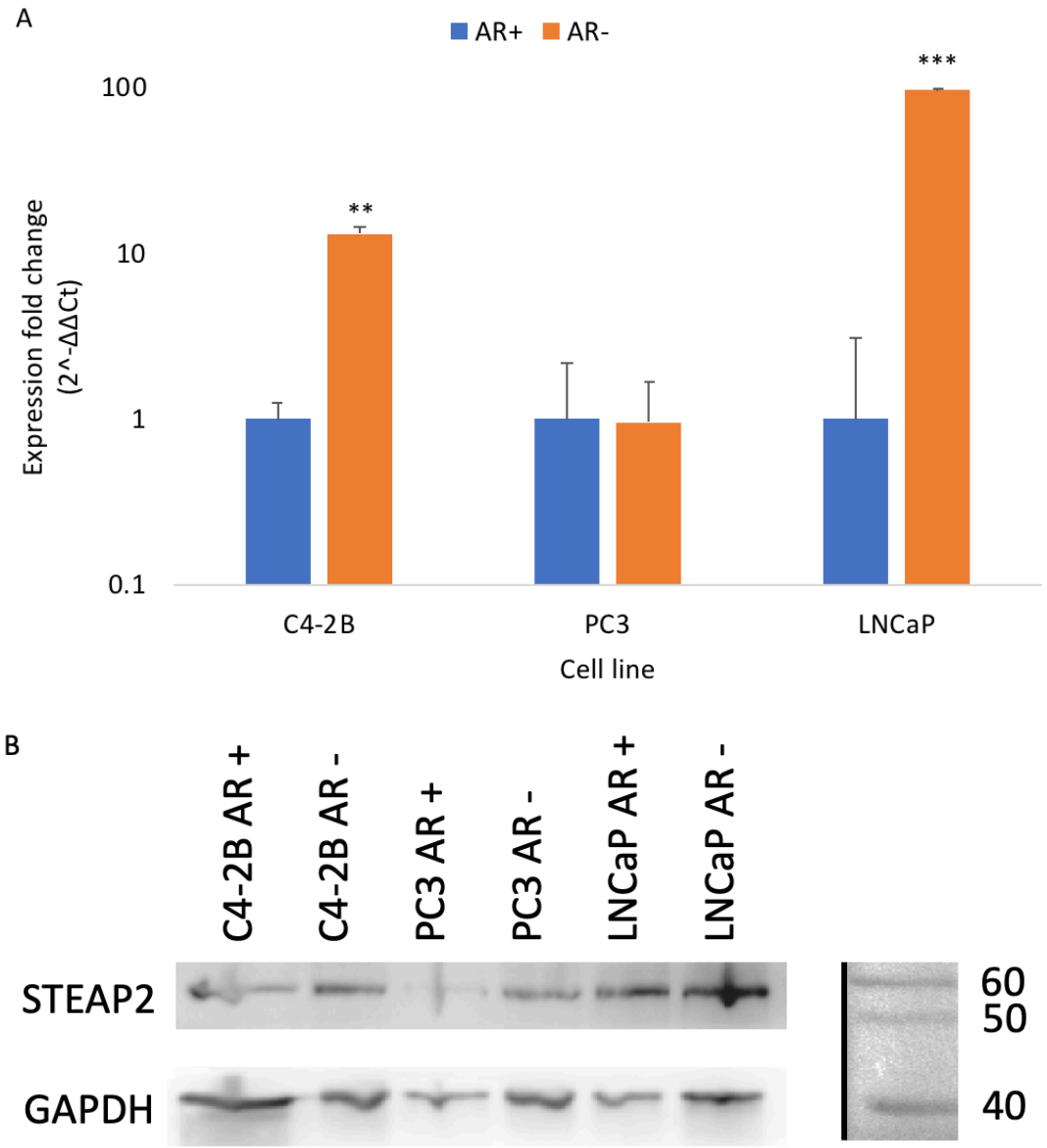

Figure 6.5. Growth of cells in charcoal stripped FBS alters STEAP2 gene and protein expression in androgen sensitive cells. Changes in STEAP2 gene expression (A) and protein expression (B) in prostate cancer cell lines grown in castrate-resistant conditions as compared to normal conditions, analysed by RT-PCR and Western blot respectively. An ANOVA post-hoc Dunnett test was performed for statistical analysis. Error bars denote S.E.M. p-value < 0.01 (**), p-value < 0.001 (***), p-value < 0.0001 (****) (N = 3). Western blot image shows STEAP2 expression in protein lysates from AR-replete and AR-deprived cells. STEAP2: approx. 56 kDa; GAPDH: approx. 37 kDa. (Loading control = GAPDH, Black lines represent where the western blot image has been edited for clarity).

6.3.6 Androgen depletion increases the expression of genes involved in prostate cancer progression

Section 5.3.4.1 demonstrated that AR is significantly overexpressed in C4-2B cells but not in LNCaP cells, following STEAP2 knockout. **Chapter 4, Section 4.3.4** found that the expression of three out of four genes known to influence *AR* expression – *PSA, FKBP5* and *TMPRSS2* – increased in response to STEAP2 polyclonal antibody treatment in both LNCaP and C4-2B cells, whilst *GPRC6A* expression was undetected. Following these results, the gene expression of the same four *AR*-regulated genes were quantified in response to androgen depletion by qRT-PCR in PC3, LNCaP and C4-2B cells. Cells grown under standard conditions were used for comparison.

Upon analysis of gene expression of the four AR regulated genes, all four genes were found to be significantly overexpressed in all three androgen-depleted prostate cancer cell lines. The highest increase was observed in *TMPRSS2* expression, which was found to be overexpressed by 43.9-, 12.2- and 9946.8-fold in androgen-depleted PC3, LNCaP and C4-2B cells respectively, ($p \leq 0.01$; **Figures 6.6A, 6.6B & 6.6C**). The highest expression of the three other genes was observed in androgen-depleted C4-2B cells, which exhibited increases of 112.1-, 96.3- and 83.2-fold in *PSA*, *FKBP5* and *GPRC6A* expression respectively ($p \leq 0.01$; **Figure 6.6C**). qRT-PCR analysis therefore demonstrated that androgen regulated genes are highly expressed in androgen depleted prostate cancer cell lines and thus, could warrant further investigations into the mechanisms of androgen-regulated prostate cancer progression.

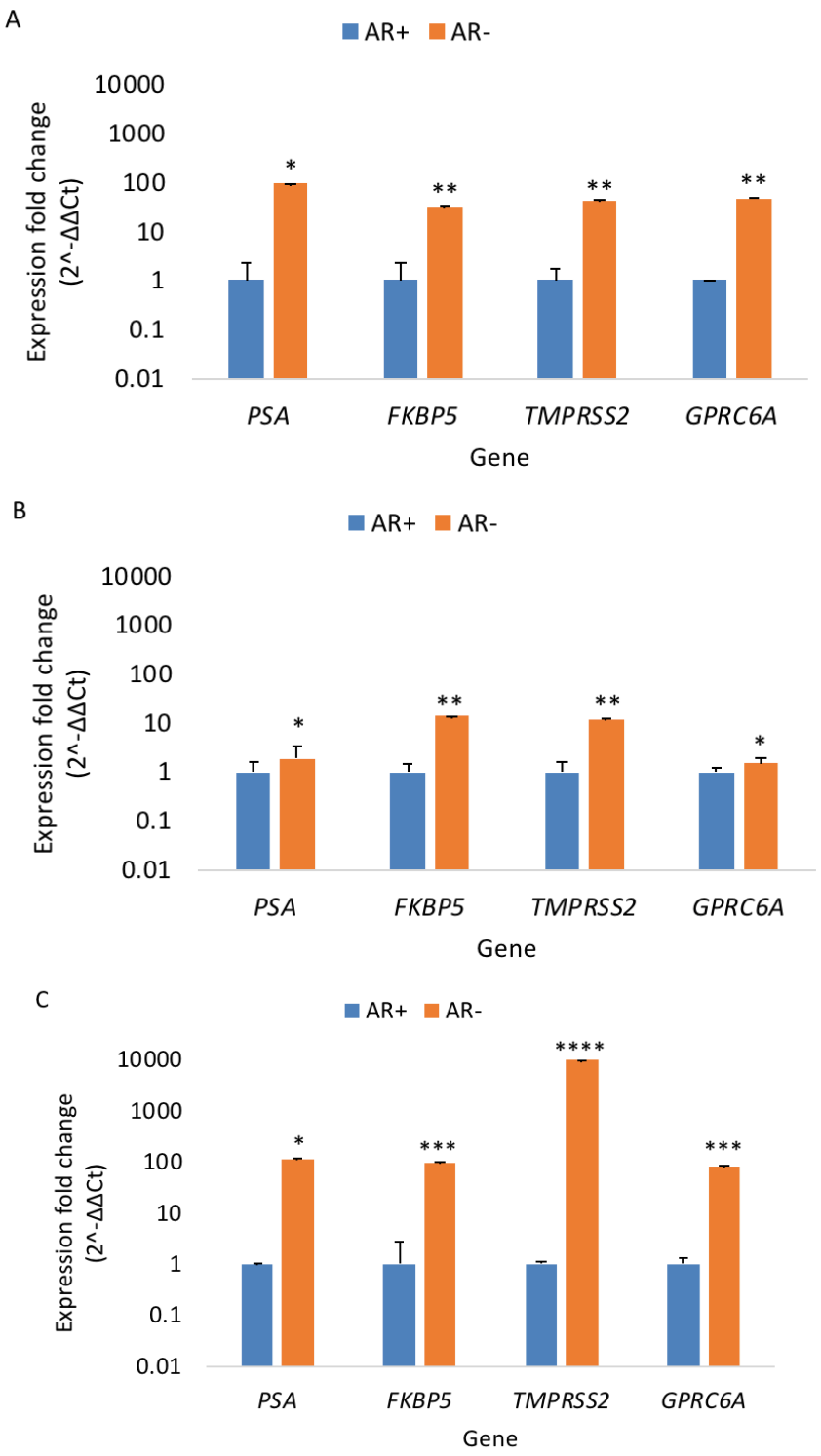

Figure 6.6. Androgen depletion increases the expression of genes regulated by *AR*. Fold changes in the gene expression of *PSA*, *FKBP5*, *TMPRSS2* and *GPRC6A* in PC3 (A), LNCaP (B) and C4-2B (C) cells grown in CSS (AR-), as compared to cells grown in FBS (AR+). An ANOVA post-hoc Dunnett test was performed for statistical analysis. GAPDH was used as the housekeeping gene. Error bars denote S.E.M. p-value < 0.05 (*), p-value < 0.01 (**), p-value < 0.001 (***), p-value < 0.0001 (****) (N = 3).

6.3.7 Androgen depletion decreases the viability and proliferation of STEAP2-knockout prostate cancer cells

To assess the impact of androgen depletion on the percentage of viable and proliferating *STEAP2* knockout C4-2B and LNCaP cells generated in **Chapter 5**, the alamarBlue assay was used. alamarBlue has the ability to be used as both a marker of cell viability and proliferation as it measures a cell's ability to metabolise resazurin to resorufin yet relies upon different manipulations of the molar extinction coefficients (E) for alamarBlue (see **Chapter 2, Sections 2.4.2 & 2.5.1**). Both the percentages of viable and proliferating cells were normalised to cells on day 1 to determine the difference over time.

The percentage of viable cells was significantly reduced in both *STEAP2*-knockout cell lines when grown in media supplemented with CSS. The percentage of viable LNCaP^{KO} cells was consistently and significantly reduced across all 3 days and was lowest on day 3 (-85%, $p < 0.05$; **Figure 6.7A**). In C4-2B^{KO} cells, the percentage of viable cellswas also significantly reduced on all 3 days (-44%, -46% and -62% respectively, $p \leq 0.01$; **Figure 6.7B**).

The percentage of proliferating cells was significantly reduced in both *STEAP2*-knockout cell lines when grown in media supplemented with CSS. Proliferative capacity was significantly reduced in LNCaP^{KO} cells on all 3 days (-88%, -87% and -89% respectively, $p < 0.0001$; **Figure 6.8A**). In C4-2B^{KO} cells, the percentage of proliferating cells was also significantly reduced on all 3 days (-40%, -50% and -59% respectively, $p < 0.0001$; **Figure 6.8B**). Based on these data combined with results displayed in **Section 6.3.7**, it can be suggested that androgen depletion significantly reduces the viability and proliferative capacity of STEAP2-knockout androgen-sensitive prostate cancer cell lines.

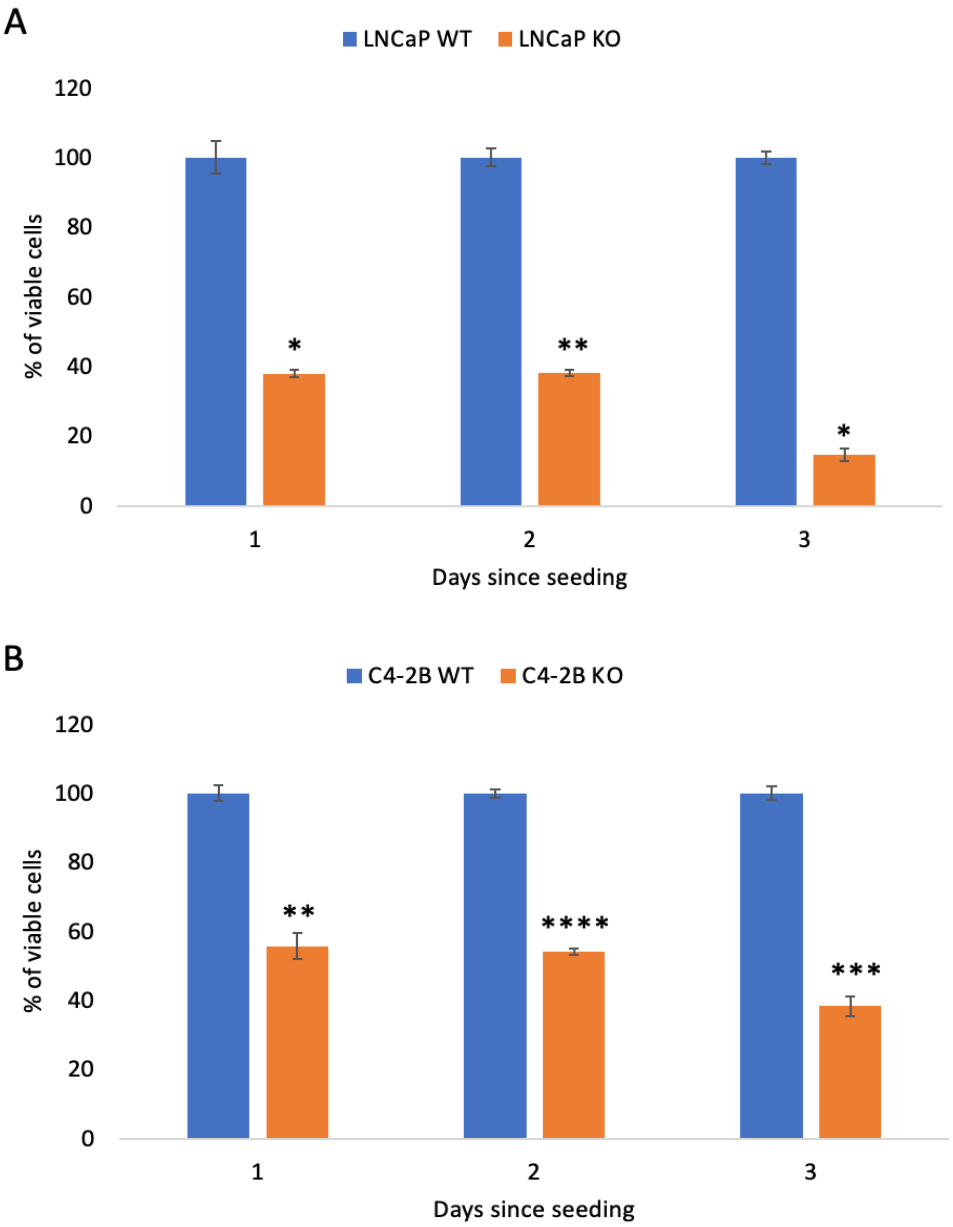

Figure 6.7. Androgen depletion significantly reduces STEAP2-knockout cell viability. Quantification by alamarBlue assay of the percentage of viable LNCaP^{KO} (A) and C4-2B^{KO} (B) cells grown in media supplemented with CSS. An ANOVA post-hoc Dunnett test was performed for statistical analysis. Error bars denote S.E.M. p-value < 0.05 (*), p-value < 0.01 (**), p-value < 0.001 (***), p-value < 0.0001 (****) (N = 3).

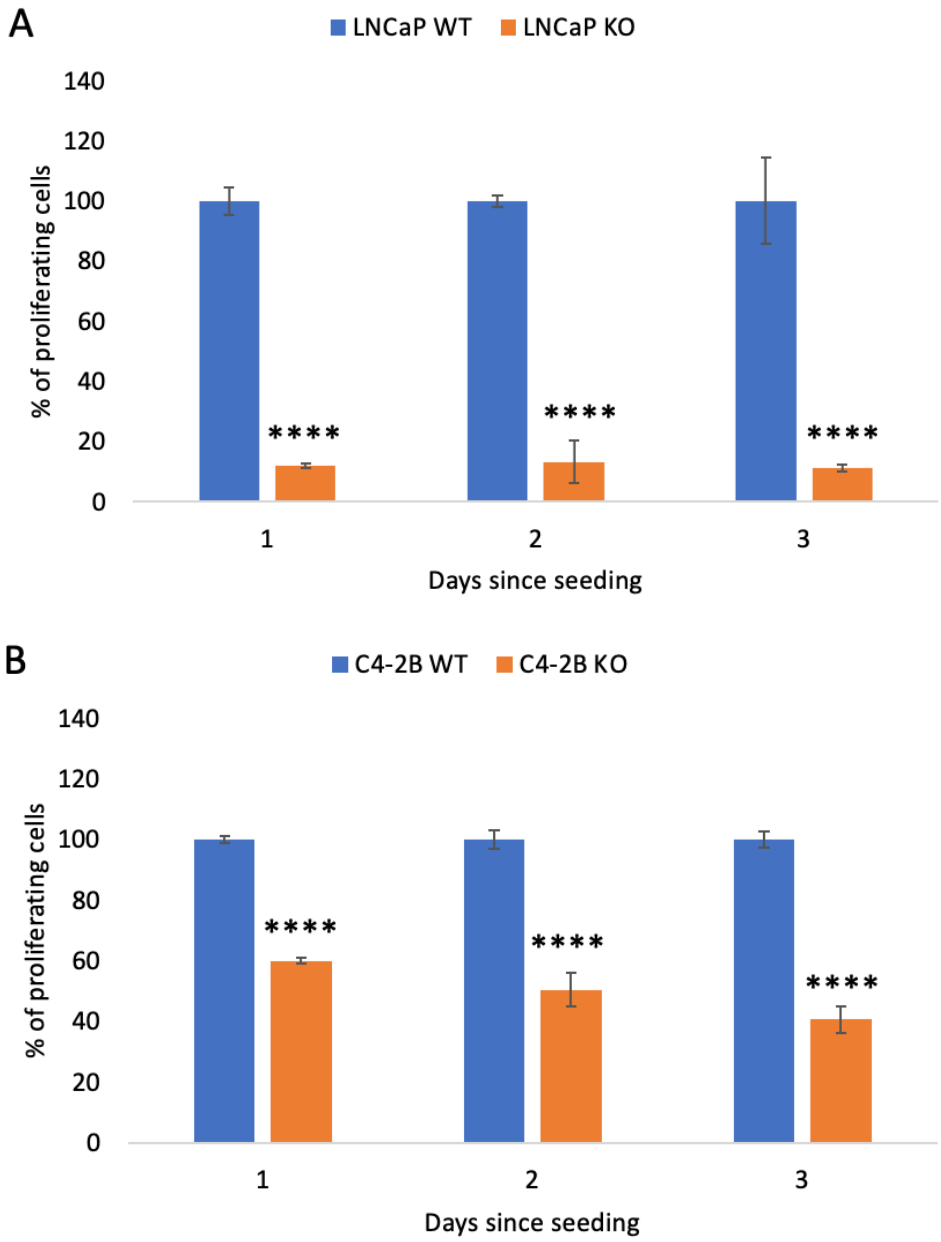

Figure 6.8. Androgen depletion significantly reduces STEAP2-knockout cell proliferation. Quantification by alamarBlue assay of the percentage of proliferating LNCaP^{KO} (A) and C4-2B^{KO} (B) cells grown in media supplemented with CSS. An ANOVA post-hoc Dunnett test was performed for statistical analysis. Error bars denote S.E.M. p-value < 0.05 (*), p-value < 0.01 (**), p-value < 0.001 (***), p-value < 0.0001 (****) (N = 3).

6.4 Discussion

The aim of this chapter was to determine the effect of androgen depletion through growth in CSS on aggressive prostate cancer traits. This chapter also aimed to determine whether androgen depletion effected *STEAP2* expression, and the expression of androgen-regulated genes. Finally, the effects of androgen depletion on the viability and proliferation of the STEAP2-knockout androgen-sensitive cells generated in **Chapter 5, Section 5.3.2** was also assessed. The results demonstrated that androgen depletion successfully reduced prostate cancer cell viability, migration and invasion. Androgen depletion also significantly increased the expression of *STEAP2* and all four androgen-regulated genes. Furthermore, cell viability and proliferation were also inhibited in STEAP2-knockout cells under androgen-depletion conditions.

To date, links between STEAP2 and AR in prostate cancer have not been well established (Gomes *et al*., 2012). Whilst **Chapter 5, Section 5.3.4** demonstrated that STEAP2-knockout significantly increased *AR* expression in C4-2B^{KO} cells, studies into the effects of androgen depletion on *STEAP2* expression were warranted. Growth in CSS removes lipophilic materials generally present in standard FBS, including hormones, growth factors and cytokines, yet leaves salts, amino acids and glucose levels unchanged, allowing for any changes observed to be the result of hormone depletion (Sedelaar *et al*., 2009). Phenol-red free media was also used alongside CSS supplementation to further limit the involvement of steroids present in the media (Fiandalo *et al*., 2018; Sedelaar *et al*., 2009). The use of CSS is warranted in this chapter to remove androgens present in standard FBS to observe any changes occurring as a result of androgen signalling (Fiandalo *et al*., 2018; Sedelaar *et al*., 2009). To further explore the downstream effects of inhibiting androgen signalling, the expression of four androgen-regulated genes was assessed. The expression of these four genes – *FKBP5, PSA, GPRC6A and TMPRSS2* – was found to increase in response to STEAP2-knockout (see **Chapter 5, Section 5.3.4**), therefore suggesting interplay between *AR* and *STEAP2*.

6.4.1 The impact of androgen depletion on aggressive prostate cancer traits

The results of the cell viability assay showed that the ability of androgen-depleted PC3 prostate cancer cells, an androgen-independent cell line, to metabolise MTT followed the same trend as PC3 cells grown under standard (androgen-replete) conditions (**Figure 6.1A**). However, in androgen-sensitive cell lines LNCaP and C4-2B, the MTT response remained consistent over the 5-day period and no significant difference was observed over time, whilst the same cell lines grown under standard conditions exhibited a significant increase in MTT absorbance over time (**Figure 6.1B & 6.1C**). MTT can only be cleaved by active mitochondria present in metabolically active cells and is therefore a relevant survival assay for distinguishing living cells from dead ones (van Meerloo *et al*., 2011). As such, the results from the MTT assay were used herein as a method of assessing the number of viable cells present.

When proliferative capacity was assessed, all three androgen-depleted cell lines followed similar proliferation trends as those grown under standard conditions, with all three androgen-depleted cell lines proliferating at a higher rate on day 5 than those under standard conditions (**Figure 6.2**). Under androgen-depleted conditions, studies have demonstrated that cells can become resistant to androgen-depletion, through the elevated expression of several peptide growth factors including EGF, TGF-α, IL-6 and IGF1 (Bartlett *et al*., 2005; Di Lorenzo *et al*., 2002; Krueckl *et al*., 2004; Tam *et al*., 2007; Traish *et al*., 2009). This overexpression can subsequently induce androgen-independent activation of *AR* transcriptional activity, or sensitise *AR* to low androgen levels, allowing for cells to continue to proliferate (Gregory *et al*., 2004). Growth of prostate cancer cells in androgen-depleted medium has been found to be significantly increased by EGF, a process which requires steroid receptor coactivator (Src) tyrosine kinase (Dasgupta *et al*., 2015; Guo *et al*., 2006). This Src promoted growth is dependent on the phosphorylation of AR-Y534, which has been found to be inhibited through Src siRNA, suggesting that Src kinase is required for the growth of hormone-refractory prostate cancer cells (Guo *et al*., 2006; Leung & Sadar, 2017). Y534 was

identified by Guo *et al*., 2006 by mass spectrometry as a major site of Src-induced tyrosine phosphorylation, which was increased in hormone-refractory tumour xenografts in comparison to their hormone-sensitive counterparts.

The expression of neutral endopeptidase 24.11 (NEP), a cell-surface enzyme, is regulated by androgens and is upregulated in androgen-sensitive cell lines such as LNCaP, yet is downregulated in cell lines lacking *AR* such as PC3 (Usmani *et al*., 2000). NEP loss has been reported to contribute to disease progression under androgen-depleted conditions through the activation of Akt, which may subsequently accelerate tumour progression (Osman *et al*., 2006). Hypermethylation of the NEP promotor has been reported in CRPC following reactivation of NEP by the demethylation agent 5-aza-2'-deoxycytidine, suggesting NEP loss may be characteristic of a switch to CRPC (Bastian *et al*., 2008; Osman *et al*., 2006; Usmani *et al*., 2000). Loss of NEP activity may therefore provide a mechanism for the sustained proliferation rates observed in all androgen-depleted cell lines (**Figure 3.2**; Osman *et al*., 2006).

Increased cellular proliferation may also be the result of EGFR activation through autophosphorylation of EGF and EGFR binding, leading to a downstream signalling cascade resulting in activation of PI3K (Migliaccio *et al*., 2006). PI3K activation leads to Akt and signal transduce and activator of transcription (STAT) activation, the downstream effects of which modulate cellular proliferation and survival (Bonnaccorsi *et al*., 2004; Migliaccio *et al*., 2006). In terms of AR activation, these pathways are involved in phosphorylation in the absence of the androgen ligand, subsequently promoting enhanced cell growth and proliferation without androgen stimulation (Traish *et al*., 2009). This signalling pathway of EGFR crosstalk with the AR pathway is of significance when regulating cell growth under androgen-depleted conditions (Bonnaccorsi *et al*., 2004; Migliaccio *et al*., 2006; Traish *et al*., 2009).

Under androgen-depleted conditions, it has been debated that growth factor induced androgen-independent activation of *AR* transcriptional activity alone may only induce relatively small (few-fold) increases in *AR* transcriptional

activity (Guo *et al*., 2006). In comparison with the optimal induction of *AR* transcriptional activity under normal conditions and in the presence of androgens, such an increase has been deemed negligible as it is in the same range as that induced by growth factors (Guo *et al*., 2006). *In vitro*, studies monitoring a dose-dependent response of LNCaP cells to androgens found that low levels of androgens (0.01-0.1 nM) promoted cellular proliferation, whilst higher levels (1-100 nM) inhibited cellular proliferation (Guo *et al*., 2006; Song & Khera, 2014). It has been suggested that this few-fold increase in *AR* transcriptional activity may be enough to regulate a subset of *AR*-regulated genes involved in the survival and proliferation of prostate cancer cells (Guo *et al*., 2006). Under androgen-depleted conditions, paracrine loops have been found to produce localised high levels of growth factors sufficient to maintain *AR* transcriptional activity and promote cell growth and survival (Guo *et al*., 2006; Song & Khera, 2014). Therefore, with respect to the data generated in this chapter, future work could involve monitoring androgen levels over time in order to determine androgen concentration in relation to proliferative capacity. It would also be of interest to conduct future work that assesses concentrations of growth factors under androgen-depleted conditions to determine a mechanism behind the observed cell survival and proliferation.

Following androgen ablation therapy, androgen-independent prostate cancers have been known to exhibit increased tumorigenicity, characterised by a more invasive phenotype (Karantanos *et al*., 2015). During prostate cancer progression, interactions between extracellular matrix proteins and prostate cancer cells change significantly (Stewart *et al*., 2004). In this present chapter, androgen-independent PC3 cells grown in CSS migrated in a similar, albeit slower, manner to PC3 cells grown in standard conditions, as shown by the partial wound closure by day 5 in **Figure 6.3A**. A possible mechanism for this is α6β4 integrin expression, which was found to decrease in PC3 cells transfected with AR cDNA to match naturally occurring levels of AR in LNCaP cells, resulting in a less invasive phenotype and migratory potential (Bonaccorsi *et al*., 2000 & 2004). α6β4, a laminin receptor, has been found to play a vital role in the migration and invasion of cancer cells through promoting the migration of laminin through association with the actin cytoskeleton (Davis

et al., 2001). A study by Bonaccorsi *et al*., 2004 implied that in androgen-independent prostate cancers, androgen withdrawal may have significant clinical implications due to the upregulation of α6β4 and subsequent increased invasion. Despite displaying similar rates of migration, androgen-depleted PC3 cells invaded through the extracellular matrix at a significantly lower rate than their androgen-replete counterparts (**Figures 6.4A, 6.4B & 6.4G**). It would therefore be warranted to conduct gene expression analysis of α6β4 integrin expression and other markers of migration and invasion to suggest a mechanism behind this observed effect.

Conversely, in androgen-sensitive LNCaP and C4-2B cells, migratory potential was inhibited by growth in CSS, as displayed by the wound gap remaining open by day 5 in **Figures 6.3B & 6.3C**. Studies have found that invasive and migratory capability of LNCaP cells has been suppressed by microRNA-185 (miR-185), coupled with cell cycle arrest at G_0/G_1 phase (Qu *et al*., 2013). In prostate cancer xenograft models, tumorigenicity was also inhibited by miR-185, thought to be the result of CDC6 upregulation (Mallik *et al*., 2008; Qu *et al*., 2013). The expression of CDC6, another AR target gene, has been found to be regulated through AR-binding in LNCaP cells, and is downregulated as a result of AR inhibition by miR-185 overexpression (Bai *et al*., 2005; Mallik *et al*., 2008; Qu *et al*., 2013). This downregulation of CDC6 in LNCaP cells has been found to reduce cell migration and invasion through cell cycle blockade at G_1 to S phase (Bai *et al*., 2005).

In this chapter, cell proliferation of androgen-depleted cells in comparison to androgen-replete cells was relatively unchanged (**Figure 6.2**), yet cell migration and invasion was significantly reduced (**Figures 6.3 & 6.4**). Protein-kinase-C-related kinase (PRK1) has been found to modulate cell migration through kinase activity, whilst not affecting cell proliferation in androgen-independent cell lines PC3 and DU145 *in vitro* and murine models *in vivo* (Jilg *et al*., 2014; Metzger *et al*., 2003). This inhibition of migration is thought to be the result of changes in the ETS domain following PRK1 depletion (Jilg *et al*., 2014; Patki *et al*., 2013). In androgen-dependent LNCaP cells, PRK1 was

found to not only inhibit cell migration and invasion, but also proliferation, suggesting crosstalk between PRK1 and AR (Metzger *et al*., 2008).

The growth of androgen-sensitive prostate cancer cells under androgen-depleted conditions has been found to be inhibited as a result of a mutation in the major tyrosine phosphorylation site in *AR* (Guo *et al*., 2006). In the absence of androgens, phosphorylation may also control the transition of *AR* from inactive to active conformation, and in turn dissociate from negative regulatory proteins, for example HSP90 (Guo *et al*., 2006). This dissociation upon tyrosine phosphorylation may allow androgen to become dimerised with the nuclear import machinery complex in the absence of androgens, promoting *AR* nuclear translocation (Guo *et al*., 2006).

The migration and invasion of prostate cancer cells has been found to be inhibited both in *in vitro* cell lines and tumour *in vivo* following *AR*-knockdown (Cinar *et al*., 2001). In androgen-independent PC3 cells, studies have found *AR*-knockdown to reduce EGFR phosphorylation and PI3K activation, implying that androgens are involved in the modulation of EGFR expression and function (Bonaccorsi *et al*., 2004 & 2007). Under normal growth conditions, EGFR expression and phosphorylation are found at high levels in androgen-independent PC3 and DU145 cells, but lower in androgen-sensitive LNCaP cells (Bonaccorsi *et al*., 2004 & 2007; Traish *et al*., 2009). The reduction in EGFR expression in PC3 cells following AR-knockdown was suggested to lead to a less invasive phenotype through AR-EGFR crosstalk, and therefore may provide a mechanism for the reduction in cell migration and invasion observed in this Chapter (**Figures 6.3 & 6.4**; Traish *et al*., 2009).

Future studies into cell viability, proliferation, migration and invasion in response to long-term culture would provide insight into whether the results observed in this chapter are sustained over time. These studies would be warranted as it has been previously noted that prostate cancer cell proliferation may occur in a biphasic manner, with increased proliferation being promoted initially at low levels of androgens (Song & Khera, 2014). Coupled with *AR* expression over the course of a longer culture period in CSS, such

data could provide information on determining whether a switch to CRPC has occurred.

6.4.2 The impact of androgen depletion on the expression of *STEAP2* and androgen-regulated genes in prostate cancer cells

STEAP2 is highly expressed in the androgen-sensitive prostate cancer cell line LNCaP and C4-2B, but not the androgen-independent cell lines PC3 and DU145 (see **Chapter 5, Figure 5.4**; Korkmaz *et al*., 2002; Porkka *et al*., 2002). In this chapter, *STEAP2* was found to be significantly overexpressed in androgen-sensitive LNCaP and C4-2B cells under androgen-depleted conditions, when compared to their androgen-replete counterparts (**Figure 6.5A**). This observed increase in STEAP2 gene expression was also mirrored in STEAP2 protein expression (**Figure 5.5B**). It has previously been found that STEAP2 expression requires an intact AR, suggesting that AR activation may have been achieved in these cells (Korkmaz *et al*., 2002). High transcript levels of STEAP2 have also been found in CRPC samples, further suggesting AR activation may have occurred (Ylitalo *et al*., 2017).

Following growth in androgen-depleted medium, the gene expression of the androgen-regulated genes *PSA, FKBP5, TMPRSS2* and *GPRC6A* was found to increase significantly in both androgen-independent PC3 cells (**Figure 6.6A**), and androgen-sensitive LNCaP and C4-2B cells (**Figures 6.6B & 6.6C**). This increase in gene expression of androgen-regulated genes could be the result of a switch to castrate-resistant disease following the *AR* transcriptional activity becoming reinstated (Cai *et al*., 2009). The transcription of these androgen-regulated genes is stimulated once nuclear *AR*, which has been translocated from the cytoplasm to the nucleus, interacts with AREs in the promoter regions of these target genes (Dehm & Tindall, 2005).

Studies have found this to be the case in LNCaP cells cultured in androgen-depleted medium, which exhibited an increase in *PSA* expression due to enhanced receptor protein tyrosine kinase ErbB2 signalling (Cai *et al*., 2009).

Cai *et al*., 2009 also showed that EGF and heregulin-β1, a ligand for ErbB2, stimulated the expression of *PSA*, suggesting that *AR* transcriptional activity can be enhanced by ErbB2 stimulation even in the absence of androgens or at low androgen levels (Cai *et al*., 2009; Liu *et al*., 2005; Mellinghoff *et al*., 2004). Activation of EGFR or ErbB2 signalling could provide a mechanism for the maintenance of *AR* protein expression in CRPC, resulting in an increased AR protein stability (Cai *et al*., 2009). In human samples matched from pre- and post-androgen therapy, EGFR was found to influence progression to androgen-independent hormone relapse and subsequent disease progression, for which elevated *PSA* expression was used to confirm biochemical relapse (Bartlett *et al*., 2005). Further studies into the levels of *AR* expression over time by qRT-PCR in cells cultured in CSS would be warranted to confirm this hypothesis.

In androgen depleted tumours, a loss of androgen regulation coupled with increased PI3K and MAPK signalling may not only account for the sustained proliferative potential of androgen-depleted prostate cancer cells, but also the increase in *FKBP5* expression (**Figures 6.2 & 6.6**; Traish *et al*., 2009). *FKBP5* expression is modulated through PI3K signalling, which can become stimulated following *AR* activation in the absence of ligand binding, triggering *AR* signalling, cellular proliferation and survival (Traish *et al*., 2009). This may also suggest a mechanism behind the sustained cell viability observed in all androgen-depleted cell lines (**Figure 6.1**). PI3K signalling may also become active in androgen-depleted cells as a result of nuclear receptor coactivator 2 (NCoA2) induction, which may also contribute to the development of CRPC (Qin *et al*., 2014). NCoA2, also known as Src-2, is a coregulator of transcription and modulates transcription once recruited to the enhancer or promoter regions of target genes (Dasgupta *et al*., 2015; Qin *et al*., 2014). NCoA2 may be involved in supporting growth and survival of androgen-depleted prostate cancer cells through glutamine metabolism (Dasgupta *et al*., 2015; Qin *et al*., 2014). In murine models, NCoA2 has been found to stimulate hyperactivation of PI3K/Akt signalling, promoting cell survival and proliferation (Qin *et al*., 2014). Similarly, the depletion of NCoA2 prevented the development of CPRC, indicating NCoA2 may provide a potential therapeutic target alongside

androgen ablation (Qin *et al*., 2014). This may provide a mechanism for the sustained viability of androgen-depleted prostate cancer cells in this chapter (**Figure 3.1**), however further studies to monitor NCoA2 expression would be required to confirm this hypothesis.

Transcription factor cyclin AMP-responsive element-binding protein 5 (CREB5) has been identified as a modulator of conferring resistance to androgen depletion in androgen-dependent prostate cancer cell lines and enhances proliferation rates under androgen-depleted conditions (Hwang *et al*., 2019). When androgen ablation therapy was delivered *in vitro*, the ability of low residual levels of nuclear *AR* to bind to *AR* target sequences was enhanced by CREB5 and *AR* transcription was subsequently promoted (Hwang *et al*., 2019). As a result, Hwang *et al*., 2019 reported that the gene expression of 16 out of 43 AR target genes was upregulated more than 2-fold in cells also overexpressing CREB5 when treated with CSS, whilst *AR* expression and localisation was not directly altered. These upregulated target genes included *PSA* and *FKBP5*, both of which were overexpressed in response to CSS in this chapter (**Figure 6.6**; Hwang *et al*., 2019). These results suggest that the expression of *AR*-regulated genes may be enhanced in parallel to CREB5 expression under androgen-depleted conditions (Hwang *et al*., 2019). To confirm this hypothesis, it would be interesting to conduct further qRT-PCR analysis to determine CREB5 expression in androgen-depleted cells in comparison to their androgen-replete counterparts to suggest a mechanism driving the overexpression of the AR-regulated genes observed in this chapter.

When treated with a peroxisome proliferator-activated receptor alpha (PPARα) androgen agonist, fenofibrate, G_1 phase cell cycle arrest and inhibition of Akt phosphorylation was induced in LNCaP cells (Zhao *et al*., 2013). *PSA* and *TMPRSS2* expression were also reduced in a dose dependent manner, whilst intracellular ROS signalling was increased (Zhao *et al*., 2013). In androgen-independent PC3 cells, fenofibrate only induced apoptosis at higher concentrations than in LNCaP cells, suggesting that G_1 phase cell cycle arrest may be mediated by downregulation of *AR* (Zhao *et al*., 2013). In CRPC,

TMPRSS2 expression and subsequent fusion with the *ERG* gene is often increased following a gain of function mutation in *AR* sufficient to drive expression of *AR*-regulated genes (Montgomery *et al*., 2008; Tomlins *et al*., 2005). *TMPRSS2* was found to be significantly overexpressed in all three androgen-depleted cell lines (**Figure 6.6**), suggesting a switch to CRPC has occurred. *TMPRSS2* expression has also been found to increase alongside *PSA,* also observed in this Chapter, in CRPC following a gain in function mutation in DHT synthesis (**Figure 6.6**; Chang *et al*., 2013).

As *GPRC6A* has been found to indirectly mediate the effects of *AR* in prostate cancer progression, its overexpression observed in this chapter in conjunction with increased proliferation could further suggest a switch to CRPC (**Figure 6.6**; Pi & Quarles, 2012; Zarif & Miranti, 2016). *GPRC6A* also regulates the non-genomic, rapid signalling responses to testosterone which activate the PI3K/Akt pathways responsible for *AR*-independent progression, onset of CRPC and subsequent resistance to ADT (Pi *et al*., 2015; Zarif & Miranti, 2016). Overexpression of *GPRC6A* may also trigger stimulation of interleukin-6 (IL-6), which may in turn promote androgen synthesis in the absence of androgens through enhancing *AKR1C3* transcription (Chun *et al*., 2009; Thulin *et al*., 2016).

Whilst growth in CSS strips cells of androgens present in the serum, complete androgen-free conditions cannot exist entirely as low levels of residual androgens remain, as observed in the serum of patients undergoing androgen ablation therapy (Chang *et al*., 2013). Transcripts encoding androgen synthesising steroidogenic enzymes such as hydroxy-delta-5-steroid dehydrogenase beta-1 (HSD3β1), cytochrome P450 17A1 (CYP17A1), and AKR1C3 have been found to be expressed in biopsies from metastatic prostate cancer tumours (Chang *et al*., 2013; Montgomery *et al*., 2008). These enzymes have been found to be capable of maintaining intratumoural androgen levels at high enough concentrations to activate *AR* target genes and maintain tumour cell survival in the absence of androgens (Chang *et al*., 2013; Montgomery *et al*., 2008). In particular, HSD3β1 has been found to limit DHT synthesis under androgen-depleted conditions (Chang *et al*., 2013). In

LNCaP cells grown in androgen-depleted media, a castrate level of testosterone remains, which cells then metabolise to produce a level of intracellular DHT similar to physiological conditions (approximately 10 nM), allowing for the stimulation of androgen-depleted LNCaP cells *in vitro* (Sedelaar *et al*., 2009). This maintenance of androgen levels may account for the activation of AR-regulated genes observed in androgen-depleted cells (**Figure 6.6**; Chang *et al*., 2013; Montgomery *et al*., 2008). To further relate the findings in this Chapter to the literature with regards to *AR*-regulated gene expression, it would be of interest to assess gene expression across a range of androgen levels, along with DHT expression (Chang *et al*., 2013; Montgomery *et al*., 2008).

6.4.3 The impact of androgen depletion on the viability and proliferation of STEAP2-knockout androgen-sensitive prostate cancer cells

STEAP2-knockout was previously found to significantly reduce the cellular proliferation rate of LNCaP and C4-2B cells in comparison to their wild-type counterparts (see **Chapter 5, Figure 5.7**). As STEAP2 was found to become upregulated in response to androgen depletion in androgen-sensitive LNCaP and C4-2B cells (**Figure 6.5A**), it was of interest to explore the impact of CRISPR/Cas9 targeted STEAP2-knockout in conjunction with androgen depletion. Here, cell viability and proliferation of STEAP2-knockout LNCaP and C4-2B cells was significantly decreased under androgen-depleted conditions, when compared to androgen-replete LNCaP^{KO} and C4-2B^{KO} cells (**Figures 6.7 & 6.8**).

Both *AR* and *STEAP2* expression have been found to be involved in cellular proliferation and survival of prostate cancer cells, yet a link between the two has not yet been fully established (Gomes *et al*., 2012; Wang *et al*., 2010). Under androgen-depleted conditions, LNCaP and C4-2B cell viability was consistent over time (**Figures 6.1B & 6.1C**), yet significantly decreased in androgen-depleted LNCaP^{KO} and C4-2B^{KO} cells (**Figure 6.7**). STEAP2 knockdown with siRNA has previously been found to increase the number of

apoptotic events in prostate cancer cells through upregulation of p21, which regulates the cell cycle during G_1 and S phase (Bertoli *et al*., 2013; Wang *et al*., 2010). p21 expression has also been found to increase over time in parallel with increased apoptosis of prostate cancer cells in response to androgen ablation (Martinez *et al*., 2002). To confirm the involvement of p21 in cell death of androgen-depleted cells, flow cytometry would be warranted to determine the phase of cell cycle arrest in response to androgen-depletion in STEAP2-knockout cells, whilst p21 expression could be explored to suggest a mechanism of cell death.

Under androgen-depleted conditions, the proliferative capacity of LNCaP and C4-2B cells increased over time (**Figures 6.2B & 6.2C**), which could be the result of EGF overexpression (Dasgupta *et al*., 2015; Guo *et al*., 2006; Traish *et al*., 2009). EGF has been found to become overexpressed when STEAP2 is ectopically expressed in prostate cancer cells, resulting in ERK pathway activation and increased proliferation due to partial cell cycle arrest in the G_0-G_1 phase (Gomes *et al*., 2012; Wang *et al*., 2010). As proliferation decreased in response to STEAP2-knockout, it could be suggested that the ERK signalling pathway driving cellular proliferation may not become activated by STEAP2 (**Figure 6.8**; Dasgupta *et al*., 2015; Guo *et al*., 2006; Traish *et al*., 2009; Wang *et al.,* 2010). However more studies to explore the signalling pathways involved would be warranted to confirm this hypothesis. It would also be of interest to explore changes in MMPs -1, -3, -7, -9, -11 and -13, which become activated upon ERK translocation (Dhillon *et al*., 2007; Gong *et al*., 2014).

These data suggest that not only does *STEAP2* provide potential as a novel therapeutic target in the treatment of prostate cancer, but this could be targeted in conjunction with androgen ablation therapy. Further studies into the effects of androgen depletion on the migratory and invasive potential of STEAP2-knockout cells are warranted, as *STEAP2* overexpression has previously been thought to enhance prostate cancer cell migration and progression (Burnell *et al*., 2018; Whiteland *et al*., 2014). Had time allowed, it would have been interesting to conduct qRT-PCR gene profiling of androgen-

depleted STEAP2-knockout cells to assess *PSA, FKBP5, TMPRSS2* and *GPRC6A* expression in order to suggest a mechanism behind the reduction in cell proliferation and viability. This would also be of importance to determine whether these genetic drivers of prostate cancer progression respond to androgen-depletion in STEAP2-knockout cells.

6.5 Conclusion

The data generated in this chapter provides strong evidence that targeted STEAP2 therapy could potentially be a viable therapeutic target alongside conventional androgen-depletion therapy in the treatment of prostate cancer for future clinical translation. Androgen-depletion through growth in CSS resulted in a promising inhibition of cell migration and invasion. Gene expression analysis of *STEAP2* and androgen-regulated genes found that androgen depletion initiates an increase in expression of key genes in the progression of prostate cancer, despite androgen-depletion inhibiting cell migration and invasion; however, the mechanisms behind this remain unclear. When STEAP2 was knocked out by CRISPR/Cas9 engineering, cell viability and proliferation decreased, further suggesting *AR* and *STEAP2* crosstalk. Further studies into the mechanisms driving the increase of *STEAP2* and androgen-regulated genes when androgen is depleted are warranted, such as RNAseq profiling. Overall, the data presented in this chapter provides further evidence that crosstalk between *AR* and *STEAP2* could be involved in the progression prostate cancer.

Chapter 7

General discussion

Prostate cancer is the most common cancer in men, with approximately 10% progressing to advanced or metastatic disease, which has a poor 5-year survival rate of approximately 30% (CRUK, 2019). For many men with metastatic disease, treatment options are limited to either palliative care or radical chemo- or radiotherapy which come with severe adverse effects (e.g., extreme fatigue, nausea and erectile dysfunction), hindering a patients' quality of life (CRUK, 2019). Prostate cancer is a highly androgen regulated disease, and as such ADT is often offered as the first-line treatment, however many men develop resistance to these drugs and go on to develop a more aggressive form of the disease; CRPC (Kirby *et al*., 2011; Scher *et al*., 2004). In order to improve the clinical management of men with advanced prostate cancer, the development of more targeted therapeutic drugs is needed. Over recent years, advances in the development of mAbs have allowed for progression to more personalised treatment strategies in the clinical management of patients with cancers such as malignant melanoma and non-Hodgkin lymphoma (Satta *et al*., 2018; Tsumoto *et al*., 2019). mAbs are highly specific and can therefore target cancer-specific proteins and trigger cell death and / or disrupt downstream pathways involved in cancer progression (Wang *et al*., 2018). Immunotherapy has become a widely studied area of research recently, with various drugs being developed to treat metastatic CRPC including ipilumumab and Sipuleucel-T (Anassi & Ndefo, 2011; Beer *et al*., 2017; Redman *et al*., 2017). These immunotherapeutics may offer clinical benefit over the standard ADT regimen currently offered, however the number of patients who may benefit from these drugs is limited (Beer *et al*., 2017; Hossain *et al*., 2018; Massard & Fizazi, 2011). To further enhance the efficacy of mAbs, ADC technology has been utilised which relies on the specificity of mAbs along with biochemical linkers to trigger a cytotoxic payload release to induce cell death (Chen *et al*., 2020). Due to their increased specificity, ADCs have the added benefit of reduced off-target effects. However, to date, a

specific mAb or mAb-ADC for the clinical management of prostate cancer patients is lacking. Another development in cancer therapeutic approaches is the use of genome editing, particularly through CRISPR/Cas9 technology to knockout genes of interest from cancer cells in order to inhibit their effects on disease progression (Yi & Li, 2016). However, to date this approach has not been applied as a treatment strategy for prostate cancer. STEAP2, a cell surface protein that functions as a metalloreductase, is highly expressed in prostate cancer cells when compared to normal tissue and is known to contribute to disease progression by modulating aggressive prostate cancer traits such as cell migration and invasion *in vitro* (Gomes *et al.,* 2012). Given these features, STEAP2 therefore offers the potential to be a future therapeutic target for prostate cancer treatment in combination with mAbs and CRISPR/Cas9 technologies.

Thus, the aim of this thesis was to evaluate whether STEAP2 is a viable drug target for the potential clinical management of prostate cancer, with a focus on the application of therapeutic anti-STEAP2 mono- and poly-clonal antibodies, and CRISPR/Cas9 gene knockout technology. This thesis also aimed to determine whether STEAP2 is involved in the expression of *AR* or androgen-regulated genes. The data generated in this thesis demonstrated:

1. Androgen-independent cell lines PC3 and DU145 form more viable 3D spheroid structures over time than androgen-sensitive LNCaP and C4-2B cells (Chapter 3);
2. Anti-STEAP2 pAb and mAb treatment reduced cell viability in 2D but not 3D models, with anti-STEAP2 mAb2 identified as a lead candidate.
    a. Anti-STEAP2 mAb2 triggered receptor internalisation in both a dose- and time-dependent manner (Chapter 4);
3. The expression of *AR* and androgen-regulated genes significantly increased in response to anti-STEAP2 pAb treatment and STEAP2 knockout (Chapter 4 & 5);
4. CRISPR/Cas9 technology successfully generated stable STEAP2-knockout LNCaP and C4-2B cells with reduced cell proliferation, migration and invasion capacities *in vitro* (Chapter 5);

5. Androgen deprivation significantly increased STEAP2 expression in androgen-sensitive cell lines, whilst reducing cell migration and invasion (Chapter 6).

In Chapter 3, gene expression profiling of a panel of prostate cancer cell lines found *STEAP2* to have the highest expression of the four *STEAP* family members. These findings were consistent with previous studies reporting *STEAP2* to be highly expressed in prostate cancer tissue, but not the normal healthy prostate, and correlates with poor prognosis and advanced disease (Burnell *et al*., 2018; Porkka *et al*., 2002). These results, along with previous work highlighting the role of STEAP2 in disease progression, confirm that *STEAP2* poses an attractive therapeutic target for the treatment of prostate cancer, hence it being the focus for further investigations throughout this thesis (Burnell *et al*., 2018). Due to its high specificity to prostate cancer tissue and low expression in normal cells, targeting *STEAP2* with therapeutic agents may allow for targeting induced cell death of prostate cancer cells, whilst preserving normal, healthy cells from the adverse effects associated with many conventional treatments (Sikkeland *et al*., 2016). Indeed, throughout this thesis, inhibition of *STEAP2* by either anti-STEAP2 antibody treatments or CRISPR/Cas9 gene knockout triggered a reduction in cell viability.

One of the key properties gained by cancer cells is the ability to migrate to distant sites from their primary tumours and form metastases (Hanahan & Weinberg, 2011; Rycaj & Tang, 2017). Disease progression can also be increased by the ability of cancer cells to invade out from their original sites (Gialeli *et al*., 2011). The main site for metastases in prostate cancer patients is the bone, yet the development of a physiologically relevant platform to assess the interactions between prostate cancer cells and bone stromal cells is lacking (Taichman *et al*., 2007; Sun *et al*., 2007). Thus, Chapter 3 also worked to fully develop, optimise and characterise a robust method for the generation of viable 3D prostate cancer spheroids for future use throughout this thesis. 3D spheroid models are more physiologically relevant representatives of the *in vivo* microenvironments and bridge the gap between *in vitro* and *in vivo* studies (Donglai *et al*., 2017; Hirschhaeuser *et al*., 2010;

Lovitt *et al*., 2014). Previous studies have reported that *STEAP2* overexpression correlated with an increased aggressive cancer phenotype, with *STEAP2* driving migration and invasion (Burnell *et al*., 2018; Gomes *et al*., 2012; Wang *et al*., 2010; Whiteland *et al*., 2014). The results of Chapter 3 demonstrated that not only did LNCaP and C4-2B cells display the highest levels of *STEAP2* expression, but they also formed the most uniformly distributed 3D co-culture models with bone stromal cells. This correlation between *STEAP2* expression and stromal cell integration, along with previous studies highlighting the role of *STEAP2* in migration and invasion, further indicate *STEAP2* as a potential target for treating metastatic disease.

STEAP2 consists of six transmembrane helices, giving rise to three ECLs which have the potential to be targeted with specific drugs (Grunewald *et al.*, 2012). The anti-STEAP2 antibodies applied in Chapter 4 all targeted the ECL3 of STEAP2, following previous work within the wider research group which identified a peptide located on ECL3 as the most immunogenic for therapeutic targeting (Nguyen-Chi, 2020). When exposed to 2D monolayers in Chapter 4, the anti-STEAP2 pAb significantly reduced cell viability in all cell lines, and of the three anti-STEAP2 mAbs evaluated, mAb2 was identified as the preferred lead candidate due to its ability to significantly reduce cell viability at lower doses across all four prostate cancer cell lines. This reduction in cell viability was not mirrored when the antibodies were applied to the 3D PC3 and LNCaP cell spheroid models generated in Chapter 3. The spheroid models generated in Chapter 3 showed variation in their viability over time, with PC3 cells generating more viable spheroids than LNCaP cells. Therefore, although the viability of LNCaP spheroids was significantly reduced at all doses of anti-STEAP2 mAb between 62.5 – 1,000 μg/ml, this may be more likely due to the time-dependent limitations in model viability. In contrast, PC3 cells did form spheroids with sustained viability over time, high cell numbers were initially seeded and dense spheroids were formed. PC3 spheroid viability was only significantly impacted at the highest dose of anti-STEAP2 mAb2 (1,000 μg/ml). However, given the dense tissue structure, the minimal induction of cell death induced by the anti-STEAP2 mAb2 is most likely to due to poor penetration

through the spheroids (Grimes *et al*., 2014; Hirschhaeuser *et al*., 2010; Lazzari *et al*., 2018; Riffle *et al*., 2017).

Cell death is initiated upon triggering the apoptotic cascade, yet it remains unclear whether it is the extrinsic or intrinsic apoptotic pathway that *STEAP2* exerts an effect on (Wang *et al*., 2010). During the extrinsic pathway, cell death is the result of the formation of the DISC, the stability of which may be reduced by STEAP2 (Dickens *et al*., 2012; Wang *et al*., 2010). *STEAP2* may also play a role in the intrinsic pathway as its knockdown has been found to trigger apoptosis through transcription factors, independent of the extrinsic pathway (Sayers, 2011; Wang *et al*., 2010). LNCaP and C4-2B cells were deemed more susceptible to targeted *STEAP2* treatment due to their naturally high expression levels determined in Chapter 3, and as such significant reductions in their viability were observed following both anti-STEAP2 pAb and mAb treatment in Chapter 4, and CRISPR/Cas9 STEAP2-knockout in Chapter 5. TRAIL-induced apoptosis may also contribute to cell death in LNCaP cells, which was found to be the case in response to *STEAP2*-knockdown (Wang *et al*., 2010). TRAIL-induced apoptosis could also contribute to DISC formation through the extrinsic apoptosis pathway via caspase-8 mediated cell death (Dickens *et al*., 2012). The heme-binding domain of STEAP2, also known as the ACRATA, has previously been suggested to inhibit cell growth and metabolism via electron transport across the membranes of STEAP proteins (Oosterheert *et al*., 2020; Sanches-Polido *et al*., 2004; Yamada *et al*., 2004).

Following previous work within the wider research group, it was of interest to assess the suitability of the lead mAb candidate, mAb2, for potential future use in ADC technology (Nguyen-Chi, 2020). One of the key properties of a successful ADC relies on the ability of its mAb to trigger receptor internalisation (Kamath & Iyer, 2015; Tarcsa *et al*., 2020). In Chapter 4, PC3, LNCaP and C4-2B cells were exposed to a range of anti-STEAP2 mAb2 doses for various lengths of time and were visually assessed under confocal microscopy to determine receptor internalisation. In LNCaP and C4-2B cells, lower doses of anti-STEAP2 mAb2 of 25 μg/ml and 50 μg/ml respectively were deemed

sufficient at triggering receptor internalisation, as higher doses appeared to saturate cells (Rhoden *et al*., 2012). A higher dose range of 100 – 500 μg/ml anti-STEAP2 mAb2 was required to trigger receptor internalisation in PC3 cells. Data from Chapter 3 showed significantly high STEAP2 expression in LNCaP and C4-2B cells, but not PC3 cells, which may also account for receptor internalisation at lower anti-STEAP2 mAb2 doses. Therefore, the data presented in Chapters 3 and 4 suggest that the use of anti-STEAP2 mAb2 along with ADC technology should be reserved for prostate cancers with high *STEAP2* levels to allow for lower doses of antibody to be administered.

Previous studies have applied siRNA to knockdown *STEAP2* expression, yet as siRNA achieves a transient gene knockdown, it was of importance to explore other technologies that would provide a complete and sustainable *STEAP2* knockout for further consideration as a future therapeutic option (Burnell *et al*., 2018). The ability of anti-STEAP2 antibodies to reduce cell viability led to the optimisation and development of CRISPR/Cas9 genome engineering to achieve a stable STEAP2 knockout. CRISPR/Cas9 has gained interest as a potential tool in the development of more personalised therapeutics, as it allows for a wide variety of genomic sequences to be targeted (Li *et al*., 2020; Yi & Li, 2016). Two oligonucleotides were designed to target either the full STEAP2 protein, or a STEAP2 transcript variant. One of the major concerns regarding the use of CRISPR/Cas9 engineering is the ability to produce clones with a stable gene knockout (Lino et al., 2018). Following the results of Chapter 3 which demonstrated *STEAP2* expression was highest in LNCaP and C4-2B cells, which was translated into protein expression as seen in Chapter 5, results demonstrated that a stable STEAP2 knockout was successfully achieved and sustained in both of these cell lines. Transient knockdown of *STEAP2* using siRNA has also been reported to decrease cell migration and invasion (Burnell *et al*., 2018). Chapter 5 therefore aimed to assess the impact of CRISPR/Cas9 targeted *STEAP2* knockout on these aggressive prostate cancer traits. Both of these traits were significantly reduced in LNCaP^{KO} and C4-2B^{KO} cells when compared to their wild-type counterparts. Cell migration and invasion were also reduced when cells were

grown in androgen-depleted conditions in Chapter 6. Previous studies have hypothesised that this inhibition of migration and invasion may be due to a reduction in EGFR signalling, and subsequent lack of PI3K/Akt activation (Bonaccorsi *et al*., 2004 & 2007). AR-knockdown has also been found to induce a less invasive phenotype through AR-EGFR interactions (Traish *et al*., 2009). Data in Chapter 5 shows that STEAP2-knockout significantly inhibits prostate cancer cell migration and invasion *in vitro*, which was also found in previous studies within the group in response to anti-STEAP2 pAb and siRNA knockdown (Burnell *et al*., 2018; Nguyen-Chi, 2020). These combined results suggest that *STEAP2* has potential to be targeted specifically in the treatment of advanced prostate cancer as its sustained inhibition using various approaches resulted in a less aggressive prostate cancer cell phenotype.

Uncontrolled proliferation is one of the key properties gained by cancer cells in order to grow exponentially (Hanahan & Weinberg, 2011). STEAP2 exerts an effect on cellular proliferation through activation of the ERK pathway, suggesting inhibition of this pathway following STEAP2-knockout (Gomes *et al*., 2012; Wang *et al.,* 2010). Throughout this thesis, proliferation was assessed in response to culture conditions and *STEAP2* inhibition. *STEAP2* was found to play a role in over-proliferation in Chapter 3, as its high expression levels correlated with increased proliferation of both 2D and 3D LNCaP and C4-2B cells. The 3D spheroids generated in Chapter 3 also recapitulated *in vitro* some of the key characteristics of *in vivo* tumours, such as the presence of a necrotic core and viable, proliferating peripheral zone (Grimes *et al*., 2014; Hirschhaeuser *et al*., 2010; Riffle *et al*., 2017). When *STEAP2* was knocked out of these cells using CRISPR/Cas9 engineering, proliferation significantly decreased (Chapter 5), which was also the case when cells were stripped of androgens (Chapter 6). The cyclin-dependent kinase inhibitor p21, which when upregulated is known to increase the number of apoptotic events in prostate cancer cells, has been reported to be overexpressed both in response to STEAP2-knockdown with siRNA, and in androgen-depleted cells (Bertoli *et al*., 2013; Martinez *et al*., 2002; Wang *et al*., 2010). As cell cycle progression through G_1 and S phase is regulated by

p21, its expression could provide a mechanism of cell death in androgen-depleted STEAP2-knockout cells (Bertoli *et al*., 2013; Wang *et al*., 2010).

Data presented in Chapter 3 showing the high expression of *STEAP2* in androgen-sensitive cell lines formed the basis of further investigations into the role of androgens throughout this thesis. Androgens play a vital role in normal prostate development and homeostasis (Davey & Grossman, 2016). Prostate cancer is a largely androgen-regulated disease, with *AR* linked to aggressive prostate cancer traits (Eder *et al*., 2000; Gonen-Korkmaz *et al*., 2014). Studies into the relationship between *AR* and *STEAP2* have been inconclusive at establishing the mechanisms between the two, yet it has been proposed that *STEAP2* expression may be influenced by *AR* (Gomes *et al*., 2012; Korkmaz *et al*., 2002). Data presented in Chapter 4 showed *AR* expression significantly increases following anti-STEAP2 pAb treatment in androgen-sensitive cell lines. This was further explored in Chapter 5 following CRISPR/Cas9 targeted *STEAP2* knockout, which similarly showed an increase in AR expression in LNCaP^{KO} and C4-2B^{KO} cells when compared to their wild-type counterparts. This increase in *AR* expression in response to *STEAP2* inhibition using two different approaches could be a cause for concern as it may induce a more invasive phenotype in patients (Hu *et al*., 2015; Whiteland *et al*., 2014). MMPs are often required for the progression of prostate cancer, and aid in the degradation of the extracellular matrix and subsequent invasion of cells from their primary site (Gialeli *et al*., 2011). Prostate cancer progression is regulated through MMPs -2, -7, -9, -13 and -14, of which MMP-9 is known to increase in response to *AR* overexpression, whilst MMPs -3, -7, -10 and -13 have been found to decrease in response to *STEAP2* inhibition (Brehmer *et al*., 2003; Burnell *et al*., 2018; Daja *et al*., 2003; Hu *et al*., 2015; Morgia *et al*., 2005). MMPs are downstream effectors of ERK signalling, which increases in response to *STEAP2* overexpression, leading to a more invasive phenotype (Wang *et al*., 2010; Whiteland *et al*., 2014). Increases in *AR* expression are often the result of mutations in AR, the most common of which is *ARv7*, which can lead to resistance to ADT (Guo *et al*., 2009; Hu *et al*., 2009; Nelson & Shah, 2019; Qu *et al*., 2015).

Whilst *AR* expression had been evaluated following *STEAP2* inhibition in Chapters 4 and 5, it was then of interest to determine whether *STEAP2* expression was altered in response to androgen depletion, which formed the basis of Chapter 6. In this Chapter, CSS-supplemented media was used to remove androgens from the growth conditions of cells (Fiandalo *et al*., 2018; Sedelaar *et al*., 2009). Crosstalk between *STEAP2* and *AR* was further evidenced in Chapter 6, as *STEAP2* expression significantly increased in cells grown in CSS when compared to their androgen-replete counterparts. As *STEAP2* is involved in driving prostate cancer progression, clinically this increase would be concerning for the patient as ADT is commonly given as a first-line treatment approach (Burnell et al., 2018). These findings suggest that *AR* expression may have been restored, as *STEAP2* requires an intact *AR* (Korkmaz et al., 2002). Biochemical resurgence of androgen levels is indicative of a switch to CRPC, a more aggressive form of the disease in which high STEAP2 levels have been reported (Ylitalo *et al*., 2017).

Along with the expression of *AR*, androgen-regulated genes including *PSA*, *FKBP5, TMPRSS2* and *GPRC6A* have also been implicated in the development and progression of prostate cancer (Velasco *et al*., 2004; Yu *et al*., 2010; Zarif & Miranti, 2016). Throughout this thesis, the expression of these genes was assessed in response to anti-STEAP2 pAb treatment, CRISPR/Cas9 targeted *STEAP2* knockout and following growth in CSS-supplemented media in Chapters 4, 5 and 6 respectively. Following anti-STEAP2 pAb treatment, the expression of all four genes increased in C4-2B cells, whilst *PSA, FKBP5* and *GPRC6A* expression increased in a dose-dependent manner in LNCaP cells. In LNCaP^{KO} cells the expression of *PSA* and *FKBP5* increased significantly, whilst *TMPRSS2* was overexpressed in both LNCaP^{KO} and C4-2B^{KO} cells. Of these, *PSA* expression is of particular interest in prostate cancer research as it serves as both a diagnostic indicator of prostate cancer and is used to determine disease relapse following conventional therapy (Cornford *et al*., 2020; Lipianskaya *et al*., 2014; Scher *et al*., 2004). The observed increases in *PSA* expression following *STEAP2* inhibition could be the result of NFκB activity, which has also been found to correlate with *STEAP2* expression in LNCaP cells (Gonen-Korkmaz *et al*.,

2014; Kikuchi *et al*., 2003; Murillo *et al*., 2001). Previous studies have hypothesised that interleukin-6 activation through the EGF signalling pathway may also induce *PSA* overexpression, whilst increased *FKBP5* expression could be the result of histone acetylation through cAMP (Lin *et al*., 2001; Magee *et al*., 2006; Zhu & Kyprianou, 2008). *TMPRSS2* overexpression often correlates with the fusion of *TMPRSS2* with *ERG*, as *AR* overexpression can increase the proximity of the two genes (Hermans *et al*., 2006; Zong *et al*., 2009). *GPRC6A* is currently the only identified receptor of osteocalcin which is involved in the formation of bone metastases from primary prostate tumours and is thought to be overexpressed (Suva *et al*., 2011; Pi *et al*., 2016; Ye *et al*., 2017).

A major challenge still faced in cancer research is the identification of novel biomarkers which can be used in the development of treatment strategies in the clinical management of patients with advanced disease. In prostate cancer, such biomarkers could also aid in providing a more specific diagnosis, risk stratification and prognosis for patients, whilst also defining those who are more likely to benefit from certain therapies. Advances in immunotherapies such as the development of immune checkpoint inhibitors and drugs such as ipilumumab and Sipuleucel-T have allowed for more tailored clinical management strategies, with trials into the optimal treatment combinations and sequences still underway. However, appropriate targeted and specific therapies are still lacking for men with advanced prostate cancer. The findings of this thesis provide proof-of-concept that targeting STEAP2 with anti-STEAP2 antibodies or complete gene knockout may be a viable treatment approach. However, given the prevalence of men who develop CRPC, the androgen responses observed following anti-STEAP2 antibody treatment are concerning and warrant further investigations.

7.1 Future Perspectives

Whilst the data presented in this thesis highlights the potential of *STEAP2* as a target in the treatment of prostate cancer, further work is needed to confirm the hypotheses suggested. Various approaches were used to achieve *STEAP2* inhibition throughout this thesis, all of which triggered a reduction in prostate cancer cell viability, yet the mechanism behind this remains unclear (**Table 7.1**). Future studies should focus on assessing interactions between anti-STEAP2 antibodies and the DISC, TRAIL and the ACRATA to determine the exact mechanism through which anti-STEAP2 antibodies induce cell death. The expression of *AR* and androgen-regulated genes was highly upregulated in response to *STEAP2* inhibition in Chapters 4 and 5, and as such future studies should focus upon determining whether these increases are the result of interactions between signalling pathways involved in both *STEAP2* and *AR* expression. The observed increases in the four androgen-regulated genes following various methods of *STEAP2* inhibition warrant further investigations due to the potential negative impact this may pose for the patient, particularly with regards to disease progression and the development of CRPC. This would allow for the identification of novel therapeutic strategies which may be delivered alongside anti-STEAP2 antibody treatment, without the associated negative impact of increased *AR* expression. The data presented in this thesis would need to be confirmed by *in vivo* studies in future to further confirm *STEAP2* as a viable drug target for the clinical management of men with advanced prostate cancer.

The anti-STEAP2 monoclonal antibody lead candidate highlighted in this thesis, along with the successful knockout of CRISPR/Cas9 STEAP2 *in vitro,* provides three possible avenues of continued research to expand upon in the future:

1. Investigation of CRISPR/Cas9 STEAP2 knockout as therapeutic agent for reducing aggressive prostate cancer traits *in vivo.*

2. Development of ADC technology based on anti-STEAP2 monoclonal antibodies in combination with various linkers and payloads to increase the efficacy of reducing aggressive prostate cancer traits *in vitro* and *in vivo*.
3. Explore the effects mAb2 has on STEAP2 metalloreductase activity to determine whether STEAP2 function remains unaffected following mAb2 treatment.

Table 7.1. Summary of the *in vitro* findings that resulted from the knock-out of *STEAP2* and androgens in androgen-sensitive LNCaP and C4-2B prostate cancer cell lines. In this study, *STEAP2* was shown to be directly involved with influencing the viability, proliferation, migration and invasion of prostate cancer cells. *STEAP2* knock-out played a major role in the expression of *AR* and androgen-regulated genes. Androgen depletion decreased aggressive prostate cancer traits whilst increasing the expression of *STEAP2* and androgen-regulated genes. Dashed line indicates experiments that were not conducted.

Treatment approach →		Anti-STEAP2 polyclonal antibody		Anti-STEAP2 monoclonal antibody		CRISPR/Cas9 *STEAP2* knockout		Androgen depletion	
Influence of treatment →		Increase	Decrease	Increase	Decrease	Increase	Decrease	Increase	Decrease
Parameters measured	Viability		✓		✓		✓		✓
	Proliferation		✓		✓		✓	No change	No change
	Migration	-----	-----	------	------		✓		✓
	Invasion	-----	-----	------	------		✓		✓
Changes in gene expression	*AR*	✓		------	------	✓		------	------
	PSA	✓		------	------	✓		✓	
	FKBP5	✓		------	------	✓		✓	
	TMPRSS2	✓		------	------	✓		✓	
	GPRC6A	✓		------	------	✓		✓	
	STEAP2	------	------	------	------	------	------	✓	

7.2 Conclusion

STEAP2 shows promise as a potential novel therapeutic target due to its overexpression being specific to prostate cancer tissues, and low expression profile in other tissues. Within this thesis a fully optimised protocol for producing viable 3D prostate cancer cell spheroids was developed. This platform was carefully characterised and can be implemented in future studies to assess the efficacy of therapeutic targets in a model that is more physiologically representative. Mono- and polyclonal antibodies have shown potential in the treatment of various cancers, yet their use in prostate cancer is limited. The anti-STEAP2 mono- and polyclonal antibodies applied within this thesis which target the ECL3 of STEAP2 showed promise in reducing prostate cancer cell viability and proliferation *in vitro*. The anti-STEAP2 monoclonal antibody lead (mAb2) showed promise for further development with ADC technology due to its capability for triggering STEAP2 receptor internalisation in a panel of prostate cancer cell lines. These findings highlight the therapeutic value of antibody-based therapeutics targeting the ECL3 of STEAP2 based on the ability of both the anti-STEAP2 pAb and mAbs to induce cell death in prostate cancer cells. CRISPR/Cas9 technology was successfully optimised and developed to generate stable STEAP2-knockout LNCaP and C4-2B cells *in vitro*. This knockout further implicates STEAP2 as a potential therapeutic target as LNCaP^{KO} and C4-2B^{KO} exhibited reduced proliferation, migration and invasive potential compared to their wild-type counterparts. However, STEAP2 inhibition both via anti-STEAP2 antibody treatment and CRISPR/Cas9 knockout triggered an overexpression of *AR* and androgen-regulated genes, which warrants further investigations as clinically this finding could result in the onset of a more aggressive form of the disease; castrate resistant prostate cancer. Crosstalk between androgens and *STEAP2* was further suggested as *STEAP2* overexpression was observed in androgen-sensitive LNCaP and C4-2B cells, and *AR* expression increased following STEAP2-knockout. The *in vitro* findings of this thesis support STEAP2 as a viable therapeutic target for reducing aggressive prostate cancer traits. The data presented in this thesis provides rationale for future investigations into the pathways involved in regulating androgen responses to STEAP2 therapy.

Overall, STEAP2 could potentially provide a target for the development of more tailored and personalised therapeutic agents to improve the clinical management of men with aggressive prostate cancer.

Chapter 8

Bibliography

AAT Bioquest, Inc. (2020, November 16). *Quest Graph™ IC50 Calculator."*. Retrieved from https://www.aatbio.com/tools/ic50-calculator

Alaia, C., Boccellino, M., Zappavigna, S., Amler, E., Quagliuolo, L., Rossetti, S., ... & Caraglia, M. (2018). Ipilimumab for the treatment of metastatic prostate cancer. *Expert opinion on biological therapy*, *18*(2), 205-213.

Alexandre, C. (2005). Androgens and bone metabolism. *Joint Bone Spine*, *72*(3), 202-206.

Alves, P. M., Faure, O., Graff-Dubois, S., Cornet, S., Bolonakis, I., Gross, D. A., ... & Lemonnier, F. A. (2006). STEAP, a prostate tumor antigen, is a target of human CD8+ T cells. *Cancer Immunology, Immunotherapy*, *55*(12), 1515-1523.

Amzallag, N., Passer, B. J., Allanic, D., Segura, E., Théry, C., Goud, B., ... & Telerman, A. (2004). TSAP6 facilitates the secretion of translationally controlled tumor protein/histamine-releasing factor via a nonclassical pathway. *Journal of Biological Chemistry*, *279*(44), 46104-46112.

Anassi, E., & Ndefo, U. A. (2011). Sipuleucel-T (provenge) injection: the first immunotherapy agent (vaccine) for hormone-refractory prostate cancer. *Pharmacy and Therapeutics*, *36*(4), 197.

Arner, P., Stenson, B. M., Dungner, E., Näslund, E., Hoffstedt, J., Ryden, M., & Dahlman, I. (2008). Expression of six transmembrane protein of prostate 2 in human adipose tissue associates with adiposity and insulin resistance. *The Journal of Clinical Endocrinology & Metabolism*, *93*(6), 2249-2254.

Arsov, C., Winter, C., Rabenalt, R., & Albers, P. (2012). Current second-line treatment options for patients with castration resistant prostate cancer (CRPC) resistant to docetaxel. In *Urologic Oncology: Seminars and Original Investigations* (Vol. 30, No. 6, pp. 762-771). Elsevier.

Artandi, S. E., & DePinho, R. A. (2010). Telomeres and telomerase in cancer. *Carcinogenesis*, *31*(1), 9-18.

Askew, E. B., Gampe, R. T., Stanley, T. B., Faggart, J. L., & Wilson, E. M. (2007). Modulation of androgen receptor activation function 2 by testosterone and dihydrotestosterone. *Journal of Biological Chemistry*, *282*(35), 25801-25816.

Aslam, S., & Eisen, T. (2013). Vascular endothelial growth factor receptor tyrosine kinase inhibitors in metastatic renal cell cancer: latest results and clinical implications. *Therapeutic advances in medical oncology*, *5*(6), 324-333.

Baek, K. H., Hong, M. E., Jung, Y. Y., Lee, C. H., Lee, T. J., Park, E. S., ... & Lee, S. W. (2012). Correlation of AR, EGFR, and HER2 expression levels in prostate cancer: immunohistochemical analysis and chromogenic in situ hybridization. *Cancer research and treatment: official journal of Korean Cancer Association*, *44*(1), 50.

Bai, V. U., Cifuentes, E., Menon, M., Barrack, E. R., & Reddy, G. P. V. (2005). Androgen receptor regulates Cdc6 in synchronized LNCaP cells progressing from G1 to S phase. *Journal of cellular physiology*, *204*(2), 381-387.

Barber, L., Gerke, T., Markt, S. C., Peisch, S. F., Wilson, K. M., Ahearn, T., ... & Mucci, L. A. (2018). Family history of breast or prostate cancer and prostate cancer risk. *Clinical Cancer Research*, *24*(23), 5910-5917.

Barroca-Ferreira, J., Pais, J. P., Santos, M. M., Goncalves, A. M., Gomes, I. M., Sousa, I., ... & Maia, C. J. (2018). Targeting STEAP1 protein in human cancer: current trends and future challenges. *Current cancer drug targets*, *18*(3), 222-230.

Bartlett, J. M., Brawley, D., Grigor, K., Munro, A. F., Dunne, B., & Edwards, J. (2005). Type I receptor tyrosine kinases are associated with hormone escape in prostate cancer. *The Journal of Pathology: A Journal of the Pathological Society of Great Britain and Ireland*, *205*(4), 522-529.

Basch, E., Oliver, T. K., Vickers, A., Thompson, I., Kantoff, P., Parnes, H. & Nam, R. K. (2012). Screening for prostate cancer with prostate-specific antigen testing: American Society of Clinical Oncology Provisional Clinical Opinion. *Journal of Clinical Oncology*, *30*(24), 3020-3025.

Bastian, P. J., Palapattu, G. S., Yegnasubramanian, S., Rogers, C. G., Lin, X., Mangold, L. A., ... & Nelson, W. G. (2008). CpG island hypermethylation profile in the serum of men with clinically localized and hormone refractory metastatic prostate cancer. *The Journal of urology*, *179*(2), 529-535.

Bauer, D. E., Canver, M. C., & Orkin, S. H. (2015). Generation of genomic deletions in mammalian cell lines via CRISPR/Cas9. *JoVE (Journal of Visualized Experiments)*, (95), e52118.

Beck, A., Goetsch, L., Dumontet, C., & Corvaïa, N. (2017). Strategies and challenges for the next generation of antibody–drug conjugates. *Nature reviews Drug discovery*, *16*(5), 315-337.

Beer, T. M., Kwon, E. D., Drake, C. G., Fizazi, K., Logothetis, C., Gravis, G., ... & Piulats, J. M. (2017). Randomized, double-blind, phase III trial of ipilimumab versus placebo in asymptomatic or minimally symptomatic patients with metastatic chemotherapy-naive castration-resistant prostate cancer. *J Clin Oncol*, *35*(1), 40-47.

Ben-Kasus, T., Schechter, B., Lavi, S., Yarden, Y., & Sela, M. (2009). Persistent elimination of ErbB-2/HER2-overexpressing tumors using combinations of monoclonal antibodies: relevance of receptor endocytosis. *Proceedings of the national academy of sciences*, *106*(9), 3294-3299.

Bertoli, C., Skotheim, J. M., & De Bruin, R. A. (2013). Control of cell cycle transcription during G1 and S phases. *Nature reviews Molecular cell biology*, *14*(8), 518-528.

Bialk, P., Rivera-Torres, N., Strouse, B., & Kmiec, E. B. (2015). Regulation of gene editing activity directed by single-stranded oligonucleotides and CRISPR/Cas9 systems. *PLoS One*, *10*(6), e0129308.

Bill-Axelson, A., Holmberg, L., Garmo, H., Rider, J. R., Taari, K., Busch, C., ... & Andrén, O. (2014). Radical prostatectomy or watchful waiting in early prostate cancer. *New England Journal of Medicine*, *370*(10), 932-942.

Bolla, M., Henry, A., Mason, M., & Wiegel, T. (2019). The role of radiotherapy in localised and locally advanced prostate cancer. *Asian journal of urology*, *6*(2), 153-161.

Bonaccorsi, L., Carloni, V., Muratori, M., Formigli, L., Zecchi, S., Forti, G., & Baldi, E. (2004). EGF receptor (EGFR) signalling promoting invasion is disrupted in androgen-sensitive prostate cancer cells by an interaction between EGFR and androgen receptor (AR). *International journal of cancer*, *112*(1), 78-86.

Bonaccorsi, L., Carloni, V., Muratori, M., Salvadori, A., Giannini, A., Carini, M., ... & Baldi, E. (2000). Androgen receptor expression in prostate carcinoma cells suppresses α6β4 integrin-mediated invasive phenotype. *Endocrinology*, *141*(9), 3172-3182.

Bonaccorsi, L., Nosi, D., Muratori, M., Formigli, L., Forti, G., & Baldi, E. (2007). Altered endocytosis of epidermal growth factor receptor in androgen receptor positive prostate cancer cell lines. *Journal of molecular endocrinology*, *38*(1), 51-66.

Borra, R. C., Lotufo, M. A., Gagioti, S. M., Barros, F. D. M., & Andrade, P. M. (2009). A simple method to measure cell viability in proliferation and cytotoxicity assays. *Brazilian oral research*, *23*(3), 255-262.

Boutros, M., & Ahringer, J. (2008). The art and design of genetic screens: RNA interference. *Nature Reviews Genetics*, *9*(7), 554-566.

Brehmer, B., Biesterfeld, S., & Jakse, G. (2003). Expression of matrix metalloproteinases (MMP-2 and-9) and their inhibitors (TIMP-1 and-2) in prostate cancer tissue. *Prostate cancer and prostatic diseases*, *6*(3), 217-222.

Breslin, S., & O'Driscoll, L. (2016). The relevance of using 3D cell cultures, in addition to 2D monolayer cultures, when evaluating breast cancer drug sensitivity and resistance. *Oncotarget*, *7*(29), 45745.

Breslin, S., & O'Driscoll, L. (2013). Three-dimensional cell culture: the missing link in drug discovery. *Drug discovery today*, *18*(5-6), 240-249. *British Journal of Urology*, *124*(1), 9–26.

Brusnahan, S. K., McGuire, T. R., Jackson, J. D., Lane, J. T., Garvin, K. L., O'Kane, B. J., ... & Sharp, J. G. (2010). Human blood and marrow side population stem cell and Stro-1 positive bone marrow stromal cell numbers decline with age, with an increase in quality of surviving stem cells: correlation with cytokines. *Mechanisms of ageing and development*, *131*(11-12), 718-722.

Bubendorf, L., Schöpfer, A., Wagner, U., Sauter, G., Moch, H., Willi, N. & Mihatsch, M. J. (2000). Metastatic patterns of prostate cancer: an autopsy study of 1,589 patients. *Human pathology*, *31*(5), 578-583.

Buchanan, G., Irvine, R. A., Coetzee, G. A., & Tilley, W. D. (2002). Contribution of the androgen receptor to prostate cancer predisposition and progression. In *Prostate Cancer: New Horizons in Research and Treatment* (pp. 71-87). Springer, Boston, MA

Burnell, S. E., Spencer-Harty, S., Howarth, S., Bodger, O., Kynaston, H., Morgan, C., & Doak, S. H. (2018). STEAP2 knockdown reduces the invasive potential of prostate cancer cells. *Scientific reports*, *8*(1), 1-12.

Bystrom, L. M., Guzman, M. L., & Rivella, S. (2014). Iron and reactive oxygen species: friends or foes of cancer cells?. *Antioxidants & redox signalling*, *20*(12), 1917-1924.

Cabarkapa, S., Perera, M., McGrath, S., & Lawrentschuk, N. (2016). Prostate cancer screening with prostate-specific antigen: A guide to the guidelines. *Prostate international*, *4*(4), 125-129.

Cai, C., Portnoy, D. C., Wang, H., Jiang, X., Chen, S., & Balk, S. P. (2009). Androgen receptor expression in prostate cancer cells is suppressed by activation of epidermal growth factor receptor and ErbB2. *Cancer research*, *69*(12), 5202-5209.

Cai, C., Wang, H., Xu, Y., Chen, S., & Balk, S. P. (2009). Reactivation of Androgen Receptor–Regulated TMPRSS2: ERG Gene Expression in Castration-Resistant Prostate Cancer. *Cancer research*, *69*(15), 6027-6032.

Cancer Research UK (2015). About prostate cancer – a quick guide, Cancer Research UK.

Cancer Research UK. (2019). Cancer Statistics.

Cao, Z., West, C., Norton-Wenzel, C. S., Rej, R., Davis, F. B., Davis, P. J., & Rej, R. (2009). Effects of resin or charcoal treatment on foetal bovine serum and bovine calf serum. *Endocrine research*, *34*(4), 101-108.

Carter, H. B., Albertsen, P. C., Barry, M. J., Etzioni, R., Freedland, S. J., Greene, K. L. & Penson, D. F. (2013). Early detection of prostate cancer: AUA Guideline. *The Journal of urology*, *190*(2), 419-426.

Center, M. M., Jemal, A., Lortet-Tieulent, J., Ward, E., Ferlay, J., Brawley, O., & Bray, F. (2012). International variation in prostate cancer incidence and mortality rates. *European urology*, *61*(6), 1079-1092.

Challita-Eid, P. M., Morrison, K., Etessami, S., An, Z., Morrison, K. J., Perez-Villar, J. J., ... & Jakobovits, A. (2007). Monoclonal antibodies to six-transmembrane epithelial antigen of the prostate-1 inhibit intercellular communication in vitro and growth of human tumor xenografts in vivo. *Cancer Research*, *67*(12), 5798-5805.

Chan, S. C., Li, Y., & Dehm, S. M. (2012). Androgen receptor splice variants activate androgen receptor target genes and support aberrant prostate cancer cell growth independent of canonical androgen receptor nuclear localization signal. *Journal of Biological Chemistry*, *287*(23), 19736-19749.

Chang, K. H., Li, R., Kuri, B., Lotan, Y., Roehrborn, C. G., Liu, J., ... & Mirzaei, H. (2013). A gain-of-function mutation in DHT synthesis in castration-resistant prostate cancer. *Cell*, *154*(5), 1074-1084.

Charoen, K. M., Fallica, B., Colson, Y. L., Zaman, M. H., & Grinstaff, M. W. (2014). Embedded multicellular spheroids as a biomimetic 3D cancer model for evaluating drug and drug-device combinations. *Biomaterials*, *35*(7), 2264-2271.

Chen, H., Libertini, S. J., George, M., Dandekar, S., Tepper, C. G., Al-Bataina, B., ... & Mudryj, M. (2010). Genome-wide analysis of androgen receptor binding and gene regulation in two CWR22-derived prostate cancer cell lines. *Endocrine-related cancer*, *17*(4), 857.

Chen, M., Mao, A., Xu, M., Weng, Q., Mao, J., & Ji, J. (2019). CRISPR-Cas9 for cancer therapy: Opportunities and challenges. *Cancer letters*, *447*, 48-55.

Chen, N., & Zhou, Q. (2016). The evolving Gleason grading system. *Chinese Journal of Cancer Research*, *28*(1), 58.

Chen, R. C., Rosenman, J. G., Hoffman, L. G., Chiu, W. K., Wang, A. Z., Pruthi, R. S., ... & Godley, P. A. (2012). Phase I study of concurrent weekly docetaxel, high-dose intensity-modulated radiation therapy (IMRT) and androgen-deprivation therapy (ADT) for high-risk prostate cancer. *BJU international*, *110*(11b), E721-E726.

Chen, S., Sanjana, N. E., Zheng, K., Shalem, O., Lee, K., Shi, X. & Lee, H. (2015). Genome-wide CRISPR screen in a mouse model of tumor growth and metastasis. *Cell*, *160*(6), 1246-1260.

Chen, W., Yuan, Y., & Jiang, X. (2020). Antibody and antibody fragments for cancer immunotherapy. *Journal of Controlled Release*, *328*, 395-406.

Chen, X., Huang, Z., Zhou, B., Wang, H., Jia, G., Liu, G., & Zhao, H. (2014). STEAP4 and insulin resistance. *Endocrine*, *47*(2), 372-379.

Chlenski, A., Nakashiro, K. I., Ketels, K. V., Korovaitseva, G. I., & Oyasu, R. (2001). Androgen receptor expression in androgen-independent prostate cancer cell lines. *The Prostate*, *47*(1), 66-75.

Chopra, D. P., Menard, R. E., Januszewski, J., & Mattingly, R. R. (2004). TNF-α-mediated apoptosis in normal human prostate epithelial cells and tumor cell lines. *Cancer letters*, *203*(2), 145-154.

Chun, J. Y., Nadiminty, N., Dutt, S., Lou, W., Yang, J. C., Kung, H. J., ... & Gao, A. C. (2009). Interleukin-6 regulates androgen synthesis in prostate cancer cells. *Clinical Cancer Research*, *15*(15), 4815-4822.

Chung, L. W. (2003). Prostate carcinoma bone-stroma interaction and its biologic and therapeutic implications. *Cancer*, *97*(S3), 772-778.

Cinar, B., De Benedetti, A., & Freeman, M. R. (2005). Post-transcriptional regulation of the androgen receptor by Mammalian target of rapamycin. *Cancer research*, *65*(7), 2547-2553.

Clines, G. A., Mohammad, K. S., Bao, Y., Stephens, O. W., Suva, L. J., Shaughnessy Jr, J. D. & Guise, T. A. (2007). Dickkopf homolog 1 mediates endothelin-1-stimulated new bone formation. *Molecular endocrinology*, *21*(2), 486-498.

Cohen, R. J., Shannon, B. A., Phillips, M., Moorin, R. E., Wheeler, T. M., & Garrett, K. L. (2008). Central zone carcinoma of the prostate gland: a distinct tumor type with poor prognostic features. *The Journal of urology*, *179*(5), 1762-1767.

Cohen, S., Shoshana, O. Y., Zelman-Toister, E., Maharshak, N., Binsky-Ehrenreich, I., Gordin, M., ... & Leng, L. (2012). The cytokine midkine and its receptor RPTPζ regulate B cell survival in a pathway induced by CD74. *The Journal of Immunology*, *188*(1), 259-269.

Cong, L., Ran, F. A., Cox, D., Lin, S., Barretto, R., Habib, N. & Zhang, F. (2013). Multiplex genome engineering using CRISPR/Cas systems. *Science*, *339*(6121), 819-823.

Cook, L. M., Shay, G., Aruajo, A., & Lynch, C. C. (2014). Integrating new discoveries into the “vicious cycle” paradigm of prostate to bone metastases. *Cancer and Metastasis Reviews*, *33*(2-3), 511-525.

Cooper, C. R., Chay, C. H., Gendernalik, J. D., Lee, H. L., Bhatia, J., Taichman, R. S., ... & Pienta, K. J. (2003). Stromal factors involved in prostate carcinoma metastasis to bone. *Cancer: Interdisciplinary International Journal of the American Cancer Society*, *97*(S3), 739-747.

Cornford, P., van den Bergh, R. C., Briers, E., Van den Broeck, T., Cumberbatch, M. G., De Santis, M., ... & Grivas, N. (2020). EAU-EANM-ESTRO-ESUR-SIOG Guidelines on Prostate Cancer. Part II—2020 Update: Treatment of Relapsing and Metastatic Prostate Cancer. *European urology*.

Crawford, E. D., Bennett, C. L., Andriole, G. L., Garnick, M. B., & Petrylak, D. P. (2013). The utility of prostate-specific antigen in the management of advanced prostate cancer. *BJU international*, *112*(5), 548-560.

Crawford, E. D., Petrylak, D., & Sartor, O. (2017). Navigating the evolving therapeutic landscape in advanced prostate cancer. In *Urologic Oncology: Seminars and Original Investigations* (Vol. 35, pp. S1-S13). Elsevier.

Cunningham, D., & You, Z. (2015). In vitro and in vivo model systems used in prostate cancer research. *Journal of biological methods*, *2*(1).

Czekanska, E. M. (2011). Assessment of cell proliferation with resazurin-based fluorescent dye. In *Mammalian Cell Viability* (pp. 27-32). Humana Press.

D'Amico, A. V. (2014). US Food and Drug Administration approval of drugs for the treatment of prostate cancer: a new era has begun. *Journal of Clinical Oncology*, *32*(4), 362-364.

D'Amico, A. V., Whittington, R., Malkowicz, S. B., Schultz, D., Blank, K., Broderick, G. A. & Wein, A. (1998). Biochemical outcome after radical prostatectomy, external beam radiation therapy, or interstitial radiation therapy for clinically localized prostate cancer. *Jama*, *280*(11), 969-974.

D'Arcy, M. S. (2019). Cell death: a review of the major forms of apoptosis, necrosis and autophagy. *Cell biology international*, *43*(6), 582-592.

Dai, J., Hall, C. L., Escara-Wilke, J., Mizokami, A., Keller, J. M., & Keller, E. T. (2008). Prostate cancer induces bone metastasis through Wnt-induced bone morphogenetic protein-dependent and independent mechanisms. *Cancer research*, *68*(14), 5785-5794.

Daja, M. M., Niu, X., Zhao, Z., Brown, J. M., & Russell, P. J. (2003). Characterization of expression of matrix metalloproteinases and tissue inhibitors of metalloproteinases in prostate cancer cell lines. *Prostate cancer and prostatic diseases*, *6*(1), 15-26.

Dallas, S. L., Rosser, J. L., Mundy, G. R., & Bonewald, L. F. (2002). Proteolysis of latent transforming growth factor-β (TGF-β)-binding protein-1 by osteoclasts A cellular mechanism for release of TGF-β from bone matrix. *Journal of Biological Chemistry*, *277*(24), 21352-21360.

Das, T. P., Suman, S., & Damodaran, C. (2014). Induction of reactive oxygen species generation inhibits epithelial–mesenchymal transition and promotes growth arrest in prostate cancer cells. *Molecular carcinogenesis*, *53*(7), 537-547.

Dasgupta, S., Putluri, N., Long, W., Zhang, B., Wang, J., Kaushik, A. K., ... & Rajapakshe, K. (2015). Coactivator SRC-2–dependent metabolic reprogramming mediates prostate cancer survival and metastasis. *The Journal of clinical investigation*, *125*(3), 1174-1188.

Dasiram, J. D., Ganesan, R., Kannan, J., Kotteeswaran, V., & Sivalingam, N. (2017). Curcumin inhibits growth potential by G1 cell cycle arrest and induces apoptosis in p53-mutated COLO 320DM human colon adenocarcinoma cells. *Biomedicine & Pharmacotherapy*, *86*, 373-380.

Davey, R. A., & Grossmann, M. (2016). Androgen receptor structure, function and biology: from bench to bedside. *The Clinical Biochemist Reviews*, *37*(1), 3.

Davis, T. L., Cress, A. E., Dalkin, B. L., & Nagle, R. B. (2001). Unique expression pattern of the α6β4 integrin and laminin-5 in human prostate carcinoma. *The Prostate*, *46*(3), 240-248.

Daya, S., & Berns, K. I. (2008). Gene therapy using adeno-associated virus vectors. *Clinical microbiology reviews*, *21*(4), 583-593.

De Bono, J. S., Oudard, S., Ozguroglu, M., Hansen, S., Machiels, J. P., Kocak, I., ... & Roessner, M. (2010). Prednisone plus cabazitaxel or mitoxantrone for metastatic castration-resistant prostate cancer progressing after docetaxel treatment: a randomised open-label trial. *The Lancet*, *376*(9747), 1147-1154.

de Castro, I. P. (2019). Cell Metabolism in Cancer: An Energetic Switch. In *Molecular and Cell Biology of Cancer* (pp. 97-116). Springer, Cham.

De Mattia, F., Gubser, C., Van Dommelen, M. M., Visch, H. J., Distelmaier, F., Postigo, A., ... & Willems, P. H. (2009). Human Golgi antiapoptotic protein modulates intracellular calcium fluxes. *Molecular biology of the cell*, *20*(16), 3638-3645.

Dearnaley, D. P., Jovic, G., Syndikus, I., Khoo, V., Cowan, R. A., Graham, J. D., ... & Matthews, J. H. (2014). Escalated-dose versus control-dose conformal radiotherapy for prostate cancer: long-term results from the MRC RT01 randomised controlled trial. *The lancet oncology*, *15*(4), 464-473.

Deftos, L. J., Barken, I., Burton, D. W., Hoffman, R. M., & Geller, J. (2005). Direct evidence that PTHrP expression promotes prostate cancer progression in bone. *Biochemical and biophysical research communications*, *327*(2), 468-472.

Degenhardt, K., Mathew, R., Beaudoin, B., Bray, K., Anderson, D., Chen, G., ... & Nelson, D. A. (2006). Autophagy promotes tumor cell survival and restricts necrosis, inflammation, and tumorigenesis. *Cancer cell*, *10*(1), 51-64.

Dehm, S. M., & Tindall, D. J. (2005). Regulation of androgen receptor signalling in prostate cancer. *Expert review of anticancer therapy*, *5*(1), 63-74.

Dehm, S. M., & Tindall, D. J. (2006). Molecular regulation of androgen action in prostate cancer. *Journal of cellular biochemistry*, *99*(2), 333-344.

Dehm, S. M., & Tindall, D. J. (2007). Androgen receptor structural and functional elements: role and regulation in prostate cancer. *Molecular endocrinology*, *21*(12), 2855-2863.

Dehm, S. M., Schmidt, L. J., Heemers, H. V., Vessella, R. L., & Tindall, D. J. (2008). Splicing of a novel androgen receptor exon generates a constitutively active androgen receptor that mediates prostate cancer therapy resistance. *Cancer research*, *68*(13), 5469-5477.

Demarest, S. J., Hariharan, K., & Dong, J. (2011). Emerging antibody combinations in oncology. In *MAbs* (Vol. 3, No. 4, pp. 338-351). Taylor & Francis.

DeNardo, D. G., Andreu, P., & Coussens, L. M. (2010). Interactions between lymphocytes and myeloid cells regulate pro-versus anti-tumor immunity. *Cancer and Metastasis Reviews*, *29*(2), 309-316.

Dhillon, A. S., Hagan, S., Rath, O., & Kolch, W. (2007). MAP kinase signalling pathways in cancer. *Oncogene*, *26*(22), 3279-3290.

Dhondt, B., Geeurickx, E., Tulkens, J., Van Deun, J., Vergauwen, G., Lippens, L., ... & Lumen, N. (2020). Unravelling the proteomic landscape of extracellular vesicles in prostate cancer by density-based fractionation of urine. *Journal of extracellular vesicles*, *9*(1), 1736935.

Dhondt, B., Rousseau, Q., De Wever, O., & Hendrix, A. (2016). Function of extracellular vesicle-associated miRNAs in metastasis. *Cell and tissue research*, *365*(3), 621-641.

Di Lorenzo, G., Tortora, G., D'Armiento, F. P., De Rosa, G., Staibano, S., Autorino, R., ... & Bianco, A. R. (2002). Expression of epidermal growth factor receptor correlates with disease relapse and progression to androgen-independence in human prostate cancer. *Clinical Cancer Research*, *8*(11), 3438-3444.

Diamantis, N., & Banerji, U. (2016). Antibody-drug conjugates—an emerging class of cancer treatment. *British journal of cancer*, *114*(4), 362-367.

Dickens, L. S., Boyd, R. S., Jukes-Jones, R., Hughes, M. A., Robinson, G. L., Fairall, L., ... & MacFarlane, M. (2012). A death effector domain chain DISC model reveals a crucial role for caspase-8 chain assembly in mediating apoptotic cell death. *Molecular cell*, *47*(2), 291-305.

Donglai, L. V., Zongtao, H., Lin, L., Lu, H., & Xu, X. (2017). Three-dimensional cell culture: A powerful tool in tumor research and drug discovery. *Oncology letters*, *14*(6), 6999-7010.

Dorstyn, L., Akey, C. W., & Kumar, S. (2018). New insights into apoptosome structure and function. *Cell Death & Differentiation*, *25*(7), 1194-1208.

Doudna, J. A., & Charpentier, E. (2014). Genome editing. The new frontier of genome engineering with CRISPR-Cas9. Sci. 346, 1258096.

Dubrovska, A., Kim, S., Salamone, R. J., Walker, J. R., Maira, S. M., García-Echeverría, C., ... & Reddy, V. A. (2009). The role of PTEN/Akt/PI3K signalling in the maintenance and viability of prostate cancer stem-like cell populations. *Proceedings of the National Academy of Sciences*, *106*(1), 268-273.

Duval, K., Grover, H., Han, L. H., Mou, Y., Pegoraro, A. F., Fredberg, J., & Chen, Z. (2017). Modeling physiological events in 2D vs. 3D cell culture. *Physiology*, *32*(4), 266-277.

Dvir-Ginzberg, M., Gamlieli-Bonshtein, I., Agbaria, R., & Cohen, S. (2003). Liver tissue engineering within alginate scaffolds: effects of cell-seeding density on hepatocyte viability, morphology, and function. *Tissue engineering*, *9*(4), 757-766.

Ebrahem, Q., Chaurasia, S. S., Vasanji, A., Qi, J. H., Klenotic, P. A., Cutler, A., ... & Anand-Apte, B. (2010). Crosstalk between vascular endothelial growth factor and matrix metalloproteinases in the induction of neovascularization in vivo. *The American journal of pathology*, *176*(1), 496-503.

Edlund, M., Sung, S. Y., & Chung, L. W. (2004). Modulation of prostate cancer growth in bone microenvironments. *Journal of cellular biochemistry*, *91*(4), 686-705.

Edmondson, R., Broglie, J. J., Adcock, A. F., & Yang, L. (2014). Three-dimensional cell culture systems and their applications in drug discovery and cell-based biosensors. *Assay and drug development technologies*, *12*(4), 207-218.

Erdogan, S., Turkekul, K., Dibirdik, I., Doganlar, O., Doganlar, Z. B., Bilir, A., & Oktem, G. (2018). Midkine downregulation increases the efficacy of quercetin on prostate cancer stem cell survival and migration through PI3K/AKT and MAPK/ERK pathway. *Biomedicine & Pharmacotherapy*, *107*, 793-805.

Fares, J., Fares, M. Y., Khachfe, H. H., Salhab, H. A., & Fares, Y. (2020). Molecular principles of metastasis: a hallmark of cancer revisited. *Signal transduction and targeted therapy*, *5*(1), 1-17.

Farhat, A., Jiang, D., Cui, D., Keller, E. T., & Jackson, T. L. (2017). An integrative model of prostate cancer interaction with the bone microenvironment. *Mathematical biosciences*, *294*, 1-14.

Febbo, P. G., Lowenberg, M., Thorner, A. R., Brown, M., Loda, M., & Golub, T. R. (2005). Androgen mediated regulation and functional implications of fkbp51 expression in prostate cancer. *The Journal of urology*, *173*(5), 1772-1777.

Ferlay, J., Soerjomataram, I., Dikshit, R., Eser, S., Mathers, C., Rebelo, M., ... & Bray, F. (2015). Cancer incidence and mortality worldwide: sources, methods and major patterns in GLOBOCAN 2012. *International journal of cancer*, *136*(5), E359-E386.

Fiandalo, M. V., Wilton, J. H., Mantione, K. M., Wrzosek, C., Attwood, K. M., Wu, Y., & Mohler, J. L. (2018). Serum-free complete medium, an alternative medium to mimic androgen deprivation in human prostate cancer cell line models. *The Prostate*, *78*(3), 213-221.

Ficarra, V., Novara, G., Rosen, R. C., Artibani, W., Carroll, P. R., Costello, A., ... & Van der Poel, H. (2012). Systematic review and meta-analysis of studies reporting urinary continence recovery after robot-assisted radical prostatectomy. *European urology*, *62*(3), 405-417.

Fine, S. W., & Reuter, V. E. (2012). Anatomy of the prostate revisited: implications for prostate biopsy and zonal origins of prostate cancer. *Histopathology*, *60*(1), 142-152.

Fitter, S., Gronthos, S., Ooi, S. S., & Zannettino, A. C. (2017). The mesenchymal precursor cell marker antibody STRO-1 binds to cell surface heat shock cognate 70. *Stem Cells*, *35*(4), 940-951.

Flavahan, W. A., Gaskell, E., & Bernstein, B. E. (2017). Epigenetic plasticity and the hallmarks of cancer. *Science*, *357*(6348).

Flint, M., McAlister, D. A., Agarwal, A., & du Plessis, S. S. (2015). Male accessory sex glands: Structure and function. In *Mammalian Endocrinology and Male Reproductive Biology* (pp. 245-257). CRC Press.

Florczyk, S. J., Liu, G., Kievit, F. M., Lewis, A. M., Wu, J. D., & Zhang, M. (2012). 3D porous chitosan–alginate scaffolds: a new matrix for studying prostate cancer cell–lymphocyte interactions in vitro. *Advanced healthcare materials*, *1*(5), 590-599.

Fong, E. L., Martinez, M., Yang, J., Mikos, A. G., Navone, N. M., Harrington, D. A., & Farach-Carson, M. C. (2014). Hydrogel-based 3D model of patient-derived prostate xenograft tumors suitable for drug screening. *Molecular pharmaceutics*, *11*(7), 2040-2050.

Fong, E. L., Wan, X., Yang, J., Morgado, M., Mikos, A. G., Harrington, D. A. & Farach-Carson, M. C. (2016). A 3D in vitro model of patient-derived prostate cancer xenograft for controlled interrogation of in vivo tumor-stromal interactions. *Biomaterials*, *77*, 164-172.

Franco, O. E., Onishi, T., Yamakawa, K., Arima, K., Yanagawa, M., Sugimura, Y., & Kawamura, J. (2003). Mitogen-activated protein kinase pathway is involved in androgen-independent PSA gene expression in LNCaP cells. *The Prostate*, *56*(4), 319-325.

Friedrich, J., Ebner, R., & Kunz-Schughart, L. A. (2007). Experimental anti-tumor therapy in 3-D: spheroids–old hat or new challenge?. *International journal of radiation biology*, *83*(11-12), 849-871.

Friedrich, J., Seidel, C., Ebner, R., & Kunz-Schughart, L. A. (2009). Spheroid-based drug screen: considerations and practical approach. *Nature protocols*, *4*(3), 309-324.

Gao, J., Ward, J. F., Pettaway, C. A., Shi, L. Z., Subudhi, S. K., Vence, L. M., ... & Troncoso, P. (2017). VISTA is an inhibitory immune checkpoint that is increased after ipilimumab therapy in patients with prostate cancer. *Nature medicine*, *23*(5), 551.

Gialeli, C., Theocharis, A. D., & Karamanos, N. K. (2011). Roles of matrix metalloproteinases in cancer progression and their pharmacological targeting. *The FEBS journal*, *278*(1), 16-27.

Giuliano, C. J., Lin, A., Girish, V., & Sheltzer, J. M. (2019). Generating single cell–derived knockout clones in mammalian cells with CRISPR/Cas9. *Current protocols in molecular biology*, *128*(1).

Glass, Z., Lee, M., Li, Y., & Xu, Q. (2018). Engineering the delivery system for CRISPR-based genome editing. *Trends in biotechnology*, *36*(2), 173-185.

Glick, D., Barth, S., & Macleod, K. F. (2010). Autophagy: cellular and molecular mechanisms. *The Journal of pathology*, *221*(1), 3-12.

Goldstein, A. S., Huang, J., Guo, C., Garraway, I. P., & Witte, O. N. (2010). Identification of a cell of origin for human prostate cancer. *Science*, *329*(5991), 568-571.

Gomes, A., Guillaume, L., Grimes, D. R., Fehrenbach, J., Lobjois, V., & Ducommun, B. (2016). Oxygen partial pressure is a rate-limiting parameter for cell proliferation in 3D spheroids grown in physioxic culture condition. *PloS one*, *11*(8).

Gomes, I. M., Arinto, P., Lopes, C., Santos, C. R., & Maia, C. J. (2014). STEAP1 is overexpressed in prostate cancer and prostatic intraepithelial neoplasia lesions, and it is positively associated with Gleason score. In *Urologic Oncology: Seminars and Original Investigations* (Vol. 32, No. 1, pp. 53-e23). Elsevier.

Gomes, I. M., Maia, C. J., & Santos, C. R. (2012). STEAP proteins: from structure to applications in cancer therapy. *Molecular Cancer Research*, *10*(5), 573-587.

Gomes, I. M., Santos, C. R., & Maia, C. J. (2014). Expression of STEAP1 and STEAP1B in prostate cell lines, and the putative regulation of STEAP1 by post-transcriptional and post-translational mechanisms. *Genes & cancer*, *5*(3-4), 142.

Gonen-Korkmaz, C., Sevin, G., Gokce, G., Zuhuri Arun, M., Yıldırım, G., Reel, B., ... & Ogut, D. (2014). Analysis of tumor necrosis factor α-induced and nuclear factor κB-silenced LNCaP prostate cancer cells by RT-qPCR. *Experimental and therapeutic medicine*, *8*(6), 1695-1700.

Gong, X., Lin, C., Cheng, J., Su, J., Zhao, H., Liu, T., ... & Zhao, P. (2015). Generation of multicellular tumor spheroids with microwell-based agarose scaffolds for drug testing. *PloS one*, *10*(6).

Gong, Y., Chippada-Venkata, U. D., & Oh, W. K. (2014). Roles of matrix metalloproteinases and their natural inhibitors in prostate cancer progression. *Cancers*, *6*(3), 1298-1327.

Graham, J., Kirkbride, P., Cann, K., Hasler, E., & Prettyjohns, M. (2014). Prostate cancer: summary of updated NICE guidance. *BMJ*, *348*, f7524.

Granchi, S., Brocchi, S., Bonaccorsi, L., Baldi, E., Vinci, M. C., Forti, G. & Maggi, M. (2001). Endothelin-1 production by prostate cancer cell lines is up-regulated by factors involved in cancer progression and down-regulated by androgens. *The Prostate*, *49*(4), 267-277.

Gravdal, K., Halvorsen, O. J., Haukaas, S. A., & Akslen, L. A. (2007). A switch from E-cadherin to N-cadherin expression indicates epithelial to mesenchymal transition and is of strong and independent importance for the progress of prostate cancer. *Clinical cancer research*, *13*(23), 7003-7011.

Gregory, C. W., Fei, X., Ponguta, L. A., He, B., Bill, H. M., French, F. S., & Wilson, E. M. (2004). Epidermal growth factor increases coactivation of the androgen receptor in recurrent prostate cancer. *Journal of Biological Chemistry*, *279*(8), 7119-7130.

Greiner, A., Richter, B., & Bastmeyer, M. (2012). Micro-Engineered 3D Scaffolds for Cell Culture Studies. *Macromolecular Bioscience*, *12*(10), 1301-1314.

Grivennikov, S. I., Greten, F. R., & Karin, M. (2010). Immunity, inflammation, and cancer. *Cell*, *140*(6), 883-899.

Grunewald, T. G. P., Ranft, A., Esposito, I., da Silva-Buttkus, P., Aichler, M., Baumhoer, D., ... & Jürgens, H. (2012). High STEAP1 expression is associated with improved outcome of Ewing's sarcoma patients. *Annals of oncology*, *23*(8), 2185-2190.

Grunewald, T. G., Bach, H., Cossarizza, A., & Matsumoto, I. (2012). The STEAP protein family: versatile oxidoreductases and targets for cancer immunotherapy with overlapping and distinct cellular functions. *Biology of the Cell*, *104*(11), 641-657.

Guo, T., Xin, Y., Zhang, Y., Gu, X., & Kong, J. (2019). A rapid and versatile tool for genomic engineering in Lactococcus lactis. *Microbial cell factories*, *18*(1), 22.

Guo, Z., Dai, B., Jiang, T., Xu, K., Xie, Y., Kim, O., ... & Njar, V. C. (2006). Regulation of androgen receptor activity by tyrosine phosphorylation. *Cancer cell*, *10*(4), 309-319.

Guo, Z., Yang, X., Sun, F., Jiang, R., Linn, D. E., Chen, H., ... & Kung, H. J. (2009). A novel androgen receptor splice variant is up-regulated during prostate cancer progression and promotes androgen depletion–resistant growth. *Cancer research*, *69*(6), 2305-2313.

Haglind, E., Carlsson, S., Stranne, J., Wallerstedt, A., Wilderäng, U., Thorsteinsdottir, T., ... & Wiklund, P. (2015). Urinary incontinence and erectile dysfunction after robotic versus open radical prostatectomy: a prospective, controlled, nonrandomised trial. *European urology*, *68*(2), 216-225.

Hahn, J., Xiao, W., Jiang, F., Simone, F., Thirman, M. J., & Wang, Z. (2007). Apoptosis induction and growth suppression by U19/Eaf2 is mediated through its ELL-binding domain. *The Prostate*, *67*(2), 146-153.

Hall, C. L., Daignault, S. D., Shah, R. B., Pienta, K. J., & Keller, E. T. (2008). Dickkopf-1 expression increases early in prostate cancer development and decreases during progression from primary tumor to metastasis. *The Prostate*, *68*(13), 1396-1404.

Hamdy, F. C., Donovan, J. L., Lane, J., Mason, M., Metcalfe, C., Holding, P., ... & Oxley, J. (2016). 10-year outcomes after monitoring, surgery, or radiotherapy for localized prostate cancer. *N Engl J Med*, *375*, 1415-1424.

Han, G., Buchanan, G., Ittmann, M., Harris, J. M., Yu, X., DeMayo, F. J., ... & Greenberg, N. M. (2005). Mutation of the androgen receptor causes oncogenic transformation of the prostate. *Proceedings of the National Academy of Sciences*, *102*(4), 1151-1156.

Han, M., Xu, R., Wang, S., Yang, N., Ni, S., Zhang, Q., ... & Ji, J. (2018). Six-transmembrane epithelial antigen of prostate 3 predicts poor prognosis and promotes glioblastoma growth and invasion. *Neoplasia*, *20*(6), 543-554.

Hanahan, D., & Weinberg, R. A. (2000). The hallmarks of cancer. *cell*, *100*(1), 57-70.

Hanahan, D., & Weinberg, R. A. (2011). Hallmarks of cancer: the next generation. *cell*, *144*(5), 646-674.

Hansen-Bruhn, M., de Ávila, B. E. F., Beltrán-Gastélum, M., Zhao, J., Ramírez-Herrera, D. E., Angsantikul, P., ... & Wang, J. (2018). Active Intracellular Delivery of a Cas9/sgRNA Complex Using Ultrasound-Propelled Nanomotors. *Angewandte Chemie International Edition*, *57*(10), 2657-2661.

Harada, S., Keller, E. T., Fujimoto, N., Koshida, K., Namiki, M., Matsumoto, T., & Mizokami, A. (2001). Long-term exposure of tumor necrosis factor α causes hypersensitivity to androgen and anti-androgen withdrawal phenomenon in LNCaP prostate cancer cells. *The Prostate*, *46*(4), 319-326.

Härmä, V., Virtanen, J., Mäkelä, R., Happonen, A., Mpindi, J. P., Knuuttila, M., ... & Nees, M. (2010). A comprehensive panel of three-dimensional models for studies of prostate cancer growth, invasion and drug responses. *PloS one*, *5*(5).

Harris, W. P., Mostaghel, E. A., Nelson, P. S., & Montgomery, B. (2009). Androgen deprivation therapy: progress in understanding mechanisms of resistance and optimizing androgen depletion. *Nature clinical practice Urology*, *6*(2), 76-85.

Harrison, R. G., Greenman, M. J., Mall, F. P., & Jackson, C. M. (1907). Observations of the living developing nerve fiber. *The Anatomical Record*, *1*(5), 116-128.

Hasegawa, H., Li, C., Alba, B. M., Penny, D. M., Xia, Z., Dayao, M. R., ... & Murawsky, C. M. (2018). Membrane cholesterol modulates STEAP2 conformation during dynamic intracellular trafficking processes leading to broad subcellular distribution. *Experimental cell research*, *370*(2), 208-226.

Hashimoto, K., Tabata, H., Shindo, T., Tanaka, T., Hashimoto, J., Inoue, R., ... & Takahashi, A. (2019). Serum testosterone level is a useful biomarker for determining the optimal treatment for castration-resistant prostate cancer. In *Urologic Oncology: Seminars and Original Investigations* (Vol. 37, No. 7, pp. 485-491). Elsevier.

Hazan, R. B., Qiao, R. U. I., Keren, R., Badano, I., & Suyama, K. (2004). Cadherin switch in tumor progression. *Annals of the New York Academy of Sciences*, *1014*(1), 155-163.

Heidenreich, A., Varga, Z., & Von Knobloch, R. (2002). Extended pelvic lymphadenectomy in patients undergoing radical prostatectomy: high incidence of lymph node metastasis. *The Journal of urology*, *167*(4), 1681-1686.

Heinlein, C. A., & Chang, C. (2004). Androgen receptor in prostate cancer. *Endocrine reviews*, *25*(2), 276-308.

Helgstrand, J. T., Røder, M. A., Klemann, N., Toft, B. G., Brasso, K., Vainer, B., & Iversen, P. (2017). Diagnostic characteristics of lethal prostate cancer. *European Journal of Cancer*, *84*, 18-26.

Hensel, J., & Thalmann, G. N. (2016). Biology of bone metastases in prostate cancer. *Urology*, *92*, 6-13.

Herai, R. H. (2019). Avoiding the off-target effects of CRISPR/cas9 system is still a challenging accomplishment for genetic transformation. *Gene*, *700*, 176-178.

Herbst, R. S., & Khuri, F. R. (2003). Mode of action of docetaxel–a basis for combination with novel anticancer agents. *Cancer treatment reviews*, *29*(5), 407-415.

Hermans, K. G., Van Marion, R., Van Dekken, H., Jenster, G., Van Weerden, W. M., & Trapman, J. (2006). TMPRSS2: ERG fusion by translocation or interstitial deletion is highly relevant in androgen-dependent prostate cancer, but is bypassed in late-stage androgen receptor–negative prostate cancer. *Cancer research*, *66*(22), 10658-10663.

Hirschhaeuser, F., Menne, H., Dittfeld, C., West, J., Mueller-Klieser, W., & Kunz-Schughart, L. (2010). Multicellular tumor spheroids: An underestimated tool is catching up again. *Journal of Biotechnology*, *148*(1), 3-15.

Hodgkins, A., Farne, A., Perera, S., Grego, T., Parry-Smith, D. J., Skarnes, W. C., & Iyer, V. (2015). WGE: a CRISPR database for genome engineering. *Bioinformatics*, *31*(18), 3078-3080.

Hoogsteen, I. J., Marres, H. A., Wijffels, K. I., Rijken, P. F., Peters, J. P., van den Hoogen, F. J., ... & Kaanders, J. H. (2005). Colocalization of carbonic anhydrase 9 expression and cell proliferation in human head and neck squamous cell carcinoma. *Clinical cancer research*, *11*(1), 97-106.

Hossain, M. K., Nahar, K., Donkor, O., & Apostolopoulos, V. (2018). Immune-based therapies for metastatic prostate cancer: an update. *Immunotherapy*, *10*(4), 283-298.

Hsiao, A. Y., Torisawa, Y. S., Tung, Y. C., Sud, S., Taichman, R. S., Pienta, K. J., & Takayama, S. (2009). Microfluidic system for formation of PC-3 prostate cancer co-culture spheroids. *Biomaterials*, *30*(16), 3020-3027.

Hsu, P. D., Lander, E. S., & Zhang, F. (2014). Development and applications of CRISPR-Cas9 for genome engineering. *Cell*, *157*(6), 1262-1278.

Hu, R., Dunn, T. A., Wei, S., Isharwal, S., Veltri, R. W., Humphreys, E., ... & Bova, G. S. (2009). Ligand-independent androgen receptor variants derived from splicing of cryptic exons signify hormone-refractory prostate cancer. *Cancer research*, *69*(1), 16-22.

Huang, K., Yang, C., Wang, Q. X., Li, Y. S., Fang, C., Tan, Y. L., ... & Zhou, B. C. (2017). The CRISPR/Cas9 system targeting EGFR exon 17 abrogates NF-κB activation via epigenetic modulation of UBXN1 in EGFRwt/vIII glioma cells. *Cancer letters*, *388*, 269-280.

Huang, X., Ding, L., Bennewith, K. L., Tong, R. T., Welford, S. M., Ang, K. K., ... & Giaccia, A. J. (2009). Hypoxia-inducible mir-210 regulates normoxic gene expression involved in tumor initiation. *Molecular cell*, *35*(6), 856-867.

Hubert, R. S., Vivanco, I., Chen, E., Rastegar, S., Leong, K., Mitchell, S. C., ... & Jakobovits, A. (1999). STEAP: a prostate-specific cell-surface antigen highly expressed in human prostate tumors. *Proceedings of the National Academy of Sciences*, *96*(25), 14523-14528.

Humphrey, P. A. (2004). Gleason grading and prognostic factors in carcinoma of the prostate. *Modern pathology*, *17*(3), 292-306.

Hurrell, T., Ellero, A. A., Masso, Z. F., & Cromarty, A. D. (2018). Characterization and reproducibility of HepG2 hanging drop spheroids toxicology in vitro. *Toxicology in Vitro*, *50*, 86-94.

Huynh, M. J., & Pautler, S. E. (2018). A clinical perspective on the application of surgical robotics for radical prostatectomy. *Encyclopedia Of Medical Robotics, The (In 4 Volumes)*, 29.

Hwang, J. H., Seo, J. H., Beshiri, M. L., Wankowicz, S., Liu, D., Cheung, A., ... & Golumb, L. (2019). CREB5 Promotes Resistance to Androgen-Receptor Antagonists and Androgen Deprivation in Prostate Cancer. *Cell reports*, *29*(8), 2355-2370.

Ibrahim, T., Flamini, E., Mercatali, L., Sacanna, E., Serra, P., & Amadori, D. (2010). Pathogenesis of osteoblastic bone metastases from prostate cancer. *Cancer*, *116*(6), 1406-1418.

Ingram, M., Techy, G. B., Saroufeem, R., Yazan, O., Narayan, K. S., Goodwin, T. J., & Spaulding, G. F. (1997). Three-dimensional growth patterns of various human tumor cell lines in simulated microgravity of a NASA bioreactor. *In Vitro Cellular & Developmental Biology-Animal*, *33*(6), 459-466.

Inman, C. K., & Shore, P. (2003). The osteoblast transcription factor Runx2 is expressed in mammary epithelial cells and mediates osteopontin expression. *Journal of Biological Chemistry*, *278*(49), 48684-48689.

Inoue, A., Matsumoto, I., Tanaka, Y., Iwanami, K., Kanamori, A., Ochiai, N., ... & Sumida, T. (2009). Tumor necrosis factor α-induced adipose-related protein expression in experimental arthritis and in rheumatoid arthritis. *Arthritis research & therapy*, *11*(4), R118.

Ivan, M., & Huang, X. (2014). miR-210: fine-tuning the hypoxic response. In *Tumor Microenvironment and Cellular Stress* (pp. 205-227). Springer, New York, NY.

Jaaskelainen, J., Deeb, A., Schwabe, J. W., Mongan, N. P., Martin, H., & Hughes, I. A. (2006). Human androgen receptor gene ligand-binding-domain mutations leading to disrupted interaction between the N-and C-terminal domains. *Journal of molecular endocrinology*, *36*(2), 361-368.

James, N. D., Sydes, M. R., Clarke, N. W., Mason, M. D., Dearnaley, D. P., Spears, M. R., ... & de Bono, J. (2016). Addition of docetaxel, zoledronic acid, or both to first-line long-term hormone therapy in prostate cancer (STAMPEDE): survival results from an adaptive, multiarm, multistage, platform randomised controlled trial. *The Lancet*, *387*(10024), 1163-1177.

Jia, S., Gao, X., Lee, S. H., Maira, S. M., Wu, X., Stack, E. C., ... & Roberts, T. M. (2013). Opposing effects of androgen deprivation and targeted therapy on prostate cancer prevention. *Cancer discovery*, *3*(1), 44-51.

Jiang, B. H., & Liu, L. Z. (2009). PI3K/PTEN signalling in angiogenesis and tumorigenesis. *Advances in cancer research*, *102*, 19-65.

Jiang, F., & Doudna, J. A. (2017). CRISPR–Cas9 structures and mechanisms. *Annual review of biophysics*, *46*, 505-529.

Jilg, C. A., Ketscher, A., Metzger, E., Hummel, B., Willmann, D., Rüsseler, V., ... & Hölz, S. (2014). PRK1/PKN1 controls migration and metastasis of androgen-independent prostate cancer cells. *Oncotarget*, *5*(24), 12646.

Jin, Y., Wang, L., Qu, S., Sheng, X., Kristian, A., Mælandsmo, G. M., ... & Alpay, N. (2015). STAMP2 increases oxidative stress and is critical for prostate cancer. *EMBO molecular medicine*, *7*(3), 315-331.

Jinek, M., Chylinski, K., Fonfara, I., Hauer, M., Doudna, J. A., & Charpentier, E. (2012). A programmable dual-RNA–guided DNA endonuclease in adaptive bacterial immunity. *Science*, *337*(6096), 816-821.

Johns, L. E., & Houlston, R. S. (2003). A systematic review and meta-analysis of familial prostate cancer risk. *BJU international*, *91*(9), 789-794.

Jørgensen, N. R., Teilmann, S. C., Henriksen, Z., Civitelli, R., Sørensen, O. H., & Steinberg, T. H. (2003). Activation of L-type calcium channels is required for gap junction-mediated intercellular calcium signalling in osteoblastic cells. *Journal of Biological Chemistry*, *278*(6), 4082-4086.

Jung, M., Mertens, C., Tomat, E., & Brüne, B. (2019). Iron as a central player and promising target in cancer progression. *International Journal of Molecular Sciences*, *20*(2), 273

Kaarbø, M., Klokk, T. I., & Saatcioglu, F. (2007). Androgen signalling and its interactions with other signalling pathways in prostate cancer. *Bioessays*, *29*(12), 1227-1238.

Kamath, A. V., & Iyer, S. (2015). Preclinical pharmacokinetic considerations for the development of antibody drug conjugates. *Pharmaceutical research*, *32*(11), 3470-3479.

Kang, Z., Jänne, O. A., & Palvimo, J. J. (2004). Coregulator recruitment and histone modifications in transcriptional regulation by the androgen receptor. *Molecular Endocrinology*, *18*(11), 2633-2648.

Kantoff, P. W., Higano, C. S., Shore, N. D., Berger, E. R., Small, E. J., Penson, D. F., ... & Xu, Y. (2010). Sipuleucel-T immunotherapy for castration-resistant prostate cancer. *New England Journal of Medicine*, *363*(5), 411-422.

Karantanos, T., Evans, C. P., Tombal, B., Thompson, T. C., Montironi, R., & Isaacs, W. B. (2015). Understanding the mechanisms of androgen deprivation resistance in prostate cancer at the molecular level. *European urology*, *67*(3), 470-479.

Karsenty, G., Kronenberg, H. M., & Settembre, C. (2009). Genetic control of bone formation. *Annual Review of Cell and Developmental*, *25*, 629-648.

Kelly, M. M., Hoel, B. D., & Voelkel-Johnson, C. (2002). Doxorubicin pretreatment sensitizes prostate cancer cell lines to TRAIL induced apoptosis which correlates with the loss of c-FLIP expression. *Cancer biology & therapy*, *1*(5), 520-527.

Kenny, P. A., Lee, G. Y., Myers, C. A., Neve, R. M., Semeiks, J. R., Spellman, P. T., ... & Gray, J. W. (2007). The morphologies of breast cancer cell lines in three-dimensional assays correlate with their profiles of gene expression. *Molecular oncology*, *1*(1), 84-96.

Kepp, O., Galluzzi, L., Lipinski, M., Yuan, J., & Kroemer, G. (2011). Cell death assays for drug discovery. *Nature reviews Drug discovery*, *10*(3), 221-237.

Khaitan, D., & Dwarakanath, B. S. (2006). Multicellular spheroids as an in vitro model in experimental oncology: applications in translational medicine. *Expert opinion on drug discovery*, *1*(7), 663-675.

Khera, E., Cilliers, C., Bhatnagar, S., & Thurber, G. M. (2018). Computational transport analysis of antibody-drug conjugate bystander effects and payload tumoral distribution: implications for therapy. *Molecular Systems Design & Engineering*, *3*(1), 73-88.

Kicinski, M., Vangronsveld, J., & Nawrot, T. S. (2011). An epidemiological reappraisal of the familial aggregation of prostate cancer: a meta-analysis. *PloS one*, *6*(10), e27130.

Kikuchi, E., Horiguchi, Y., Nakashima, J., Kuroda, K., Oya, M., Ohigashi, T., ... & Murai, M. (2003). Suppression of hormone-refractory prostate cancer by a novel nuclear factor κB inhibitor in nude mice. *Cancer Research*, *63*(1), 107-110.

Kim, S., Kim, D., Cho, S. W., Kim, J., & Kim, J. S. (2014). Highly efficient RNA-guided genome editing in human cells via delivery of purified Cas9 ribonucleoproteins. *Genome research*, *24*(6), 1012-1019.

Kim, Y., Ahn, B., Na, Y., Shin, T., Rha, K., & Kim, J. (2014). Digital rectal examination in a simulated environment using sweeping palpation and mechanical localization. *International journal of precision engineering and manufacturing*, *15*(1), 169-175.

Kirby, M., Hirst, C., & Crawford, E. D. (2011). Characterising the castration-resistant prostate cancer population: a systematic review. *International journal of clinical practice*, *65*(11), 1180-1192.

Kitagawa, Y., Mizokami, A., & Namiki, M. (2013). Trends of clinical symptoms and prognosis of middle-aged prostate cancer patients after instigation of prostate specific antigen-based population screening. *Prostate international*, *1*(2), 65-68.

Klein, M., Eslami-Mossallam, B., Arroyo, D. G., & Depken, M. (2018). Hybridization kinetics explains CRISPR-Cas off-targeting rules. *Cell reports*, *22*(6), 1413-1423.

Knerr, K., Ackermann, K., Neidhart, T., & Pyerin, W. (2004). Bone metastasis: Osteoblasts affect growth and adhesion regulons in prostate tumor cells and provoke osteomimicry. *International journal of cancer*, *111*(1), 152-159.

Knutson, M. D. (2007). Steap proteins: implications for iron and copper metabolism. *Nutrition reviews*, *65*(7), 335-340.

Kole, L., Sarkar, M., Deb, A., & Giri, B. (2016). Pioglitazone, an anti-diabetic drug requires sustained MAPK activation for its anti-tumor activity in MCF7 breast cancer cells, independent of PPAR-γ pathway. *Pharmacological Reports*, *68*(1), 144-154.

Korkmaz, C. G., Korkmaz, K. S., Kurys, P., Elbi, C., Wang, L., Klokk, T. I., ... & Saatcioglu, F. (2005). Molecular cloning and characterization of STAMP2, an androgen-regulated six transmembrane protein that is overexpressed in prostate cancer. *Oncogene*, *24*(31), 4934-4945.

Korkmaz, K. S., Elbi, C., Korkmaz, C. G., Loda, M., Hager, G. L., & Saatcioglu, F. (2002). Molecular cloning and characterization of STAMP1, a highly prostate-specific six transmembrane protein that is overexpressed in prostate cancer. *Journal of Biological Chemistry*, *277*(39), 36689-36696.

Kotterman, M. A., & Schaffer, D. V. (2014). Engineering adeno-associated viruses for clinical gene therapy. *Nature Reviews Genetics*, *15*(7), 445-451.

Kovtun, Y. V., Audette, C. A., Ye, Y., Xie, H., Ruberti, M. F., Phinney, S. J., ... & Goldmacher, V. S. (2006). Antibody-drug conjugates designed to eradicate tumors with homogeneous and heterogeneous expression of the target antigen. Cancer research, 66(6), 3214-3221.

Krueckl, S. L., Sikes, R. A., Edlund, N. M., Bell, R. H., Hurtado-Coll, A., Fazli, L., ... & Cox, M. E. (2004). Increased insulin-like growth factor I receptor expression and signalling are components of androgen-independent progression in a lineage-derived prostate cancer progression model. *Cancer research*, *64*(23), 8620-8629.

Krupa, M., Canamero, M., Gomez, C. E., Najera, J. L., Gil, J., & Esteban, M. (2011). Immunization with recombinant DNA and modified vaccinia virus Ankara (MVA) vectors delivering PSCA and STEAP1 antigens inhibits prostate cancer progression. *Vaccine*, *29*(7), 1504-1513.

Kuban, D. A., Tucker, S. L., Dong, L., Starkschall, G., Huang, E. H., Cheung, M. R., ... & Pollack, A. (2008). Long-term results of the MD Anderson randomized dose-escalation trial for prostate cancer. *International Journal of Radiation Oncology* Biology* Physics*, *70*(1), 67-74.

Kue, P. F., Taub, J. S., Harrington, L. B., Polakiewicz, R. D., Ullrich, A., & Daaka, Y. (2002). Lysophosphatidic acid-regulated mitogenic ERK signalling in androgen-insensitive prostate cancer PC-3 cells. *International journal of cancer*, *102*(6), 572-579.

Kunz-Schughart, L. A., Freyer, J. P., Hofstaedter, F., & Ebner, R. (2004). The use of 3-D cultures for high-throughput screening: the multicellular spheroid model. *Journal of biomolecular screening*, *9*(4), 273-285.

Lam, T. B., MacLennan, S., Willemse, P. P. M., Mason, M. D., Plass, K., Shepherd, R., ... & Briers, E. (2019). EAU-EANM-ESTRO-ESUR-SIOG prostate cancer guideline panel consensus statements for deferred treatment with curative intent for localised prostate cancer from an international collaborative study (Detective study). *European urology*, *76*(6), 790-813.

Lambe, T., Simpson, R. J., Dawson, S., Bouriez-Jones, T., Crockford, T. L., Lepherd, M., ... & Villarreal Jr, G. (2009). Identification of a Steap3 endosomal targeting motif essential for normal iron metabolism. *Blood, The Journal of the American Society of Hematology*, *113*(8), 1805-1808.

Lambert, A. W., Pattabiraman, D. R., & Weinberg, R. A. (2017). Emerging biological principles of metastasis. *Cell*, *168*(4), 670-691.

Lambeth, J. D. (2004). NOX enzymes and the biology of reactive oxygen. *Nature Reviews Immunology*, *4*(3), 181-189.

Lamm, M. L., Podlasek, C. A., Barnett, D. H., Lee, J., Clemens, J. Q., Hebner, C. M., & Bushman, W. (2001). Mesenchymal factor bone morphogenetic protein 4 restricts ductal budding and branching morphogenesis in the developing prostate. *Developmental biology*, *232*(2), 301-314.

Lamouille, S., Xu, J., & Derynck, R. (2014). Molecular mechanisms of epithelial–mesenchymal transition. *Nature reviews Molecular cell biology*, *15*(3), 178-196.

Langley, R. R., & Fidler, I. J. (2011). The seed and soil hypothesis revisited—The role of tumor-stroma interactions in metastasis to different organs. *International journal of cancer*, *128*(11), 2527-2535.

Laurent, J., Frongia, C., Cazales, M., Mondesert, O., Ducommun, B., & Lobjois, V. (2013). Multicellular tumor spheroid models to explore cell cycle checkpoints in 3D. *BMC cancer*, *13*(1), 73.

Lazzari, G., Nicolas, V., Matsusaki, M., Akashi, M., Couvreur, P., & Mura, S. (2018). Multicellular spheroid based on a triple co-culture: A novel 3D model to mimic pancreatic tumor complexity. *Acta biomaterialia*, *78*, 296-307.

Lee, C. H., Chen, S. L., Sung, W. W., Lai, H. W., Hsieh, M. J., Yen, H. H., ... & Chen, M. L. (2016). The prognostic role of STEAP1 expression determined via immunohistochemistry staining in predicting prognosis of primary colorectal cancer: a survival analysis. *International journal of molecular sciences*, *17*(4), 592.

Lee, D. J., Mallin, K., Graves, A. J., Chang, S. S., Penson, D. F., Resnick, M. J., & Barocas, D. A. (2017). Recent changes in prostate cancer screening practices and prostate cancer epidemiology. *The Journal of Urology*.

Leitzmann, M. F., & Rohrmann, S. (2012). Risk factors for the onset of prostatic cancer: age, location, and behavioral correlates. *Clinical epidemiology*, *4*, 1.

Lespagnol, A., Duflaut, D., Beekman, C., Blanc, L., Fiucci, G., Marine, J. C., ... & Telerman, A. (2008). Exosome secretion, including the DNA damage-induced p53-dependent secretory pathway, is severely compromised in TSAP6/Steap3-null mice. *Cell Death & Differentiation*, *15*(11), 1723-1733.

Leung, J. K., & Sadar, M. D. (2017). Non-genomic actions of the androgen receptor in prostate cancer. *Frontiers in endocrinology*, *8*, 2.

Li, D., Zhou, H., & Zeng, X. (2019). Battling CRISPR-Cas9 off-target genome editing. *Cell Biol Toxicol* 35**,** 403–406 (2019).

Li, F., Emmerton, K. K., Jonas, M., Zhang, X., Miyamoto, J. B., Setter, J. R., ... & Law, C. L. (2016). Intracellular released payload influences potency and bystander-killing effects of antibody-drug conjugates in preclinical models. *Cancer research*, *76*(9), 2710-2719.

Li, L., Lou, Z., & Wang, L. (2011). The role of FKBP5 in cancer aetiology and chemoresistance. *British journal of cancer*, *104*(1), 19-23.

Li, M., Xie, H., Liu, Y., Xia, C., Cun, X., Long, Y., ... & He, Q. (2019). Knockdown of hypoxia-inducible factor-1 alpha by tumor targeted delivery of CRISPR/Cas9 system suppressed the metastasis of pancreatic cancer. *Journal of Controlled Release*, *304*, 204-215.

Li, S., Fong, K. W., Gritsina, G., Zhang, A., Zhao, J. C., Kim, J., ... & Nelson, P. S. (2019). Activation of MAPK signalling by CXCR7 leads to enzalutamide resistance in prostate cancer. *Cancer research*, *79*(10), 2580-2592.

Li, Y., Glass, Z., Huang, M., Chen, Z. Y., & Xu, Q. (2020). Ex vivo cell-based CRISPR/Cas9 genome editing for therapeutic applications. *Biomaterials*, 119711.

Liao, J., Li, X., Koh, A. J., Berry, J. E., Thudi, N., Rosol, T. J. & McCauley, L. K. (2008). Tumor expressed PTHrP facilitates prostate cancer-induced osteoblastic lesions. *International journal of cancer*, *123*(10), 2267-2278.

Lim, S. D., Sun, C., Lambeth, J. D., Marshall, F., Amin, M., Chung, L., ... & Arnold, R. S. (2005). Increased Nox1 and hydrogen peroxide in prostate cancer. *The Prostate*, *62*(2), 200-207.

Lin, D. L., Whitney, M. C., Yao, Z., & Keller, E. T. (2001). Interleukin-6 induces androgen responsiveness in prostate cancer cells through up-regulation of androgen receptor expression. *Clinical Cancer Research*, *7*(6), 1773-1781.

Lin, R. Z., & Chang, H. Y. (2008). Recent advances in three-dimensional multicellular spheroid culture for biomedical research. *Biotechnology Journal: Healthcare Nutrition Technology*, *3*(9-10), 1172-1184.

Lines, J. L., Pantazi, E., Mak, J., Sempere, L. F., Wang, L., O'Connell, S., ... & Noelle, R. (2014). VISTA is an immune checkpoint molecule for human T cells. *Cancer research*, *74*(7), 1924-1932.

Lino, C. A., Harper, J. C., Carney, J. P., & Timlin, J. A. (2018). Delivering CRISPR: a review of the challenges and approaches. *Drug delivery*, *25*(1), 1234-1257.

Lipianskaya, J., Cohen, A., Chen, C. J., Hsia, E., Squires, J., Li, Z., ... & Huang, J. (2014). Androgen-deprivation therapy-induced aggressive prostate cancer with neuroendocrine differentiation. *Asian journal of andrology*, *16*(4), 541.

Liu, J. J., Lin, M., Yu, J. Y., Liu, B., & Bao, J. K. (2011). Targeting apoptotic and autophagic pathways for cancer therapeutics. *Cancer letters*, *300*(2), 105-114.

Liu, M., Zhao, Y., Yang, F., Wang, J., Shi, X., Zhu, X. & Yang, K. (2016). Evidence for a role of GPRC6A in prostate cancer metastasis based on case-control and in vitro analyses. *Eur Rev Med Pharmacol Sci*, *20*(11), 2235-2248.

Liu, R. M., Li, Y. B., & Zhong, J. J. (2012). Cytotoxic and pro-apoptotic effects of novel ganoderic acid derivatives on human cervical cancer cells in vitro. *European journal of pharmacology*, *681*(1-3), 23-33.

Liu, T. Y., Tan, Z. J., Jiang, L., Gu, J. F., Wu, X. S., Cao, Y., ... & Liu, Y. B. (2013). Curcumin induces apoptosis in gallbladder carcinoma cell line GBC-SD cells. *Cancer cell international*, *13*(1), 64.

Liu, T., Shen, J. K., Li, Z., Choy, E., Hornicek, F. J., & Duan, Z. (2016). Development and potential applications of CRISPR-Cas9 genome editing technology in sarcoma. *Cancer letters*, *373*(1), 109-118.

Liu, Y., Majumder, S., McCall, W., Sartor, C. I., Mohler, J. L., Gregory, C. W., ... & Whang, Y. E. (2005). Inhibition of HER-2/neu kinase impairs androgen receptor recruitment to the androgen responsive enhancer. *Cancer research*, *65*(8), 3404-3409.

Logothetis, C. J., & Lin, S. H. (2005). Osteoblasts in prostate cancer metastasis to bone. *Nature Reviews Cancer*, *5*(1), 21-28.

Lonergan, P. E., & Tindall, D. J. (2011). Androgen receptor signalling in prostate cancer development and progression. *Journal of carcinogenesis*, *10*.

Lovitt, C. J., Shelper, T. B., & Avery, V. M. (2013). Miniaturized three-dimensional cancer model for drug evaluation. *Assay and drug development technologies*, *11*(7), 435-448.

Lovitt, C. J., Shelper, T. B., & Avery, V. M. (2014). Advanced cell culture techniques for cancer drug discovery. *Biology*, *3*(2), 345-367.

Loy, C. J., Sim, K. S., & Yong, E. L. (2003). Filamin-A fragment localizes to the nucleus to regulate androgen receptor and coactivator functions. *Proceedings of the National Academy of Sciences*, *100*(8), 4562-4567.

Luca, A. C., Mersch, S., Deenen, R., Schmidt, S., Messner, I., Schäfer, K. L., ... & Krieg, A. (2013). Impact of the 3D microenvironment on phenotype, gene expression, and EGFR inhibition of colorectal cancer cell lines. *PloS one*, *8*(3).

Lulkiewicz, M., Bajsert, J., Kopczynski, P., Barczak, W., & Rubis, B. (2020). Telomere length: how the length makes a difference. *Molecular Biology Reports*, 1-8.

Macheret, M., & Halazonetis, T. D. (2015). DNA replication stress as a hallmark of cancer. *Annual Review of Pathology: Mechanisms of Disease*, *10*, 425-448.

Machlenkin, A., Paz, A., Haim, E. B., Goldberger, O., Finkel, E., Tirosh, B., ... & Lemonnier, F. (2005). Human CTL epitopes prostatic acid phosphatase-3 and six-transmembrane epithelial antigen of prostate-3 as candidates for prostate cancer immunotherapy. *Cancer research*, *65*(14), 6435-6442.

Magee, J. A., Chang, L. W., Stormo, G. D., & Milbrandt, J. (2006). Direct, androgen receptor-mediated regulation of the FKBP5 gene via a distal enhancer element. *Endocrinology*, *147*(1), 590-598.

Maia, J., Caja, S., Strano Moraes, M. C., Couto, N., & Costa-Silva, B. (2018). Exosome-based cell-cell communication in the tumor microenvironment. *Frontiers in cell and developmental biology*, *6*, 18.

Mallik, I., Davila, M., Tapia, T., Schanen, B., & Chakrabarti, R. (2008). Androgen regulates Cdc6 transcription through interactions between androgen receptor and E2F transcription factor in prostate cancer cells. *Biochimica et Biophysica Acta (BBA)-Molecular Cell Research*, *1783*(10), 1737-1744.

Marques, R. B., Dits, N. F., Erkens-Schulze, S., van IJcken, W. F., van Weerden, W. M., & Jenster, G. (2011). Modulation of androgen receptor signalling in hormonal therapy-resistant prostate cancer cell lines. *PLoS One*, *6*(8), e23144.

Marques, R. B., Dits, N. F., Erkens-Schulze, S., Van Weerden, W. M., & Jenster, G. (2010). Bypass mechanisms of the androgen receptor pathway in therapy-resistant prostate cancer cell models. *PloS one*, *5*(10).

Marshall, H. T., & Djamgoz, M. (2018). Immuno-oncology: emerging targets and combination therapies. *Frontiers in oncology*, *8*, 315.

Martin, R. M., Donovan, J. L., Turner, E. L., Metcalfe, C., Young, G. J., Walsh, E. I., ... & Sterne, J. A. (2018). Effect of a low-intensity PSA-based screening intervention on prostate cancer mortality: the CAP randomized clinical trial. *Jama*, *319*(9), 883-895.

Martinez, L. A., Yang, J., Vazquez, E. S., del Carmen Rodriguez-Vargas, M., Olive, M., Hsieh, J. T., ... & Navone, N. M. (2002). p21 modulates threshold of apoptosis induced by DNA-damage and growth factor withdrawal in prostate cancer cells. *Carcinogenesis*, *23*(8), 1289-1296.

Massard, C., & Fizazi, K. (2011). Targeting continued androgen receptor signalling in prostate cancer. *Clinical Cancer Research*, *17*(12), 3876-3883.

Matsumoto, I., Zhang, H., Yasukochi, T., Iwanami, K., Tanaka, Y., Inoue, A., ... & Sumida, T. (2008). Therapeutic effects of antibodies to tumor necrosis factor-α, interleukin-6 and cytotoxic T-lymphocyte antigen 4 immunoglobulin in mice with glucose-6-phosphate isomerase induced arthritis. *Arthritis research & therapy*, *10*(3), 1-8.

Mavragani, I. V., Nikitaki, Z., Kalospyros, S. A., & Georgakilas, A. G. (2019). Ionizing radiation and complex DNA damage: from prediction to detection challenges and biological significance. *Cancers*, *11*(11), 1789.

McAllister, M. J., Underwood, M. A., Leung, H. Y., & Edwards, J. (2019). A review on the interactions between the tumor microenvironment and androgen receptor signalling in prostate cancer. *Translational Research*, *206*, 91-106.

McGowan, P. M., Kirstein, J. M., & Chambers, A. F. (2009). Micrometastatic disease and metastatic outgrowth: clinical issues and experimental approaches. *Future Oncology*, *5*(7), 1083-1098.

McPhaul, M. J. (2016). Androgen Insensitivity Due to Mutations of the Androgen Receptor. In *Genetic Diagnosis of Endocrine Disorders* (pp. 279-288). Academic Press.

Mehta, G., Hsiao, A. Y., Ingram, M., Luker, G. D., & Takayama, S. (2012). Opportunities and challenges for use of tumor spheroids as models to test drug delivery and efficacy. *Journal of controlled release*, *164*(2), 192-204.

Mellinghoff, I. K., Vivanco, I., Kwon, A., Tran, C., Wongvipat, J., & Sawyers, C. L. (2004). HER2/neu kinase-dependent modulation of androgen receptor function through effects on DNA binding and stability. *Cancer cell*, *6*(5), 517-527.

Metzakopian, E., Strong, A., Iyer, V., Hodgkins, A., Tzelepis, K., Antunes, L., ... & Hoffmann, C. (2017). Enhancing the genome editing toolbox: genome wide CRISPR arrayed libraries. *Scientific reports*, *7*(1), 1-9.

Metzger, E., Müller, J. M., Ferrari, S., Buettner, R., & Schüle, R. (2003). A novel inducible transactivation domain in the androgen receptor: implications for PRK in prostate cancer. *The EMBO journal*, *22*(2), 270-280.

Migita, T., & Inoue, S. (2012). Implications of the Golgi apparatus in prostate cancer. *The international journal of biochemistry & cell biology*, *44*(11), 1872-1876.

Migliaccio, A., Castoria, G., DOMENICO, M. D., Ciociola, A., Lombardi, M., De Falco, A., ... & Auricchio, F. (2006). Crosstalk between EGFR and extranuclear steroid receptors. *Annals of the New York Academy of Sciences*, *1089*(1), 194-200.

Milowsky, M. I., Galsky, M. D., Morris, M. J., Crona, D. J., George, D. J., Dreicer, R., ... & Nanus, D. M. (2016). Phase 1/2 multiple ascending dose trial of the prostate-specific membrane antigen-targeted antibody drug conjugate MLN2704 in metastatic castration-resistant prostate cancer. In *Urologic Oncology: Seminars and Original Investigations* (Vol. 34, No. 12, pp. 530-e15). Elsevier.

Mitsuzuka, K., & Arai, Y. (2018). Metabolic changes in patients with prostate cancer during androgen deprivation therapy. *International Journal of Urology*, *25*(1), 45-53.

Mittal, D., Gubin, M. M., Schreiber, R. D., & Smyth, M. J. (2014). New insights into cancer immunoediting and its three component phases—elimination, equilibrium and escape. *Current opinion in immunology*, *27*, 16-25.

Monroe, K. R., Mimi, C. Y., Kolonel, L. N., Coetzee, G. A., Wilkens, L. R., Ross, R. K., & Henderson, B. E. (1995). Evidence of an X-linked or recessive genetic component to prostate cancer risk. *Nature medicine*, *1*(8), 827-829.

Montgomery, R. B., Mostaghel, E. A., Vessella, R., Hess, D. L., Kalhorn, T. F., Higano, C. S., ... & Nelson, P. S. (2008). Maintenance of intratumoral androgens in metastatic prostate cancer: a mechanism for castration-resistant tumor growth. *Cancer research*, *68*(11), 4447-4454.

Moreaux, J., Kassambara, A., Hose, D., & Klein, B. (2012). STEAP1 is overexpressed in cancers: a promising therapeutic target. *Biochemical and biophysical research communications*, *429*(3-4), 148-155.

Morgia, G., Falsaperla, M., Malaponte, G., Madonia, M., Indelicato, M., Travali, S., & Mazzarino, M. C. (2005). Matrix metalloproteinases as diagnostic (MMP-13) and prognostic (MMP-2, MMP-9) markers of prostate cancer. *Urological research*, *33*(1), 44-50.

Mosaad, E. O., Chambers, K. F., Futrega, K., Clements, J. A., & Doran, M. R. (2018). The Microwell-mesh: A high-throughput 3D prostate cancer spheroid and drug-testing platform. *Scientific reports*, *8*(1), 1-12.

Moschini, M., Spahn, M., Mattei, A., Cheville, J., & Karnes, R. J. (2016). Incorporation of tissue-based genomic biomarkers into localized prostate cancer clinics. *BMC medicine*, *14*(1), 67.

Mosmann, T. (1983). Rapid colorimetric assay for cellular growth and survival: application to proliferation and cytotoxicity assays. *Journal of immunological methods*, *65*(1-2), 55-63.

Muir, C., Chung, L., Carson, D., & Farach-Carson, M. (2006). Hypoxia increases VEGF-A production by prostate cancer and bone marrow stromal cells and initiates paracrine activation of bone marrow endothelial cells. *Clinical & Experimental Metastasis*, *23*(1), 75-86.

Muranen, T., Selfors, L. M., Worster, D. T., Iwanicki, M. P., Song, L., Morales, F. C. & Brugge, J. S. (2012). Inhibition of PI3K/mTOR leads to adaptive resistance in matrix-attached cancer cells. *Cancer cell*, *21*(2), 227-239.

Murillo, H., Huang, H., Schmidt, L. J., Smith, D. I., & Tindall, D. J. (2001). Role of PI3K signalling in survival and progression of LNCaP prostate cancer cells to the androgen refractory state. *Endocrinology*, *142*(11), 4795-4805.

Myung, J. K., Banuelos, C. A., Fernandez, J. G., Mawji, N. R., Wang, J., Tien, A. H., ... & McEwan, I. J. (2013). An androgen receptor N-terminal domain antagonist for treating prostate cancer. *The Journal of clinical investigation*, *123*(7), 2948-2960.

Na, H., Li, X., Zhang, X., Xu, Y., Sun, Y., Cui, J., ... & Zuo, Y. (2020). LncRNA STEAP3-AS1 modulates cell cycle progression via affecting CDKN1C expression through STEAP3 in colon cancer. *Molecular Therapy-Nucleic Acids*, *21*, 480-491.

Nagy, J. A., & Dvorak, H. F. (2012). Heterogeneity of the tumor vasculature: the need for new tumor blood vessel type-specific targets. *Clinical & experimental metastasis*, *29*(7), 657-662.

Naji, L., Randhawa, H., Sohani, Z., Dennis, B., Lautenbach, D., Kavanagh, O., ... & Profetto, J. (2018). Digital rectal examination for prostate cancer screening in primary care: a systematic review and meta-analysis. *The Annals of Family Medicine*, *16*(2), 149-154.

Nakamura, I., Duong, L. T., Rodan, S. B., & Rodan, G. A. (2007). Involvement of α v β 3 integrins in osteoclast function. *Journal of bone and mineral metabolism*, *25*(6), 337-344.

Nakazawa, M., Antonarakis, E. S., & Luo, J. (2014). Androgen receptor splice variants in the era of enzalutamide and abiraterone. *Hormones and Cancer*, *5*(5), 265-273.

Nath, S., & Devi, G. R. (2016). Three-dimensional culture systems in cancer research: Focus on tumor spheroid model. *Pharmacology & therapeutics*, *163*, 94-108.

National Cancer Intelligence Network (2015), Stage Breakdown by CCG 2013, London.

Navaei, A. H., Walter, B. A., Moreno, V., Pack, S. D., Pinto, P., & Merino, M. J. (2017). Correlation between erg fusion protein and androgen receptor expression by immunohistochemistry in prostate, possible role in diagnosis and therapy. *Journal of Cancer*, *8*(13), 2604.

Naveed, M., Tehreem, S., Mubeen, S., Nadeem, F., Zafar, F., & Irshad, M. (2016). In-silico analysis of non-synonymous-SNPs of STEAP2: To provoke the progression of prostate cancer. *Open Life Sciences*, *11*(1), 402-416.

National Comprehensive Cancer Network. (2018). *Prostate Cancer.*

Negri, E., Pelucchi, C., Talamini, R., Montella, M., Gallus, S., Bosetti, C. & La Vecchia, C. (2005). Family history of cancer and the risk of prostate cancer and benign prostatic hyperplasia. *International journal of cancer*, *114*(4), 648-652.

Negrini, S., Gorgoulis, V. G., & Halazonetis, T. D. (2010). Genomic instability—an evolving hallmark of cancer. *Nature reviews Molecular cell biology*, *11*(3), 220-228.

Nelson, A. W. & Shah, N. (2019) Prostate cancer. *Renal and urological surgery, 37*(9), 500-507.

Nelson, A. W., Tilley, W. D., Neal, D. E., & Carroll, J. S. (2014). Estrogen receptor beta in prostate cancer: friend or foe?. *Endocrine-related cancer*, *21*(4), T219-T234.

Nelson, J. B., Nabulsi, A. A., Vogelzang, N. J., Breul, J., Zonnenberg, B. A., Daliani, D. D. & Carducci, M. A. (2003). Suppression of prostate cancer induced bone remodeling by the endothelin receptor A antagonist atrasentan. *The Journal of urology*, *169*(3), 1143-1149.

Nevedomskaya, E., Baumgart, S. J., & Haendler, B. (2018). Recent advances in prostate cancer treatment and drug discovery. *International journal of molecular sciences*, *19*(5), 1359.

Nguyen, D. P., Li, J., & Tewari, A. K. (2014). Inflammation and prostate cancer: the role of interleukin 6 (IL-6). *BJU international*, *113*(6), 986-992.

Nguyen-Chi, A. (2020). *Design and evaluation of anti-STEAP2 antibodies to treat aggressive prostate cancer* (PhD). Swansea University.

Ni, L., Yang, C. S., Gioeli, D., Frierson, H., Toft, D. O., & Paschal, B. M. (2010). FKBP51 promotes assembly of the Hsp90 chaperone complex and regulates androgen receptor signalling in prostate cancer cells. *Molecular and cellular biology*, *30*(5), 1243-1253.

NICE. (2019). NICE Guidance - Prostate cancer: diagnosis and management.

Nimmanapalli, R., Perkins, C. L., Orlando, M., O'Bryan, E., Nguyen, D., & Bhalla, K. N. (2001). Pretreatment with paclitaxel enhances apo-2 ligand/tumor necrosis factor-related apoptosis-inducing ligand-induced apoptosis of prostate cancer cells by inducing death receptors 4 and 5 protein levels. *Cancer research*, *61*(2), 759-763.

Nishimasu, H., Ran, F. A., Hsu, P. D., Konermann, S., Shehata, S. I., Dohmae, N., ... & Nureki, O. (2014). Crystal structure of Cas9 in complex with guide RNA and target DNA. *Cell*, *156*(5), 935-949.

Nishimori, H., Ehata, S., Suzuki, H. I., Katsuno, Y. & Miyazono, K. (2012). Prostate cancer cells and bone stromal cells mutually interact with each other through bone morphogenetic protein-mediated signals. *Journal of Biological Chemistry*, *287*(24), 20037-20046.

Nyquist, M. D., & Dehm, S. M. (2013). Interplay between genomic alterations and androgen receptor signalling during prostate cancer development and progression. *Hormones and Cancer*, *4*(2), 61-69.

O'brien, J., Wilson, I., Orton, T., & Pognan, F. (2000). Investigation of the Alamar Blue (resazurin) fluorescent dye for the assessment of mammalian cell cytotoxicity. *European journal of biochemistry*, *267*(17), 5421-5426.

O'Connor, J. C., Farach-Carson, M. C., Schneider, C. J., & Carson, D. D. (2007). Coculture with prostate cancer cells alters endoglin expression and attenuates transforming growth factor-β signalling in reactive bone marrow stromal cells. *Molecular cancer research*, *5*(6), 585-603.

Odedina, F. T., Akinremi, T. O., Chinegwundoh, F., Roberts, R., Yu, D., Reams, R. R., ... & Kumar, N. (2009). Prostate cancer disparities in Black men of African descent: a comparative literature review of prostate cancer burden among Black men in the United States, Caribbean, United Kingdom, and West Africa. In *Infectious agents and cancer*(Vol. 4, No. 1, pp. 1-8). BioMed Central.

Ohgami, R. S., Campagna, D. R., Greer, E. L., Antiochos, B., McDonald, A., Chen, J., ... & Fleming, M. D. (2005). Identification of a ferrireductase required for efficient transferrin-dependent iron uptake in erythroid cells. *Nature genetics*, *37*(11), 1264-1269.

Ohgami, R. S., Campagna, D. R., McDonald, A., & Fleming, M. D. (2006). The Steap proteins are metalloreductases. *Blood*, *108*(4), 1388-1394.

Okamoto, M., Lee, C., & Oyasu, R. (1997). Interleukin-6 as a paracrine and autocrine growth factor in human prostatic carcinoma cells in vitro. *Cancer research*, *57*(1), 141-146.

Onishi, K., Tanaka, N., Miyake, M., Nakai, Y., Anai, S., Torimoto, K., ... & Konishi, N. (2019). Changes in lower urinary tract symptoms after iodine-125 brachytherapy for prostate cancer. *Clinical and translational radiation oncology*, *14*, 51-58.

Ono, M., Kubota, S., Fujisawa, T., Sonoyama, W., Kawaki, H., Akiyama, K. & Takigawa, M. (2007). Promotion of attachment of human bone marrow stromal cells by CCN2. *Biochemical and biophysical research communications*, *357*(1), 20-25.

Oosterheert, W., Reis, J., Gros, P., & Mattevi, A. (2020). An Elegant Four-Helical Fold in NOX and STEAP Enzymes Facilitates Electron Transport across Biomembranes—Similar Vehicle, Different Destination. *Accounts of Chemical Research*, *53*(9), 1969-1980.

Oosterhoff, J. K., Penninkhof, F., Brinkmann, A. O., Grootegoed, J. A., & Blok, L. J. (2003). REPS2/POB1 is downregulated during human prostate cancer progression and inhibits growth factor signalling in prostate cancer cells. *Oncogene*, *22*(19), 2920-2925.

Oraiopoulou, M. E., Tampakaki, M., Tzamali, E., Tamiolakis, T., Makatounakis, V., Vakis, A. F., ... & Papamatheakis, J. (2019). A 3D tumor spheroid model for the T98G Glioblastoma cell line phenotypic characterization. *Tissue and Cell*, *59*, 39-43.

Osman, I., Dai, J., Mikhail, M., Navarro, D., Taneja, S. S., Lee, P., ... & Nanus, D. M. (2006). Loss of neutral endopeptidase and activation of protein kinase B (Akt) is associated with prostate cancer progression. *Cancer: Interdisciplinary International Journal of the American Cancer Society*, *107*(11), 2628-2636.

Ozmen, F., Ozmen, M. M., Gelecek, S., Bilgic, İ., Moran, M., & Sahin, T. T. (2016). STEAP4 and HIF-1α gene expressions in visceral and subcutaneous adipose tissue of the morbidly obese patients. *Molecular immunology*, *73*, 53-59.

Packer, J. R., & Maitland, N. J. (2016). The molecular and cellular origin of human prostate cancer. *Biochimica et Biophysica Acta (BBA)-Molecular Cell Research*, *1863*(6), 1238-1260.

Paget, S. (1889). The distribution of secondary growths in cancer of the breast. *Lancet*, 571-573.

Pal, M., Bhattacharya, S., Kalyan, G., & Hazra, S. (2018). Cadherin profiling for therapeutic interventions in Epithelial Mesenchymal Transition (EMT) and tumorigenesis. *Experimental cell research*, *368*(2), 137-146.

Palmer, T. D., Ashby, W. J., Lewis, J. D., & Zijlstra, A. (2011). Targeting tumor cell motility to prevent metastasis. *Advanced drug delivery reviews*, *63*(8), 568-581.

Pan, Y. Z., Li, Y., Guo, L. R., Zhao, Y. Y., & Zhao, X. J. (2008). Influence of expression of six transmembrane epithelial antigen of the prostate-1 on intracellular reactive oxygen species level and cell growth: an in vitro experiment. *Chinese Medical Journal, 88*(9), 641-644.

Passer, B. J., Nancy-Portebois, V., Amzallag, N., Prieur, S., Cans, C., de Climens, A. R., ... & Morchoisne, S. (2003). The p53-inducible TSAP6 gene product regulates apoptosis and the cell cycle and interacts with Nix and the Myt1 kinase. *Proceedings of the National Academy of Sciences*, *100*(5), 2284-2289.

Patel, P. H., & Kockler, D. R. (2008). Sipuleucel-T: a vaccine for metastatic, asymptomatic, androgen-independent prostate cancer. *Annals of Pharmacotherapy*, *42*(1), 91-98.

Patki, M., Chari, V., Sivakumaran, S., Gonit, M., Trumbly, R., & Ratnam, M. (2013). The ETS domain transcription factor ELK1 directs a critical component of growth signalling by the androgen receptor in prostate cancer cells. *Journal of Biological Chemistry*, *288*(16), 11047-11065.

Patrikidou, A., Loriot, Y., Eymard, J. C., Albiges, L., Massard, C., Ileana, E., ... & Fizazi, K. (2014). Who dies from prostate cancer?. *Prostate cancer and prostatic diseases*, *17*(4), 348-352.

Pavlova, N. N., & Thompson, C. B. (2016). The emerging hallmarks of cancer metabolism. *Cell metabolism*, *23*(1), 27-47.

Pernar, C. H., Ebot, E. M., Wilson, K. M., & Mucci, L. A. (2018). The epidemiology of prostate cancer. *Cold Spring Harbor Perspectives in Medicine*, *8*(12), a030361.

Peschel, R. E., Colberg, J. W., Chen, Z., Nath, R., & Wilson, L. D. (2004). Iodine 125 versus palladium 103 implants for prostate cancer: clinical outcomes and complications. *The Cancer Journal*, *10*(3), 170-174.

Pfeil, K., Eder, I. E., Putz, T., Ramoner, R., Culig, Z., Ueberall, F., ... & Klocker, H. (2004). Long-term androgen-ablation causes increased resistance to PI3K/Akt pathway inhibition in prostate cancer cells. *The Prostate*, *58*(3), 259-268.

Pi, M., & Quarles, L. D. (2012). GPRC6A regulates prostate cancer progression. *The Prostate*, *72*(4), 399-409.

Pi, M., Kapoor, K., Wu, Y., Ye, R., Senogles, S. E., Nishimoto, S. K., ... & Baudry, J. (2015). Structural and functional evidence for testosterone activation of GPRC6A in peripheral tissues. *Molecular endocrinology*, *29*(12), 1759-1773.

Pi, M., Kapoor, K., Ye, R., Nishimoto, S. K., Smith, J. C., Baudry, J., & Quarles, L. D. (2016). Evidence for osteocalcin binding and activation of GPRC6A in β-cells. *Endocrinology*, *157*(5), 1866-1880.

Platz, E. A., Rimm, E. B., Willett, W. C., Kantoff, P. W., & Giovannucci, E. (2000). Racial variation in prostate cancer incidence and in hormonal system markers among male health professionals. *JNCI: Journal of the National Cancer Institute*, *92*(24), 2009-2017.

Pollack, A., Zagars, G. K., Starkschall, G., Antolak, J. A., Lee, J. J., Huang, E., ... & Rosen, I. (2002). Prostate cancer radiation dose response: results of the MD Anderson phase III randomized trial. *International Journal of Radiation Oncology* Biology* Physics*, *53*(5), 1097-1105.

Porkka, K. P., Helenius, M. A., & Visakorpi, T. (2002). Cloning and characterization of a novel six-transmembrane protein STEAP2, expressed in normal and malignant prostate. *Laboratory investigation*, *82*(11), 1573-1582.

Porkka, K. P., Pfeiffer, M. J., Waltering, K. K., Vessella, R. L., Tammela, T. L., & Visakorpi, T. (2007). MicroRNA expression profiling in prostate cancer. *Cancer research*, *67*(13), 6130-6135.

Potters, L., Klein, E. A., Kattan, M. W., Reddy, C. A., Ciezki, J. P., Reuther, A. M., & Kupelian, P. A. (2004). Monotherapy for stage T1–T2 prostate cancer: radical prostatectomy, external beam radiotherapy, or permanent seed implantation. *Radiotherapy and Oncology*, *71*(1), 29-33.

Präbst, K., Engelhardt, H., Ringgeler, S., & Hübner, H. (2017). Basic colorimetric proliferation assays: MTT, WST, and resazurin. In *Cell viability assays* (pp. 1-17). Humana Press, New York, NY.

Prior, L., Bordet, S., Trifiro, M. A., Mhatre, A., Kaufman, M., Pinsky, L., ... & Trapman, J. (1992). Replacement of arginine 773 by cysteine or histidine in the human androgen receptor causes complete androgen insensitivity with different receptor phenotypes. *American journal of human genetics*, *51*(1), 143.

Pullar, B. & Shah, N. (2016). Prostate cancer. *Surgery Oxford International, 34*(10), 505-511.

Putzke, A. P., Ventura, A. P., Bailey, A. M., Akture, C., Opoku-Ansah, J., Çeliktaş, M., ... & Nguyen, H. M. (2011). Metastatic progression of prostate cancer and e-cadherin: Regulation by Zeb1 and Src family kinases. *The American journal of pathology*, *179*(1), 400-410.

Qi, Y., Yu, Y., Wu, Y., Wang, S., Yu, Q., Shi, J., ... & Kou, C. (2015). Genetic variants in six-transmembrane epithelial antigen of prostate 4 increase risk of developing metabolic syndrome in a Han Chinese population. *Genetic testing and molecular biomarkers*, *19*(12), 666-672.

Qin, D. N., Kou, C. Z., Ni, Y. H., Zhang, C. M., Zhu, J. G., Zhu, C., ... & Guo, X. R. (2010). Monoclonal antibody to the six-transmembrane epithelial antigen of prostate 4 promotes apoptosis and inhibits proliferation and glucose uptake in human adipocytes. *International journal of molecular medicine*, *26*(6), 803-811.

Qin, D. N., Zhu, J. G., Ji, C. B., Kou, C. Z., Zhu, G. Z., Zhang, C. M., ... & Guo, X. R. (2011). Monoclonal antibody to six transmembrane epithelial antigen of prostate-4 influences insulin sensitivity by attenuating phosphorylation of P13K (P85) and Akt: possible mitochondrial mechanism. *Journal of bioenergetics and biomembranes*, *43*(3), 247-255.

Qin, J., Lee, H. J., Wu, S. P., Lin, S. C., Lanz, R. B., Creighton, C. J., ... & Tsai, M. J. (2014). Androgen deprivation–induced NCoA2 promotes metastatic and castration-resistant prostate cancer. *The Journal of clinical investigation*, *124*(11), 5013-5026.

Qu, Y., Dai, B., Ye, D., Kong, Y., Chang, K., Jia, Z., ... & Shi, G. (2015). Constitutively active AR-V7 plays an essential role in the development and progression of castration-resistant prostate cancer. *Scientific reports*, *5*(1), 1-6.

Qu, F., Cui, X., Hong, Y., Wang, J., Li, Y., Chen, L., ... & Wang, Q. (2013). MicroRNA-185 suppresses proliferation, invasion, migration, and tumorigenicity of human prostate cancer cells through targeting androgen receptor. *Molecular and cellular biochemistry*, *377*(1-2), 121-130.

Quail, D. F., & Joyce, J. A. (2013). Microenvironmental regulation of tumor progression and metastasis. *Nature medicine*, *19*(11), 1423-1437.

Quero, L., Dubois, L., Lieuwes, N. G., Hennequin, C., & Lambin, P. (2011). miR-210 as a marker of chronic hypoxia, but not a therapeutic target in prostate cancer. *Radiotherapy and Oncology*, *101*(1), 203-208.

Quinn, D. I., Sandler, H. M., Horvath, L. G., Goldkorn, A., & Eastham, J. A. (2017). The evolution of chemotherapy for the treatment of prostate cancer. *Annals of Oncology*, *28*(11), 2658-2669.

Ramlee, M. K., Yan, T., Cheung, A. M., Chuah, C. T., & Li, S. (2015). High-throughput genotyping of CRISPR/Cas9-mediated mutants using fluorescent PCR-capillary gel electrophoresis. *Scientific reports*, *5*(1), 1-13.

Rampersad, S. N. (2012). Multiple applications of Alamar Blue as an indicator of metabolic function and cellular health in cell viability bioassays. *Sensors*, *12*(9), 12347-12360.

Ran, F. A., Hsu, P. D., Wright, J., Agarwala, V., Scott, D. A., & Zhang, F. (2013). Genome engineering using the CRISPR-Cas9 system. *Nature protocols*, *8*(11), 2281.

Ratajczak, T., Ward, B. K., & Minchin, R. F. (2003). Immunophilin chaperones in steroid receptor signalling. *Current topics in medicinal chemistry*, *3*(12), 1348-1357.

Rebbeck, T. R., Devesa, S. S., Chang, B. L., Bunker, C. H., Cheng, I., Cooney, K., ... & Haiman, C. A. (2013). Global patterns of prostate cancer incidence, aggressiveness, and mortality in men of african descent. *Prostate cancer*, *2013*.

Redman, J. M., Gulley, J. L., & Madan, R. A. (2017). Combining immunotherapies for the treatment of prostate cancer. In *Urologic Oncology: Seminars and Original Investigations* (Vol. 35, No. 12, pp. 694-700). Elsevier.

Reichert, J. C., Quent, V. M., Burke, L. J., Stansfield, S. H., Clements, J. A., & Hutmacher, D. W. (2010). Mineralized human primary osteoblast matrices as a model system to analyse interactions of prostate cancer cells with the bone microenvironment. *Biomaterials*, *31*(31), 7928-7936.

Reichert, J. M., Rosensweig, C. J., Faden, L. B., & Dewitz, M. C. (2005). Monoclonal antibody successes in the clinic. *Nature biotechnology*, *23*(9), 1073-1078.

Reuvers, T. G., Kanaar, R., & Nonnekens, J. (2020). DNA damage-inducing anticancer therapies: from global to precision damage. *Cancers*, *12*(8), 2098.

Rhoden, J. J., & Wittrup, K. D. (2012). Dose dependence of intratumoral perivascular distribution of monoclonal antibodies. *Journal of pharmaceutical sciences*, *101*(2), 860-867.

Ridge, S. M., Sullivan, F. J., & Glynn, S. A. (2017). Mesenchymal stem cells: key players in cancer progression. *Molecular cancer*, *16*(1), 31.

Riffle, S., Pandey, R. N., Albert, M., & Hegde, R. S. (2017). Linking hypoxia, DNA damage and proliferation in multicellular tumor spheroids. *BMC cancer*, *17*(1), 338.

Rini, B. I., Weinberg, V., Fong, L., Conry, S., Hershberg, R. M., & Small, E. J. (2006). Combination immunotherapy with prostatic acid phosphatase pulsed antigen-presenting cells (provenge) plus bevacizumab in patients with serologic progression of prostate cancer after definitive local therapy. *Cancer: Interdisciplinary International Journal of the American Cancer Society*, *107*(1), 67-74.

Rodeberg, D. A., Nuss, R. A., Elsawa, S. F., & Celis, E. (2005). Recognition of six-transmembrane epithelial antigen of the prostate–expressing tumor cells by peptide antigen–induced cytotoxic T lymphocytes. *Clinical cancer research*, *11*(12), 4545-4552.

Roehrborn, C. G. (2002). Etiology, pathophysiology, epidemiology and natural history of benign prostatic hyperplasia. *Campbell's urology*.

Rokhlin, O. W., Taghiyev, A. F., Guseva, N. V., Glover, R. A., Chumakov, P. M., Kravchenko, J. E., & Cohen, M. B. (2005). Androgen regulates apoptosis induced by TNFR family ligands via multiple signalling pathways in LNCaP. *Oncogene*, *24*(45), 6773-6784.

Romanuik, T. L., Wang, G., Morozova, O., Delaney, A., Marra, M. A., & Sadar, M. D. (2010). LNCaP Atlas: Gene expression associated with in vivoprogression to castration-recurrent prostate cancer. *BMC medical genomics*, *3*(1), 43.

Ryan, D. E., Taussig, D., Steinfeld, I., Phadnis, S. M., Lunstad, B. D., Singh, M., ... & Roy, S. (2018). Improving CRISPR–Cas specificity with chemical modifications in single-guide RNAs. *Nucleic acids research*, *46*(2), 792-803.

Ryan, K. M. (2011). p53 and autophagy in cancer: guardian of the genome meets guardian of the proteome. *European journal of cancer*, *47*(1), 44-50.

Rycaj, K., & Tang, D. G. (2017). Molecular determinants of prostate cancer metastasis. *Oncotarget*, *8*(50), 88211.

Ryu, N. E., Lee, S. H., & Park, H. (2019). Spheroid Culture System Methods and Applications for Mesenchymal Stem Cells. *Cells*, *8*(12), 1620.

Sak, M. M. (2007). *Characterization of human STAMP2 promoter and 5'flanking sequence* (Master's thesis).

Sanchez-Pulido, L., Rojas, A. M., Valencia, A., Martinez-A, C., & Andrade, M. A. (2004). ACRATA: a novel electron transfer domain associated to apoptosis and cancer. *BMC cancer*, *4*(1), 98.

Sánchez-Rivera, F. J., & Jacks, T. (2015). Applications of the CRISPR-Cas9 system in cancer biology. *Nature reviews cancer*, *15*(7), 387-395.

Sander, J. D., & Joung, J. K. (2014). CRISPR-Cas systems for editing, regulating and targeting genomes. *Nature biotechnology*, *32*(4), 347.

Sanjana, N. E., Shalem, O., & Zhang, F. (2014). Improved vectors and genome-wide libraries for CRISPR screening. *Nature methods*, *11*(8), 783.

Sarisozen, C., Abouzeid, A. H., & Torchilin, V. P. (2014). The effect of co-delivery of paclitaxel and curcumin by transferrin-targeted PEG-PE-based mixed micelles on resistant ovarian cancer in 3-D spheroids and in vivo tumors. *European Journal of Pharmaceutics and Biopharmaceutics*, *88*(2), 539-550.

Sathianathen, N. J., Philippou, Y. A., Kuntz, G. M., Konety, B. R., Gupta, S., Lamb, A. D., & Dahm, P. (2018). Taxane-based chemohormonal therapy for metastatic hormone-sensitive prostate cancer. *Cochrane Database of Systematic Reviews*, (10).

Satta, A., Mezzanzanica, D., Caroli, F., Frigerio, B., Di Nicola, M., Kontermann, R. E., ... & Gianni, A. M. (2018). Design, selection and optimization of an anti-TRAIL-R2/anti-CD3 bispecific antibody able to educate T cells to recognize and destroy cancer cells. In *MAbs* (Vol. 10, No. 7, pp. 1084-1097). Taylor & Francis.

Savas, S., Azorsa, D. O., Jarjanazi, H., Ibrahim-Zada, I., Gonzales, I. M., Arora, S., ... & Tuzmen, S. (2011). NCI60 cancer cell line panel data and RNAi analysis help identify EAF2 as a modulator of simvastatin and lovastatin response in HCT-116 cells. *PLoS One*, *6*(4), e18306.

Saxena, P., Trerotola, M., Wang, T., Li, J., Sayeed, A., VanOudenhove, J., ... & Languino, L. R. (2012). PSA regulates androgen receptor expression in prostate cancer cells. *The Prostate*, *72*(7), 769-776.

Sayers, T. J. (2011). Targeting the extrinsic apoptosis signalling pathway for cancer therapy. *Cancer Immunology, Immunotherapy*, *60*(8), 1173-1180.

Scarl, R. T., Lawrence, C. M., Gordon, H. M., & Nunemaker, C. S. (2017). STEAP4: its emerging role in metabolism and homeostasis of cellular iron and copper. *Journal of Endocrinology*, *234*(3), R123-R134.

Schaid, D. J. (2004). The complex genetic epidemiology of prostate cancer. *Human molecular genetics*, *13*, 103-121.

Scher, H. I., Buchanan, G., Gerald, W., Butler, L. M., & Tilley, W. D. (2004). Targeting the androgen receptor: improving outcomes for castration-resistant prostate cancer. *Endocrine-related cancer*, *11*(3), 459-476.

Scher, H. I., Fizazi, K., Saad, F., Taplin, M. E., Sternberg, C. N., Miller, K., ... & Armstrong, A. J. (2012). Increased survival with enzalutamide in prostate cancer after chemotherapy. *New England Journal of Medicine*, *367*(13), 1187-1197.

Scher, H. I., Graf, R. P., Schreiber, N. A., Jayaram, A., Winquist, E., McLaughlin, B., ... & Anderson, A. (2018). Assessment of the validity of nuclear-localized androgen receptor splice variant 7 in circulating tumor cells as a predictive biomarker for castration-resistant prostate cancer. *JAMA oncology*, *4*(9), 1179-1186.

Schlüter, K. D., Katzer, C., & Piper, H. M. (2001). AN-terminal PTHrP peptide fragment void of a PTH/PTHrP-receptor binding domain activates cardiac ETA receptors. *British journal of pharmacology*, *132*(2), 427-432.

Schmidt, L. J., & Tindall, D. J. (2011). Steroid 5 α-reductase inhibitors targeting BPH and prostate cancer. *The Journal of Steroid Biochemistry and Molecular Biology*, *125*(1-2), 32-38.

Schneider, J. G., Amend, S. R., & Weilbaecher, K. N. (2011). Integrins and bone metastasis: integrating tumor cell and stromal cell interactions. *Bone*, *48*(1), 54-65.

Schröder, F. H., Hugosson, J., Roobol, M. J., Tammela, T. L., Ciatto, S., Nelen, V., ... & Denis, L. J. (2009). Screening and prostate-cancer mortality in a randomized European study. *New England Journal of Medicine*, *360*(13), 1320-1328.

Schweers, R. L., Zhang, J., Randall, M. S., Loyd, M. R., Li, W., Dorsey, F. C., ... & Ney, P. A. (2007). NIX is required for programmed mitochondrial clearance during reticulocyte maturation. *Proceedings of the National Academy of Sciences*, *104*(49), 19500-19505.

Sedelaar, J. M., & Isaacs, J. T. (2009). Tissue culture media supplemented with 10% foetal calf serum contains a castrate level of testosterone. *The Prostate*, *69*(16), 1724-1729.

Shalem, O., Sanjana, N. E., Hartenian, E., Shi, X., Scott, D. A., Mikkelsen, T. S., ... & Zhang, F. (2014). Genome-scale CRISPR-Cas9 knockout screening in human cells. *Science*, *343*(6166), 84-87.

Shankar, E., Franco, D., Iqbal, O., Moreton, S., Kanwal, R., & Gupta, S. (2020). Dual targeting of EZH2 and androgen receptor as a novel therapy for castration-resistant prostate cancer. *Toxicology and Applied Pharmacology*, *404*, 115200.

Sharma, P. R., Mackey, A. J., Dejene, E. A., Ramadan, J. W., Langefeld, C. D., Palmer, N. D., ... & Nunemaker, C. S. (2015). An islet-targeted genome-wide association scan identifies novel genes implicated in cytokine-mediated islet stress in type 2 diabetes. *Endocrinology*, *156*(9), 3147-3156.

Shaw, G. L., Whitaker, H., Corcoran, M., Dunning, M. J., Luxton, H., Kay, J., ... & Russell, R. (2016). The early effects of rapid androgen deprivation on human prostate cancer. *European urology*, *70*(2), 214-218.

Shen, B., Zhang, W., Zhang, J., Zhou, J., Wang, J., Chen, L., ... & Skarnes, W. C. (2014). Efficient genome modification by CRISPR-Cas9 nickase with minimal off-target effects. *Nature methods*, *11*(4), 399.

Shi, L., Meng, T., Zhao, Z., Han, J., Zhang, W., Gao, F., & Cai, J. (2017). CRISPR knock out CTLA-4 enhances the anti-tumor activity of cytotoxic T lymphocytes. *Gene*, *636*, 36-41.

Shields, R. L., Namenuk, A. K., Hong, K., Meng, Y. G., Rae, J., Briggs, J., ... & Fox, J. A. (2001). High resolution mapping of the binding site on human IgG1 for FcγRI, FcγRII, FcγRIII, and FcRn and design of IgG1 variants with improved binding to the FcγR. *Journal of Biological Chemistry*, *276*(9), 6591-6604.

Shiozawa, Y., Pedersen, E. A., Havens, A. M., Jung, Y., Mishra, A., Joseph, J. & Pienta, M. J. (2011). Human prostate cancer metastases target the hematopoietic stem cell niche to establish footholds in mouse bone marrow. *The Journal of clinical investigation*, *121*(4), 1298.

Shukla, M. E., Yu, C., Reddy, C. A., Stephans, K. L., Klein, E. A., Abdel-Wahab, M., ... & Tendulkar, R. D. (2015). Evaluation of the current prostate cancer staging system based on cancer-specific mortality in the surveillance, epidemiology, and end results database. *Clinical genitourinary cancer*, *13*(1), 17-21.

Shyamsundar, R., Kim, Y. H., Higgins, J. P., Montgomery, K., Jorden, M., Sethuraman, A., ... & Pollack, J. R. (2005). A DNA microarray survey of gene expression in normal human tissues. *Genome biology*, *6*(3), R22.

Sievers, E. L., & Senter, P. D. (2013). Antibody-drug conjugates in cancer therapy. *Annual review of medicine*, *64*.

Sikkeland, J., Sheng, X., Jin, Y., & Saatcioglu, F. (2016). STAMPing at the crossroads of normal physiology and disease states. *Molecular and cellular endocrinology*, *425*, 26-36.

Sikora, M. J., Johnson, M. D., Lee, A. V., & Oesterreich, S. (2016). Endocrine response phenotypes are altered by charcoal-stripped serum variability. *Endocrinology*, *157*(10), 3760-3766.

Simmons, P. J., & Torok-Storb, B. (1991). Identification of stromal cell precursors in human bone marrow by a novel monoclonal antibody, STRO-1.

Singh, D., Sternberg, S. H., Fei, J., Doudna, J. A., & Ha, T. (2016). Real-time observation of DNA recognition and rejection by the RNA-guided endonuclease Cas9. *Nature communications*, *7*(1), 1-8.

Singh, R., Letai, A., & Sarosiek, K. (2019). Regulation of apoptosis in health and disease: the balancing act of BCL-2 family proteins. *Nature Reviews Molecular Cell Biology*, *20*(3), 175-193.

Slee, E., Adrain, C., & Martin, S. (2001). Executioner Caspase-3, -6, and -7 Perform Distinct, Non-redundant Roles during the Demolition Phase of Apoptosis. *Journal Of Biological Chemistry*, *276*(10), 7320-7326.

Smith, D. F., & Toft, D. O. (2008). Minireview: the intersection of steroid receptors with molecular chaperones: observations and questions. *Molecular endocrinology*, *22*(10), 2229-2240.

Smith, H. A., & Kang, Y. (2013). The metastasis-promoting roles of tumor-associated immune cells. *Journal of molecular medicine*, *91*(4), 411-429.

Sobel, R. E., & Sadar, M. D. (2005). Cell lines used in prostate cancer research: a compendium of old and new lines—part 1. *The Journal of urology*, *173*(2), 342-359.

Sobin, L. H. (2009). Kidney (ICD-O C64). *TNM Classification of Malignant Tumors*, 255-257.

Song, W., & Khera, M. (2014). Physiological normal levels of androgen inhibit proliferation of prostate cancer cells in vitro. *Asian journal of andrology*, *16*(6), 864.

Soni, P. D., Short, E. P., Heckman, P., Narayana, V., & McLaughlin, P. W. (2017). Using Gradient Optimization in Place of Volumetric Constraints to Improve Rectal Dose Distribution During Dose-Escalated Radiation Therapy Planning for Prostate Cancer. *International Journal of Radiation Oncology• Biology• Physics*, *99*(2), E723-E724.

Spratt, D. E., Dess, R. T., Hartman, H. E., Mahal, B. A., Jackson, W. C., Soni, P. D., ... & Pisansky, T. M. (2018). Androgen receptor activity and radiotherapeutic sensitivity in African-American men with prostate cancer: a large scale gene expression analysis and meta-analysis of RTOG trials. *International Journal of Radiation Oncology• Biology• Physics*, *102*(3), S3.

Stewart, B., & Wild, C. (2014). *World Cancer Report 2014*. Lyon: International Agency for Research on Cancer.

Stewart, D. A., Cooper, C. R., & Sikes, R. A. (2004). Changes in extracellular matrix (ECM) and ECM-associated proteins in the metastatic progression of prostate cancer. *Reproductive Biology and Endocrinology*, *2*(1), 2.

Stiehm, E. R., Keller, M. A., & Vyas, G. N. (2008). Preparation and use of therapeutic antibodies primarily of human origin. *Biologicals*, *36*(6), 363-374.

Stish, B. J., Davis, B. J., Mynderse, L. A., Deufel, C. L., & Choo, R. (2017). Brachytherapy in the management of prostate cancer. *Surgical Oncology Clinics*, *26*(3), 491-513.

Strebhardt, K., & Ullrich, A. (2008). Paul Ehrlich's magic bullet concept: 100 years of progress. *Nature Reviews Cancer*, *8*(6), 473-480.

Sun, B. L., Sun, X., Casanova, N., Garcia, A. N., Oita, R., Algotar, A. M., ... & Garcia, J. G. (2020). Role of secreted extracellular nicotinamide phosphoribosyltransferase (eNAMPT) in prostate cancer progression: Novel biomarker and therapeutic target. *EBioMedicine*, *61*, 103059.

Sun, H. Z., Yang, T. W., Zang, W. J., & Wu, S. F. (2010). Dehydroepiandrosterone-induced proliferation of prostatic epithelial cell is mediated by NFKB via PI3K/AKT signalling pathway. *Journal of endocrinology*, *204*(3), 311.

Sun, X., Cheng, G., Hao, M., Zheng, J., Zhou, X., Zhang, J., ... & Wang, J. (2010). CXCL12/CXCR4/CXCR7 chemokine axis and cancer progression. *Cancer and Metastasis Reviews*, *29*(4), 709-722.

Sun, Y. X., Fang, M., Wang, J., Cooper, C. R., Pienta, K. J., & Taichman, R. S. (2007). Expression and activation of αvβ3 integrins by SDF-1/CXC12 increases the aggressiveness of prostate cancer cells. *The Prostate*, *67*(1), 61-73.

Sun, Y., Clair, D. K. S., Xu, Y., Crooks, P. A., & Clair, W. H. S. (2010). A NADPH oxidase–dependent redox signalling pathway mediates the selective radiosensitization effect of parthenolide in prostate cancer cells. *Cancer research*, *70*(7), 2880-2890.

Sung, S. Y., Hsieh, C. L., Law, A., Zhau, H. E., Pathak, S., Multani, A. S. & Dahut, W. L. (2008). Coevolution of prostate cancer and bone stroma in three-dimensional coculture: implications for cancer growth and metastasis. *Cancer research*, *68*(23), 9996-10003.

Suva, L. J., Washam, C., Nicholas, R. W., & Griffin, R. J. (2011). Bone metastasis: mechanisms and therapeutic opportunities. *Nature Reviews Endocrinology*, *7*(4), 208-218.

Taichman, R. S., Cooper, C., Keller, E. T., Pienta, K. J., Taichman, N. S., & McCauley, L. K. (2002). Use of the stromal cell-derived factor-1/CXCR4 pathway in prostate cancer metastasis to bone. *Cancer research*, *62*(6), 1832-1837.

Takagi, A., Watanabe, M., Ishii, Y., Morita, J., Hirokawa, Y., Matsuzaki, T., & Shiraishi, T. (2007). Three-dimensional cellular spheroid formation provides human prostate tumor cells with tissue-like features. *Anticancer research*, *27*(1A), 45-53.

Takayama, K., Kaneshiro, K., Tsutsumi, S., Horie-Inoue, K., Ikeda, K., Urano, T., ... & Inoue, S. (2007). Identification of novel androgen response genes in prostate cancer cells by coupling chromatin immunoprecipitation and genomic microarray analysis. *Oncogene*, *26*(30), 4453-4463.

Tam, L., McGlynn, L. M., Traynor, P., Mukherjee, R., Bartlett, J. M., & Edwards, J. (2007). Expression levels of the JAK/STAT pathway in the transition from hormone-sensitive to hormone-refractory prostate cancer. *British journal of cancer*, *97*(3), 378-383.

Tamura, T., & Chiba, J. (2009). STEAP4 regulates focal adhesion kinase activation and CpG motifs within STEAP4 promoter region are frequently methylated in DU145, human androgen-independent prostate cancer cells. *International journal of molecular medicine*, *24*(5), 599-604.

Tan, M. E., Li, J., Xu, H. E., Melcher, K., & Yong, E. L. (2015). Androgen receptor: structure, role in prostate cancer and drug discovery. *Acta Pharmacologica Sinica*, *36*(1), 3-23.

Tanaka, Y., Matsumoto, I., Iwanami, K., Inoue, A., Minami, R., Umeda, N., ... & Sugihara, M. (2012). Six-transmembrane epithelial antigen of prostate4 (STEAP4) is a tumor necrosis factor alpha-induced protein that regulates IL-6, IL-8, and cell proliferation in synovium from patients with rheumatoid arthritis. *Modern rheumatology*, *22*(1), 128-136.

Tang, H., & Shrager, J. B. (2019). *U.S. Patent No. 10,240,145*. Washington, DC: U.S. Patent and Trademark Office.

Tang, L., Zeng, Y., Du, H., Gong, M., Peng, J., Zhang, B., ... & Liu, J. (2017). CRISPR/Cas9-mediated gene editing in human zygotes using Cas9 protein. *Molecular genetics and genomics*, *292*(3), 525-533.

Tanner, M. J., Welliver Jr, R. C., Chen, M., Shtutman, M., Godoy, A., Smith, G., ... & Buttyan, R. (2011). Effects of androgen receptor and androgen on gene expression in prostate stromal fibroblasts and paracrine signalling to prostate cancer cells. *PloS one*, *6*(1).

Tannock, I. F., De Wit, R., Berry, W. R., Horti, J., Pluzanska, A., Chi, K. N., ... & Rosenthal, M. A. (2004). Docetaxel plus prednisone or mitoxantrone plus prednisone for advanced prostate cancer. *New England Journal of Medicine*, *351*(15), 1502-1512.

Tarcsa, E., Guffroy, M. R., Falahatpisheh, H., Phipps, C., & Kalvass, J. C. (2020). Antibody-drug conjugates as targeted therapies: Are we there yet? A critical review of the current clinical landscape. *Drug Discovery Today: Technologies*.

ten Freyhaus, H., Calay, E. S., Yalcin, A., Vallerie, S. N., Yang, L., Calay, Z. Z., ... & Hotamisligil, G. S. (2012). Stamp2 controls macrophage inflammation through nicotinamide adenine dinucleotide phosphate homeostasis and protects against atherosclerosis. *Cell metabolism*, *16*(1), 81-89.

Thalmann, G. N., Anezinis, P. E., Chang, S. M., Zhau, H. E., Kim, E. E., Hopwood, V. L., ... & Chung, L. W. (1994). Androgen-independent cancer progression and bone metastasis in the LNCaP model of human prostate cancer. Cancer research, 54(10), 2577-2581.

Thalmann, G. N., Sikes, R. A., Wu, T. T., Degeorges, A., Chang, S. M., Ozen, M., ... & Chung, L. W. (2000). LNCaP progression model of human prostate cancer: Androgen-independence and osseous metastasis. The Prostate, 44(2), 91-103.

Thoma, C. R., Zimmermann, M., Agarkova, I., Kelm, J. M., & Krek, W. (2014). 3D cell culture systems modeling tumor growth determinants in cancer target discovery. *Advanced drug delivery reviews*, *69*, 29-41.

Thulin, M. H., Nilsson, M. E., Thulin, P., Céraline, J., Ohlsson, C., Damber, J. E., & Welén, K. (2016). Osteoblasts promote castration-resistant prostate cancer by altering intratumoral steroidogenesis. *Molecular and cellular endocrinology*, *422*, 182-191.

Tolkach, Y., Joniau, S., & Van Poppel, H. (2013). Luteinizing hormone-releasing hormone (LHRH) receptor agonists vs antagonists: a matter of the receptors?. *BJU international*, *111*(7), 1021-1030.

Tomlins, S. A., Laxman, B., Dhanasekaran, S. M., Helgeson, B. E., Cao, X., Morris, D. S., ... & Yu, J. (2007). Distinct classes of chromosomal rearrangements create oncogenic ETS gene fusions in prostate cancer. *Nature*, *448*(7153), 595-599.

Tomlins, S. A., Laxman, B., Varambally, S., Cao, X., Yu, J., Helgeson, B. E., ... & Mehra, R. (2008). Role of the TMPRSS2-ERG gene fusion in prostate cancer. *Neoplasia (New York, NY)*, *10*(2), 177.

Tomlins, S. A., Rhodes, D. R., Perner, S., Dhanasekaran, S. M., Mehra, R., Sun, X. W., ... & Lee, C. (2005). Recurrent fusion of TMPRSS2 and ETS transcription factor genes in prostate cancer. *science*, *310*(5748), 644-648.

Towers, C. G., Wodetzki, D., & Thorburn, A. (2020). Autophagy and cancer: Modulation of cell death pathways and cancer cell adaptations Autophagy and cancer. *The Journal of cell biology*, *219*(1).

Traish, A. M., & Morgentaler, A. (2009). Epidermal growth factor receptor expression escapes androgen regulation in prostate cancer: a potential molecular switch for tumour growth. *British journal of cancer*, *101*(12), 1949-1956.

Trimboli, A. J., Fukino, K., de Bruin, A., Wei, G., Shen, L., Tanner, S. M., ... & Ostrowski, M. C. (2008). Direct evidence for epithelial-mesenchymal transitions in breast cancer. *Cancer research*, *68*(3), 937-945.

Troyer, J. K., Beckett, M. L., & Wright, G. L. (1997). Location of prostate-specific membrane antigen in the LNCaP prostate carcinoma cell line. *The Prostate*, *30*(4), 232-242.

Tsumoto, K., Isozaki, Y., Yagami, H., & Tomita, M. (2019). Future perspectives of therapeutic monoclonal antibodies. *Immunotherapy*, *11*(2), 119-127.

Tuladhar, R., Yeu, Y., Piazza, J. T., Tan, Z., Clemenceau, J. R., Wu, X., ... & Hwang, T. H. (2019). CRISPR-Cas9-based mutagenesis frequently provokes on-target mRNA misregulation. *Nature communications*, *10*(1), 1-10.

Turgeon, M. O., Perry, N. J., & Poulogiannis, G. (2018). DNA damage, repair, and cancer metabolism. *Frontiers in oncology*, *8*, 15.

Usmani, B. A., Shen, R., Janeczko, M., Papandreou, C. N., Lee, W. H., Nelson, W. G., ... & Nanus, D. M. (2000). Methylation of the neutral endopeptidase gene promoter in human prostate cancers. *Clinical Cancer Research*, *6*(5), 1664-1670.

Vainshtein, I., Roskos, L. K., Cheng, J., Sleeman, M. A., Wang, B., & Liang, M. (2015). Quantitative measurement of the target-mediated internalization kinetics of biopharmaceuticals. *Pharmaceutical research*, *32*(1), 286-299

Vajdic, C. M., & van Leeuwen, M. T. (2009). Cancer incidence and risk factors after solid organ transplantation. *International journal of cancer*, *125*(8), 1747-1754.

Valastyan, S., & Weinberg, R. A. (2011). Tumor metastasis: molecular insights and evolving paradigms. *Cell*, *147*(2), 275-292.

Van der Steen, T., Tindall, D. J., & Huang, H. (2013). Posttranslational modification of the androgen receptor in prostate cancer. *International journal of molecular sciences*, *14*(7), 14833-14859.

van Meerloo J., Kaspers G.J.L., Cloos J. (2011). Cell Sensitivity Assays: The MTT Assay. In: Cree I. (eds) Cancer Cell Culture. Methods in Molecular Biology (Methods and Protocols), vol 731. Humana Press

Varisli, L., Gonen-Korkmaz, C., Debelec-Butuner, B., Erbaykent-Tepedelen, B., Muhammed, H. S., Bogurcu, N., ... & Korkmaz, K. S. (2011). Ubiquitously expressed hematological and neurological expressed 1 downregulates Akt-mediated GSK3β signalling, and its knockdown results in deregulated G2/M transition in prostate cells. *DNA and cell biology*, *30*(6), 419-429.

Varisli, L., Gonen-Korkmaz, C., Syed, H. M., Bogurcu, N., Debelec-Butuner, B., Erbaykent-Tepedelen, B., & Korkmaz, K. S. (2012). Androgen regulated HN1 leads proteosomal degradation of androgen receptor (AR) and negatively influences AR mediated transactivation in prostate cells. *Molecular and cellular endocrinology*, *350*(1), 107-117.

Vela, I., Gregory, L., Gardiner, E. M., Clements, J. A., & Nicol, D. L. (2007). Bone and prostate cancer cell interactions in metastatic prostate cancer. *BJU international*, *99*(4), 735-742.

Velasco, A. M., Gillis, K. A., Li, Y., Brown, E. L., Sadler, T. M., Achilleos, M., ... & Zhang, Y. (2004). Identification and validation of novel androgen-regulated genes in prostate cancer. *Endocrinology*, *145*(8), 3913-3924.

Vento, J. M., Crook, N., & Beisel, C. L. (2019). Barriers to genome editing with CRISPR in bacteria. *Journal of industrial microbiology & biotechnology*, *46*(9-10), 1327-1341.

Vinci, M., Gowan, S., Boxall, F., Patterson, L., Zimmermann, M., Lomas, C., ... & Eccles, S. A. (2012). Advances in establishment and analysis of three-dimensional tumor spheroid-based functional assays for target validation and drug evaluation. *BMC biology*, *10*(1), 29.

Von Rozycki, T., Yen, M. R., Lende, E. E., & Saier Jr, M. H. (2004). The YedZ family: possible heme binding proteins that can be fused to transporters and electron carriers. *Journal of molecular microbiology and biotechnology*, *8*(3), 129-140.

Wang, H., Yang, H., Shivalila, C. S., Dawlaty, M. M., Cheng, A. W., Zhang, F., & Jaenisch, R. (2013). One-step generation of mice carrying mutations in multiple genes by CRISPR/Cas-mediated genome engineering. *cell*, *153*(4), 910-918.

Wang, L., Jin, Y., Arnoldussen, Y. J., Jonson, I., Qu, S., Mælandsmo, G. M. & Saatcioglu, F. (2010). STAMP1 is both a proliferative and an antiapoptotic factor in prostate cancer. *Cancer research*, *70*(14), 5818-5828.

Wang, R. (2019). *Sodium salicylate effects on prostate cancer aggressiveness and development of prostate cancer spheroids for drug evaluation* (PhD). Swansea University.

Wang, X. Z., Coljee, V. W., & Maynard, J. A. (2013). Back to the future: recombinant polyclonal antibody therapeutics. *Current opinion in chemical engineering*, *2*(4), 405-415.

Wang, X., An, Z., Luo, W., Xia, N., & Zhao, Q. (2018). Molecular and functional analysis of monoclonal antibodies in support of biologics development. *Protein & Cell*, *9*(1), 74-85.

Wang, Y., Singhal, U., Qiao, Y., Kasputis, T., Chung, J. S., Zhao, H., ... & Zaslavsky, A. B. (2020). Wnt Signalling Drives Prostate Cancer Bone Metastatic Tropism and Invasion. *Translational oncology*, *13*(4), 100747.

Wang, Y., Xue, H., Cutz, J. C., Bayani, J., Mawji, N. R., Chen, W. G. & Gout, P. W. (2005). An orthotopic metastatic prostate cancer model in SCID mice via grafting of a transplantable human prostate tumor line. *Laboratory investigation*, *85*(11), 1392-1404.

Wawrzynow, B., Zylicz, A., & Zylicz, M. (2018). Chaperoning the guardian of the genome. The two-faced role of molecular chaperones in p53 tumor suppressor action. *Biochimica et Biophysica Acta (BBA)-Reviews on Cancer*, *1869*(2), 161-174.

Wei, C., Liu, J., Yu, Z., Zhang, B., Gao, G., & Jiao, R. (2013). TALEN or Cas9–rapid, efficient and specific choices for genome modifications. *Journal of Genetics and Genomics*, *40*(6), 281-289.

Weinberg, R. (2014). *The biology of cancer*. New York: Garland Science.

Weiner, G. J. (2015). Building better monoclonal antibody-based therapeutics. *Nature Reviews Cancer*, *15*(6), 361-370.

Welch, D. R., & Hurst, D. R. (2019). Defining the hallmarks of metastasis. *Cancer Research*, *79*(12), 3011-3027.

Wellen, K. E., Fucho, R., Gregor, M. F., Furuhashi, M., Morgan, C., Lindstad, T., ... & Hotamisligil, G. S. (2007). Coordinated regulation of nutrient and inflammatory responses by STAMP2 is essential for metabolic homeostasis. *Cell*, *129*(3), 537-548.

Whitbread, A. K., Veveris-Lowe, T. L., Lawrence, M. G., Nicol, D. L., & Clements, J. A. (2006). The role of kallikrein-related peptidases in prostate cancer: potential involvement in an epithelial to mesenchymal transition. *Biological chemistry*, *387*(6), 707-714.

Whiteland, H., Spencer-Harty, S., Morgan, C., Kynaston, H., Thomas, D. H., Bose, P. & Doak, S. H. (2014). A role for STEAP2 in prostate cancer progression. *Clinical & experimental metastasis*, *31*(8), 909-920.

Wilt, T. J., Brawer, M. K., Jones, K. M., Barry, M. J., Aronson, W. J., Fox, S. & Nsouli, I. (2012). Radical prostatectomy versus observation for localized prostate cancer. *New England Journal of Medicine*, *367*(3), 203-213.

Windus, L. C., Glover, T. T., & Avery, V. M. (2013). Bone-stromal cells up-regulate tumourigenic markers in a tumour-stromal 3D model of prostate cancer. *Molecular cancer*, *12*(1), 112.

Windus, L. C., Kiss, D. L., Glover, T., & Avery, V. M. (2012). In vivo biomarker expression patterns are preserved in 3D cultures of Prostate Cancer. *Experimental cell research*, *318*(19), 2507-2519.

Witsch, E., Sela, M., & Yarden, Y. (2010). Roles for growth factors in cancer progression. *Physiology*.

Wright, H. L., McCarthy, H. S., Middleton, J., & Marshall, M. J. (2009). RANK, RANKL and osteoprotegerin in bone biology and disease. *Current reviews in musculoskeletal medicine*, *2*(1), 56-64.

Wright, M. E., Tsai, M. J., & Aebersold, R. (2003). Androgen receptor represses the neuroendocrine transdifferentiation process in prostate cancer cells. *Molecular endocrinology*, *17*(9), 1726-1737.

Wu, C. T., Altuwaijri, S., Ricke, W. A., Huang, S. P., Yeh, S., Zhang, C., ... & Chang, C. (2007). Increased prostate cell proliferation and loss of cell differentiation in mice lacking prostate epithelial androgen receptor. *Proceedings of the National Academy of Sciences*, *104*(31), 12679-12684.

Wu, J. B., Tang, Y. L., & Liang, X. H. (2018). Targeting VEGF pathway to normalize the vasculature: an emerging insight in cancer therapy. *OncoTargets and therapy*, *11*, 6901.

Wu, W., Yang, Y., & Lei, H. (2019). Progress in the application of CRISPR: from gene to base editing. *Medicinal research reviews*, *39*(2), 665-683.

Wu, X. X., Kakehi, Y., Mizutani, Y., Kamoto, T., Kinoshita, H., Isogawa, Y. O. S. H. I. A. K. I., ... & Ogawa, O. S. A. M. U. (2002). Doxorubicin enhances TRAIL-induced apoptosis in prostate cancer. *International journal of oncology*, *20*(5), 949-954.

Xie, J., Yang, Y., Sun, J., Jiao, Z., Zhang, H., & Chen, J. (2019). STEAP1 Inhibits Breast Cancer Metastasis and Is Associated With Epithelial–Mesenchymal Transition Procession. *Clinical breast cancer*, *19*(1), e195-e207.

Xing, L., & Boyce, B. F. (2005). Regulation of apoptosis in osteoclasts and osteoblastic cells. *Biochemical and biophysical research communications*, *328*(3), 709-720.

Xu, J., Wang, W., Kapila, Y., Lotz, J., & Kapila, S. (2009). Multiple differentiation capacity of STRO-1+/CD146+ PDL mesenchymal progenitor cells. *Stem cells and development*, *18*(3), 487-496.

Xu, K., Ganapathy, K., Andl, T., Wang, Z., Copland, J. A., Chakrabarti, R., & Florczyk, S. J. (2019). 3D porous chitosan-alginate scaffold stiffness promotes differential responses in prostate cancer cell lines. *Biomaterials*, *217*, 119311.

Xu, L. L., Su, Y. P., Labiche, R., Segawa, T., Shanmugam, N., McLeod, D. G., ... & Srivastava, S. (2001). Quantitative expression profile of androgen-regulated genes in prostate cancer cells and identification of prostate-specific genes. *International journal of cancer*, *92*(3), 322-328.

Yamada, T., Hiraoka, Y., Gupta, T. K. D., & Chakrabarty, A. M. (2004). Regulation of mammalian cell growth and death by bacterial redox proteins: relevance to ecology and cancer therapy. *Cell Cycle*, *3*(6), 750-753.

Yan, M., & Jurasz, P. (2016). The role of platelets in the tumor microenvironment: from solid tumors to leukemia. *Biochimica et Biophysica Acta (BBA)-Molecular Cell Research*, *1863*(3), 392-400.

Ye, R., Pi, M., Cox, J. V., Nishimoto, S. K., & Quarles, L. D. (2017). CRISPR/Cas9 targeting of GPRC6A suppresses prostate cancer tumorigenesis in a human xenograft model. *Journal of Experimental & Clinical Cancer Research*, *36*(1), 90.

Yi, L., & Li, J. (2016). CRISPR-Cas9 therapeutics in cancer: promising strategies and present challenges. *Biochimica et Biophysica Acta (BBA)-Reviews on Cancer*, *1866*(2), 197-207.

Yin, H., Song, C. Q., Suresh, S., Kwan, S. Y., Wu, Q., Walsh, S., ... & Koteliansky, V. (2018). Partial DNA-guided Cas9 enables genome editing with reduced off-target activity. *Nature chemical biology*, *14*(3), 311.

Yin, J. J., Mohammad, K. S., Käkönen, S. M., Harris, S., Wu-Wong, J. R., Wessale, J. L. & Guise, T. A. (2003). A causal role for endothelin-1 in the pathogenesis of osteoblastic bone metastases. *Proceedings of the National Academy of Sciences*, *100*(19), 10954-10959.

Ylitalo, E. B., Thysell, E., Jernberg, E., Lundholm, M., Crnalic, S., Egevad, L., ... & Wikström, P. (2017). Subgroups of castration-resistant prostate cancer bone metastases defined through an inverse relationship between androgen receptor activity and immune response. *European urology*, *71*(5), 776-787.

Yoo, S. K., Cheong, J., & Kim, H. Y. (2014). STAMPing into mitochondria. *International Journal of Biological Sciences*, *10*(3), 321.

Yu, J., Yu, J., Mani, R. S., Cao, Q., Brenner, C. J., Cao, X., ... & Gong, Y. (2010). An integrated network of androgen receptor, polycomb, and TMPRSS2-ERG gene fusions in prostate cancer progression. *Cancer cell*, *17*(5), 443-454.

Yu, S., Yeh, C. R., Niu, Y., Chang, H. C., Tsai, Y. C., Moses, H. L., ... & Yeh, S. (2012). Altered prostate epithelial development in mice lacking the androgen receptor in stromal fibroblasts. *The Prostate*, *72*(4), 437-449.

Yu, X., Harris, S. L., & Levine, A. J. (2006). The regulation of exosome secretion: a novel function of the p53 protein. *Cancer research*, *66*(9), 4795-4801.

Yue, X., Zhao, Y., Xu, Y., Zheng, M., Feng, Z., & Hu, W. (2017). Mutant p53 in cancer: accumulation, gain-of-function, and therapy. *Journal of molecular biology*, *429*(11), 1595-1606.

Yuen, G., Khan, F. J., Gao, S., Stommel, J. M., Batchelor, E., Wu, X., & Luo, J. (2017). CRISPR/Cas9-mediated gene knockout is insensitive to target copy number but is dependent on guide RNA potency and Cas9/sgRNA threshold expression level. *Nucleic acids research*, *45*(20), 12039-12053.

Yun, C. W., & Lee, S. H. (2018). The roles of autophagy in cancer. *International journal of molecular sciences*, *19*(11), 3466.

Zaffuto, E., Pompe, R., Zanaty, M., Bondarenko, H. D., Leyh-Bannurah, S. R., Moschini, M., ... & Zorn, K. C. (2017). Contemporary incidence and cancer control outcomes of primary neuroendocrine prostate cancer: a SEER database analysis. *Clinical Genitourinary Cancer*, *15*(5)

Zanoni, M., Piccinini, F., Arienti, C., Zamagni, A., Santi, S., Polico, R., ... & Tesei, A. (2016). 3D tumor spheroid models for in vitro therapeutic screening: a systematic approach to enhance the biological relevance of data obtained. *Scientific reports*, *6*(1), 1-11.

Zarif, J. C., & Miranti, C. K. (2016). The importance of non-nuclear AR signalling in prostate cancer progression and therapeutic resistance. *Cellular signalling*, *28*(5), 348-356.

Zhang, C. M., Chi, X., Wang, B., Zhang, M., Ni, Y. H., Chen, R. H., ... & Guo, X. R. (2008). Downregulation of STEAP4, a highly-expressed TNF-α-inducible gene in adipose tissue, is associated with obesity in humans 1. *Acta Pharmacologica Sinica*, *29*(5), 587-592.

Zhang, C., Soori, M., Miles, F., Sikes, R., Carson, D., Chung, L., & Farach-Carson, M. (2010). Paracrine factors produced by bone marrow stromal cells induce apoptosis and neuroendocrine differentiation in prostate cancer cells. *The Prostate*, *71*(2), 157-167.

Zhang, F., Tao, Y., Zhang, Z., Guo, X., An, P., Shen, Y., ... & Wang, F. (2012). Metalloreductase Steap3 coordinates the regulation of iron homeostasis and inflammatory responses. *Haematologica*, *97*(12), 1826-1835.

Zhang, L., Charron, M., Wright, W. W., Chatterjee, B., Song, C. S., Roy, A. K., & Brown, T. R. (2004). Nuclear factor-κB activates transcription of the androgen receptor gene in Sertoli cells isolated from testes of adult rats. *Endocrinology*, *145*(2), 781-789.

Zhao, H., Zhu, C., Qin, C., Tao, T., Li, J., Cheng, G., ... & Shao, P. (2013). Fenofibrate down-regulates the expressions of androgen receptor (AR) and AR target genes and induces oxidative stress in the prostate cancer cell line LNCaP. *Biochemical and biophysical research communications*, *432*(2), 320-325.

Zhao, P., Zhang, Y., Li, W., Jeanty, C., Xiang, G., & Dong, Y. (2020). Recent advances of antibody drug conjugates for clinical applications. *Acta Pharmaceutica Sinica B*.

Zhen, S., Takahashi, Y., Narita, S., Yang, Y. C., & Li, X. (2017). Targeted delivery of CRISPR/Cas9 to prostate cancer by modified gRNA using a flexible aptamer-cationic liposome. *Oncotarget*, *8*(6), 9375.

Zhou, Y., Bolton, E. C., & Jones, J. O. (2015). Androgens and androgen receptor signalling in prostate tumorigenesis. *J Mol Endocrinol*, *54*(1), R15-R29.

Zhu, M. L., & Kyprianou, N. (2008). Androgen receptor and growth factor signalling crosstalk in prostate cancer cells. *Endocrine-related cancer*, *15*(4), 841.

Zhuang, X., Herbert, J. M. J., Lodhia, P., Bradford, J., Turner, A. M., Newby, P. M., ... & Cross, D. A. E. (2015). Identification of novel vascular targets in lung cancer. *British journal of cancer*, *112*(3), 485-494.

Zoetemelk, M., Rausch, M., Colin, D. J., Dormond, O., & Nowak-Sliwinska, P. (2019). Short-term 3D culture systems of various complexity for treatment optimization of colorectal carcinoma. *Scientific reports*, *9*(1), 1-14.

Zong, Y., Xin, L., Goldstein, A. S., Lawson, D. A., Teitell, M. A., & Witte, O. N. (2009). ETS family transcription factors collaborate with alternative signalling pathways to induce carcinoma from adult murine prostate cells. *Proceedings of the National Academy of Sciences*, *106*(30), 12465-12470.

Zugazagoitia, J., Guedes, C., Ponce, S., Ferrer, I., Molina-Pinelo, S., & Paz-Ares, L. (2016). Current challenges in cancer treatment. *Clinical therapeutics*, *38*(7), 1551-1566.

Zunich, S. M., Douglas, T., Valdovinos, M., Chang, T., Bushman, W., Walterhouse, D., ... & Lamm, M. L. (2009). Paracrine sonic hedgehog signalling by prostate cancer cells induces osteoblast differentiation. *Molecular cancer*, *8*(1), 12.

Chapter 9

Appendices

Appendix 1

Additional supporting data for Chapter 3

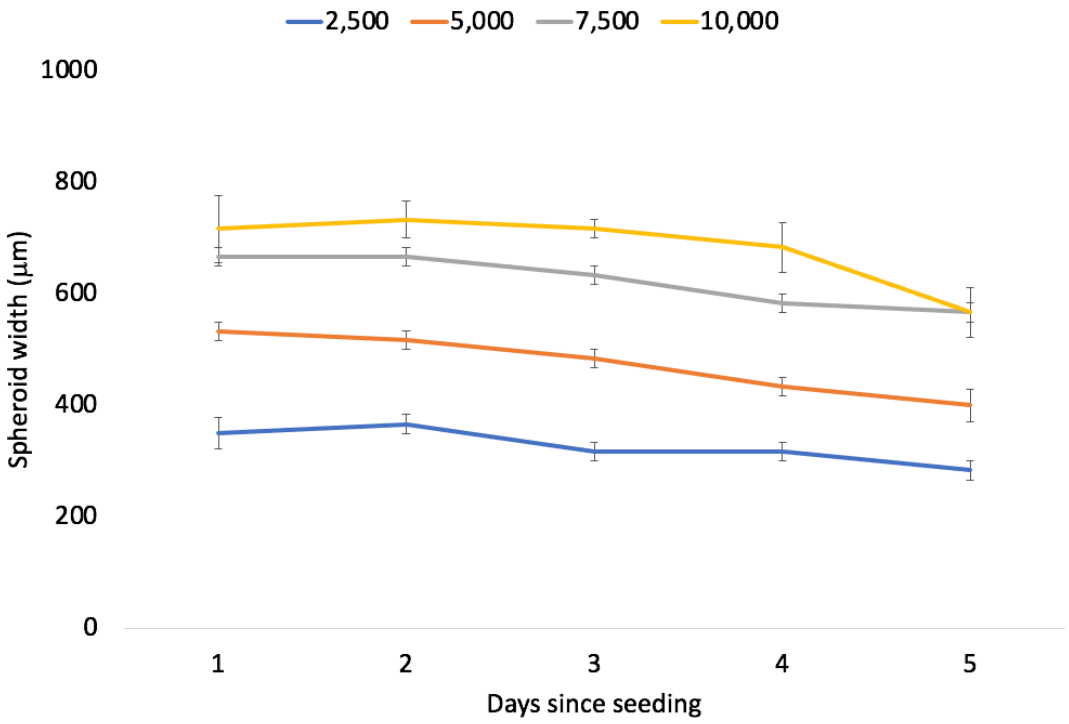

Figure A1.1. Growth curve showing the effects of different initial seeding densities on the size of 3D monoculture HS5 bone stromal cell spheroids over time. Bone stromal cell line HS5 were cultured at various initial seeding densities on agarose coated 96-well flat-bottomed plates to generate cultures of reproducibly sized, single spheroids in each well. The diameter of each spheroid was measured (μm) every day for 5 days. Measurements were taken from images acquired from 3 separate spheroids per cell line, per seeding density using a standard light microscope (AxioCam ERC55, Zeiss, Germany) using a 5x objective. An ANOVA post-hoc Dunnett test was performed for statistical analysis. Error bars denote S.E.M. p-value < 0.05 (*), p-value < 0.01 (**), p-value < 0.001 (***), p-value < 0.0001 (****) (N = 3).

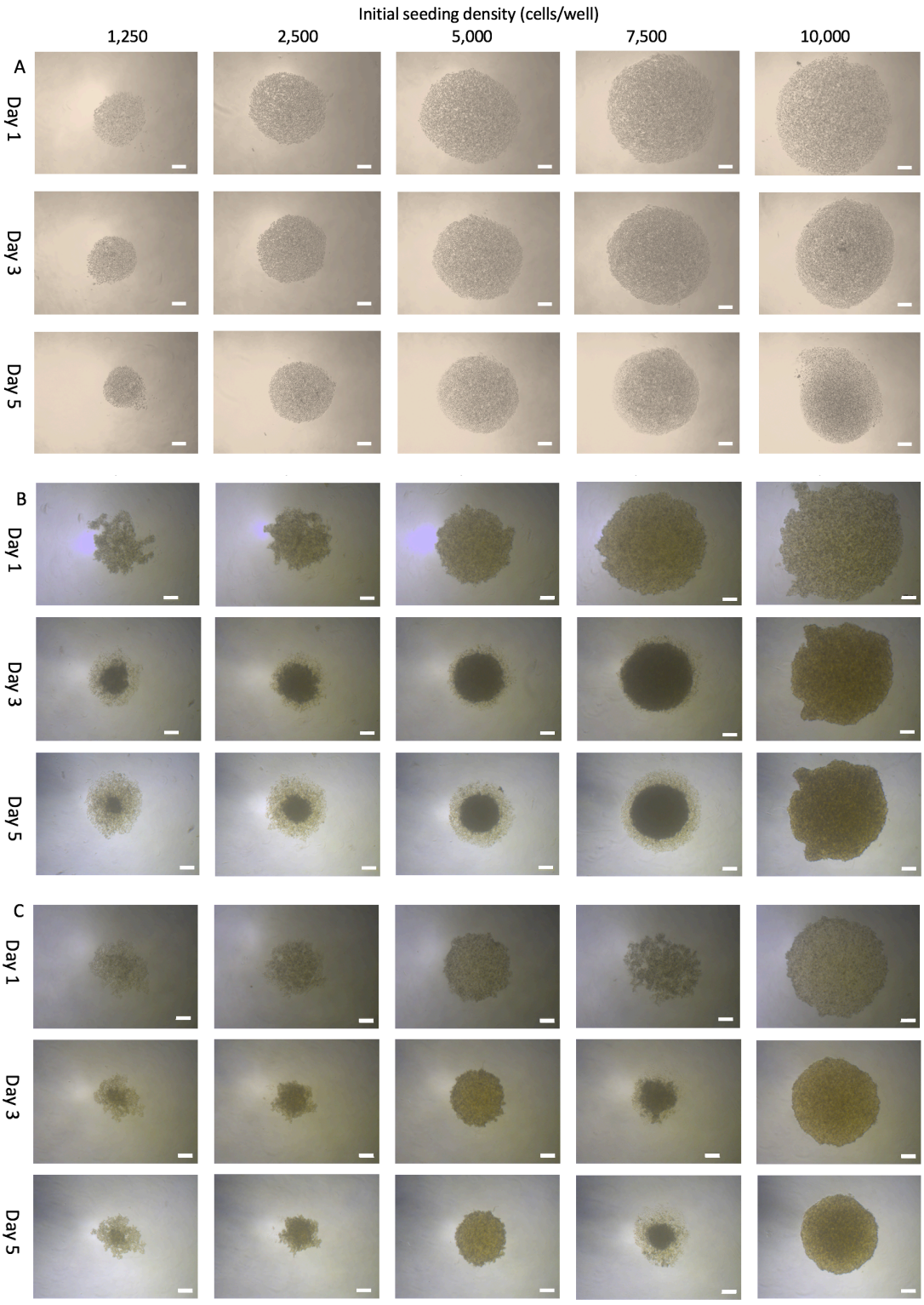
Initial seeding density (cells/well)
1,250
2,500
5,000
7,500
10,000
A
Day 1
Day 3
Day 5
B
Day 1
Day 3
Day 5
C
Day 1
Day 3
Day 5

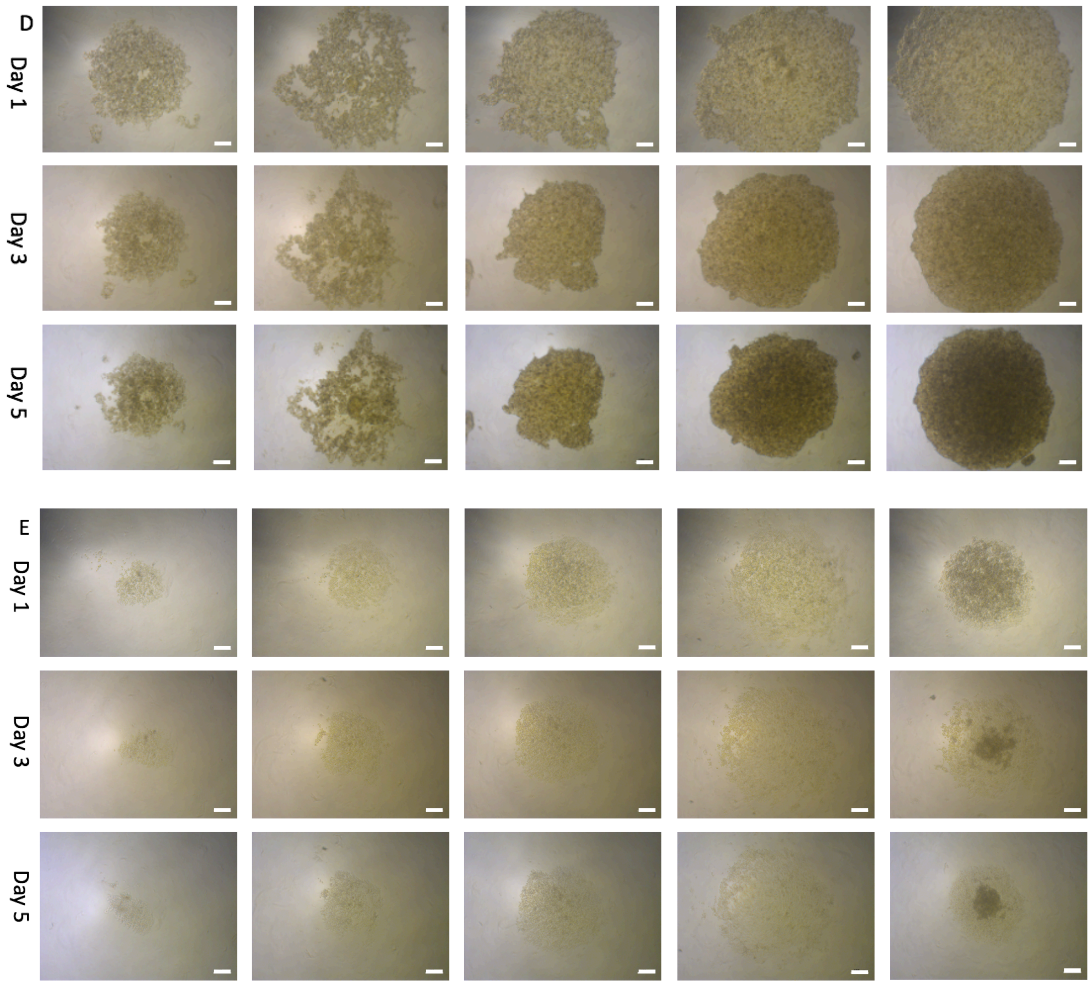

Figure A1.2. Representative light microscopy images of prostate cancer and stromal cell monoculture spheroids over time. (A) PC3, (B) DU145, (C) LNCaP and (D) C4-2B prostate cancer cells and (E) bone stromal cells were cultured as 3D spheroids with a range of initial seeding densities. Images were taken 1, 3 and days after seeding and were acquired using a standard light microscope (AxioCam ERC55, Zeiss, Germany) using a 5x objective. Scale bar = 100 μm.

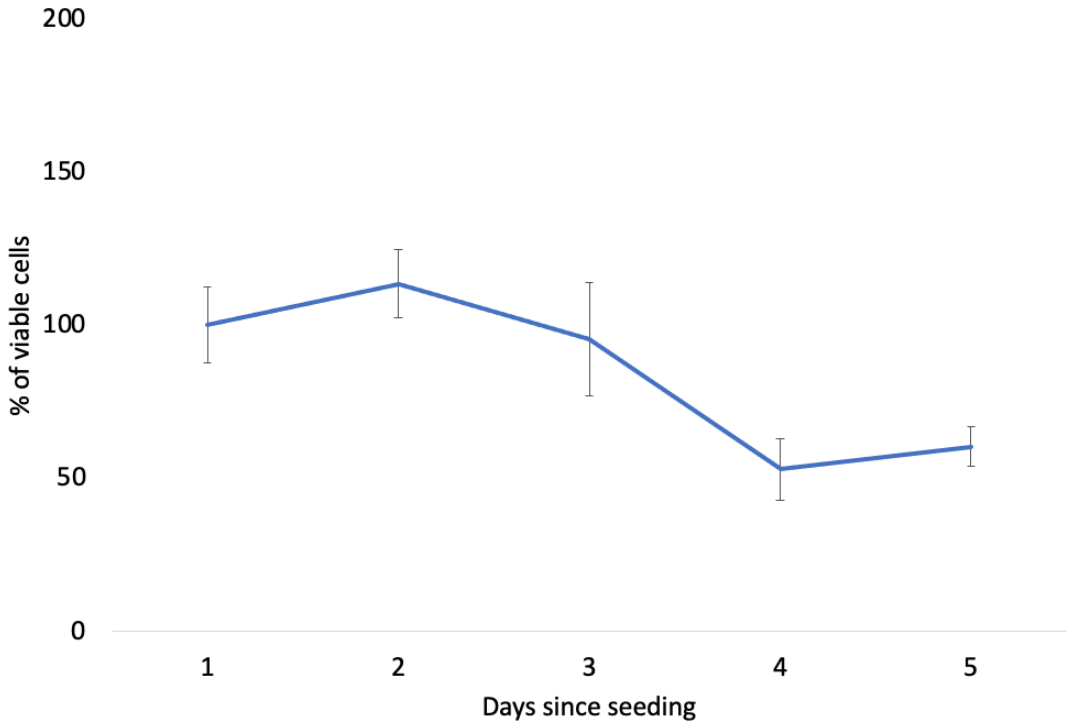

Figure A1.3. Viability of 3D HS5 cell spheroids over time. HS5 bone stromal cells were cultured at a density of 10,000 cells per well as 3D spheroids. An MTT viability assay was carried out each day for 5 days, with viability calculated as a percentage of day 1. An ANOVA post-hoc Dunnett test was performed for statistical analysis. Error bars denote S.E.M. p-value < 0.05 (*), p-value < 0.001 (***), p-value < 0.0001 (****) (N = 3).

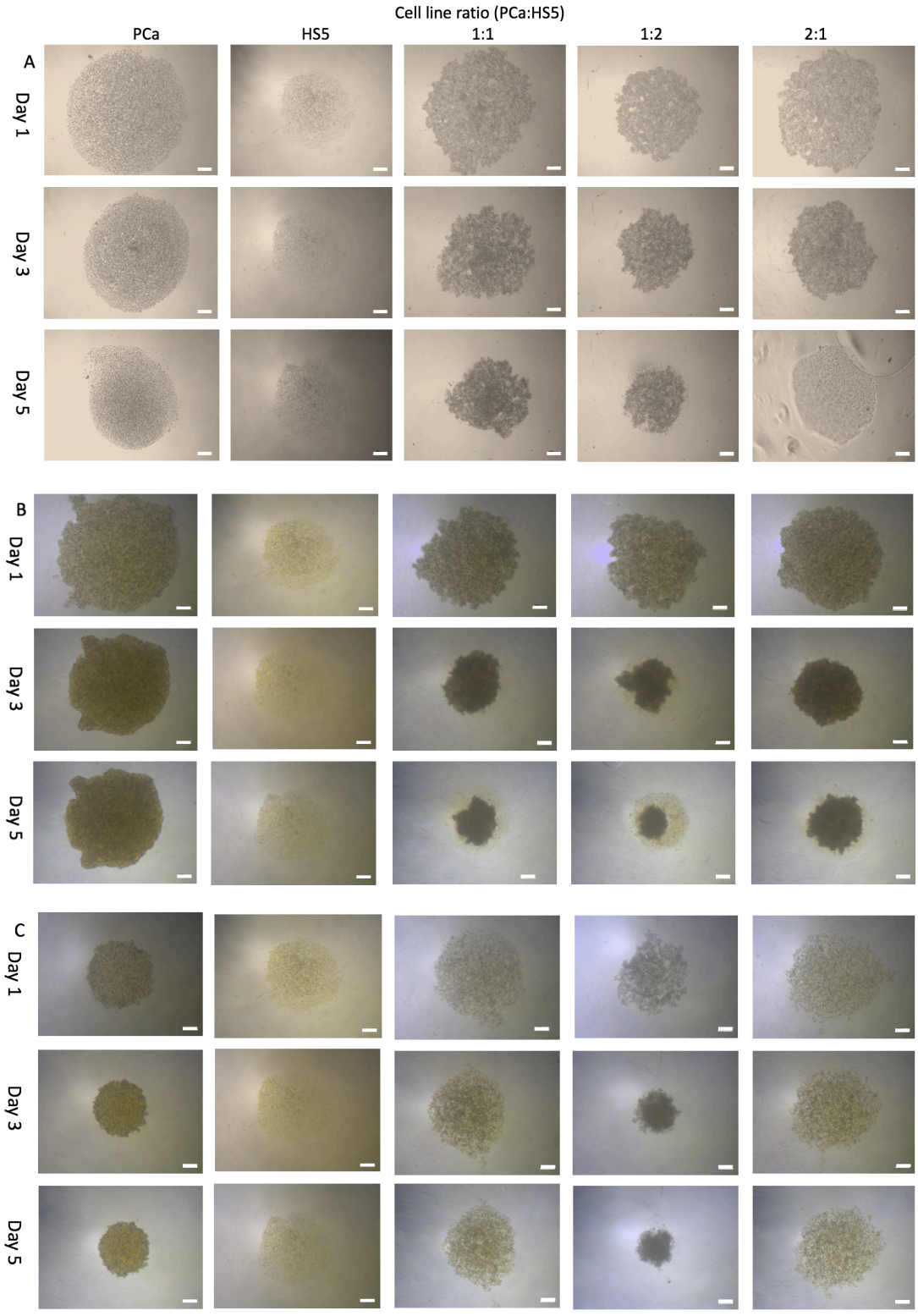
Cell line ratio (PCa:HS5)
PCa
HS5
1:1
1:2
2:1
A
Day 1
Day 3
Day 5
B
Day 1
Day 3
Day 5
C
Day 1
Day 3
Day 5

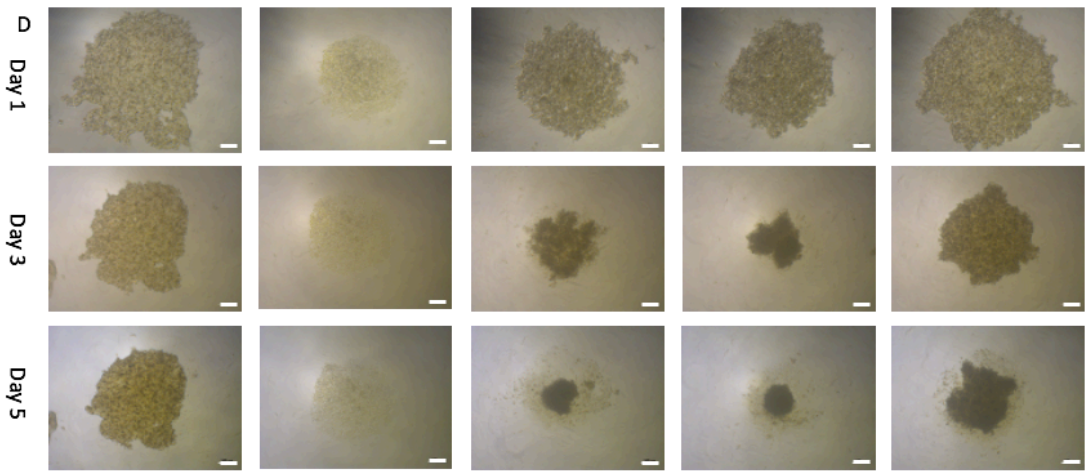

Figure A1.4. Representative light microscopy images of prostate cancer co-culture spheroids over time. (A) PC3, (B) DU145, (C) LNCaP and (D) C4-2B prostate cancer cells were cultured with different ratios of HS5 stromal cells as 3D spheroids. Images were taken every 5 days and were acquired using a standard light microscope (AxioCam ERC55, Zeiss, Germany) using a 5x objective. Scale bar = 100 μm.

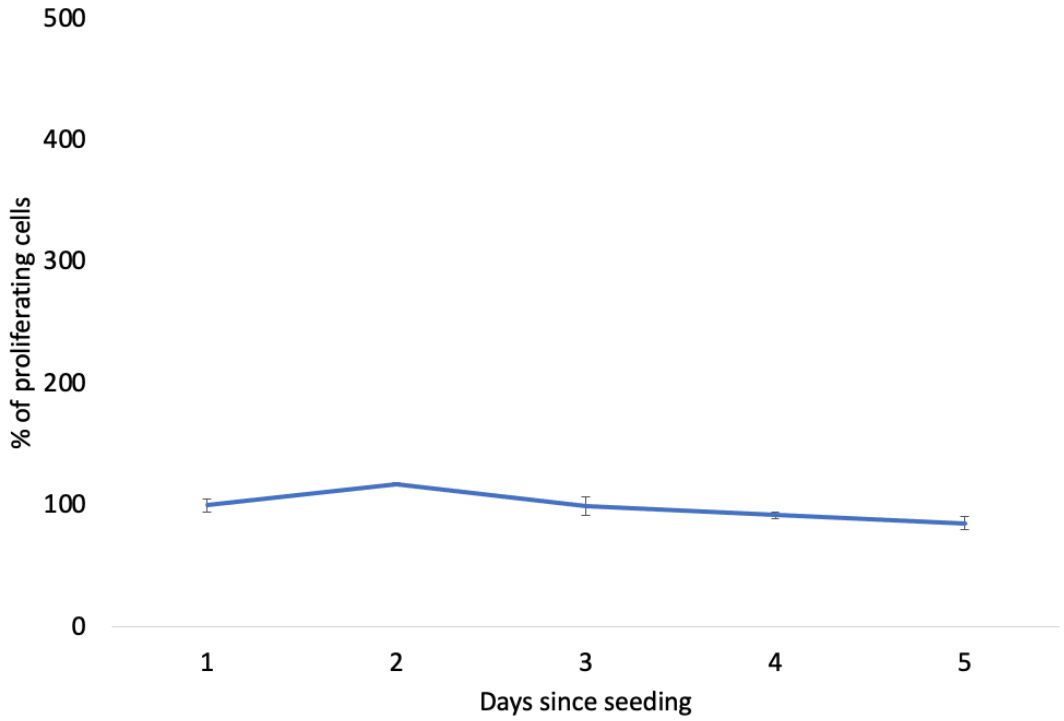

Figure A1.5. Proliferation rate of 3D HS5 cell spheroids over time. HS5 bone stromal cells were cultured at a density of 10,000 cells per well as 3D spheroids. An alamarBlue proliferation assay was carried out each day for 5 days, with viability calculated as a percentage of day 1. An ANOVA post-hoc Dunnett test was performed for statistical analysis. Error bars denote S.E.M. p-value < 0.05 (*), p-value < 0.001 (***), p-value < 0.0001 (****) (N = 3).

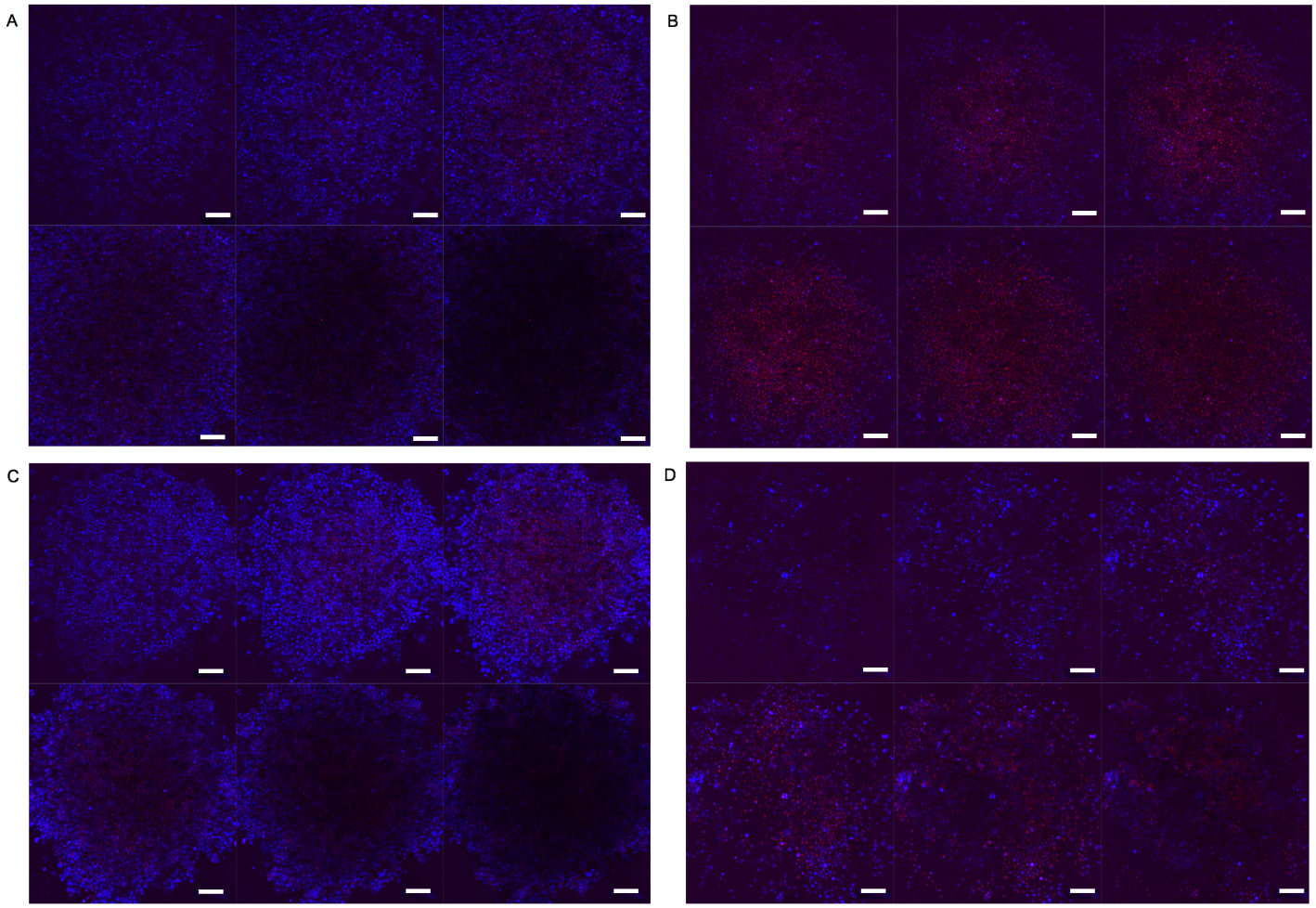

Figure A1.6. Z-stack showing PI staining of 3D PC3 co-culture spheroids by fluorescence microscopy. PI / Hoechst co-staining of 3D mono- (A & B) and co-culture (C & D) spheroids at 10x magnification showing an increase in PI uptake in both mono- and co-culture spheroids, indicative of cell death. Scale bar = 100 μm. Blue: nuclei; red: cell death. Images were taken on days 3 (A & C) and 5 (B & D) after seeding and were acquired with the Confocal LSM 710 (ZEISS, Germany) (N = 3).

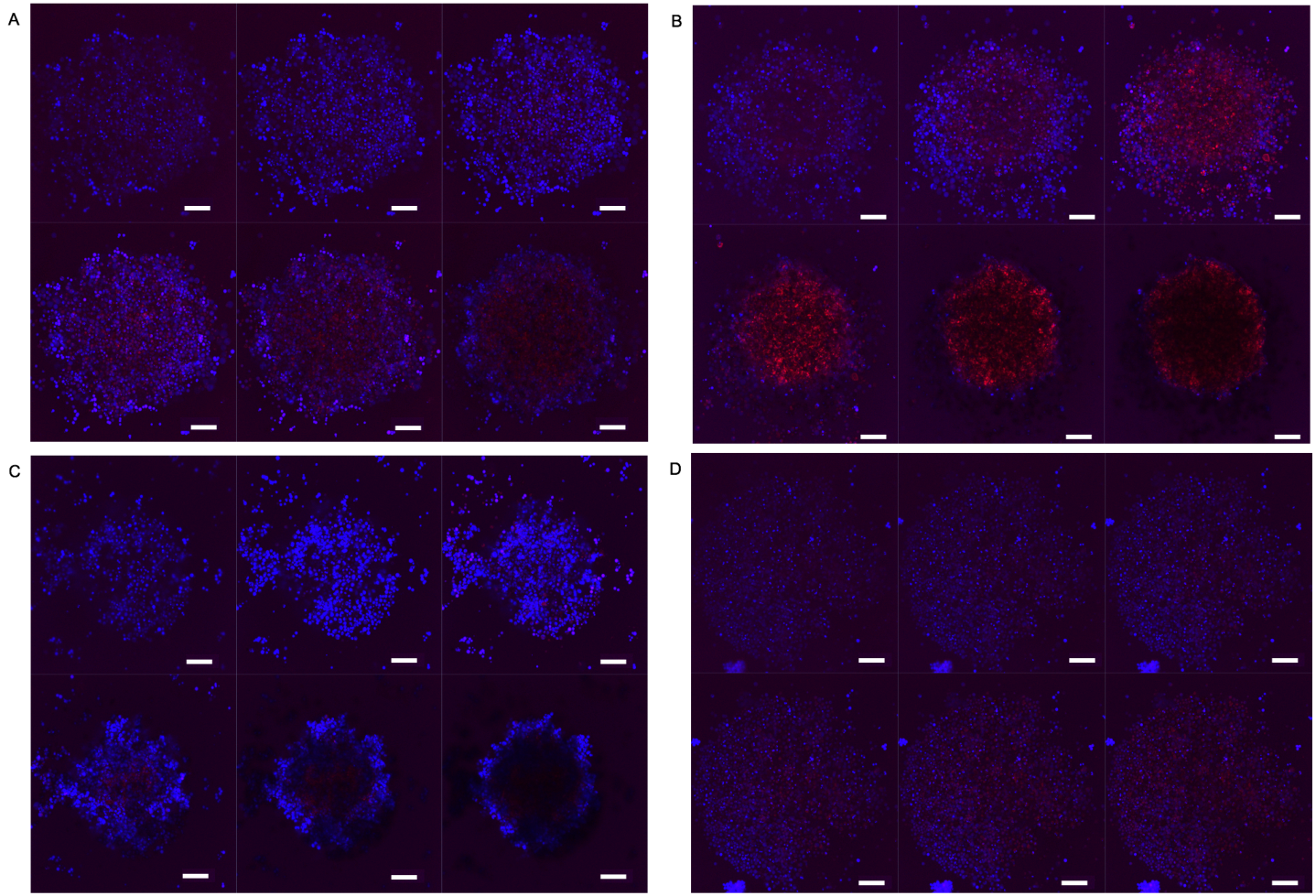

Figure A1.7. Z-stack showing PI staining of 3D DU145 co-culture spheroids by fluorescence microscopy. PI / Hoechst co-staining of 3D mono- (A & B) and co-culture (C & D) spheroids at 10x magnification showing an increase in PI uptake in both mono- and co-culture spheroids, indicative of cell death. Scale bar = 100 μM. Blue: nuclei; red: cell death. Images were taken on days 3 (A & C) and 5 (B & D) after seeding and were acquired with the Confocal LSM 710 (ZEISS, Germany) (N = 3).

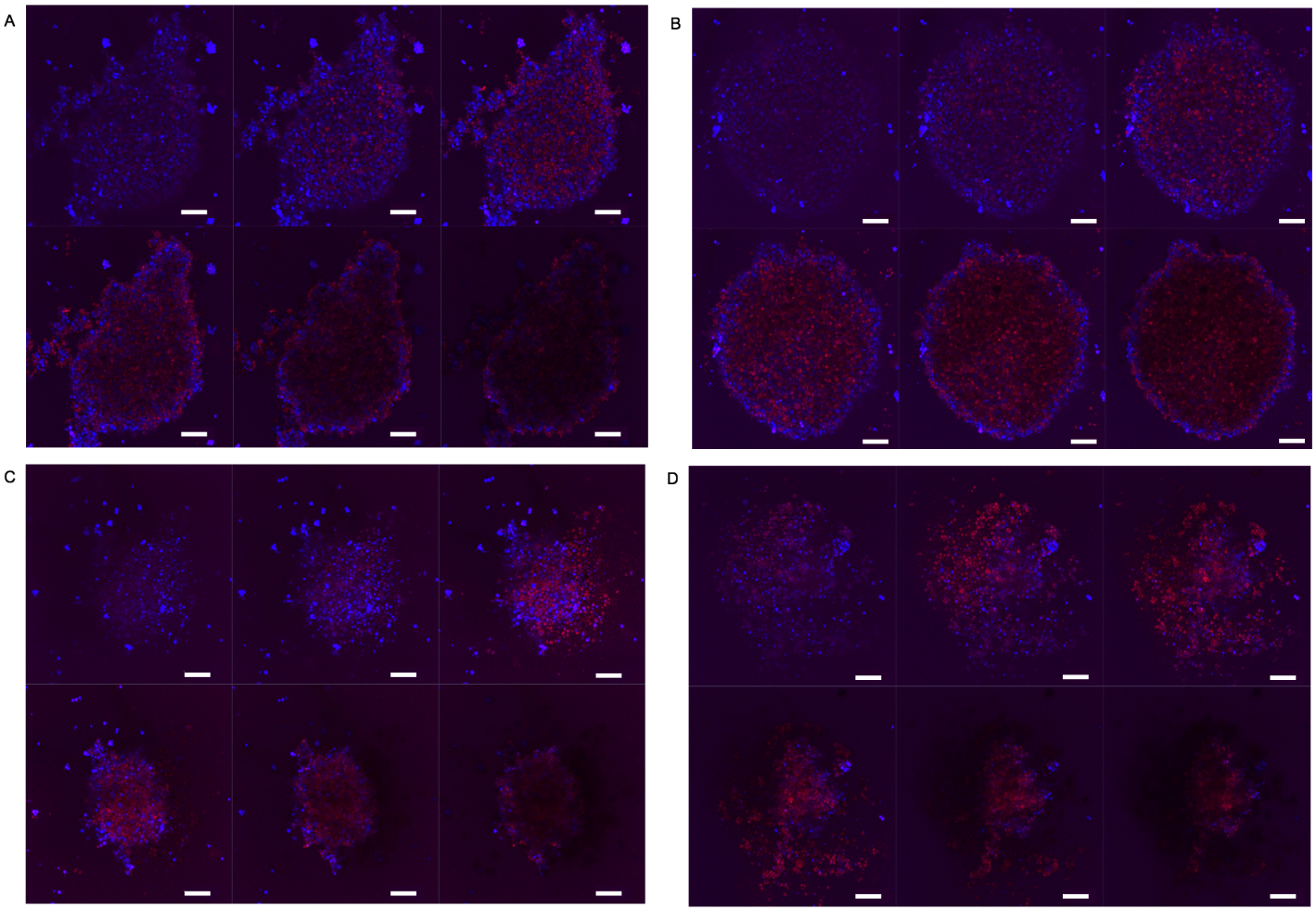

Figure A1.8. Z-stack showing PI staining of 3D LNCaP co-culture spheroids by fluorescence microscopy. PI / Hoechst co-staining of 3D mono- (A & B) and co-culture (C & D) spheroids at 10x magnification showing an increase in PI uptake in both mono- and co-culture spheroids, indicative of cell death. Scale bar = 100 μM. Blue: nuclei; red: cell death. Images were taken on days 3 (A & C) and 5 (B & D) after seeding and were acquired with the Confocal LSM 710 (ZEISS, Germany) (N = 3).

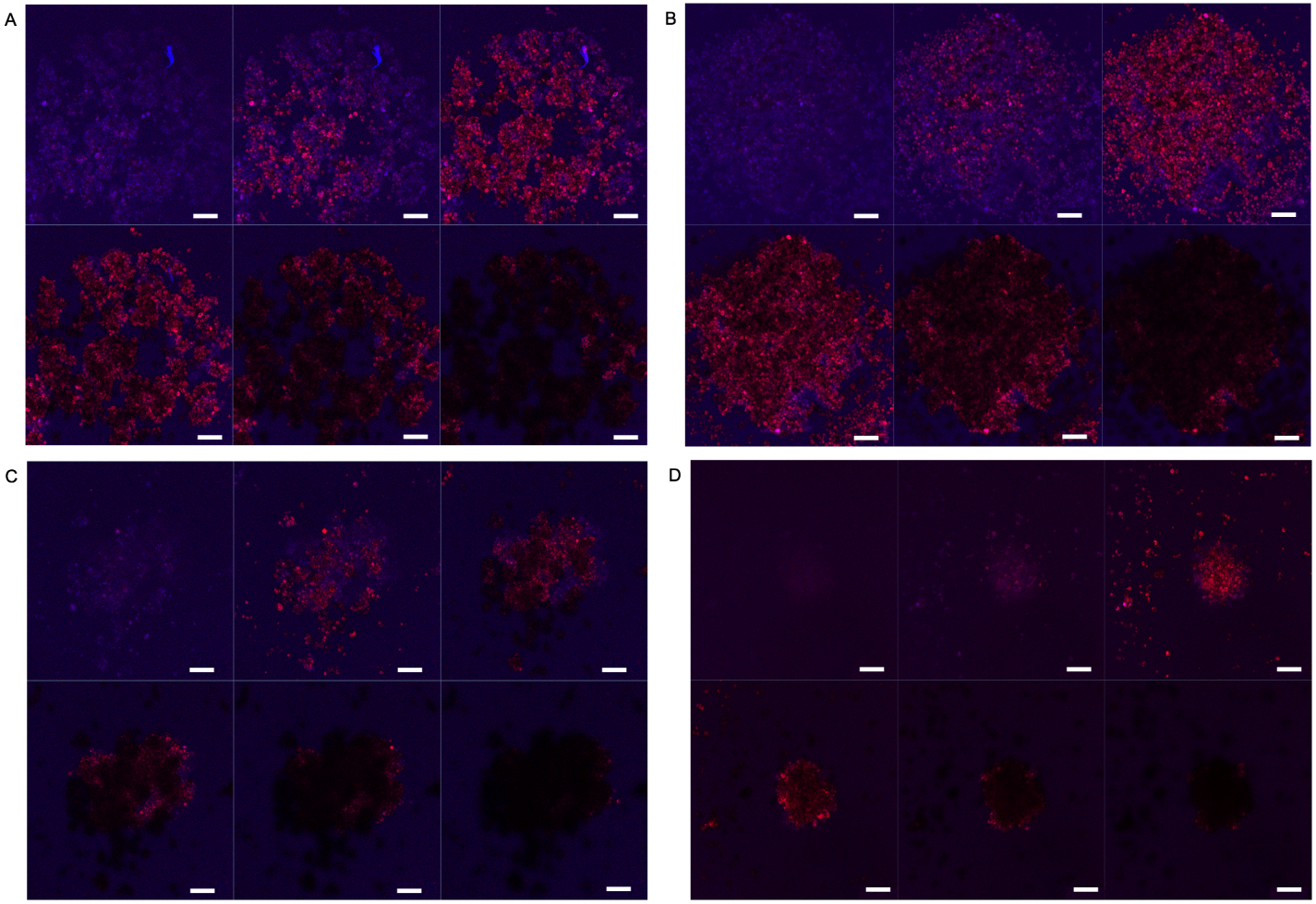

Figure A1.9. Z-stack showing PI staining of 3D C4-2B co-culture spheroids by fluorescence microscopy. PI / Hoechst co-staining of 3D mono- (A & B) and co-culture (C & D) spheroids at 10x magnification showing an increase in PI uptake in both mono- and co-culture spheroids, indicative of cell death. Scale bar = 100 μM. Blue: nuclei; red: cell death. Images were taken on days 3 (A & C) and 5 (B & D) after seeding and were acquired with the Confocal LSM 710 (ZEISS, Germany) (N = 3).

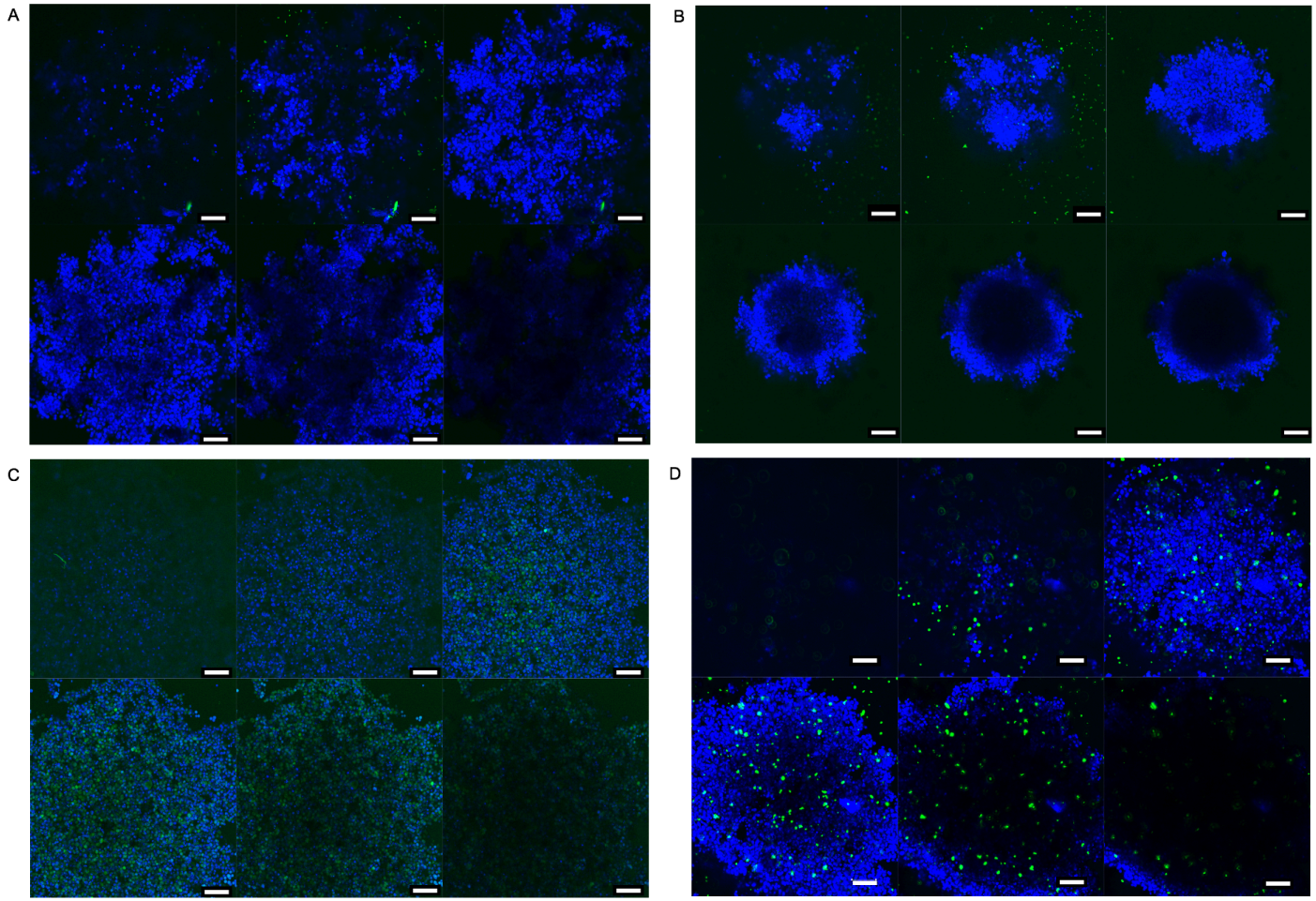

Figure A1.10. Z-stack showing integration of bone stromal (HS5) cells when co-cultured as 3D spheroids with prostate cancer cells. (A) PC3, (B) DU145, (C) LNCaP and (D) C4-2B prostate cancer cells were cultured with HS5 stromal cells as 3D spheroids. Confocal microscopy revealed HS5 cells were better integrated into androgen-sensitive prostate cancer cell spheroids (C & D). Scale bar = 100 μM. Blue: nuclei; green: STRO-1 stromal-specific antibody expression. Images were taken 3 days after seeding and were acquired with the Confocal LSM 710 (ZEISS, Germany) (N = 3)**.**

Appendix 2

Additional supporting data for Chapter 4

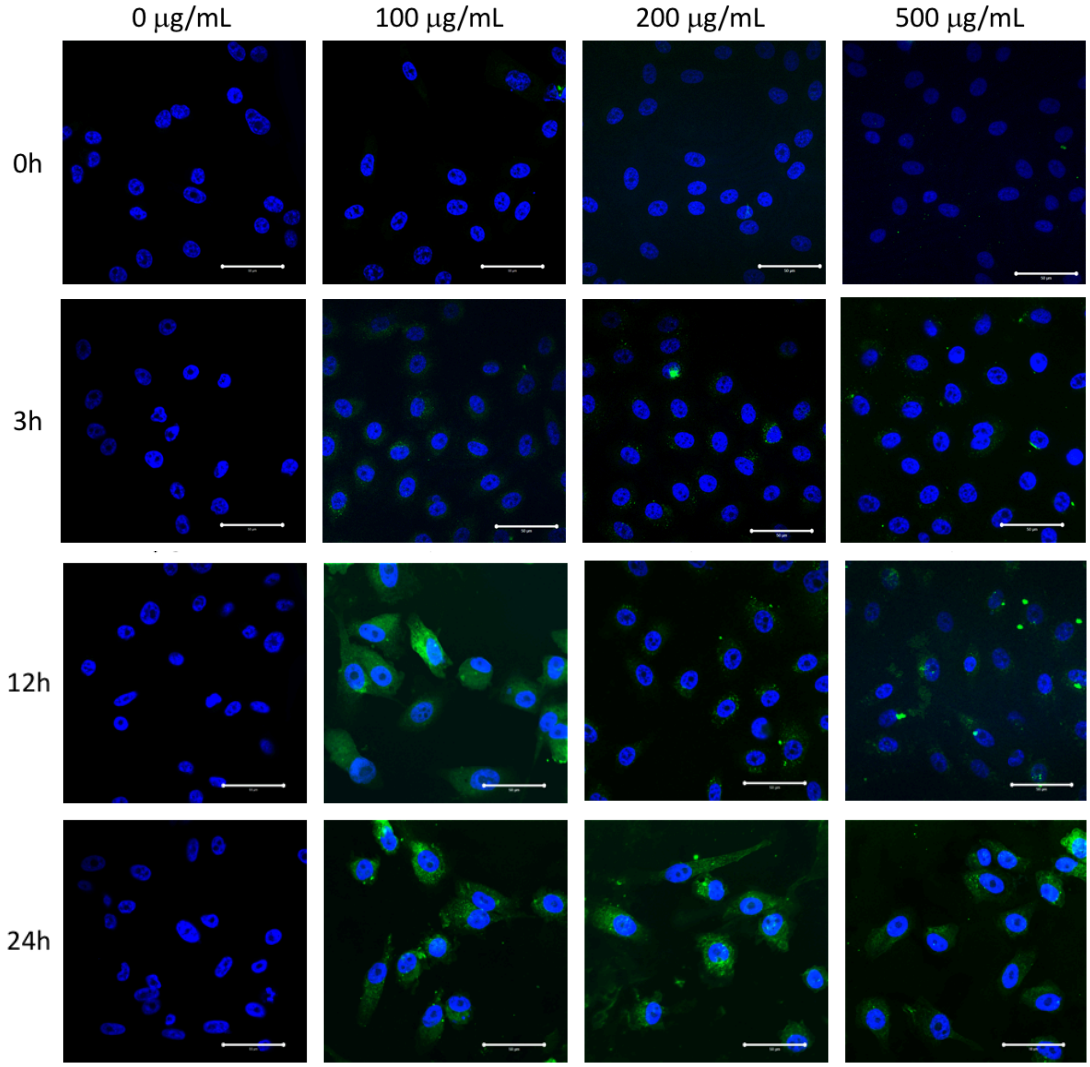

Figure A2.1. Anti-STEAP2 mAb2 exposure triggers STEAP2 receptor internalisation in PC3 cells. PC3 cells were exposed to anti-STEAP2 mAb2 for 0, 3, 12 and 24h at doses of 0, 100, 200 and 500 µg/ml. 0h: cell surface STEAP2 was visualised before receptor internalisation. 3h & 12h: STEAP2 receptor internalisation was initiated. 24h: fully internalised STEAP2 was evident. Blue: nuclei; green: STEAP2. Images were acquired with a Confocal LSM 710 with a 63x zoom objective (ZEISS, Germany). Scale bar = 50 µm. (N = 2).

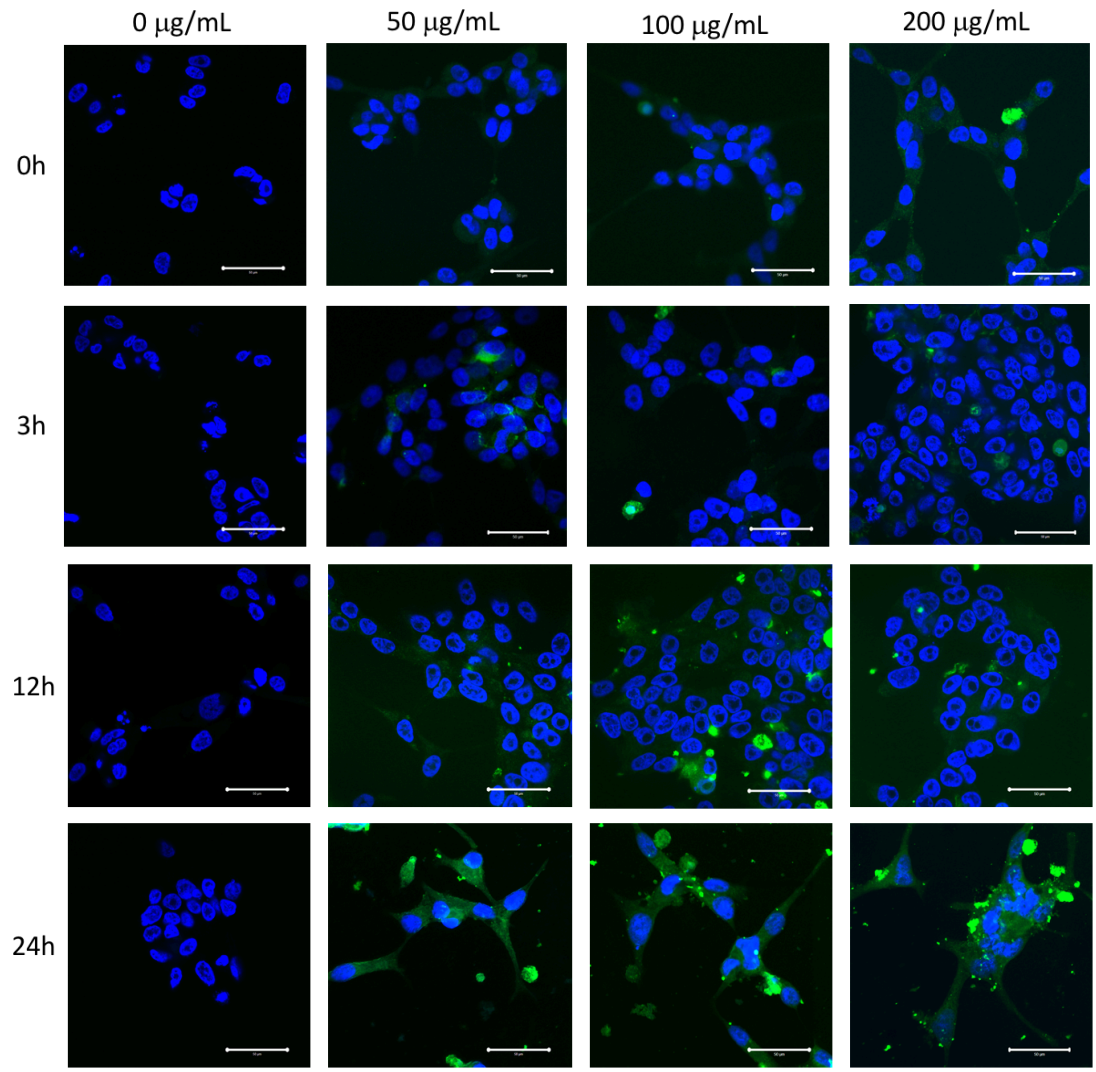

Figure A2.2. Anti-STEAP2 mAb2 exposure triggers STEAP2 receptor internalisation in LNCaP cells. PC3 cells were exposed to anti-STEAP2 mAb2 for 0, 3, 12 and 24h at doses of 0, 100, 200 and 500 µg/ml. 0h: cell surface STEAP2 was visualised before receptor internalisation. 3h & 12h: STEAP2 receptor internalisation was initiated. 24h: fully internalised STEAP2 was evident. Blue: nuclei; green: STEAP2. Images were acquired with a Confocal LSM 710 with a 63x zoom objective (ZEISS, Germany). Scale bar = 50 µm. (N = 2).

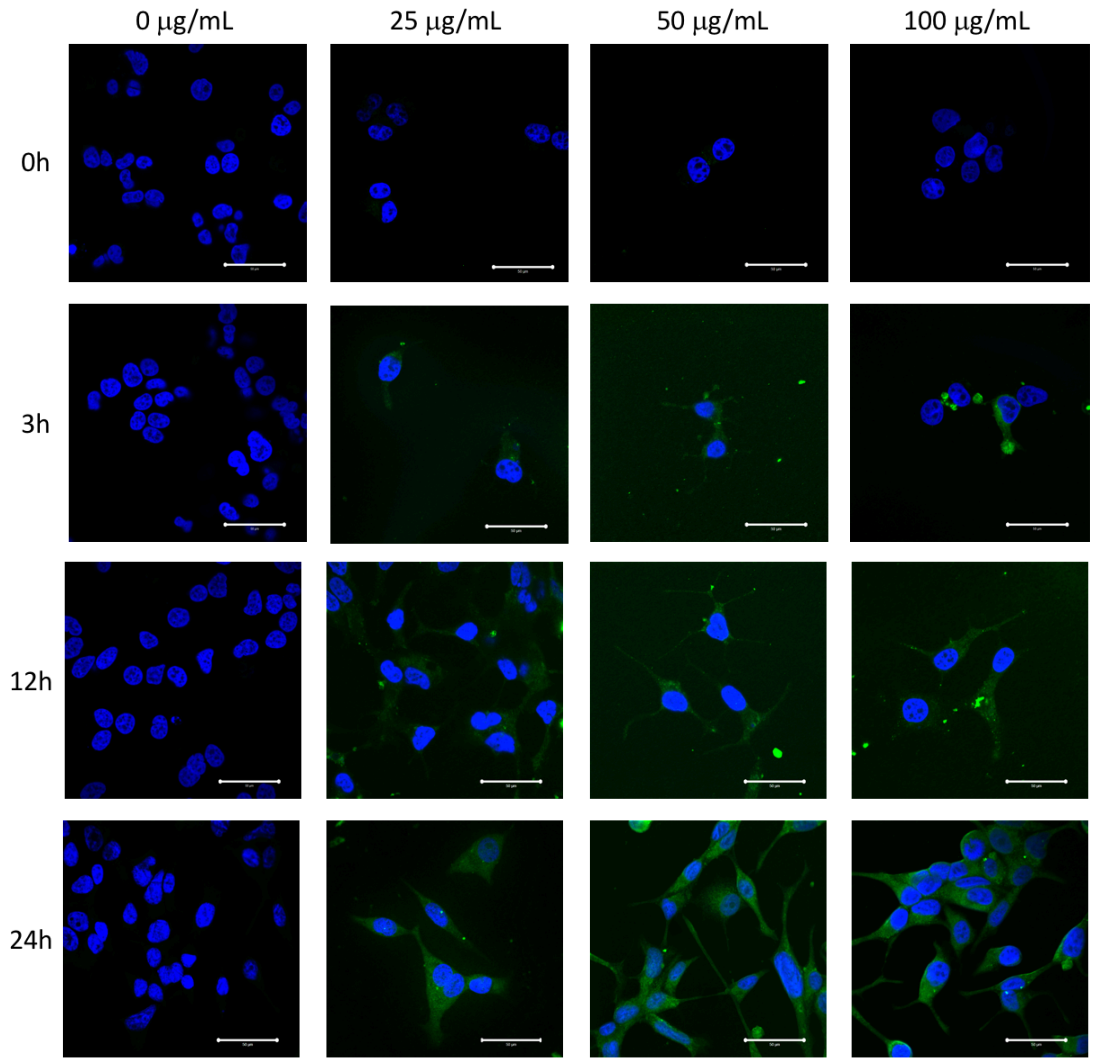

Figure A2.3. Anti-STEAP2 mAb2 exposure triggers STEAP2 receptor internalisation in C4-2B cells. PC3 cells were exposed to anti-STEAP2 mAb2 for 0, 3, 12 and 24h at doses of 0, 100, 200 and 500 µg/ml. 0h: cell surface STEAP2 was visualised before receptor internalisation. 3h & 12h: STEAP2 receptor internalisation was initiated. 24h: fully internalised STEAP2 was evident. Blue: nuclei; green: STEAP2. Images were acquired with a Confocal LSM 710 with a 63x zoom objective (ZEISS, Germany). Scale bar = 50 µm. (N = 2).

Appendix 3

Additional supporting data for Chapter 5

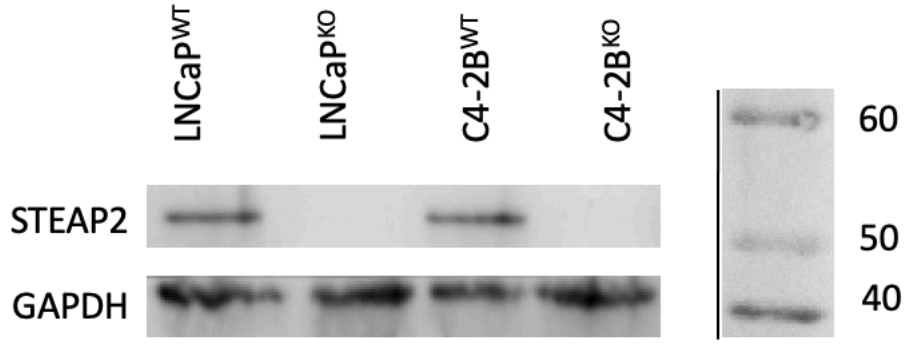

Figure A3.1. Analysis of STEAP2 knockout by Western blotting. Protein llysates were periodically obtained from passaged LNCaP^{WT},LNCaP^{KO}, C4-2B^{WT} and C4-2B^{KO} cells and passaged LNCaP^{KO} and C4-2B^{KO} cells to LNCaP^{WT} and C4-2B^{WT} cells represent high STEAP2 levels. Western blot image shows STEAP2 expression in wild-type and knock-out cells 10 passages after colony expansion. STEAP2: approx. 56 kDa; GAPDH: approx. 37 kDa. (Loading control = GAPDH, Black lines represent where the western blot image has been edited for clarity).

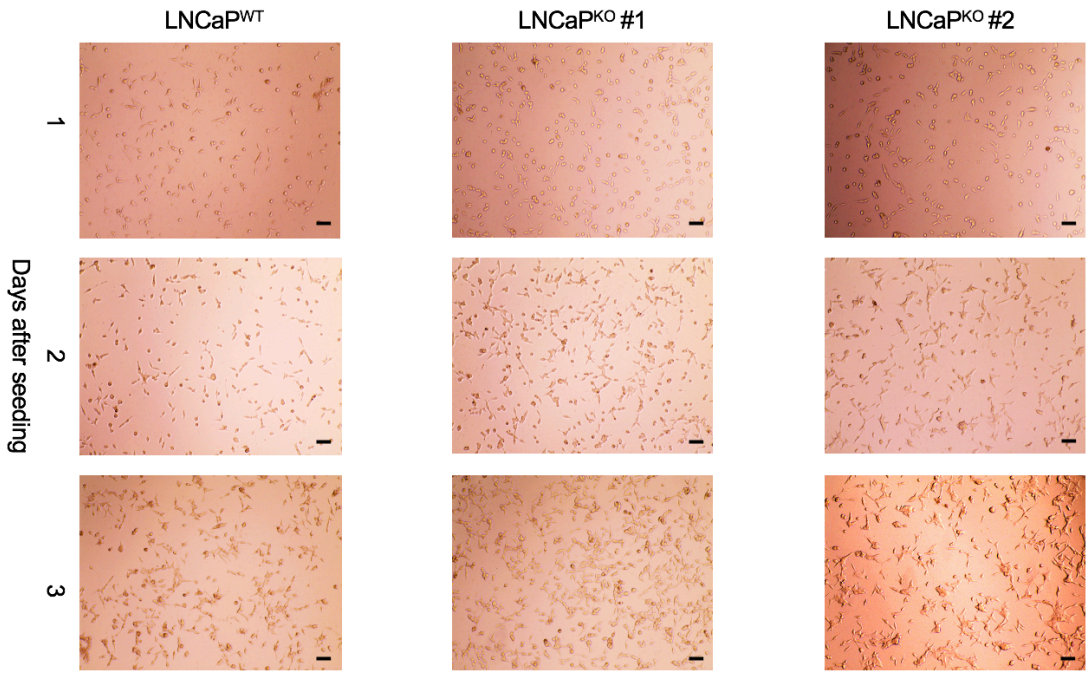

Figure A3.2. LNCaP wild-type and *STEAP2*-knockout cells over time. Morphology of LNCaP prostate cancer cells shown as wild-type cells and with CRISPR/Cas9 targeted *STEAP2* knockout via plasmid #1 and plasmid #2 prior to the isolation of single colonies. Images were taken every 24 h and were acquired using a standard light microscope (Invitrogen, EVOS XL Core, USA) using a 5x objective. Scale bar = 100 μm.

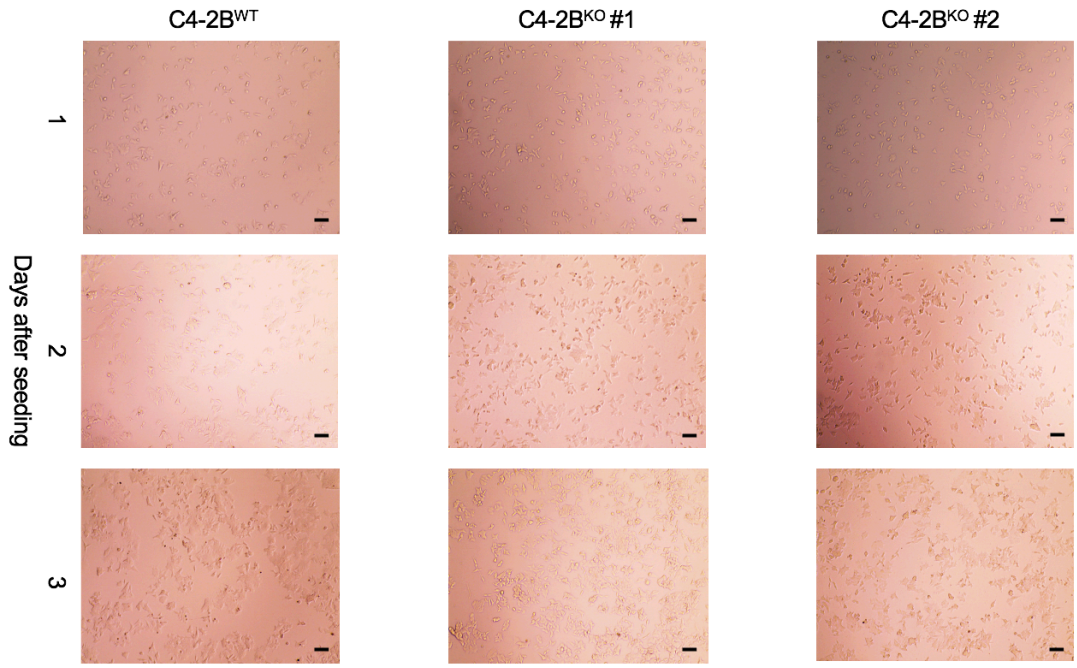

Figure A3.3. C4-2B wild-type and *STEAP2*-knockout cells over time. Morphology of C4-2B prostate cancer cells shown as wild-type cells and with CRISPR/Cas9 targeted *STEAP2* knockout via plasmid #1 and plasmid #2 prior to the isolation of single colonies. Images were taken every 24 h and were acquired using a standard light microscope (Invitrogen, EVOS XL Core, USA) using a 5x objective. Scale bar = 100 μm.

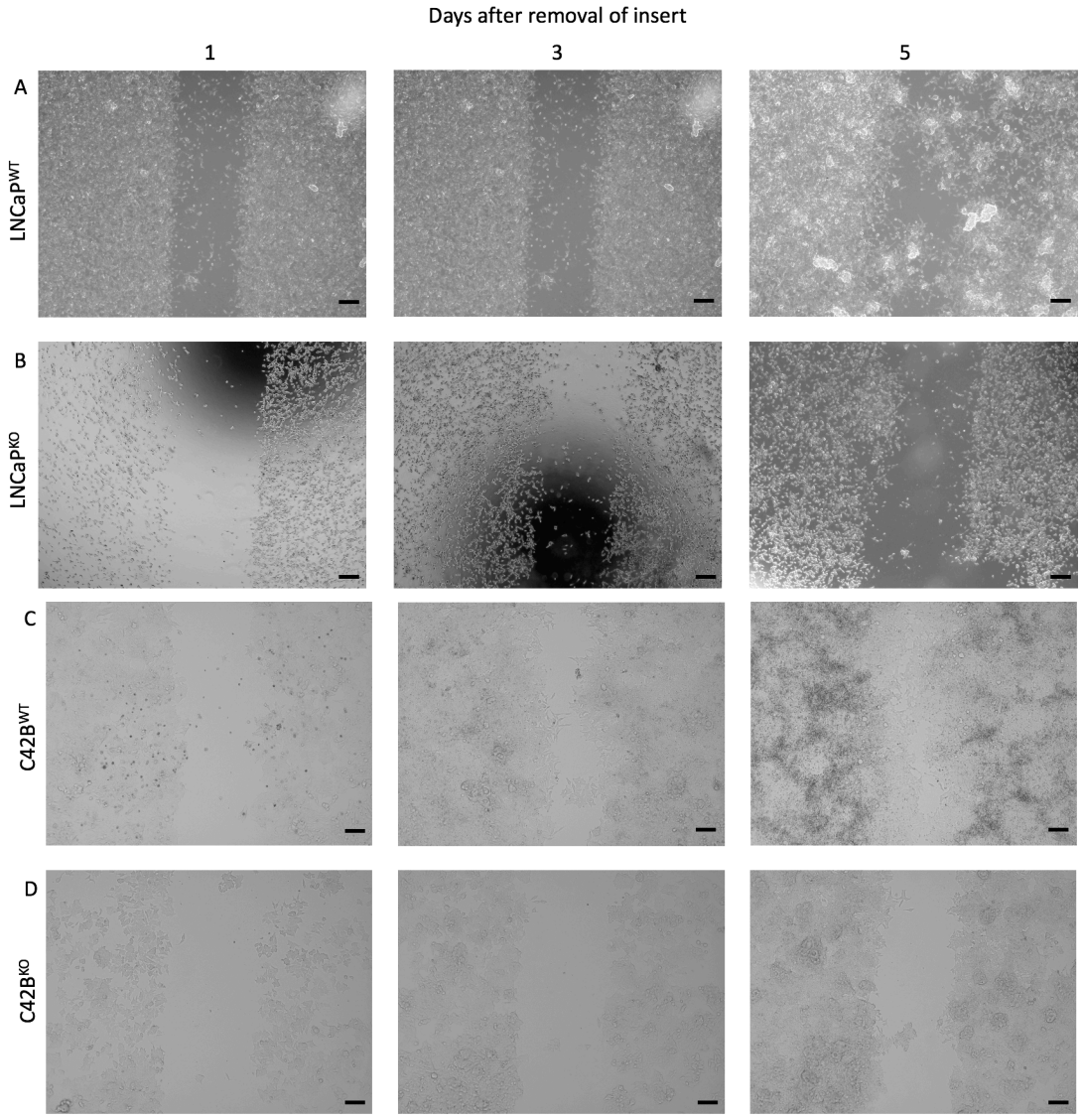

Figure A3.4. *STEAP2* knockout decreases the migratory potential of LNCaP and C4-2B cells. Each panel represents A) LNCaP^{WT}, B) LNCaP^{KO} cells and C) C4-2B^{WT}, D) C4-2B^{KO} cells. Time points at which the images were taken: 0 days, 3 days and 6 days. Wild-type LNCaP and C4-2B cells were used as positive controls. Images were acquired using an inverted light microscope with a 10x objective (Invitrogen, EVOS XL Core, USA). Scale bar = 100 μm. (Illustrated are representative images; the experiment was however conducted in triplicate with N = 3).

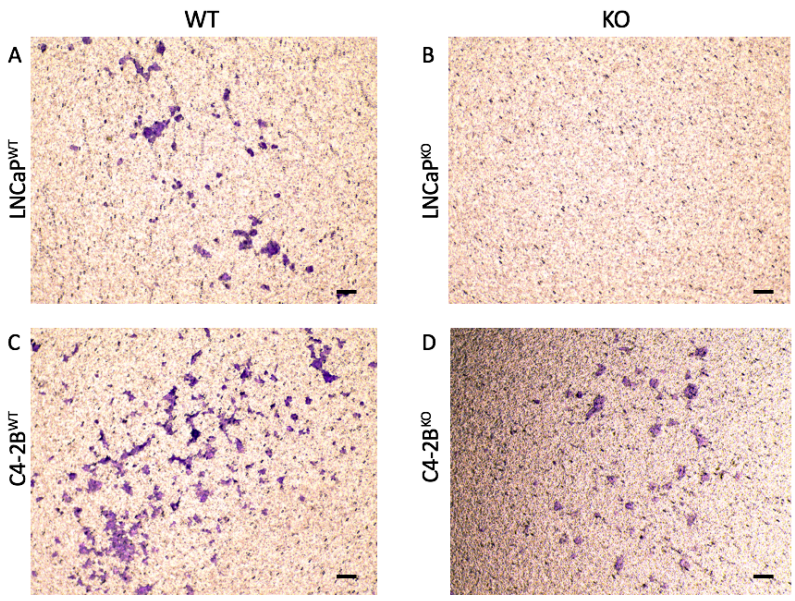

Figure A3.5. *STEAP2* knockout reduces the invasive potential of LNCaP and C4-2B cells. Images of stained cells were taken to give a visual representation of invasion. Each panel represents A) LNCaP^{WT}, B) LNCaP^{KO} cells and C) C4-2B^{WT}, D) C4-2B^{KO} cells. LNCaP^{WT} and C4-2B^{WT} cells show invasive potential. STEAP2 knockout of LNCaP^{KO} and C4-2B^{KO} reduces invasive capacity. Invaded cells were stained with crystal violet. Images were taken 48 h (C4-2B) and 72 h (LNCaP) after seeding. E) The number of stained cells that had invaded through the Transwell insert were counted and calculated as a percentage of the wild-type control. An unpaired t-test was performed for statistical analysis. Error bars denote S.E.M. p-value < 0.05 (*), p-value < 0.01 (**), p-value < 0.001 (***), p-value < 0.0001 (****). Images were taken with an inverted light microscope at a 10x objective (Invitrogen, EVOS XL Core, USA). Scale bar = 100 μm. (N = 2).

Appendix 4

Additional supporting data for Chapter 6

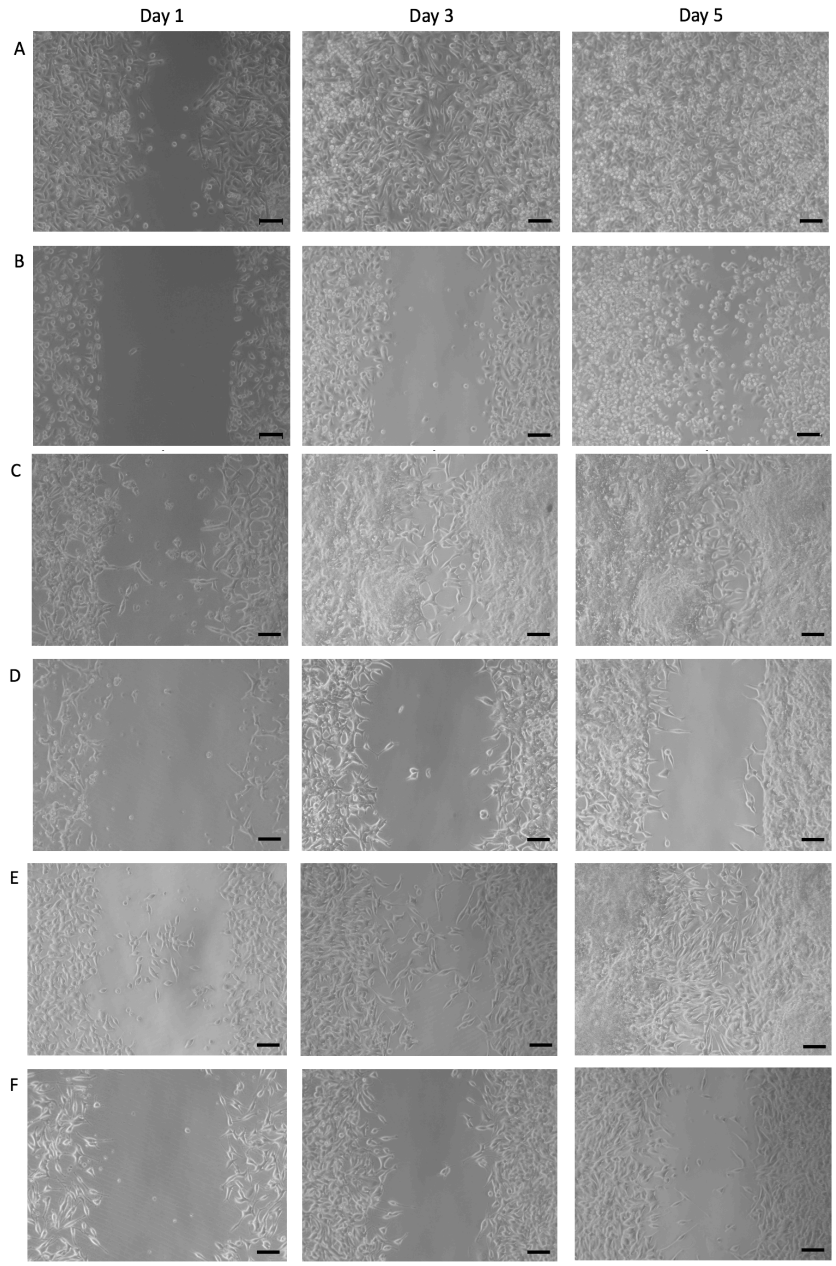

Figure A4.1. Androgen depletion by charcoal stripped FBS decreases the migratory potential of PC3, LNCaP and C4-2B cells. Time points at which the images were taken: 0 days, 3 days and 5 days. PC3 (A), LNCaP (C) and C4-2B (E) cells cultured in FBS-supplemented media (AR+). Androgen depleted PC3 (B), LNCaP (D) and C4-2B (F) cells were cultured in CSS-supplemented media (AR-). Images were acquired using an inverted light microscope with a 10x objective (AxioCam ERC55, Zeiss, Germany). Scale bar = 50 μm. (N = 2).

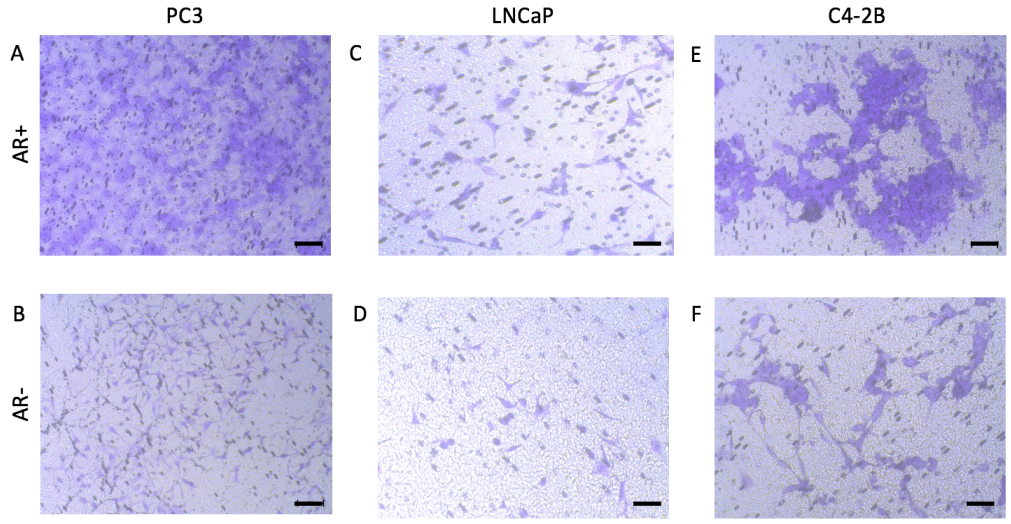

Figure A4.2. Androgen depletion reduces the invasive potential of PC3, LNCaP and C4-2B cells. Images of stained cells were taken to give a visual representation of invasion. PC3 (A), LNCaP (C) and C4-2B (E) cells cultured in FBS-supplemented media (AR+). Androgen depleted PC3 (B), LNCaP (D) and C4-2B (F) cells were cultured in CSS-supplemented media (AR-). Each panel represents A) PC3 AR+, B) PC3 AR- C) LNCaP AR+ D) LNCaP AR-, E) C4-2B AR+ and F) C4-2B AR-. AR+ cells show invasive potential. Invaded cells were stained with crystal violet and images were taken 48 h after seeding. Images were acquired using an inverted light microscope with a 10x objective (AxioCam ERC55, Zeiss, Germany). Scale bar = 50 μm. (N = 2).